DOCTOR OF PHILOSOPHY

Investigation Of Residual Stress Redistribution During Elastic Shakedown In Welded Plates

Chukkan, Jazeel Rahman

Award date:
2020

Awarding institution:
Coventry University

Investigation Of Residual Stress Redistribution During Elastic Shakedown In Welded Plates

By

Jazeel R Chukkan

May 2019

A thesis submitted in partial fulfilment of the University's requirements for the Degree of Doctor of Philosophy

Certificate of Ethical Approval

Applicant:

Jazeel Chukkan

Project Title:

Investigation of shake-out effects on the redistribution of residual stress in welded structures

This is to certify that the above named applicant has completed the Coventry University Ethical Approval process and their project has been confirmed and approved as Low Risk

Date of approval:

17 April 2018

Project Reference Number:

P69910

ABSTRACT

This research investigated the effect of the elastic shakedown on the redistribution of as-welded residual stresses under a limited number of load cycles in butt and fillet welded specimens. Elastic shakedown is said to have occurred in a component under external cyclic load when the material responds plastically in the first few cycles followed by an elastic response.

Four separate specimens manufactured from DH36 (shipbuilding steel) and Gas Metal Arc Welding were studied in which two were butt-welded plates, and two were fillet welded plates. Residual stress redistribution in the transverse and the longitudinal direction was investigated separately under cyclic load. Ten and three load cycles were applied on the butt, and fillet welded plates respectively. The variation of longitudinal and transverse residual stresses through-the-thickness of the plates were also investigated.

Neutron diffraction was carried out to determine residual stresses. The measurement was conducted in the as-welded condition and, after one, three and ten load cycles. The measured as-welded residual stress in both butt and fillet welded plate indicated that the magnitude recommended by structural integrity codes are conservative. Also, an applied load in any direction induced redistribution of residual stresses in both transverse and longitudinal component. Residual stress state in each specimen were predicted using 3D welding process simulations. Subsequently, numerical simulation of residual stress redistribution under cyclic loads were performed on weld plates. Shakedown limit analysis was implemented to define the shakedown limit of each weld plate using plastic work done as shakedown criterion. Based on the determined shakedown limit, a shakedown region was defined. A methodology of assessment using the defined shakedown region is used to investigate residual stress redistribution.

The study indicates that, under the considered load levels, the butt-welded plates were achieving shakedown state whereas the fillet welded plates did not achieve shakedown state. The numerical methods and experimental data presented in this work can offer guidance to structural integrity assessment of welded components undergoing shakedown and help produce more accurate and less conservative residual stress predictions. The proposed shakedown region can be upscaled to bigger structures for subsequent development of a procedure for allowance of elastic shakedown in design calculations.

DECLARATION

I, Jazeel R Chukkan hereby state that no portion of the work referred to in the thesis has been submitted in support of an application for another degree or qualification of this or any other university or another institute of learning.

ACKNOWLEDGEMENT

This research would not have been possible without the efforts and support of several people. I take this opportunity to express my sincere gratitude and appreciation to all.

I would like to express my appreciation and thanks to my supervisors, Prof. Michael Fitzpatrick and Prof. Xiang Zhang of Coventry University, Dr Guiyi Wu and Dr Elvin Eren of TWI Ltd., supportive supervision and invaluable guidance throughout my research.

Special thanks to instrument scientist Dr Joe Kelleher and Dr Tung Lik Lee of STFC Rutherford Appleton Laboratory, Oxford for their efforts in helping me to use the equipment, ENGINX at ISIS Neutron and Muon Source and supporting resources where the neutron diffraction stress measurement was carried out.

I also wish to thank Dr Shengming Zhang of Lloyd's Register Marine for his invaluable guidance from the start to the concluding level to develop an understanding of ship structures.

I also greatly appreciate the help of Prof Steve Jones for his insights and guidance on specimen manufacturing.

This work was made possible by the sponsorship and support of Coventry University and Lloyd's Register Foundation, a charitable foundation helping protect life and property by supporting engineering-related education, public engagement, and the application of research. The work was enabled through, and undertaken at, the National Structural Integrity Research Centre (NSIRC), a postgraduate engineering facility for industry-led research into structural integrity established and managed by TWI through a network of both national and international Universities.

Last but not least, I would like to thank all my friends and family members, without their incredible love, support and patience, I would never have been able to attempt this work.

CONTENTS

LIST OF TABLES

LIST OF FIGURES

CHAPTER 1.INTRODUCTION

1.1 Background

Ship structures are operated in a complex and challenging environment, but they should be self-sustaining in their environment for long periods with a high degree of reliability. The research work was evolved from a specific problem, which is the fatigue crack propagation in load bearing members of double bottom arrangement in ships as briefly explained in the following section.

1.1.1 Double bottom

Ship structures are most commonly made of combinations of plating and stiffeners (Stokoe 1996). A double bottom arrangement consists of the outer shell (bottom) and an inner skin or tank top (inner bottom) as shown in Figure 1.1. This provides a form of protection in the event of damage to the bottom shell. The inner bottom, being continuous, increases the longitudinal strength and acts as a platform for cargo and machinery.

Figure 1.1: Illustration of a double bottom deck (Eyres 2007)

In the double bottom structure, flat bar stiffeners or longitudinal end connections are welded on to the transverse frame, inner bottom longitudinal and bottom longitudinal. It has been reported that the weld connection between flat bar stiffeners and the longitudinal

stiffeners are critical in fatigue crack propagation (Erny et al. 2012; Fricke, von Lilienfeld-Toal and Paetzold 2012; Lotsberg and Landet 2005). There have been numerous reports on crack initiation from this weld, with crack ultimately propagating to longitudinal stiffeners (Fricke and Paetzold 2010; Hodapp, Collette and Troesch 2015; Kim et al. 2010). This is primarily due to the stress concentration in the weld toes, high tensile residual stresses in the welds and the load condition in longitudinal stiffeners as a result of various service loads such as wave load. It is known that tensile residual stresses are detrimental for weld structures to resist crack initiation and propagation. Therefore, the primary focus of this work is to investigate the residual stress redistribution in welded plates representing these connections.

1.1.2 Fatigue and residual stresses in ship structure

The fatigue design rule for welded structures including ship structures requires design based on the applied load range regardless of whether this is tensile or compressive (BS 7608 2014; Hobbacher 2009). This is to allow for the effect of tensile residual stresses due to welding in the vicinity of welds. Welding residual stresses in ship structures can introduce magnitudes equivalent to the yield strength of the material (Maddox 1991; Withers et al. 2008). Residual stresses can be beneficial or damaging depending on the type of stress and working conditions. Residual stresses can add to the applied load and causes premature failure and is not desirable in the design. Compressive residual stresses are generally beneficial in most engineering applications (Fricke and Kahl 2005). High tensile residual stress and its superposition with fatigue loading under service result in stress cycling about high tensile mean stress (Gurney 1979). The consequence of welding residual stress can be best illustrated by considering fracture mechanics. In linear elastic materials, the stress intensity factor due to residual stress is superimposed with the stress intensity factor due to external cyclic loading (Anderson 1991). As a result, with an increase in tensile residual stresses, stress intensity factor also increases, which is considered undesirable.

1.1.3 Shakedown in ship structures

However, there is a growing body of opinion that in practice the initial residual stress state will redistribute/relax as a result of loading (Eckerlid and Ulfvarson 1995; Polezhayeva et al. 2010). It is understood that this change in residual stress is primarily

due to plastic flow (Dawson and Moffat 1980; Walker 2011). Because plasticity does not depend on the loading direction, relaxation of residual stress in a particular direction can often result in an increase of tensile stress in other directions because of redistribution of the whole residual stress field around the plasticity zone. On the other hand, relaxation of residual stress can be beneficial, to allow an increase in allowable stress levels or reduced fatigue damage index. However, recommendations such as IIW (Hobbacher 2009) and BS 7608 (BS 7608 2014) do not allow any fatigue enhancement as a result of global residual stress relief in welded components of a ship structure.

In marine applications, along with random wave loading, significant static loadings as a result of tank testing and ballasting is experienced before service. Also, occasional high wave loads may cause welding residual stress redistribution in stress concentration areas. These occasional high wave loads result in incompatible strains. Typical ship structural steels are ductile materials and can, therefore, deform plastically to accommodate these incompatible strains. Hence ship structural steels could accommodate a few overloads safely by redistributing or relaxing residual stresses internally. However, as a result of these relaxations or redistributions, small plastic strains are formed which would not result in a catastrophic failure from high tensile or compressive loads. These are localised plastic strain in the order of elastic strains.

It should be noted that if the plastic strains are accumulated (ratcheting) very fast as a result of very high external loads (with or without secondary loads) or repeatedly cycled under high magnitudes causing alternating plastic strains (reverse plasticity), the component under load will fail due to low cycle fatigue. While ratchetting and reverse plasticity need to be considered in the design, small plastic strains as a result of less frequent load cycle may be tolerated. In ship structures, this type of loading is less frequent. Hence the quantification and study of the effect and redistribution of residual stress after the structure has undergone cyclic load become important.

The benefits and importance of defining a boundary between the above-mentioned small plastic strain during the first few cycles and the subsequent elastic behaviour of a structure is the main subject of this thesis. Greater focus is on the redistribution of residual stresses during these initial cycles. For many years, methods for determining the boundary limits called shakedown limits have been proposed in different forms which are defined mostly

for high-temperature applications. For high-temperature applications, creep, or time-dependent plasticity, modern structural integrity standards state recommendations to define shakedown limits (R5 2014). This study focuses on the welding residual stresses which is greatly dependent on the external load due to redistribution.

Here, a numerical technique supported has been implemented on widely used commercial FE software ABAQUS using plastic work done as a shakedown criterion, and optimised for the specific problem in this work, thus making it more straightforward than others presented before. Similar to the previous analysis techniques, the technique implemented in this work also focuses on the identification of the shakedown limit below which the structure will achieve steady state. If a structure operates below this limit indefinitely, the applied loading will eventually fail the component due to fatigue which will not be discussed in this work.

A shakedown region is defined in which a conservative maximum weld residual stress equal to yield strength and the shakedown limit is considered. This has been shown in Chapters 6. This method is adapted from recent work by Sun et al. (Sun et al. 2013). Their work primarily is based upon the reduced basis technique proposed by Johannes (Groβ-Weege 1997). The method is defined for the specific problem case studied in this work; however, it is expected that the method presents valuable information and new facet towards mechanical design and life assessment.

A summary of the various methods used to study the problems mentioned above is discussed in the following section.

1.2 Problem definition

As mentioned in the preceding section, the primary objective of this work is to investigate the residual stress redistribution in the double bottom configuration used in ship structures. Therefore, the selection of material and the manufacturing process were in line with those for the double bottom structure in a ship. Moreover, a cyclic load which represents the loading experienced in a double bottom, in the range of the elastic shakedown limit, was required to see the main load cycles which affect the stress redistribution. Also, it was essential to select a residual stress measurement technique which can adequately support the research. It was essential to use a non-destructive test

which can probe through-the-thickness values to measure redistribution of residual stress under cyclic loading and its effects through the thickness of the plates.

In traditional offshore structures, the welding is performed manually using Gas Metal Arc Welding, or Flux cored Arc Welding, both being high heat input processes compared to a laser/electron beam or automatic arc welding. On thick components such as longitudinal stiffeners, welding is performed at higher heat input, which can introduce higher levels of residual stresses (Paradowska et al. 2006). Measurement and simulation of residual stresses to determine the magnitude and orientation in welded plates have been ongoing for several years, both at the surface and through the thickness (Heinze, Schwenk and Rethmeier 2012; Tekriwal and Mazumder 1991). Even though there are established destructive and non-destructive (ND) techniques, ND testing is increasingly being more commonly used. Among the ND techniques, neutron diffraction which uses a neutron beam wavelength comparable to the atomic spacing in many standard metallic materials enables the neutron beam to penetrate the bulk of material up to several centimetres. This technique, therefore, can provide data on the full 3-dimensional residual stress state in the specimen under study (Withers and Webster 2001). The technique has been successfully utilised to determine residual stresses butt and fillet welded plates.

1.3 Objectives

This thesis aims to investigate the redistribution of residual stress due to elastic shakedown in welded structures using experimental and numerical methods. The following are the objectives of this work:

- Objective 1: To implement a shakedown limit analysis optimised to the problem in hand to define shakedown limits in the specimens under study.
- Objective 2: To quantify residual stresses in butt and fillet welded plate fabricated using established welding procedures in shipbuilding using both numerical and experimental methods.
- Objective 3: To evaluate the extent of residual stress redistribution under selected cyclic loads representing extreme loads experienced in ship structures and, in the range of the elastic shakedown using experimental techniques.
- Objective 4: To characterise the residual stress state under cyclic load applied and to define an effective FE model to simulate residual stress redistribution.

- Objective 5: To investigate the effects of shakedown limit on the redistribution of residual stresses.

1.4 Outline of the thesis

The work carried out in this PhD project is presented in detail in nine chapters:

Chapter 1 introduces the research background, problem definition, objectives and thesis outline.

Chapter 2 reviews previous studies related to residual stress evaluation and shakedown analysis including residual stress measurement techniques, and residual stress redistribution.

Chapter 3 describes in detail the experimental procedure to fabricate butt and fillet welded plates along with the cyclic load application and the methodology using neutron diffraction for residual stress measurement in the as-welded condition, and after a specific number of load cycles. The determination of the mechanical properties of the material used in work is also included in this chapter.

Chapter 4 presents the numerical simulation of welding process and compares the thermal cycles and predicted residual stresses obtained from FEA model with the results from the welding process and neutron diffraction measurement. Additionally, a residual stress mapping technique is also presented.

Chapter 5 presents the redistribution of residual stress in butt and fillet welded specimens after cyclic loading. Experimental results from neutron diffraction is initially presented. Further corresponding numerical model and its comparison with experimental measurements are presented.

Chapter 6 establishes a shakedown limit analysis to determine the shakedown limits on each specimen. Using the determined shakedown limits, a shakedown region is defined in which the redistribution of residual stress in each specimen at critical locations are investigated.

Chapter 7 defines the key findings and the limitations of this work.

Chapter 8 summarises the relevance of this work in industry and makes recommendations for future work.

CHAPTER 2.LITERATURE REVIEW

2.1 Introduction

The work presented here is of welding residual stress redistribution under cyclic loading and is hence very much based upon shakedown theory. This chapter therefore initially introduces principles of shakedown theory in order to form a sound basis for the described work. Following the principles of shakedown, the state of the art on welding residual stress, its consequences in service and the redistribution and relaxation of welding residual stresses under shakedown are presented.

The aspects of shakedown phenomenon investigated by researchers can be broadly classified into:

I. determination of the shakedown limit, and
II. the behaviour of the structure during shakedown.

The first class comes under the shakedown limit analysis along with bounding theorems and methods for determining the structure response at the various shakedown boundaries. As the focus of this work touches upon both, slightly greater importance is given to the effect of shakedown on residual stress redistribution.

2.2 Theory of shakedown

2.2.1 Welded structures under Cyclic Loading

Welding process on components during fabrication introduce high tensile residual stresses in the welds. In subsequent operation, welded structures are often subjected to complex cyclic loads. A numerical method to understand the structural integrity by considering the complete load history during service in the presence of residual stress is often tricky and computationally very demanding. However, a clear distinction between the shakedown limits, in general, can simplify these matters considerably. Shakedown theory in its simple form accommodates a load domain consisting of all possible load combination and paths applied on a simple material models like elastic-perfectly-plastic. Therefore, the numerical model becomes simplified in terms of non-linear step-by-step analysis without knowing complete and accurate material and load details.

Loading in welded structures can be compared with many industrial applications in terms of loading. That is, in many applications a constant load such as inertia, thermal stress or internal pressure exists along with the second load of cyclic nature. For example, this second load could be wave loads or thermal loads applied to offshore structures or pressure vessels respectively.

Consider a metallic body with yield strength σ_y subjected to a combination of cyclic loading. The metallic body may respond in any of the four elastic-plastic responses given below:

I. Purely elastic behaviour: - During the total period of cyclic loading the stress everywhere in the structure responds elastically. In this case, no yielding occurs.
II. Elastic Shakedown: - The initial plastic flow in the first few applied load cycles could result in a finite amount of plastic strain. This initial plastic strains will create residual stresses or redistribution of already existing residual stress. After that, the material behaves elastically again and is said to have undergone elastic shakedown (Abdel-Karim 2005). The term elastic shakedown is often abbreviated as shakedown, and hence, this thesis refers to elastic shakedown as shakedown. A typical stress-strain response of elastic shakedown is shown in Figure 2.1a.

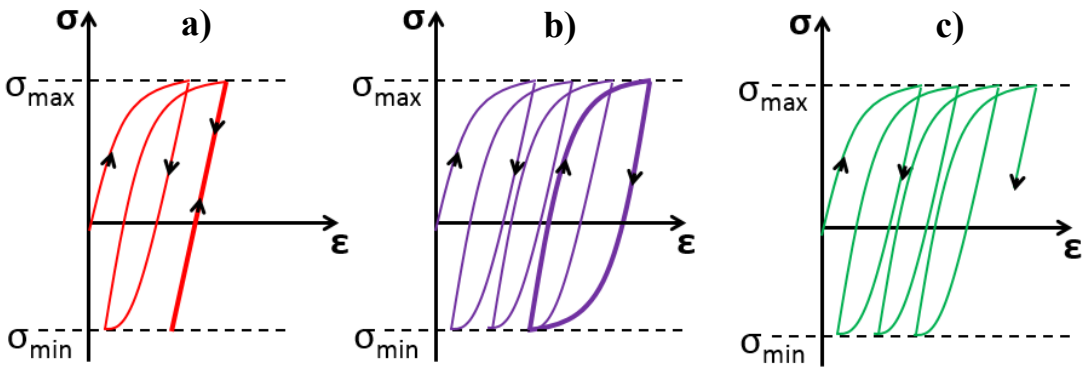

Figure 2.1: Stress-strain response under cyclic loads; a) Elastic-Shakedown b) Reverse Plasticity c) Ratchetting

III. Plastic Shakedown: - Also known as reverse plasticity, during each load cycle, the material undergoes plastic straining within the surrounding elastic material. A closed plastic strain cycle exists somewhere in the structure alternating in tension and

compression to ultimately fail the structure due to low cycle fatigue (LCF) (König 2012). A typical stress-strain response of plastic shakedown is shown in Figure 2.1b.

IV. Ratchetting: - Also known as incremental collapse, during each load cycle small plastic strain occurs and the failure will be due to the accumulation of plastic strains over successive load cycles (König 2012). A typical stress-strain response of ratchetting is shown in Figure 2.1c.

As the cyclic loads under service could cause the above states, a common benchmark method is used in elastic-plastic structures to describe the behaviour. Bree (Bree 1967) initially presented a diagram known as Bree diagram having regions comprising structural responses explained above as shown in Figure 2.2. Bree presented this figure during his research on thermal stress and axial stress acting in a thin-walled tube for nuclear industry application (Bree 1967).

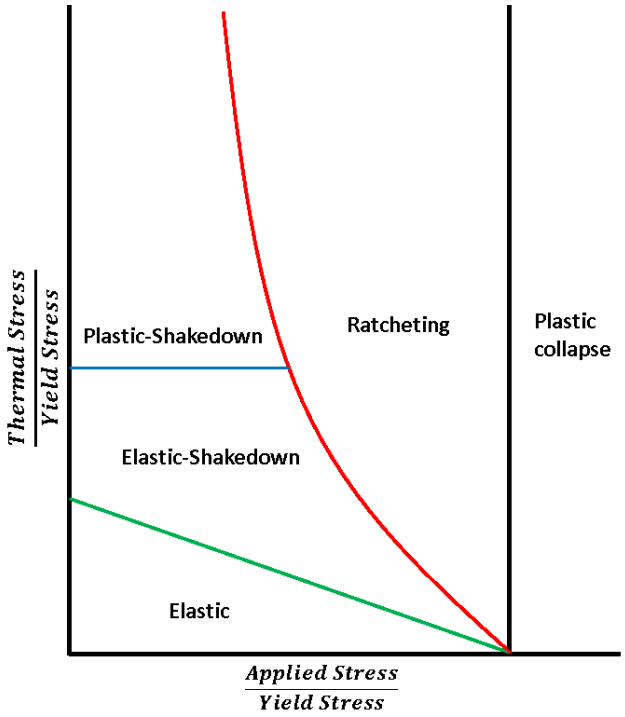

Figure 2.2: BREE diagram showing various material responses under cyclic load.

It is evident from the Bree diagram that a component designed only for the elastic region would be overly conservative. On the other hand, the region depicting ratchetting should be avoided in design. Today, the material requirements and the cost associated with a conservative design should be avoided. In welded structures, as a result of weld residual stress, designing for the elastic region could mean an operation in the elastic shakedown/shakedown region. In the case of plastic shakedown, it can be endured in

some cases. For example, structures fabricated using steel could endure more than a few thousand load cycles under low cycle fatigue. In case of ship structures, overloads due to wave actions under storms may be endured as they only occur a few cycles in its life.

A structure designed based considering above mentioned shakedown limit can only be considered safe and less conservative if other aspects such as the deflection and deformation caused as a result of plastic strain should also be safe (König 2012). Also, residual stresses may be developed in components in the near surface layers (for example a bending beam) as a result of loads sufficient to induce plastic deformation to be accommodated elastically in the longer term (Williams, Dyson and Kapoor 1999). The resulting design considering shakedown allows for a much more efficient and cost-effective design as the shakedown region is much bigger compared to purely elastic behaviour (Figure 2.2).

2.2.2 Bounding Theorems for shakedown

The initial discussions on the bound on shakedown can be traced back to 1932 by Bleich (Bleich 1932) who considered trusses and frame structures based on the concept of shakedown mentioned by Grüning (Grüning 1926). Later Melan (Melan 1938b) introduced a general theorem on shakedown for elastic-plastic structures. It stated that in a system, if self-equilibrating residual stresses exists, which in combination with the repeated stresses due to the applied load, do not exceed yield at any time, then the system will undergo shakedown. Koiter (Koiter 1964) delivered a simple mathematical formulation in 1964, which resulted in a lower bound shakedown limit.

Melan's Shakedown theorem is hence called a lower bound theorem, and the exact shakedown limit is when the maximum applied load together with the distribution of residual stress, just touches the yield. Prior to Koiter's formulation of Melan's shakedown theorem, Koiter (Koiter 1956) derived an upper bound shakedown theorem. This states that shakedown cannot occur under an external work done due to a set of bounded load variations bigger than the dissipated internal energy attributable to the admissible plastic strain in the system. Martin (Martin 1975) investigated the similarity between both lower and upper bound shakedown theorems and the general case of the shakedown limit theory.

The lower bound theorem tries to define an equilibrium solution for a given load problem such that a shakedown behaviour exists whereas the upper bound theorem tries to define

a kinematic solution for a given load problem such that it minimises the ratchet strain energy. Ratchet strains are not common in offshore structures when compared to pressure vessels. In pressure vessels such as in nuclear reactors, the constant thermal loads along with a much more complex load combination are critical whereas in offshore structures; the combination load is primarily due to the initial welding residual stress and occasional overloads. Hence it was decided to focus on the lower bound theorem to find out the shakedown limit in this work.

Moreover, both these theorems assume linear kinematics and elastic-perfectly-plastic material. Hence it does not categorically give appropriate shakedown limits for all practical situations, such as large nonlinearity and strain softening materials. This can be overcome by using a suitable material model.

2.2.3 Effect of hardening models on shakedown

There have been many papers in the literature intended to overcome various limitations of Melan's and Koiter's formulations. The best example is the basic unlimited kinematic hardening by Melan (Melan 1938) and further studies on Melan's approach by Maier (Maier 1972) and Ponter (Ponter 1975). Many researchers have studied shakedown analysis of hardening structures. When considering hardening models, there are two basic types of hardening behaviours called as the isotropic hardening model in which the magnitude of the yield stress increases to compensate increased stresses and the kinematic hardening model in which the yield surface can displace in stress space to compensate increased stresses.

Using isotropic hardening models only is not reasonable in cyclic loading because it cannot consider the Bauschinger effect and hence rejects the condition of ratchetting or incremental plasticity (Phạm and Staat 2014). In other words, unbounded isotropic hardening will only yield elastic shakedown under any condition. The unbounded kinematic hardening model was introduced by Melan (Melan 1938b) and later by Prager (Prager 1956). When using the unbounded kinematic hardening model where the yield surface remains the same size can in principle provide alternating plasticity but not ratchetting and plastic collapse which makes it suitable only for low cycle fatigue. It can be concluded that incremental ratchetting can never happen using unbounded models.

The bounded hardening will put a limit to the maximum stress which can be supported by a section of the component. If this limit stress is reached over an entire section of a component for any combination of load cases, ratchetting will occur. Due to this, the information about shakedown provided by bounded hardening is more suitable for the practical case than unbounded hardening. However, recently it was noted (Indermohan and Reinhardt 2012) that even if bounded hardening models are used, while ratcheting will be predicted the plastic strains at the resulting ratchet boundary can be very high. They question that if large plastic strains are required to induce shakedown then whether shakedown would be achieved before the structure fails due to some other mechanisms.

Modern standards such as the R5 standard (R5 2014), recommends the use of combined hardening models in line with the Chaboche nonlinear hardening model for numerical modelling of shakedown. In this work, to numerically predict residual stress redistribution and the implementation of shakedown limit analysis, prediction of the evolution of plastic strains under the applied loads would be very critical.

2.2.4 Shakedown limit analysis

Broadly speaking, there are three approaches to implementing the shakedown limit analysis. The most common approach used today, which are called direct methods, are using classical or modified bounding theorems. Direct methods assume a simple material model thereby simplifying the problem. The elastic-perfectly-plastic material model is often used in direct methods. This helps to define bounds in the load domain avoiding the requirement for an exact load path.

Direct Methods directly determine the critical states without performing step-by-step inelastic structural response analysis. The main drive for developing Direct Methods is to help in analysing high-temperature applications where the component goes through complex cyclic loading conditions. Although the computational time to perform direct methods is low, they can only be done with specialised codes. There are many different direct methods stated in literature as given below:

- Linear Matching Method (Chen, Ponter and Ainsworth 2006; Li et al. 2011).
- Uniform Modified Yield surface method (Abou-Hanna and McGreevy 2011; Gokhfeld and Charniavsky 1980).
- Generalised Local Stress-Strain r-node method (Seshadri 1995).

- Elastic Compensation Method (ECM) (Mackenzie et al. 1996; Mackenzie, Boyle and Hamilton 2000).
- Mathematical programming methods (Liu, Carvelli and Maier 1997; Staat and Heitzer 2001).

Since this work did not use this technique, it is not explained in this thesis. For more details on the implementation of these techniques, the reader is referred to the references.

Another approach based on a theorem of Konig and Kleiber (Konig and Kleiber 1978) is the basis of the method implemented in this work. In this approach, a load domain is assumed along with a representative material model to analyse the response of a structure numerically. In this method, an FEA code can be employed for a step-by-step application of load cycles to determine the response of the structure, hence called as an incremental FEA method. The accuracy of the solutions tends to improve with better implementation of the material model and the information of the load cycle which are often difficult to define as mentioned in previous sections (Borkowski and Kleiber 1980).

The incremental FEA method is rarely used in applications such as nuclear where the load path is often complex and is computationally very demanding and can become very expensive. The advantages are that it can give an estimate of strains accumulated as the structure approaches limit state. The method also allows considering large deformations into account. Direct methods are very efficient in addressing the load interaction diagrams. However, unlike the incremental FEA approach, they will not provide details on the plastic strain accumulation and cannot consider large deformations.

One method to overcome the computational complexity in the incremental FEA method can be using the so-called reduction technique (Groβ-Weege 1997; Sun et al. 2013). The method and the implementation in this work are presented in Chapter 5. Finally, there are experimental methods for determining shakedown limits on a structure. A typical experiment to determine shakedown limits would be to measure the displacement of the structure after each load cycle and check whether the strains increase with time (ratcheting) or decrease/stabilise with time (shakedown) (Del Puglia and Nerli 1973; Eyre and Galambos 1970; Sun et al. 2013).

2.3 Residual stresses in welded structures

Residual stresses are self-equilibrating stresses which are present in a structure without external loads. They may be generated or modified at every stage in the component's fabrication and life cycle. A typical ship structure consists of miles of welding which results in rapid heating and cooling in the structure under restraint to cause high tensile residual stresses in members such as stiffeners (Fricke and Paetzold 2010). Moreover, the welding residual stresses formed are often as high as the yield strength of the material (Barsoum and Barsoum 2009; Withers et al. 2008).

Residual stresses can be broadly classified into three types (Withers 2007). Type 1: Macro residual stresses are homogenous and are distributed in macroscopic dimensions and are considered in design calculations. Type 2: Micro residual stresses are distributed over the order of the grain size and are created by microstructural differences within materials. Type 3: Submicron residual stresses are in the order of atomic dimensions and are created by lattice defects. The residual stresses under type 1 are of most importance in ship structures and hence are primarily considered in this work.

Due to high temperature gradients introduced during welding, thermal expansion of the fusion zone, HAZ (heat affected zone) and the parent material becomes different. As a result of this difference in thermal expansion, during cooling, the contraction of fusion zone is restrained by the surrounding parent metal. In some cases, subsequent phase transformation will also constrain the weld zone during cooling (Kou 2002). Therefore, in a single-pass welded plate, longitudinal residual stresses are predominantly tensile in the weld zone and are balanced by compressive stresses away from the weld.

A typical residual stress profile in the longitudinal and transverse direction of a butt-welded plate is illustrated in Figure 2.3 (Zerbst et al. 2014). In the case of a fillet weld where weld passes are run on both sides of the web plate, Figure 2.4 shows typical residual stress evolved during fillet welding (Connor and American 1987). Here the residual stresses on the flange are tensile near the welds and become compressive away from the weld. Additionally, there are tensile stresses in the upper part of the web because of the longitudinal bending distortion (Nur Syahroni 2012).

Figure 2.3: Typical residual stress profiles following butt welding, a) Longitudinal residual stresses, and b) Transverse residual stresses (Zerbst et al. 2014)

Figure 2.4: Typical residual stress profiles in T-butt plate (Connor and American 1987)

The factors which result in the as-welded residual stresses present in welded structures (Leggatt 2008) include:

- Residual stresses present in the part as a result of any manufacturing or machining process before welding.
- Material properties (mechanical, metallurgical and thermal) of the parent and weld metal.
- External restraints employed during the welding process.
- Welding procedures including joint configuration, geometry and thickness, welding position, welding pass sequence etc.,
- Residual stress redistributed or relaxed as a result of subsequent manufacturing operations or thermal treatment and/or mechanical loading.

Restraints during welding are any mechanical connections which restrict the free thermal expansion and contraction. It includes the geometry of the part, and welding aids such as jigs, tacks etc. The effect of membrane restraints on transverse residual stresses was studied by Leggatt in which he showed that the stresses were significantly higher compared with low restraint welding (Leggatt 1986). In ship structures, the welding is usually under high restraint due to the surrounding assembly and/or the dimensions of the plates used.

2.4 Residual stress measurement using neutron diffraction

2.4.1 Introduction to residual stress measurement

Modern structural integrity assessment procedures like BS 7910, R6 and API RP-579 need more accurate residual stress details for evaluation of the life assessment of a fatigue loaded structure (Withers et al. 2008). Since residual stresses are self-equilibrating and internal, it is challenging to quantify residual stresses easily.

Broadly classified, there are two types of residual stress measurement techniques: Non-destructive testing and destructive testing. "Non-destructive" are used for components that are returned to service or used in the same service after measurement methods, and the stress fields are evaluated. A few commonly used techniques are listed in Table 2.1. Typically, the selection of technique should be based on material, geometry, accessibility, and volumetric resolution of stress. Also, the variation of a through-the-thickness variation of residual stress and the destruction/damage caused because of measurement are usually considered.

Table 2.1: Residual stress measurement methods

Non-destructive	Destructive
Neutron diffraction	Hole drilling and Ring coring
X-ray diffraction	Contour method
Ultrasonic testing	Block removal, splitting, slitting etc...
Magnetic methods	Layering

2.4.1.1 Destructive methods

The destructive techniques work under the basis of measuring strain release because of the removal of material from the stressed component due to the equilibrium state of initial

residual stress. Hence, they are also known as Mechanical Strain Release (MSR) techniques. Using compliance functions, the recorded strain release as a result of material removal is used to back-calculate the original residual stresses. A subset of destructive methods is semi-destructive techniques where only a small amount of material is removed from the component, so maintaining its overall structural integrity intact for operations.

Destructive methods were not possible in this work as the redistribution of residual stress under cyclic load required the weld plates to be used after the measurement of residual stress.

2.4.1.2 Non-destructive methods

The non-destructive techniques are developed based on the relationship between the physical properties of the material under internal/external stress. The variation in speed of ultrasound waves through a stressed material form the basis for the Ultrasound Technique. However, in non-destructive techniques, the diffraction techniques are arguably the most used. The diffraction techniques exploit the fact that when a material is under applied/residual stress, the resultant elastic strains cause a change in lattice spacing (spacing of the atomic planes) in the crystal structure which can be detected using Bragg's law as given below (Bragg 1929):

$$n\lambda = 2d_{hkl}\, sin\, \theta \qquad (2.1)$$

Where n is an integer, λ is the wavelength of the incident beam, d is the lattice spacing of hkl interatomic planes and θ is the Bragg angle. Depending on the wavelength and energy of the incident beam, it can interact with the various particles in the atom.

A typical laboratory X-ray diffraction (XRD) equipment use characteristic X-rays with wavelengths ranging from 0.7 to 2 Å (18 to 5 keV in energy) as an incident beam to find the stresses in the irradiated area. X-rays interact with the orbiting electrons, hence get absorbed when it goes beyond 100 micrometres (Stacey et al. 1985). Hence, the most commonly used X-ray wavelengths applied in stress measurement are not capable of penetrating deeply into most materials (Schajer 2010). The advantage of the XRD technique is that the shallow penetration enables us to assume the gauge volume under investigation to be in plane stress. This condition allows for simplification of the stress-strain equations (Prevey 1996).

The XRD technique is still to-date a rapid, economical, accurate and high-resolution technique for use on weldments. However, due to its limitation of penetration alternative methods are pursued in this work. Also, the X-ray emitting probes need to be reasonably close to the specimen for accurate measurement. This is often cumbersome to implement in components with attachments. It is worth pointing out that XRD can be combined with a layer removal technique to determine stresses through-the-thickness of the sample, but then the method becomes destructive (Kandil et al. 2001).

Synchrotron X-ray diffraction has become a capable method for measurement of triaxial residual stress states (Reimers et al. 1998). A synchrotron X-ray source provides high energy X-ray millions of times more intense and much higher penetration depth (Withers and Webster 2001).

2.4.2 Neutron diffraction

Neutron diffraction uses penetrating neutron beams which interact directly with the nucleus of the atom. Neutrons can penetrate both high and low atomic number materials. This penetration allows for the measurement of bulk stresses (Rossini et al. 2012). The principle of measurement is similar to XRD, in which residual strains are determined by comparing lattice spacing in the stressed and stress-free condition (Lodini 2003). Three normal components of stress can be determined in a material by ignoring shear stress present. Ignoring the shear stress present will not lead to an error in the three normal components (Krawitz and Winholtz 1994; Lodini 2003).

For the accurate measurement of tri-axial stress state in a component, a precise value of stress-free lattice spacing, d_0 is required. Relying on published materials for stress-free lattice spacing is not recommended because the heat effect of welding across a welded plate is often unique from one location to the other. Therefore, to measure weld residual stress, an appropriate stress-free sample should be used to determine the stress-free reference (Ganguly, Edwards and Fitzpatrick 2011).

One of the methods is by measuring lattice spacing on far locations assuming the locations are unaffected by any stresses. However, these are very crude assumptions. A common practice is by extracting small cubes sufficiently small to be assumed free of elastic stress from equivalent spatial location of the main component (Holden et al. 2006; Krawitz and Winholtz 1994). Another method is machining out a comb-like sample across the weld,

with the assumption that each tooth in a comb would be of incapable of holding an internal residual stress field (Taran et al. 2008). A comb-like sample is useful in butt-welded plates as it enables stress-free lattice measurement from corresponding locations in the stressed component. However, the extraction of comb-like samples for specimens such as fillet welded joints can be complicated. In all cases, the machining process should relax all the stress and should not introduce any new residual stresses. Electro-discharge machining (EDM) can be used in this case.

Neutron Diffraction technique is applied in two types depending on the neutron beam source namely, Time-of-Flight and monochromatic 2θ Strain Scanning approach. Monochromatic 2θ Strain Scanning technique uses a monochromatic neutron beam whereas the time of flight technique uses different wavelength neutrons generated from a spallation source travelling with different velocities.

Monochromatic 2θ Strain Scanning technique measures changes in the peak diffraction angle of a single diffraction peak, 2θ. The peak diffraction angle is related to a lattice spacing, d. Differentiating equation 2.1 for an incident beam of constant wavelength:

$$\Delta\theta_{hkl} = -\frac{\Delta d}{d_0} tan\,\theta_0 \qquad (2.2)$$

$$\varepsilon = \frac{\Delta d}{d_0} = -\Delta\theta \cdot cot\,\theta_0 \qquad (2.3)$$

where $\Delta\theta$ is the change in diffraction angle, Δd is the change in lattice spacing, $2\theta_0$ is the change in diffraction angle for corresponding stress-free sample and ε is the lattice strain.

In Time of flight, the detector is typically placed at 90º to consider a diamond-shaped (cuboidal) gauge volume. The incident neutron beam consisting of different wavelength is diffracted to the detectors at 90º. The wavelength of the incident and diffracted beams at a constant Bragg angle is monitored and the lattice spacing can be determined (Haigh et al. 2013). Differentiating equation 2.1 for an incident beam of at constant Bragg angle:

$$\Delta\lambda = \frac{\Delta d}{d_0}\lambda_0 \qquad (2.4)$$

where $\Delta\lambda$ is the change in beam wavelength and λ_0 is the wavelength corresponding to the stress-free sample.

2.5 Welding residual stress relaxation/redistribution

Several papers decades ago highlighted the significance of residual stresses on the fatigue performance of a welded structure (Bertini, Fontanari and Straffelini 1998; Trufyakov 1956; Trufyakov 1958). The interaction between the applied cyclic load and the residual stress present in the structure is still not well understood. One reason is the difficulty in measuring residual stresses in welded structures. The fact that modern structural integrity codes still recommend conservative assumptions proves this.

Residual stress relaxation during cyclic loading was observed by Mattson and Coleman (Mattson, R. and Coleman, W. 1954) many years ago. This work concluded that even if there is a relaxation of induced compressive residual stress, they still improved the fatigue life of the component. Morrow and Sinclair (Morrow J 1958) were some of the early researchers to study and predict mean stress relaxation due to axial fatigue loading. Later Jhansale and Topper (Jhansale and Topper 1973) proposed a linear, logarithmic relationship between mean stress relaxation and strain-controlled cycles. Wyman Z Zhuang reported that Kodama (Kodama S 1972) measured the surface residual stress relaxation on a shot peened specimen using X-ray diffraction figure. It can be inferred from the figure that compressive residual stresses have relaxed almost 50%. This relationship was further investigated by Holzapfel (Holzapfel et al. 1998) in which he interpolated the residual stress relaxation in both thermal and cyclic stress relaxation. W.Z Zhuang (Zhuang and Halford 2001) investigated the residual stress relaxation mechanisms and developed an analytical model to predict the behaviour under different loading parameters (discussed later in Chapter 5). Many researchers have studied the interaction between residual stresses and the operating loads resulting in relaxation during service.

It is understood that by the application of thermal or mechanical load on to a stressed material, the elastic strain components of residual stresses are being converted into plastic strains (Farajian-Sohi, Nitschke-Pagel and Dilger 2009; Gordo 2013; Holzapfel et al. 1998; Lee, Chang and Do 2015; Qian et al. 2013; Zhuang and Halford 2001). Moreover, the fact that tensile residual stresses in combination with operating loads can take elastic strains in some regions of a structure to plastic strain shows that the underlying principle behind residual stress redistribution is localised plastic flow. Residual stress relaxation

under plastic flow is not considered beneficial as the plastic flow can lead to fatigue damage (Gao et al. 2017).

Alternatively, if the applied loads under question are occasional overloads which are above the elastic range but below the plastic shakedown limits, it could be beneficial because of tensile residual stress relaxation. A study conducted by K. Yuan (Yuan and Sumi 2013) shows the relaxation of residual stresses due to overloads in a T-joint fillet weldment and its benefits on fatigue crack propagation. Residual stresses were predicted using numerical simulation. The shakedown mechanisms in these weldments are then studied by applying static preloads (both tensile and compressive) in such a way that they may act with the region where crack propagation is severe. The numerical simulation results show that high tensile preload in the range of 80% of the yield stress of the material shakes down residual stresses. However, it was noted that the results are purely numerical, and the shakedown limits are assumed to be yield limits which are not realistic.

The residual stress relaxation has also been linked with the resistance against the dislocation movement. Zhongyouan Qian (Qian et al. 2013) studied the relaxation of residual stress in low carbon steel AISI 1008, low alloy steel ASTM A572 and AISI 4142 by the application of 25% yield stress cyclic loading and above. The XRD measurement at the surface of the specimens revealed that, in AISI 1008, even a load of 25% yield stress resulted in a relaxation of transverse residual stresses; whereas, in AISI 4142 steel, there was no residual stress relaxation even for 90% yield stress loading. This has been attributed to the fact that large grains of essentially single-phase ferrite in AISI 1008 have a little resistance to dislocation movement whereas the fine perlite in AISI 4142 has very high resistance against dislocation movement.

Another feature in the relaxation/redistribution of residual stresses is that a significant change in residual stress is observed in the initial few cycles (Hao et al. 2015a; Holzapfel, Vöhringer and Macherauch 1990). After the initial cycle, the residual stress remains stable, or it continues to relax but with a lower rate. This was demonstrated using quasi-static loading (M. Farajian and T. Nitschke-Pagel 2012). Figure 2.5 illustrates the relaxation in his study on butt welded plate. After initial residual stress measurements, quasi-static tensile loads of 100, 200, 300, 400 and 500MPa were applied in the transverse direction. Increasing loads resulted in increased relaxation of transverse residual stresses.

On the other hand, less relaxation was seen in longitudinal residual stress since the load was applied in the transverse direction.

Figure 2.5: Residual stress relaxation under quasi-static tensile loading a) relaxation in transverse residual stress b) relaxation in longitudinal residual stress (M. Farajian and T. Nitschke-Pagel 2012).

Based on the salient features of residual stress redistribution or relaxation as a result of mechanical loading, it is evident that the shakedown phenomenon plays a role. There has been much research on the shakedown analysis of components under thermal loads. However, little research is available on the shakedown analysis of components with a pre-existing weld residual stress field. These problems are generally considered as stress relaxation or stress redistribution problems as explained above. One of the reasons could be that in the presence of a residual stress field, shakedown can result in relaxation or redistribution of the existing residual stress. However, shakedown analysis on these components could be used for understanding the effect of relaxation or redistribution of residual stresses on the state of shakedown.

2.6 Discussion and summary

This chapter has reviewed literature which is considered essential to form the basis of this work. It primarily aims to understand the shakedown phenomenon along with the formation and redistribution of residual stresses in welded structures. Unlike a typical residual stress relaxation study, the focus is given to draw the similarity and the influence of shakedown limit on the residual stress redistribution.

From the few published works reviewed here, perhaps the critical point is that while we now have accurate residual stress measurement techniques, it is usually prohibitively expensive to perform a complete residual stress measurement. Therefore, analytical or numerical tools still plays a vital role in characterising residual stress. So, it is necessary to continue to improve numerical or analytical methods to predict better the state of residual stress and its redistribution and substantially simplify the methodology for easy application. It is understood that even though the accuracy of the predictions is of utmost importance, achieving a numerical model with high accuracy still requires actual loading cases, control over material behaviour under sudden heating and cooling to name just a few factors.

Research carried out previously has provided valuable information on shakedown phenomenon, shakedown limit analysis, residual stress measurements, residual stress redistribution and the numerical simulation of welding and subsequent relaxation/redistribution models. The literature relating to the numerical simulations are included in corresponding chapters. The following key points were drawn from this study:

I. The study will be conducted on butt and fillet welded plates manufactured in line with shipbuilding materials and manufacturing process. It was decided to use DH 36 material and GMAW process to manufacture the weld plates.
II. As-welded residual stresses are relaxing or redistributing when the applied load is capable of inducing plastic flow. Shakedown limit analysis can identify the limit below which the structure can operate safely after a few initial plastic flows.
III. The Incremental FEA method for shakedown limit analysis can be simplified to suit the specific problem in this work to address the computational efficiency associated with the technique.
IV. Even though there have been many studies on the residual stress states in T-joint fillet welds, experimental measurements conducted through-the-thickness are still rare.
V. Residual stresses will be measured in the as-welded condition and after a specific number of load cycles using neutron diffraction because it can obtain stresses in a thick-walled component.

CHAPTER 3.MATERIALS AND EXPERIMENTAL DETAILS

3.1 Introduction

In this chapter, the experimental programme implemented to determine material data and to validate numerical models is described. A general description of the mechanical properties along with the mechanical testing performed for determining the mixed hardening constitutive model parameters is given. Following this, the manufacturing of the weld plates and the cyclic loading testing is described. Further, the method and setup used for the measurement of residual stress using neutron diffraction are presented. The approved Welding procedure specification (WPS) and supporting Welding Procedure Qualification Record (WPQR) qualified for the butt-welded specimens are given in Appendix A. The residual stresses in all specimens determined from neutron diffraction are presented in Appendix B.

3.2 Material

3.2.1 Typical ship structural steels

In ship structural materials, some of the main criteria for consideration are the material properties, ease of use in construction, ease of availability and cost. Material properties such as strength, fracture toughness, corrosion resistance, and fatigue strength along with the ease of use in construction in terms of weldability are a few factors in choosing material for marine applications.

For hull material, mostly ordinary-strength or high-strength low alloy steels with low carbon are used. They are also grouped into three as 32, 36 and 40 for which yield strengths are at 315, 355 and 390 N/mm^2 respectively. Depending on their toughness properties, they are again grouped into grades GL–A32/36/40, GL–D32/36/40, GL–E32/36/40 and GL–F32/36/40 (Eyres 2007).

Under the direction of Lloyds Register Marine, which assisted in choosing relevant material used in double bottom configuration and the ease of availability, all experimental work was undertaken using DH36 ferritic steel, a low alloy steel.

3.2.2 DH 36 ferritic low alloy steel

DH 36 is a high-strength low-alloy steel which contains niobium (Nb), vanadium (V) and titanium (Ti), which are strong carbide and nitride formers. The composition of DH36 is

given in Table 3.1. Carbide and nitrides in a material can act as effective grain growth inhibitors. Due to less grain growth, both high strength and high toughness are obtained in DH36. Steels containing titanium oxide tend to have better toughness due to its high-temperature stability (Homma et al. 1987). These are structural steels with good toughness, higher strength, and strong corrosion-resistance, processing properties, and welding properties.

Table 3.1: Composition in wt. % of the DH36 low alloy steel used in this work.

C	Si	Mn	P	Nb	V	Cu	Cr	Ni	Al	Mo	Fe
0.15	0.22	1.39	0.012	0.031	0.05	0.016	0.024	0.021	0.035	0.04	Bal.

The plate considered in this work was 12.7 mm thick and the section of the original plate, used to extract plates required for the weld specimen manufacturing, was 2000 x 500 mm^2. The thickness of the plate was according to the typical thickness used for the flat bar stiffeners in a double bottom configuration. The mechanical properties, modulus of elasticity and yield strength of the steel plate were determined as 200GPa and 350MPa respectively from the first load cycle of the strain-controlled fatigue test explained in Section 3.4, carried out on the as-delivered material.

3.3 Manufacturing of welded plates

3.3.1 Selection of welding procedure

Currently, the application of welding in ship structures is mostly fusion welding in the form of metallic arc welding. The most commonly used joining techniques in shipbuilding are Gas Metal Arc Welding (GMAW) and Flux Cored Arc Welding (FCAW). Semi-automatic welding is used as much as possible. In places or positions where automatic machines cannot access, manual welding is employed. Thick sections are sometimes welded with the submerged arc welding process (SAW). GMAW welding is again used wherever possible, and SMAW welding is used elsewhere.

In Gas Metal arc welding the metal is melted and joined using the arc struck between a continuous filler wire electrode and the job. Figure 3.1 shows a schematic of GMAW (Kou 2003). Shielding gas is supplied externally (Kou 2003). It has an automatic feeding of the consumable electrode that is shielded by an external shielding gas. Inert gases are often used as shielding gas for the process; hence the process is also called Metal Inert

Gas welding or MIG. Since CO_2 is used frequently, GMAW is the most suitable name for the process.

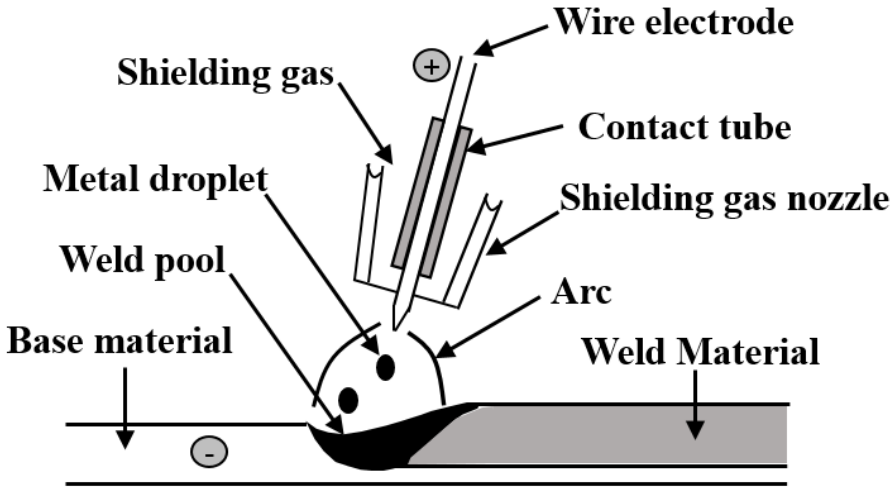

Figure 3.1: Schematic of GMAW process

GMAW is the most common method used to weld flat bar stiffeners with longitudinal load members because of its simplicity and efficiency. As this work was interested in the in flat bar stiffeners, and as recommended by Lloyds Register Marine, Gas Metal Arc welding process was selected to manufacture the coupon samples required for this work.

For the initial investigation, a multi-pass butt weld configuration was selected due to its simplicity and ease of manufacturing. Two butt welded specimens with two weld orientations were manufactured. Following the investigation on the butt-welded specimens, two fillet welded specimens with two orientations were manufactured. All welding was carried out using Gas Metal Arc welding process. The following sections explain the manufacturing process and specifications in detail.

An overmatched weld was chosen to implement in this work. The benefits of using an overmatched weld is well defined (Kirk and Dodds Jr 1991). The overmatch helps to avoid any crack propagation into weld material and any undesirable plastic deformation in the weld metal (Zerbst et al. 2014).

3.3.2 Butt-welded specimens

A joint configuration of single-vee butt joint profile aligned to the BS EN ISO 9692-1 standard as illustrated in Figure 3.2a was used. The dimensions for the joint preparation are shown in Figure3.2a. The joint was prepared using milling machine at TWI Ltd. Butt welding was performed in two different orientations with respect to the plate dimensions.

In the first orientation, two plates of 200 × 140 × 12.7 mm^3 were welded together along the 140mm edge, and in the second orientation, two plates of 400 × 70 × 12.7 mm^3 were welded together along the 400mm edge as illustrated in Figure 3.2a and 3.2b.

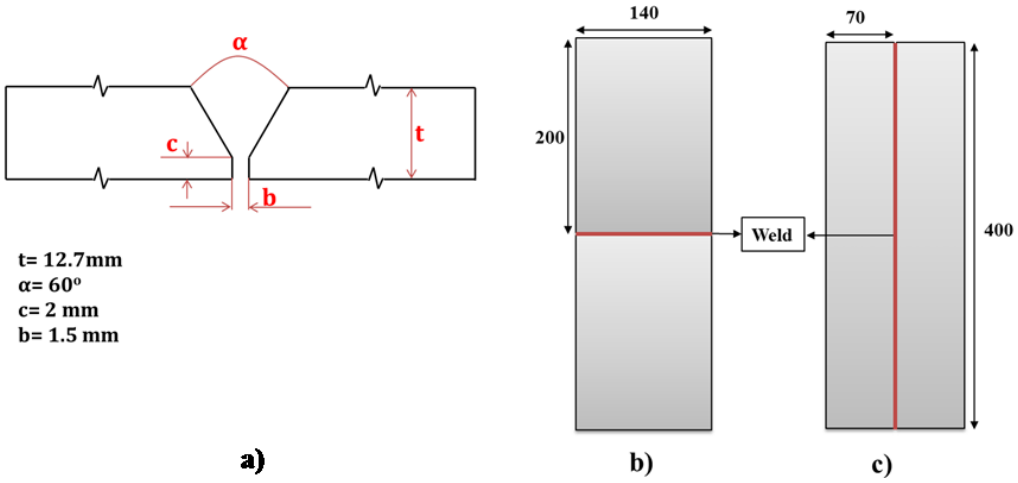

Figure 3.2: Illustration of joint and oriententation details on butt-welded plates: a) Joint configuration, b) butt-welded plate with the short weld along 140mm edge, and c) butt-welded plate with the long weld along 400mm edge.

Gas Metal Arc welding process was performed using a Fronius VR 7000 CMT machine fitted with an ABB robotic arm. A welding wire of G3Si1 wire chemistry classified to EN ISO 14341-A with a 1.2mm diameter was used as the weld filler wire to achieve an overmatched weld. The shielding gas used was a mixture of argon and carbon dioxide to the classification/Designation: ISO 14175 – M21 – ArC-20 at 15-20 litre per minute flow rate. The Welding procedure specification, according to Lloyd's Register Classification typically used for flat bar stiffeners, was qualified for the butt weld and is given in Appendix A.

Prior to welding, thermocouples and strain gauges were spot welded on to the plates to capture transient thermal response during the welding and subsequent cooling period. For the butt-welded plate with the longer weld, one platinum thermocouple, 11 K-type thermocouples and four strain gauges were placed in positions as illustrated in Figure 3.3a to monitor thermal history. For the butt-welded plate with the shorter weld, one platinum and 7 K-type thermocouples and four strain gauges as illustrated in Figure 3.3b were used. One platinum thermocouple in each weld plate was employed due to its temperature range of up to 1000 °C whereas a K-type thermocouple can only record up to 800 °C.

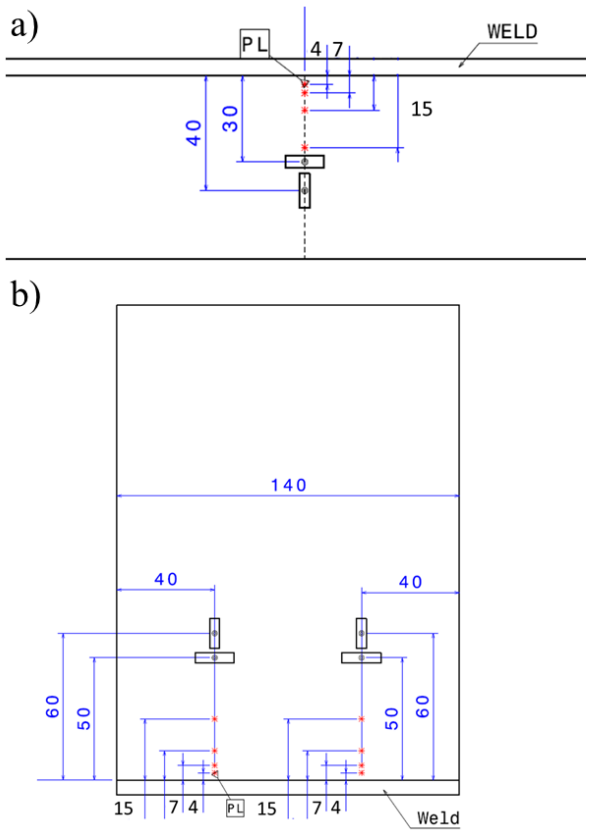

Figure 3.3: Thermocouple and strain gauge locations on the butt-welded plates: a) butt-welded plate with the long weld along 400mm edge and, b) butt-welded plate with the short weld along 140mm edge.

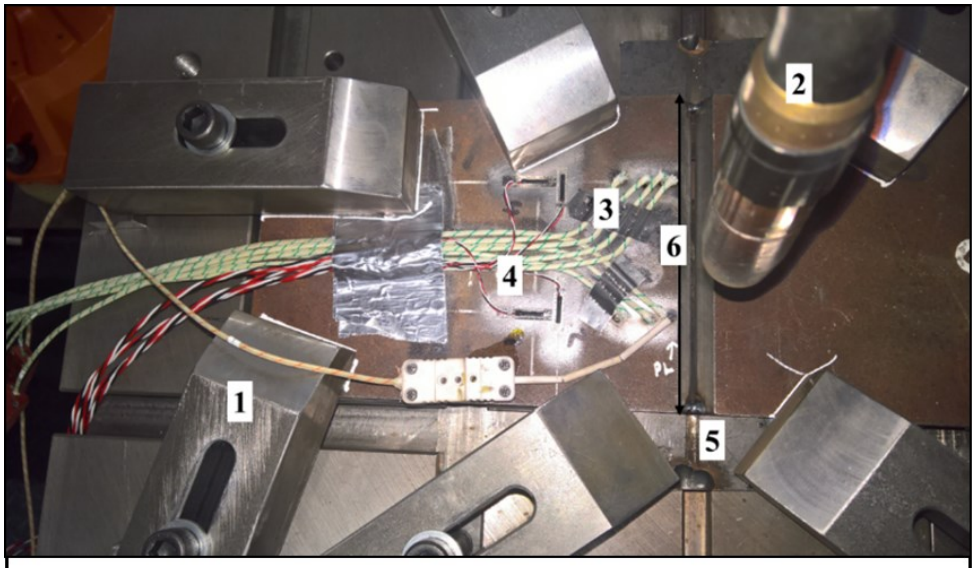

1) Restraints 2) Welding robotic arm 3) Thermocouples 4) Strain gauges 5) Run-in and run-off plates 6) Weld length of 140 mm

Figure 3.4: Photograph showing the welding set-up used for manufacturing the butt-welded plate with the short weld.

A photograph of the welding set-up used for butt welding is shown in Figure 3.4. Run-in and run-off plates were used to avoid any crater formation on the plate due to welding start and stop. The length of the weld seam was 180 and 440mm for each orientation. The temperature and strain data during the heating and the cooling period were connected to a data logger with a sampling rate of 0.001s (1kHz).

Multi-pass welding with a root pass, fill pass, and two cap passes were performed by maintaining an inter-pass temperature of 100 ^{o}C. A special fixture was manufactured to introduce maximum restraint during welding. The welding parameters used in the process are listed in Table 3.2.

Table 3.2: Welding parameters for DH36 plates.

Parameters	Root	Fill	Cap 1 & 2
Shielding gas	ISO 14175 – M21 – ArC-20.		
Filler wire diameter (mm)	1.2	1.2	1.2
Wire feed speed (m/min)	5.0	4.8	4.8 & 5.5
Voltage (V)	22.6	24.3	23.1 & 23.6
Current (A)	125	125	128 & 150
Travel Speed (mm/s)	4	4	4 & 4
Heat input (kJ/mm)	0.706	0.706	0.739 & 0.885

3.3.3 Fillet Welded specimens

Fillet welded specimens were manufactured on a rectangular base plate of dimensions 400×140×12.7mm^3. Like the butt welds, two types of fillet welds were manufactured as shown in Figure 3.5. The first orientation consisted of a web plate of dimension 140×80×12.7mm^3 welded along the 140mm edge (Figure 3.5a). The second orientation consisted of a web plate of dimension 400×80×12.7mm^3 welded along the 400mm edge (Figure 3.5b).

Gas Metal Arc welding was performed manually at TWI Ltd. Like the butt welding, a welding wire of G3Si1 wire chemistry classified to EN ISO 14341-A with a 1.2mm diameter was used as the weld filler wire to achieve an overmatched weld. The shielding gas used was a mixture of argon and carbon dioxide at 15-20 litre per minute flow rate to the classification/designation: ISO 14175 – M21 – ArC-20.

Prior to welding, thermocouples were spot welded on to the base plates of the fillet weld to monitor and record temperature during the welding and the cooling period. For the fillet welded plates with the long weld and the short weld, five and four K-type thermocouples were spot welded respectively in positions illustrated in Figure 3.6.

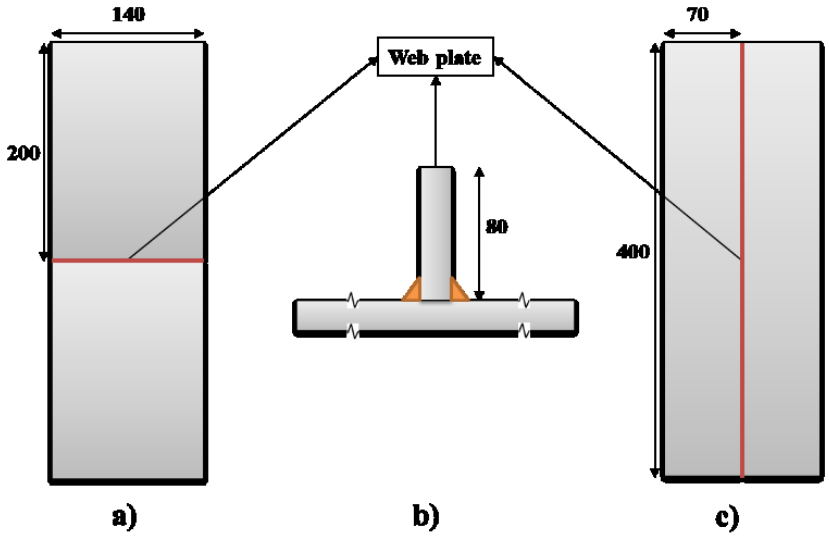

Figure 3.5: Illustration of oriententation details on fillet welded plates: a) Fillet welded plate with the short weld along 140mm edge, b) fillet weld cross-setion and wen plate details, and c) fillet welded plate with the long weld along 400mm edge.

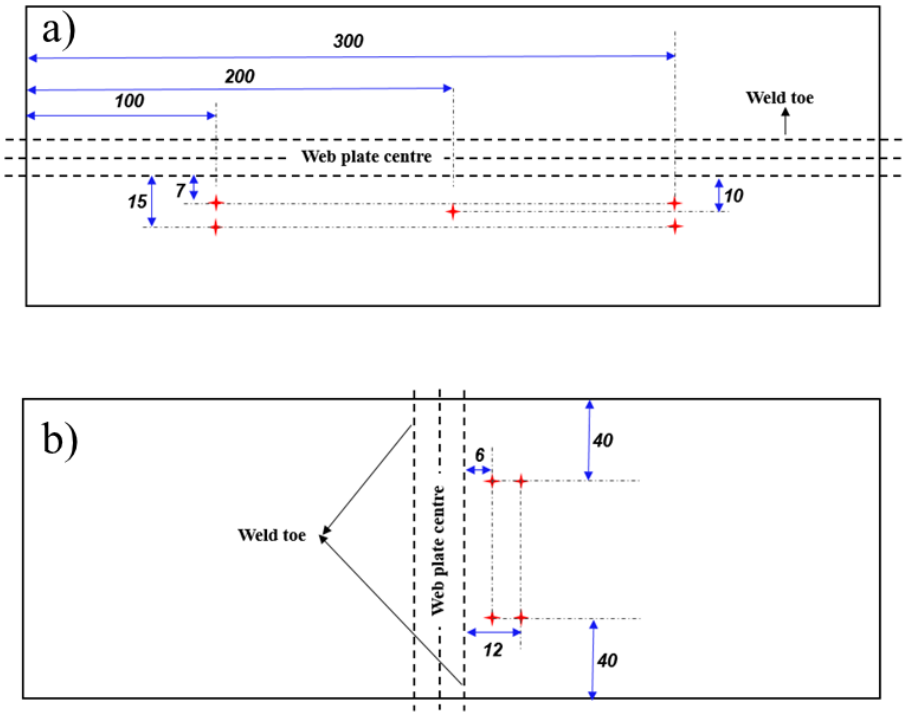

Figure 3.6: Thermocouple locations on the fillet welded plates: a) Fillet welded plate with the long weld along 400mm edge and, b) fillet welded plate with the short weld along 140mm edge.

A photograph of the welding set-up used for fillet welding is shown in Figure 3.7. A strong back was used to constrain the plates and achieve maximum restraint throughout welding. Fillet welding was also performed with run-in and run-off plates, tack welded to the main welding plate to avoid any crater and unstable weldments on the main plate. Two passes, one on each side with a leg length of 7mm, were deposited.

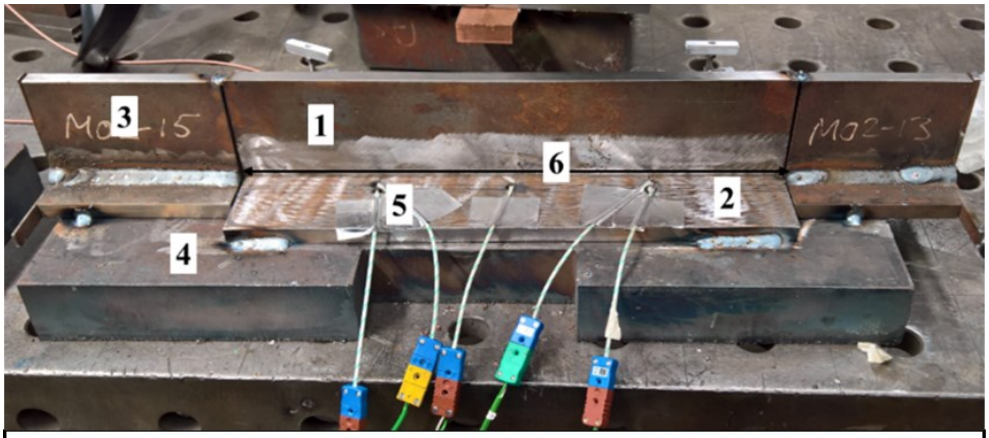

1) Web plate 2) Base plate 3) run in and run off plate 4) Strong backs
5) Thermocouples 6) Weld length of 400 mm

Figure 3.7: Photograph showing the welding set-up used for manufacturing the fillet welded plate with the long weld.

Following welding, both butt welded plates and fillet welded plates were cooled down to room temperature before unclamping. After the plates were cooled down to room temperature, the run-in plate, run-off plate and sensors were ground off, and the surface of the plates was cleaned.

3.4 EDM cutting

The weld plates were subjected to Electro-Discharge Machining (EDM) to prepare mechanical loading specimens. A specimen was designed in finite element (FE) to ensure a uniform distribution of stresses under cyclic load. A rectangular dog bone specimen with a nominal gauge area of 150×100mm^2 was selected based on the FE model. EDM cutting was implemented to produce the designed specimen. All plates were cut using EDM in order to reduce plasticity during cutting and hence to reduce any unnecessary relaxation of residual stresses. The four specimens after EDM cutting are shown in Figure 3.8 and 3.9.

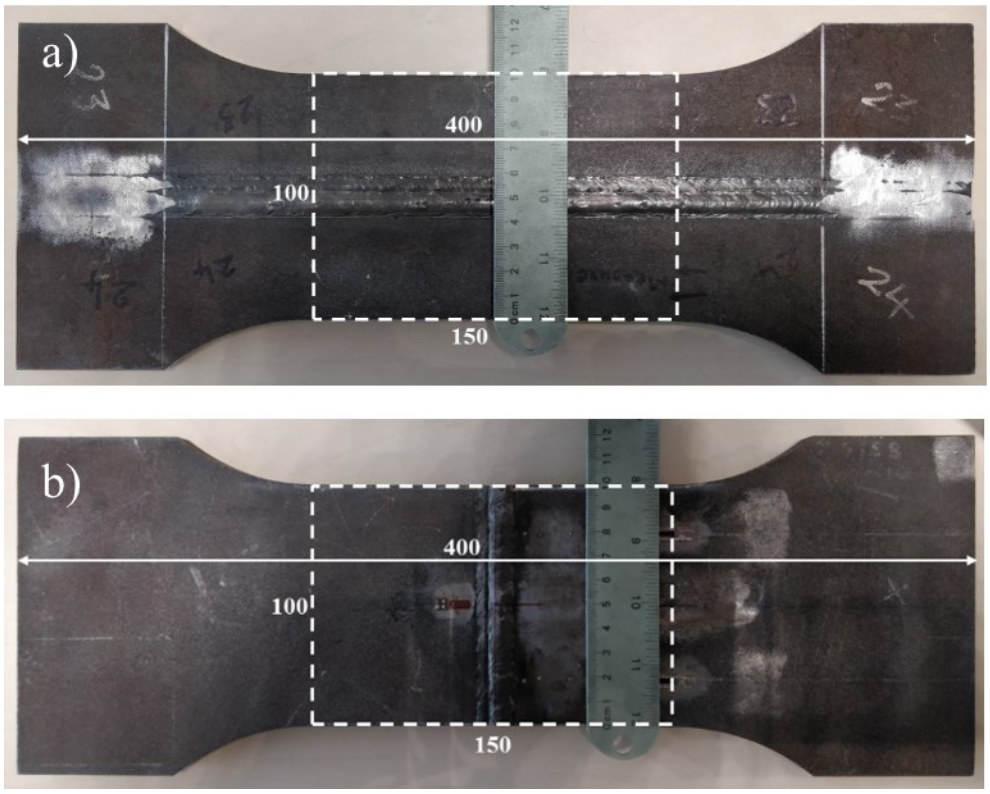

Figure 3.8: Photographs of the butt-welded plates after EDM cutting: a) Butt-welded plate with the long weld, and b) butt-welded plate with the short weld.

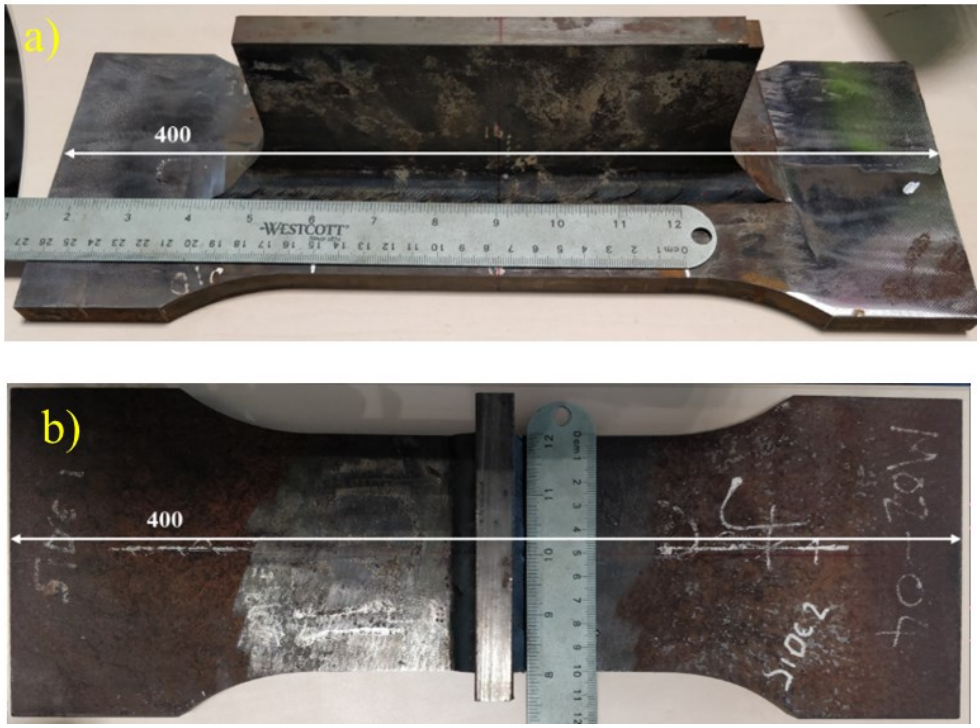

Figure 3.9: Photographs of the fillet welded plates after EDM cutting: a) Fillet welded plate with the long weld, and b) fillet welded plate with the short weld.

3.5 Testing for hardening parameters

Cyclic plasticity is fundamentally based on two different hardening behaviours: isotropic hardening and kinematic hardening. Isotropic hardening reflects an increase in the magnitude of yield stress, and kinematic hardening allows the yield surface to move in stress space during plastic flow. Numerical modelling of cyclic plasticity requires a combination of isotropic and kinematic hardening behaviours to simulate both elastic shakedown and plastic shakedown. The following Section describes the hardening model used in this work.

3.5.1 The concept of Chaboche constitutive equation

The Chaboche constitutive elastic-plastic model was initially developed by Lemaitre and Chaboche (Lemaitre and Chaboche 1994). The cyclic plasticity model is implemented with a combination of one isotropic hardening R and three kinematic hardenings α_1, α_2 and α_3. The initial yield criterion representing the elastic domain is described by a typical von Mises yield criterion f=0, where f is defined as:

$$f = J(\sigma - \alpha_1 - \alpha_2 - \alpha_3) - R - \sigma_y \tag{3.1}$$

where σ_y is the yield strength of the material, σ is the Cauchy stress tensor and J is the von Mises equivalent stress defined as:

$$J(\sigma) = \sqrt{\frac{3}{2}\sigma_d : \sigma_d} \tag{3.2}$$

where σ_d is the deviatoric stress tensor. Total strains ε_{ij}^t are decomposed into elastic strains ε_{ij}^e and plastic strains ε_{ij}^p. The isotropic hardening R and the kinematic hardening α_i are defined as below:

$$R = b(Q - R)\dot{p} \tag{3.3}$$

$$\dot{\alpha}_1 = \frac{2}{3}C_1\dot{\varepsilon}_p - \gamma_1\dot{\alpha}_1\dot{p} \tag{3.4}$$

$$\dot{\alpha}_2 = \frac{2}{3}C_2\dot{\varepsilon}_p - \gamma_2\dot{\alpha}_2\dot{p} \tag{3.5}$$

$$\dot{\alpha}_3 = \frac{2}{3}C_3\dot{\varepsilon}_p - \gamma_3\dot{\alpha}_3\dot{p} \tag{3.6}$$

where $\dot{p}$ is the rate of accumulated plasticity, $b, Q, C_1, C_2, C_3, \gamma_1, \gamma_2$ and γ_3 are material parameters. To determine the material parameters defined above, strain-controlled fatigue tests were performed as explained in the following section.

3.5.2 Strain-controlled fatigue tests for hardening model parameters

The tests aimed to determine the parameters representing the plasticity response of the material. A strain-controlled fatigue test according to ASTM E606 was performed on both base material and weld material. Tests were performed with an INSTRON servo-hydraulic testing machine, series 8000, on ASTM standard 6mm gauge diameter with a 25mm gauge length specimen and M12 threaded grips as shown in Figure 3.10.

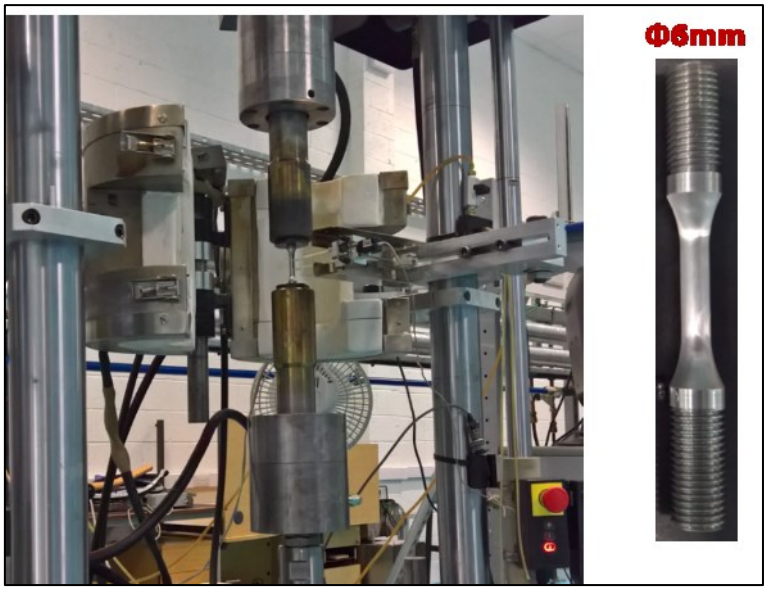

Figure 3.10: Strain-controlled fatigue test set-up and the 6mm gauge diameter specimens used for the test.

A triangular strain waveform at a constant strain range was applied, and a clip-gauge extensometer was used for measuring the total strain at ambient temperature. The specimens were fixed to the testing apparatus through a thread, with the aim of reducing clearances and possible bending in the loading train.

Eight specimens were tested with standard strain-controlled low cycle fatigue testing, with strain amplitudes ranging between 0.5% and 1.27%. Two strain ranges of 0.5% and 0.75% on four specimens (two parent material and two weld material) were used to collect the initial and stable hysteresis loops from the experiment. A cyclic tension-compression test of completely reverse ($R = -1$) cycle was applied to the specimens. To avoid buckling due to non-linearity in the loading train, the adjustment was made by means of suitable taper rings in series with the upper grip of the hydraulic machine. However, initial tests with strain ranges of 1.2% showed a tendency of buckling in the specimens which led to the selection of low strain ranges for determining the material parameters. The first cycle and the stable hysteresis cycle recorded from the clip gauge length of 12.67mm for weld and parent material are shown in Figure 3.11.

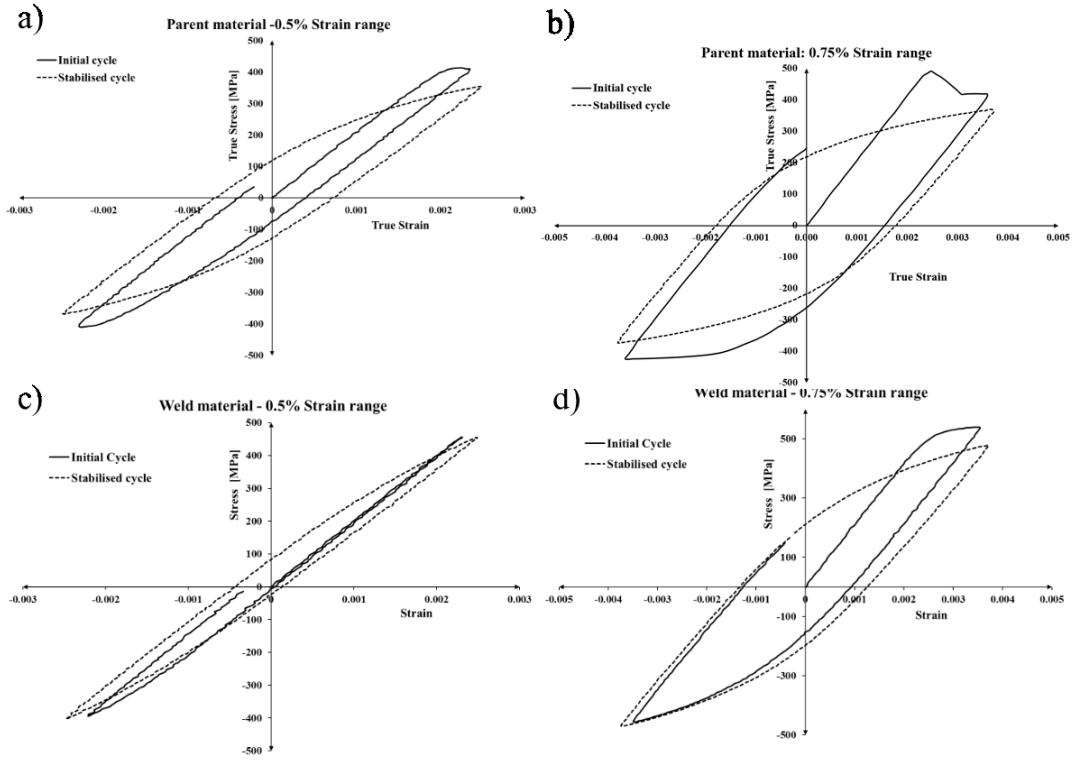

Figure 3.11: Initial and stabilised cycles for parent material and weld material after cyclic tension-compression strain controlled fatigue test: a) Parent material under 0.5% strain range, b) parent material under 0.75% strain range, c) weld material under 0.5% strain range, and d) weld material under 0.75% strain range.

3.5.3 FE implementation and determination of parameters from numerical minimisation

The hardening parameters are determined using an FE model which simulates the clip gauge volume of the specimens. The clip gauge length of the specimen was 12.67mm. Encastre boundary condition was applied on one end of the gauge volume, and the opposite end was applied with displacement cycles. A displacement cycle of range ±0.0317 mm and ±0.0475 mm was applied on the gauge volume to simulate 0.5% and 0.75% strain range respectively.

The FE model is initially run on a set of initial isotropic hardening parameters, Q and b chosen from the literature (Erny et al. 2012) which studied DH36 hardening behaviour. At first, a single load cycle was simulated to obtain the initial cycle and compared with the experimental result. Parameters Q and b were slightly changed from the initial values to find a close match with the experiment and simulation. After isotropic parameters were optimised, in the second phase, the FE model is run for 100 cycles with an initial set of kinematic back stresses. In the second phase, the objective was to minimise the error

between the experimental and numerical stabilised loops by varying kinematic hardening parameters $C_1, C_2, C_3, \gamma_1, \gamma_2$ and γ_3. The stable hysteresis loop from the experiment is compared with the FE stable hysteresis loop to optimise the initial set of parameters.

Four separate FE models were generated, where two were parent material, and two were weld material. On the same material parameters, two sets of strain ranges were analysed, and average values obtained from both FE models were considered as the final value of the parameters. The material parameters obtained for DH36 parent material and weld material are shown in Table 3.3.

Table 3.3: Parameters of DH36 and weld Elastic-Plastic model used in FEA.

DH36	*Elastic Modulus* *E*/GPa	*Poissions ratio* *v*	*Yield strength* σ_y/ Mpa
Parent	197	0.3	350
Weld	197	0.3	400

DH36	*Q*	*b*	C_1/ MPa	γ_2	C_1/ MPa	γ_2	C_1/ MPa	γ_2
Parent	-48.6	87.5	4360	16.4	38524	116	8000	40
Weld	-102	14	8912	29.65	102300	400	8000	40

Yield strength and elastic modulus of both parent and weld material were determined from the first quarter cycle applied on the specimen and were based on the average value from all experiments. Figure 3.12 compares the initial and stabilised cycles from both FE model and experimental data.

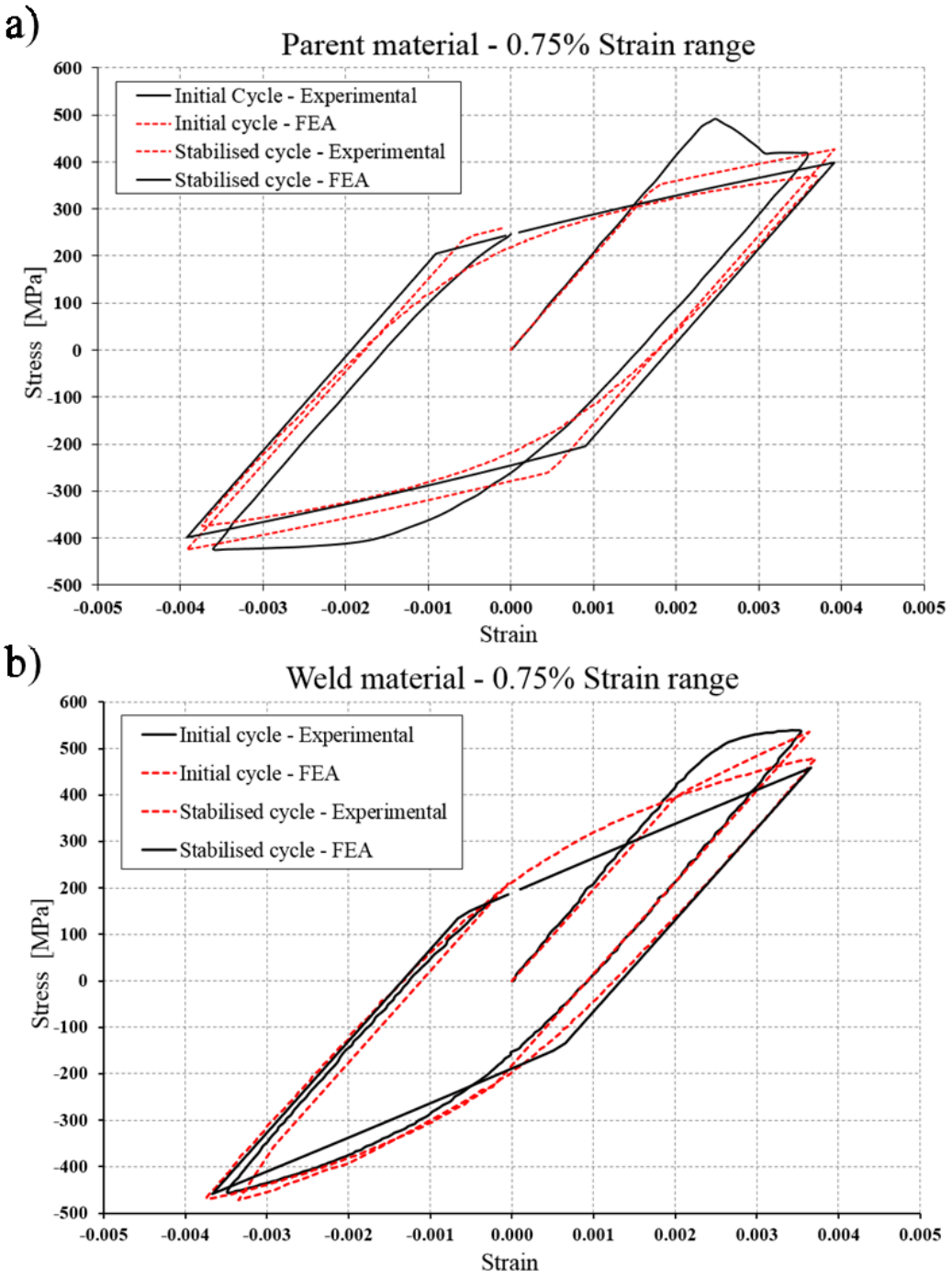

Figure 3.12: Comparison of hyterisis loop obtained from the experiment and finite element model: a) Parent material under 0.75% strain range, and b) weld material under 0.75% strain range.

3.6 Fatigue loading

The cyclic load was applied to the specimens to induce residual stress shakedown. The cyclic loads on all plates were applied using an INSTRON servo-hydraulic stress rig of capacity 1000kN at TWI's Cambridge facility shown in Figure 3.13. Prior to commencing any cyclic loading tests, preliminary 2D FE models were evaluated to estimate an approximate shakedown limit using incremental FEA method for each specimen. These models are not included in this thesis. The determined shakedown limits and, extreme loads experienced in secondary load bearing members in a ship were considered to choose a cyclic load for the experimental procedures explained in the following section.

Figure 3.13: INSTRON servo-hydraulic test machine at TWI Ltd used for the application of tensile load cycles.

3.6.1 Cyclic loading in butt-welded specimens

The preliminary finite element model on the cyclic behaviour of the butt-welded specimen indicated that a load corresponding to 75% of the yield strength of the weld material would induce residual stress redistribution. The butt-welded plate with the long weld was subjected to cyclic loading along the weld line to induce shakedown in the longitudinal residual stress component whereas the butt-welded plate with the short weld

was subjected to cyclic loading across the weld line to induce shakedown in the transverse residual stress component. The load direction and set-up are illustrated in Figure 3.14.

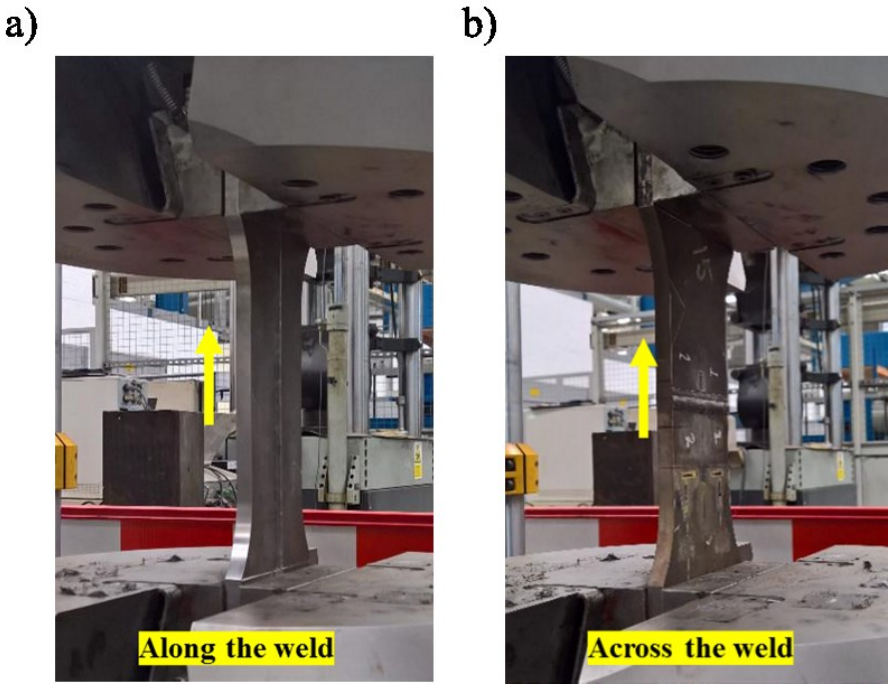

Figure 3.14: Photograph of the set-up used for the cyclic loading of butt welded plates: a) Butt-welded plate with the long weld and, b) butt-welded plate with the short weld.

A total of 10 load cycles were applied on each butt-welded specimen. Load cycles were tensile sine waves of constant amplitude with an R-ratio of 0. The frequency of the load was 0.25Hz. The maximum load in the machine was 370kN in both specimens. This was to ensure that there is residual stress redistribution in the plates within the first few cycles. After one cycle, three cycles and ten cycles the specimens were removed from the test rig to investigate the residual stress state as explained in section 3.7. An R-ratio of 0 was chosen as the specimen had to be removed from the test rig between load cycles.

3.6.2 Cyclic loading in fillet-welded specimens

Like the butt-welded specimens, a preliminary finite element model of the cyclic behaviour of fillet-welded specimen indicated that a load corresponding to 65% of the yield strength of the material would induce residual stress redistribution. Moreover, the design load criterion in the double bottom configuration of a container ship is typically considered as about 68% of the yield strength of the parent material. The load was applied such that the nominal stress at the base plate cross-section close to the lower weld toe is equivalent to 65% of the yield strength of the parent material. The fillet-welded plate with the long weld was subjected to cyclic loading along the weld line to induce shakedown

in the longitudinal residual stress component, whereas the fillet-welded plate with the short weld was subjected to cyclic loading across the weld line to induce shakedown in the transverse residual stress component. The load direction and set-up are shown in Figure 3.15.

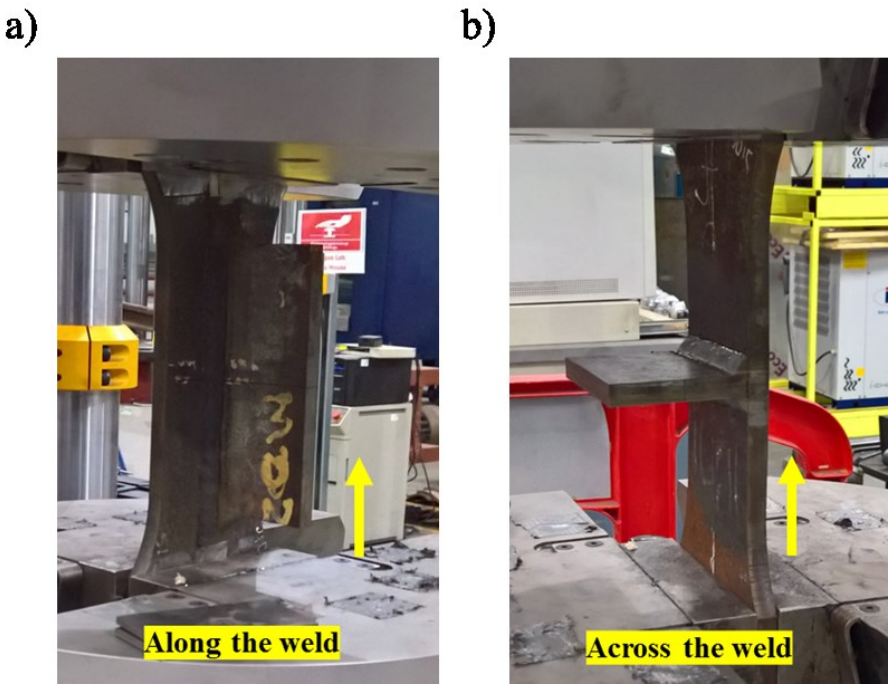

Figure 3.15: Photograph of the set-up used for the cyclic loading of fillet welded plates: a) Fillet welded plate with the long weld and, b) fillet welded plate with the short weld.

A total of three load cycles were applied on each fillet-welded specimen. Load cycles were tensile sine waves of constant amplitude with an R-ratio of 0. The frequency of the load was 0.25Hz. The maximum load was about 310kN in the fillet-welded plate with the short weld and 400kN in the fillet-welded plate with the long weld.

3.7 Residual stress measurement using neutron diffraction

As the purpose of this work was to study redistribution of residual stresses in a weld sample under cyclic loading, non-destructive techniques were required. Moreover, through-thickness residual stresses were expected to redistribute under cyclic load. Hence the neutron diffraction technique was used for these investigations.

Several neutron diffraction experiments were performed to determine the residual stress state in the welded specimens in the as-welded condition as well as after a specific number of load cycles. The time-of-flight neutron diffraction instrument ENGIN-X at the UK's ISIS neutron source, Rutherford Appleton Laboratory (RAL), Oxford was used for all diffraction measurements (Santisteban et al. 2006). The primary flight path of the neutron

beam in this instrument is 50m. The beam travels through a curved super mirrorguide to minimise the loss of neutrons in the travelled path.

The ENGIN-X instrument has two detectors fixed at 90° angles to the incident beam, to provide two strain measurement directions along the scattering vectors Q_1 and Q_2 as shown in Figure 3.16. In Figure 3.16 Q_1 corresponds to the strain parallel to the longer side received at the first detector bank, and Q_2 corresponds to the strain perpendicular to the longer side received at the second detector bank. In front of each detectors, radial collimators consisting of a number of vertical foils are arranged radially about a fixed focal point. In ENGIN-X, slits are motorised to enable control over the beam size in the vertical axis using a computer. Similarly, the secondary beam size is defined based on the selected collimator. There are multiple collimators to define the secondary beam size having a fixed width (full width at half maximum) of 0.5, 1, 2, 3 and 4mm. In this work, all measurements were obtained using 3mm collimators. The collimators will narrow the diffracted neutron beams from the chosen gauge volume to the detector banks.

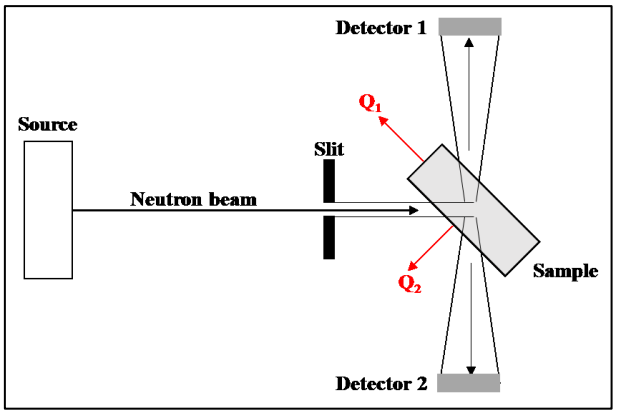

Figure 3.16: Illustartion of ENGIN-X time-of-flight neutron strain scanner.

Using neutron diffraction, the objective was to measure residual stress in all three orthogonal directions with respect to the plate dimensions, i.e. the longitudinal component parallel to the weld line, transverse component perpendicular to the weld line and normal component through the thickness of the plate. While the residual stress redistribution and elastic shakedown are described in Chapter 5 and 6, this section is dedicated to the presentation of the setup, method and the results obtained from the time-of-flight neutron diffraction.

3.7.1 Butt Welded plates

In both butt-welded specimens, neutron diffraction was used to determine stress in the as-welded condition and after one, three and ten load cycles.

Prior to neutron diffraction, a total of 30 measurement points was selected on each butt-welded specimen as shown in Figure 3.17. In Figure 3.17, '*O*' represents the origin of the local coordinates. Symmetry along the weld centre line was assumed on the butt-welded specimens. Assuming a symmetric residual stress profile along the weld centre line (x-axis in Figure 3.17) passing through the origin, the 30 measurement points were on the midplane thickness and were on one side of the symmetry plane in both plates as illustrated in Figure 3.17.

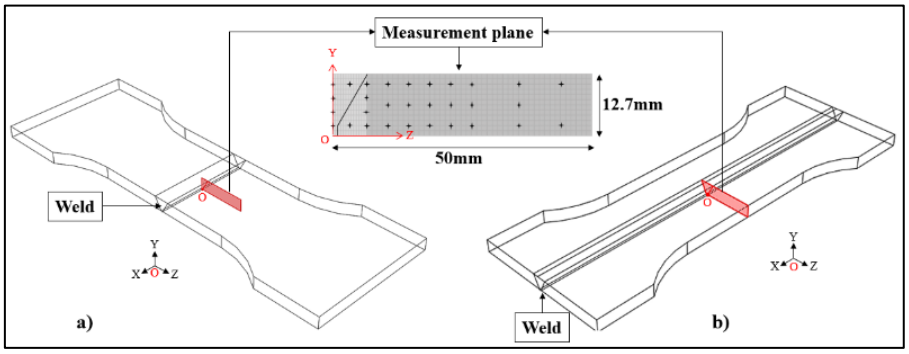

Figure 3.17: Illustration of 30 measurement points on butt welded plates: a) Butt-welded plate with the short weld and, b) butt-welded plate with the long weld.

Three line-scans across the weld were performed at the mid-thickness plane of the specimen. The line scan locations were 2.5mm below the top surface, at the mid-thickness, and 2.5mm above the bottom surface. Additionally, through-thickness measurements were performed at the weld centre and weld toe. Each measurement location among the 30 measurement points represented on the YZ plane shown in Figure 3.17 are defined as below;

- Ten measurement points at y=10.2mm from z=0 to z=42.5mm.
- Six measurement points at y=6.25mm from z=0 to z=35mm.
- Ten measurement points at y=2.5mm from z=0 to z=42.5mm.
- Two measurement points at z=0mm from y=5 to y=7.5mm.
- Two measurement points at z=6.25 from y=5 to y=7.5mm.

A reference sample for the measurement of the stress-free lattice parameter d_0 was manufactured according to a comb-like design. A comb-like sample with a $4\times4\times10mm^3$ (width x depth x height) was used as a stress-free sample as shown in Figure 3.18. In Figure 3.18, 'O' refers to the origin of the local coordinates in each plate. The comb-like sample was manufactured from a small plate exactly oriented with the measurement plate extracted from x=50mm and x=200mm on the butt-welded plate with the short weld and the butt-welded plate with the long weld respectively.

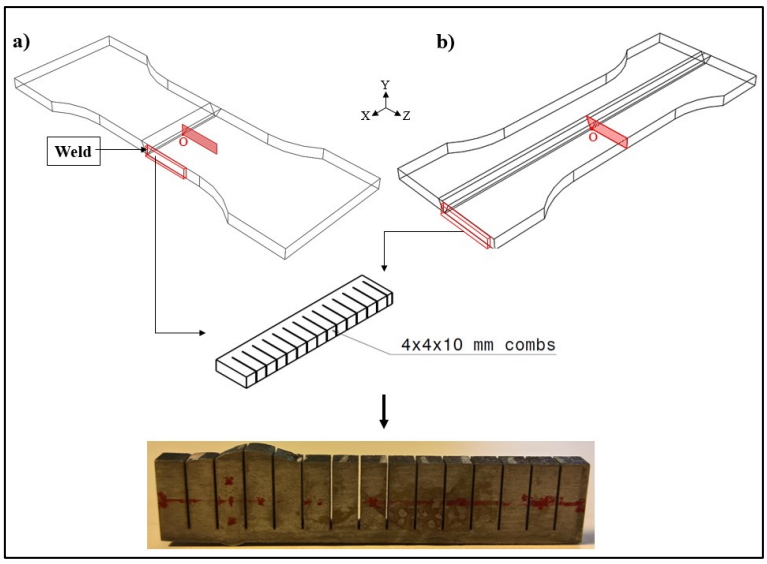

Figure 3.18: Illustarting the location where the stress-free samples were extracted and a photoghraph of comb-like stress-free sample manufactured from the main specuimen.

In the first orientation, both butt welded samples were set-up together to measure lattice spacing in two orthogonal components as shown in Figure 3.19. With two detector banks at ±90˚ to the incident beam, it was possible to measure strains in two directions simultaneously. In Figure 3.19, for both plates, transverse and normal residual strain scanning was performed. The transverse strain scanning was done by horizontal scanning using X-translation with the weld direction vertical at y=2.5, 5, 6.25, 7.5 and 10.2mm to measure lattice spacing at 30 points in each plate. Here the y-direction is through the thickness of the plates. The horizontal and vertical opening of the incident beam slit was kept at $3\times10mm^2$ to include large number of grains in one run.

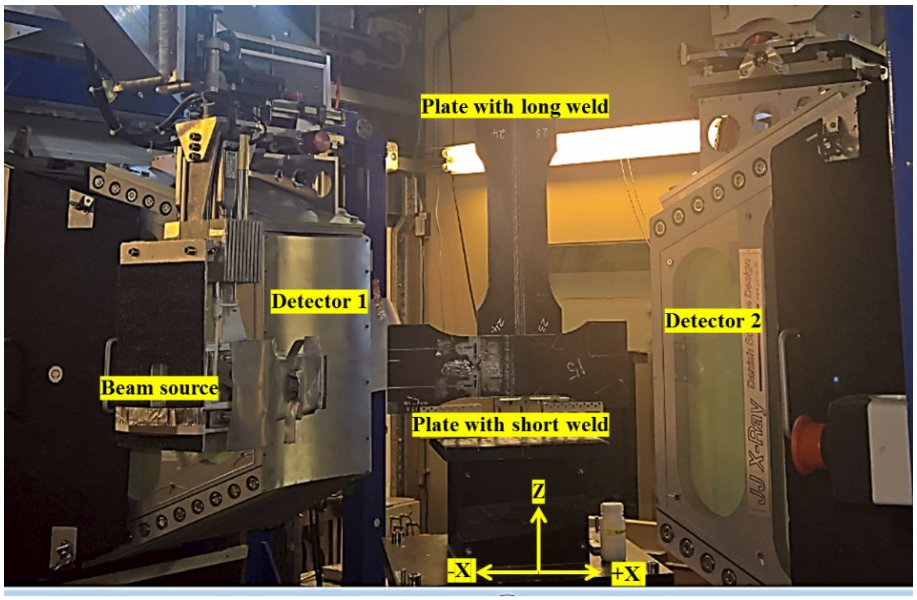

Figure 3.19: Neutron diffraction setup on butt welded plates during the measurement of transverse and normal strain directions (first orientation).

After the measurement of 60 lattice spacings to obtain residual strain in the transverse and normal directions in the first orientation, the plates were interchanged as shown in Figure 3.20 to measure the second orientation. In the second orientation, the measurement was along the longitudinal and normal directions. The longitudinal strain scanning was done by vertical scanning using Z-translation with the weld direction horizontal and at y=2.5, 5, 6.25, 7.5 and 10.2mm to measure lattice spacing at 30 points in each plate. The incident beam slit was kept at $3\times3mm^2$ to maintain the spatial resolution of the measurements. A 3mm collimator was used to define the spatial resolution in the through-thickness direction.

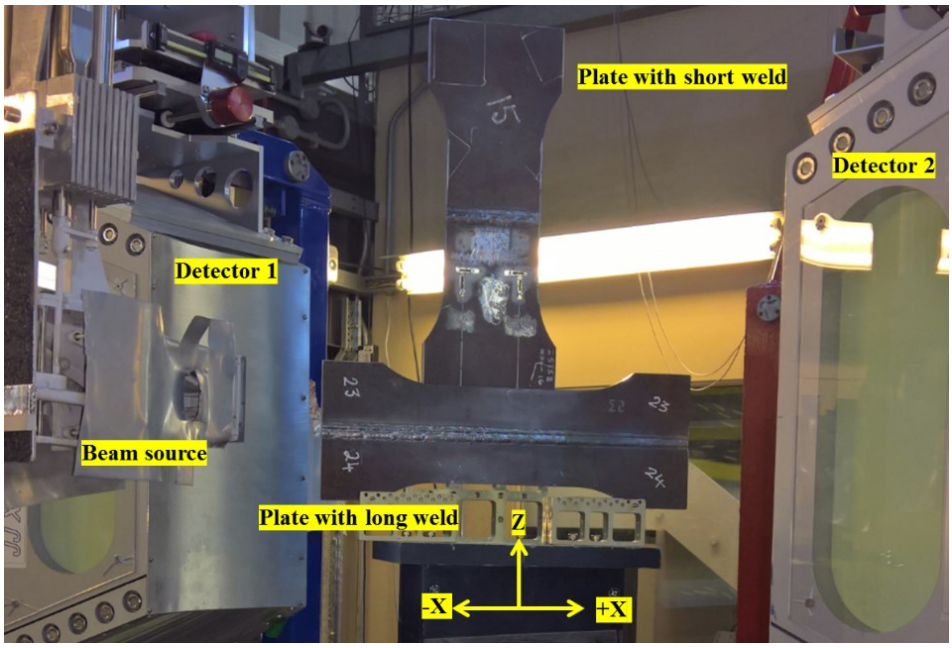

Figure 3.20: Neutron diffraction setup on butt welded plates during the measurement of longitudinal and normal strain directions (second orientation).

The reference comb sample was also measured in the longitudinal, transverse and normal directions to determine the stress-free references, henceforth referred to as d_0 for weld, Heat Affected Zone (HAZ) and parent material. A $3\times3\times3mm^3$ gauge volume was used to measure lattice spacing in the reference comb sample. It was ensured that the gauge volume was completely immersed inside each tooth of the comb. Three locations from the weld, two locations from the HAZ, and three locations on the parent material were measured in two separate orientations to determine lattice stress-free references in longitudinal, transverse and normal directions. An average value of each measured value in each area was used to define the stress-free lattice spacing.

As mentioned before, neutron strain scanning in the butt-welded plates was performed in the as-welded condition, and after one, three and ten load cycles. After a set of

measurements in all three orthogonal directions, the plates were removed from the neutron compartment and subjected to tensile load cycles in TWI as explained in Section 3.6.

3.7.2 Fillet Welded plates

Similar to the butt-welded specimens, neutron diffraction was used to determine stress in the as-welded condition, and after one and three load cycles. On each fillet welded specimen, the base plate is defined as the horizontal plate, and the web plate is defined as the vertical plate for ease. The objective was to measure residual stress in all three orthogonal directions with respect to the plate dimensions in both horizontal and vertical plates of each specimen.

Prior to neutron diffraction set-up, a total of 30 measurement points was selected on each fillet-welded specimen as shown in Figure 3.21. In Figure 3.21a and 3.21b, '*O*' represents the origin of the local coordinates.

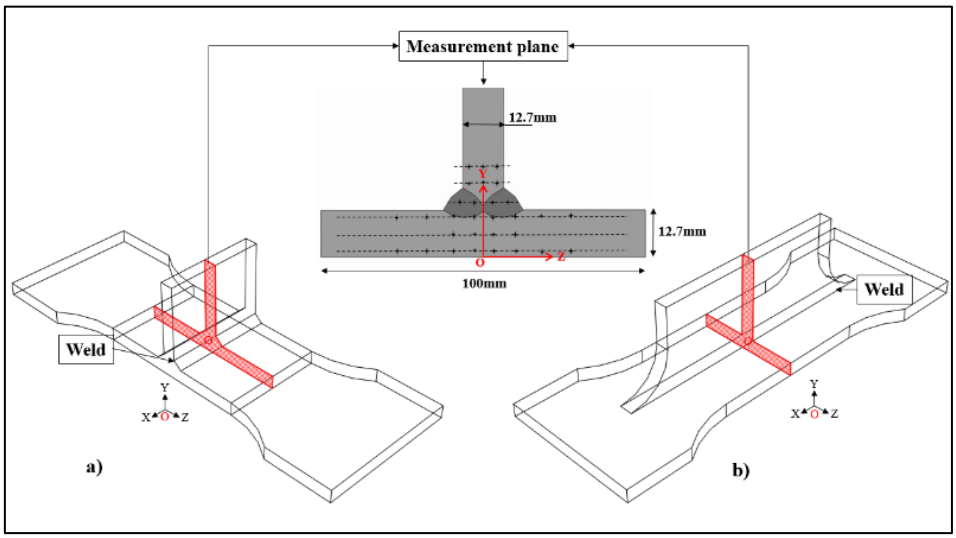

Figure 3.21: Illustration of 30 measurement points on fillet welded plates: a) Fillet-welded plate with the short weld and, b) fillet-welded plate with the long weld.

The 30 measurement points on each plate were on the midplane thickness and consisted of 20 points from both sides of the weld centre line on the horizontal plate and 10 points from the area of the vertical plate as illustrated in Figure 3.21. The measurement locations among the 30 points represented on the YZ plane shown in Figure 3.21 are defined as below:

- Eight measurement points at y=2.5mm from z = –21 to z = +21mm.
- Four measurement points at y=6.25mm from z = –9 to z = +9mm.
- Eight measurement points at y=10.2mm from z = –21 to z = +21mm.

- Four measurement points at y=15.2mm from z = –9 to y = +9mm.
- Three measurement points at y=20.2mm from z = –3.9 to z = +3.9mm.
- Three measurement points at y=25.2mm from z = –3.9 to z = +3.9mm.

A reference sample for the measurement of the stress-free lattice parameter d_0 was extracted for both fillet welded plates. A 4mm thick section of the T-joint was extracted from the joint cross-section. For each plate, four 4×4×4mm^3 cubes were extracted from weld 1, weld 2, the horizontal plate and the vertical plate as shown in Figure 3.22. The reference stress-free sample was extracted from the same fillet welded plates and exactly oriented with the measurement plane extracted from x=50mm and x=200mm on the fillet-welded plate with the short weld and fillet-welded plate with the long weld respectively.

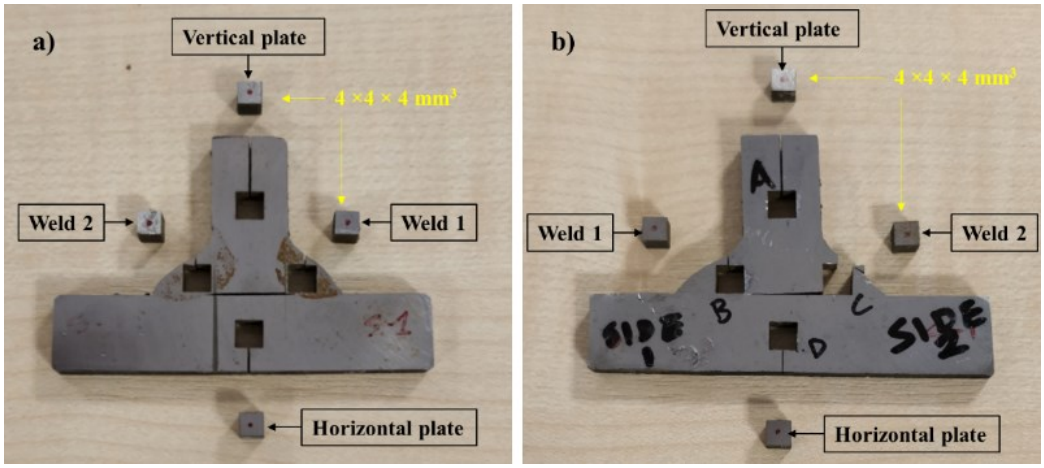

Figure 3.22: Reference stress-free samples from fillet welded plates: a) Stress-free cubes from fillet welded plate with the long weld, and b) stress-free cubes from fillet -welded plate with the short weld.

A total of four orientations with respect to the incident neutron beam direction were employed to measure 30 points on the measurement cross-section in order to reduce the neutron beam path length. The first orientation measured the transverse and normal strain components on 20 measurement locations in the horizontal plate of each fillet welded specimen. The first orientation setup for both fillet welded samples in the neutron diffraction compartment is shown in Figure 3.23.

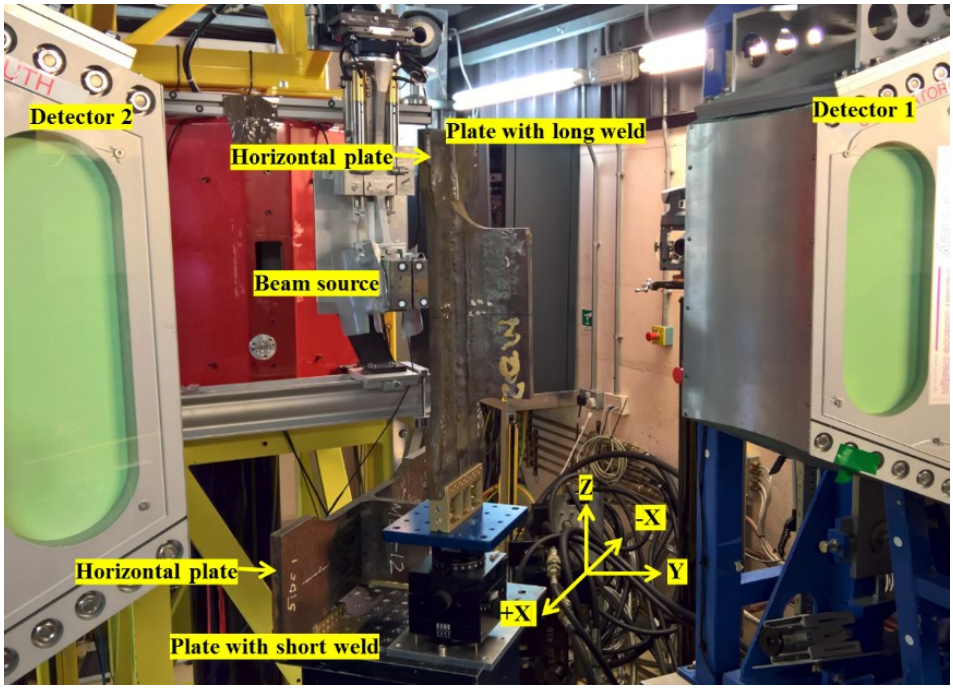

Figure 3.23: Neutron diffraction setup on fillet welded plates during the measurement of transverse and normal strain directions (first orientation) only on the horizontal plate.

The transverse strain scanning was done by horizontal scanning using X-translation with the weld direction vertical at y=2.5, 6.25 and 10.2mm to measure lattice spacing at 20 points on each plate. The horizontal and vertical opening of the incident beam slit was $3\times10mm^2$ to reduce measurement time by including a large number of grains in one run during the measurement of transverse and normal components. The spatial resolution in the through-thickness direction was defined using a 3mm collimator.

After the measurement of 40 lattice spacings to obtain residual strain in the transverse and normal direction in the horizontal plate, the plates were reoriented. In the second orientation, the longitudinal and normal residual stresses were recorded on the same points thereby completing the measurement of all three orthogonal components. The longitudinal strain scanning was done by vertical scanning using Z-translation with the weld direction horizontal and at y=2.5, 6.25 and 10.2mm. To maintain the spatial resolution, the slit was kept at 3×3 mm^2. A 3mm collimator was used to define the spatial resolution in the through-thickness direction.

After completing measurement in the horizontal plate on each specimen, for the measurement of the vertical plate and the welds, a third orientation was measured in which the fillet welded specimens were rotated 180° so that the weld surface was turned towards the incident beam as shown in Figure 3.24.

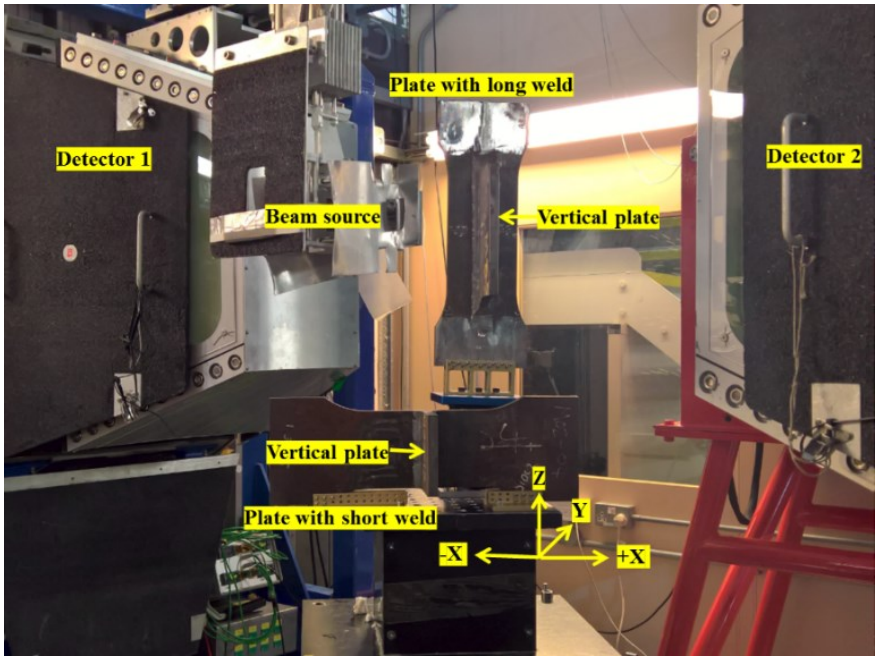

Figure 3.24: Neutron diffraction setup on fillet welded plates during the measurement of longitudinal and normal strain directions (third orientation).

In the third orientation, transverse and normal strain components on the vertical plate and weld passes were measured, consisting of 10 points. For the measurement of longitudinal strain, each plate was independently set-up in a fourth orientation. The fourth orientation employed for the fillet welded plate with the short weld is shown in Figure 3.25.

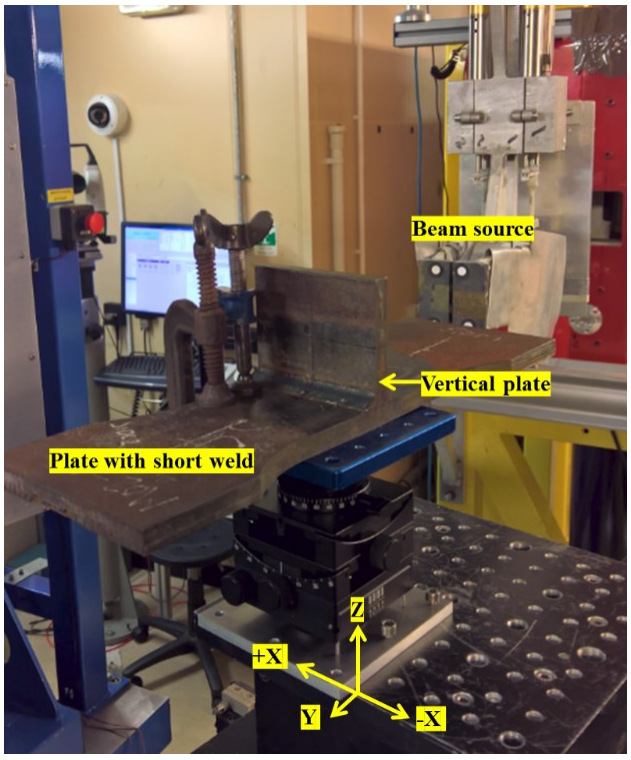

Figure 3.25: Neutron diffraction setup on fillet welded plate with the short weld during the measurement of: of longitudinal strain in vertical plate (fourth Orientation).

The reference stress-free sample was also measured in the longitudinal, transverse and normal directions to determine the stress-free reference, d_0 for weld 1, weld 2, horizontal parent material and vertical parent material. A 3×3×3 mm^3 gauge volume was used to measure lattice spacing in the reference sample. Like earlier samples, it was ensured that the gauge volume is completely immersed inside each cube. Each cube was measured in two separate orientations to determine lattice stress-free reference, d_0, in longitudinal, transverse and normal directions.

As mentioned before, neutron strain scanning in the fillet-welded plates was performed in the as-welded condition and after one and three load cycles. After a set of measurements in all three orthogonal directions, the plates were removed from the neutron compartment and subjected to tensile load cycles in TWI as explained in Section 3.6.

3.8 Neutron diffraction data analysis

The lattice parameters were determined from the diffraction spectra data obtained from each measurement location. The lattice parameters in three orthogonal directions at selected locations were measured. The lattice parameter in the butt-welded plate, d and the corresponding lattice parameter in the stress-free sample, d_0 are used to determine the residual strain at each location. The ENGIN-X computer uses GSAS code to apply a least squares fit to each diffraction spectrum to highlight the diffraction peaks. The peak shift, $\Delta\lambda$ is then determined from the diffraction peaks. Since the diffraction angles are kept constant for the neutron beam in ENGIN-X, the strain component ε is determined from Equation 3.7.

$$\varepsilon = \frac{\Delta\lambda}{\lambda} = \frac{d-d_0}{d_0} \qquad (3.7)$$

Further, the stress components were calculated using Hooke's law in its generalised expression:

$$\begin{aligned} \sigma_{xx} &= 2\mu\varepsilon_{xx} + \phi(\varepsilon_{xx} + \varepsilon_{yy} + \varepsilon_{zz}) \\ \sigma_{yy} &= 2\mu\varepsilon_{yy} + \phi(\varepsilon_{xx} + \varepsilon_{yy} + \varepsilon_{zz}) \\ \sigma_{zz} &= 2\mu\varepsilon_{zz} + \phi(\varepsilon_{xx} + \varepsilon_{yy} + \varepsilon_{zz}) \end{aligned} \qquad (3.8)$$

where $\mu = \frac{E}{2(1+\nu)}$, $\phi = \frac{\nu E}{(1+\nu)(1-2\nu)}$, ν is Poisson's ratio, E is the elastic modulus (210 GPa), v is the Poisson's ratio for steel (0.3) and x, y and z denote three orthogonal directions relative to the plate's dimensions.

Due to several factors in the neutron diffraction instrument, uncertainty can arise during the measurement of lattice spacing. However, these are very small errors during the measurement and hence were neglected. The error during peak fitting was considered as they are higher when compared to measurement errors and the error in strain, $\Delta\varepsilon$ formulated based on statistical error analysis is determined using (Goudar et al. 2008):

$$\Delta\varepsilon = \left[\left(\frac{\Delta d}{d_0}\right)^2 + \left(\frac{d * \Delta d_0}{d_0^2}\right)^2\right]^{1/2} \quad (3.9)$$

where Δd and Δd_0 are the measurement errors in lattice parameter of the specimen and stress-free sample respectively. The resulting error in corresponding residual stress components was calculated using the equation (Goudar et al. 2008):

$$\Delta\sigma_{xx} = \frac{E}{(1+v)(1-2v)} \sqrt{(1-v)^2(\Delta\varepsilon_{xx})^2 + v^2\left[(\Delta\varepsilon_{yy})^2 + (\Delta\varepsilon_{zz})^2\right]} \quad (3.10)$$

Equation 3.10 was used to calculate the error in measured stresses in x, y and z orthogonal directions.

3.9 Lattice spacings from reference comb samples

The comb-like stress-free reference samples for butt welded plates and individual cube samples for fillet welded specimens are presented first because this is vital in the determination of the strain values in the corresponding weld plate.

3.9.1 Reference lattice spacings from butt welded specimens

The measured lattice spacings in the reference comb sample from the butt welded plates with the short weld and the long weld are shown in Figure 3.26 and 3.27 respectively. In both cases, three measurements from the weld material, one measurement from the HAZ and four measurements from the parent material as illustrated in Figure 3.26 and 3.27 were obtained. An average value of each measurement region was considered for further analysis. The average values extracted from the measurements are listed in Table 3.4 and 3.5.

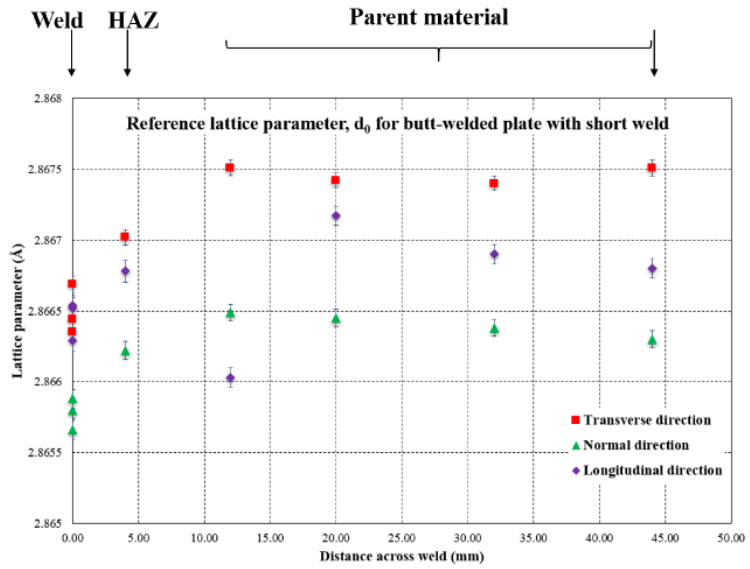

Figure 3.26: Reference lattice parameter, d_0 measured on the weld, HAZ and parent material in the butt-welded plate with the short weld

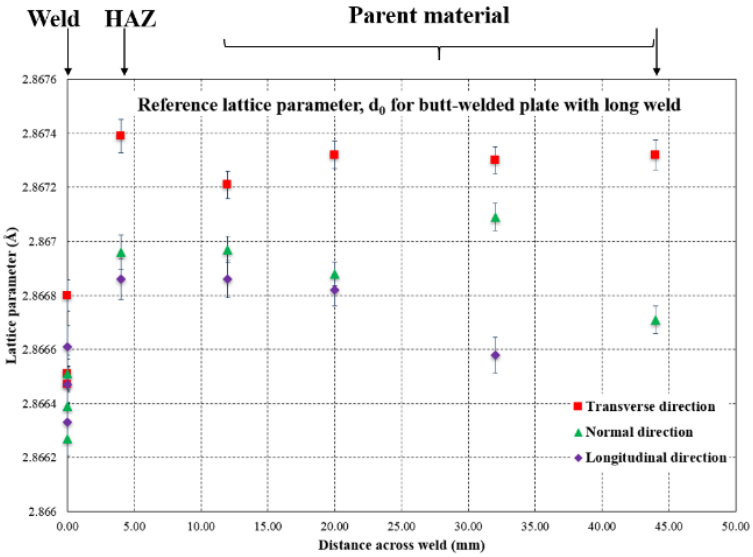

Figure 3.27: Reference lattice parameter, d_0 measured on the weld, HAZ and parent material in the butt-welded plate with the long weld

Table 3.4: Reference lattice parameter measured for butt welded specimen with the short weld.

	d_0(Å) Transverse	*d_0(Å) Longitudinal*	*d_0(Å) Normal*
Weld Material	2.86649	2.86645	2.865985
HAZ	2.86702	2.86678	2.86651
Parent Material	2.86746	2.8666	2.86661

Table 3.5: Reference lattice parameter measured for butt welded specimen with the long weld.

	d_0(Å) Transverse	d_0(Å) Longitudinal	d_0(Å) Normal
Weld Material	2.86659	2.86647	2.86636
HAZ	2.86739	2.86686	2.86691
Parent Material	2.86728	2.86675	2.86708

3.9.2 Reference lattice spacings from fillet welded specimens

From both fillet welded specimens, reference lattice spacings in three orthogonal directions were measured from cubes corresponding to the weld 1, weld 2, vertical plate and horizontal plate from both fillet welded specimens. The reference lattice spacing obtained for each material are listed in Table 3.6 and 3.7. Stresses in longitudinal, transverse and normal directions in the welded plates were calculated using the corresponding stress-free lattice spacing listed in Table 3.6 and 3.7 from each region of the fillet-welded stress-free sample.

Table 3.6: Reference lattice parameter measured for fillet welded plate with the short weld.

	d_0(Å) Transverse	d_0(Å) Longitudinal	d_0(Å) Normal
Weld 1	2.86648	2.86654	2.86604
Weld 2	2.86621	2.86656	2.86622
Vertical plate	2.86692	2.86717	2.86687
Horizontal plate	2.8667	2.86679	2.86676

Table 3.7: Reference lattice parameter measured for fillet welded specimen with the long weld.

	d_0(Å) Transverse	d_0(Å) Longitudinal	d_0(Å) Normal
Weld 1	2.86589	2.86654	2.86667
Weld 2	2.86657	2.86615	2.86615
Vertical plate	2.86667	2.86676	2.86676
Horizontal plate	2.86680	2.86679	2.86679

3.9.3 Measured residual strains in three orthogonal directions

This section presents the complete measurement results in terms of stresses calculated using the corresponding reference lattice spacing obtained in Sections 3.9.1 and 3.9.2 using equations 3.7 to 3.10. The residual strains determined from neutron diffraction for the as-welded sample, and after a specific number of load cycles in each plate are given in Appendix B. The residual strains in three orthogonal directions in the butt-welded specimens are shown for which the local coordinates are defined in Figure 3.17. The residual strains in three orthogonal directions in the fillet welded specimens are shown in which the local coordinates are defined in Fig. 3.20. The residual stresses calculated will be discussed further in Chapter 4 and 5.

3.10 Summary

This chapter discussed the various methods and processes used to manufacture specimens required for the investigation of residual stresses and the validation of FE models. Gas Metal Arc Welding was used to manufacture all specimens. Two butt welded plates and two fillet welded plates were manufactured. The welded plates were cut using EDM to prepare loading samples. Residual stresses were measured using neutron diffraction in all specimens. The method and setup used for the measurement of residual stresses in each specimen were described. The next chapter will discuss the numerical prediction and mapping of residual stresses using FE models along with the validation of FE results with each specimen.

CHAPTER 4.NUMERICAL SIMULATION OF AS-WELDED RESIDUAL STRESSES

4.1 Introduction

Numerical simulation of residual stress redistribution under elastic shakedown requires an accurate and complete description of the residual stress field in the specimens under study. Welding process simulation is implemented in this work to simulate the initial as-welded residual stress distribution on the specimens under study. Welding process simulation enables the determination of macroscopic transient temperature, displacement, stress and strains during the process, and are generally performed in what is known as an uncoupled analysis. Additionally, a novel iterative technique to establish the state of residual stress in a butt-welded plate by using a limited set of experimental measurements obtained using neutron diffraction is presented as an alternative to traditional 3D welding process simulations. 3D welding process simulations are computationally demanding when the intended application is to assess the structural integrity of a small region of welded structures such as the effect of residual stress son localised cracks.

Initially, the general FEA details for the implementation of welding process simulation such as material properties and governing equations are discussed. Following this, a description of butt-welding and fillet welding process simulations and the validation of thermal history with corresponding experimental measurements are presented. After the numerical simulation of the welding process, the EDM cutting performed on each specimen was simulated using element activation/deactivation technique. Finally, the predicted residual stress from the same locations was compared to experimental residual stress values measured using neutron diffraction. Following the welding process simulation, a novel iterative technique for residual stress mapping applied in the butt-welded plate with the short weld is presented and compared with predicted residual stresses from welding simulation

4.2 Principles of welding process simulation

4.2.1 The physics of arc welding

The arc welding process introduces complex physical interactions in the material to be welded. The physical interactions consist of processes such as heat transfer from the arc source to the component to be welded, melting, fluid flow with mass transport, the interaction between liquid and solid phases, metallurgical phase transformation, and

solidification (Kou 2003). In all arc welding processes, the arc source is defined as the heat source, and it is quantified by arc energy. Arc energy is the energy supplied by the welding arc to the component to be welded. Arc energy in kJ/mm is defined as:

$$AE = \frac{60VI}{1000v} \quad (4.1)$$

where V is the applied arc voltage in volts, I is the arc current in amperes and v is the travel speed of the welding torch (mm/min). The arc energy produces an electromagnetic force in the weld pool which enables the hot liquid metal to flow to the bottom of the weld pool to produce deep weld penetration. The proportion of the arc energy transferred to the component to be welded is defined as welding efficiency η. Most of the arc energy is transferred to the weld pool, with some energy lost due to the efficiency of the welding process via thermal conduction and radiation. Heat input is the heat energy transferred to the workpiece after factoring the welding efficiency. Heat input is most relevant as it considers the effect of the specific arc welding process. For Gas Metal Arc Welding, the efficiency (η) is considered as 0.8 as recommended in (R6 Revision 4 2015). The heat input, Q is then defined as:

$$Q = \eta VI \quad (4.2)$$

The weld pool starts to solidify when the arc moves away. The solidification is affected by various factors such as cooling rate, temperature gradient and compositional gradient. In the weld pool during solidification, different phases could solidify over a range of temperatures which could give rise to solid-state phase transformation upon cooling. The composition of a transformed phase depends on the cooling rate which in turn is dependent on various welding parameters.

The residual stress evolution strongly depends on the solidification process and hence can be numerically predicted to a reasonable accuracy using thermal strains and the cooling rate of the material. However, a complete simulation of all the physical interactions is difficult to employ in an analytical or numerical model (Dong and Hong 2002).

Apart from the physical processes described above, residual stresses are also affected by the restraints or boundary conditions on the workpiece. It is not always a requirement to involve all the arc welding physical aspects in simulation as long as the predicted stresses are reasonably accurate (Bate and Smith 2016; Dong and Hong 2002).

4.2.2 Implementation of welding process simulation

Numerical techniques using finite element analysis for the prediction of welding residual stresses have been in practice since the late 1970s. Due to steady advancements in computing, data processing speed, storage capacity and numerical algorithms, numerical techniques have been favoured in comparison to experimental methods. Moreover, the development of commercial finite element software packages such as ABAQUS, SYSWELD and ANSYS etc. have enabled easy implementation of welding process simulations.

Experimental measurements of temperature history and residual stress values have been used for the validation of weld model predictions and also to improve the accuracy of the predictions. Currently, there are huge amounts of documented data on welding residual stresses, including in open publication, and this show scatter in both magnitudes and distributions. This implies that for a more consistent, accurate and realistic prediction, experimental techniques and numerical procedures still require further enhancement. However, it is worth noting that much of the scatter in the distribution and magnitudes is due to the incapability of numerical methods to account for all the complex physical interactions, which often varies considerably from workpiece to workpiece depending on several variables such as environment, welder (if manual welding) and welding parameters.

Guidelines for welding process simulations are described in R6 Rev.4 (R6 Revision 4 2015) Section III.15, which defines the main steps, heat input definitions, material property requirements, convection and radiation boundary conditions for heat transfer analysis and hardening mechanisms for mechanical stress analysis.

A 3D sequentially uncoupled analysis is adopted in this work. Initially, a heat conduction problem is solved independently to obtain thermal solutions by implementing a heat transfer analysis. This analysis predicts the transient temperature distribution in a weld following the welding process. Subsequently, a mechanical analysis is performed on the same FE model with the thermal solutions from the heat transfer analysis used to calculate corresponding thermal strain. Both heat transfer and mechanical analysis were simulated under “static” step type in ABAQUS. The material’s temperature-dependent response to these thermal strains is determined numerically to calculate residual stresses.

4.2.3 Heat transfer analysis and associated governing equations

A transient thermal analysis is required for the heat transfer simulation. This can be implemented by modelling the heat flow either in two-dimensional (2D) or three-dimensional (3D) configuration. The main step involved in heat transfer analysis is to introduce the heat input defined in Equation 4.2 under thermal boundary conditions involved during the process.

The introduction of the heat input in the numerical model can be using three approaches in the order of increasing complexity and accuracy (R6 Revision 4 2015);

- a static heat source with prescribed temperature (generally melting temperature),
- a static heat source with volumetric flux, and
- a moving heat source with volumetric flux

A static heat source with prescribed temperature defines heat input by a fixed temperature above the material melting temperature (T_m) for a specific time period (Δt). In this method, a reasonable time period is critical as too long a hold time results in an excessive amount of heat input to the weld region and too short a hold time may not be able to introduce sufficient molten zone size. As a result, the accuracy of the predicted residual stress field is difficult to achieve.

A static heat source with volumetric flux, in comparison, defines the heat flux instead of temperature and welding efficiency. With the flux duration and weld pool dimensions obtained from actual welding, the heat flux is applied simultaneously to the whole weldment. In 2D this means applying heat flux in the weld cross-section and along the length of the weld, on the whole weldment.

A moving heat source with volumetric flux is only implemented in 3D welding simulation. The heat source is moved along a welding path which represents the most realistic form of welding process. In Abaqus, a subroutine code is often required to implement a moving heat source, in which the voltage, current, efficiency, travel speed, heat flux and the volume to which heat flux is applied or a heat source model should be defined.

The heat source models for arc welding processes can be traced back to the 1940s led by Rosenthal (Rosenthal 1946) who proposed a point or line moving heat source model to analytically predict the temperature in the region of the fusion zone (FZ) and the heat affected zone (HAZ) on an infinite material. However, the residual stress in the region

where the point source is incident was inaccurate. Pavelic (Pavelic 1969) developed a moving heat source based on a Gaussian distribution of flux on the surface of the workpiece, which enabled better prediction of temperature fields in the HAZ in comparison with Rosenthal's.

Later Goldak (Goldak, Chakravarti and Bibby 1984) proposed a double-ellipsoidal model, which is a non-axisymmetric 3D heat source model suitable for simulating arc welds and welds produced by high-power-density processes. Among all the heat source models, the moving double ellipsoidal heat source model proposed by Goldak has been widely used to date for introducing heat input in the arc welding process simulation.

In ABAQUS, the double ellipsoidal model can accurately be implemented to impose the heat input in the FE model with a user subroutine which performs the weld deposition continuously and sequentially. However, it becomes increasingly complex if the welding consists of multi-pass welds, and the computer resource is restricted. Hence, it is often simple to define a volumetric heat flux in multi-pass welding in comparison to a particular heat source model. It can be applied by simply dividing a weld pass into smaller weld blocks called 'weld chunks' and consider sequentially heating each block in the weld material with constant heat input. For example, on a welding process with two passes, each pass can be divided into N number of chunks introducing 2*N* number of chunks altogether. The heat flux, h (W/m^3), applied to a weld chunk can be defined as:

$$h = \frac{Q}{V_{wc}} \qquad (4.3)$$

where V_{wc} is the volume of the weld chunks corresponding to a heating time Δt defined as:

$$\Delta t = \frac{L_{wc}}{v} \qquad (4.4)$$

where L_{wc} is the length of the weld chunks along the weld travel direction and v is the welding torch travel speed in m/s.

In the arc welding process, heat transfer occurs from the hot molten fusion zone to the surrounding weld plate. The heat transfer mode from the fusion zone to the base material is primarily through conduction. On a plate where x, y and z represent three orthogonal axes, the heat transfer due to conduction from the weld zone is dictated according to the heat equation:

$$\nabla(K\nabla T) + h(x,y,z,t) = \rho C_p(\frac{\partial T}{\partial t}) \qquad (4.5)$$

Where *h,* heat flux is defined in equation 4.3 (W/m^3), ρ is the density of the material (kg/m^3), *K* is the thermal conductivity (Wm^{-1}°C^{-1}), C_p is the specific heat (J kg^{-1}°C^{-1}), *T* is the transient temperature (°C) and *t* is time (s). Newton's law of cooling and the Stefan-Boltzmann relation govern the convective and radiative heat losses during welding according to the initial and boundary conditions specified (Rahman Chukkan et al. 2015). For a given body temperature *T* surrounded by a fluid or gas, radiation to the surrounding medium follows the Stefan–Boltzmann law and heat convection assumes that a thermal layer exists with a heat transfer coefficient, which follows Newton's law of cooling.

4.2.4 Mechanical analysis and associated governing equations

The second part of the sequentially coupled welding simulation consists of mechanical analysis, namely the welding residual stress simulation. The mechanical model reads the transient temperature solution from the heat transfer analysis. Apart from inputting the temperature field from a heat transfer model on a time-dependent basis, the stress analysis determines the mechanical behaviour of the workpiece based on a material model which aims to realistically represent the elastic and plastic behaviours including plastic strain hardening in the thermal cycles of rapid heating and cooling.

In the mechanical model, the equilibrium equation (Equ. 4.6) and thermo-elastoplastic constitutive equations (Equ. 4.7) can be defined as,

$$\sigma_{ij} + \rho b_{ij} = 0 \qquad (4.6)$$

$$[d\sigma] + ([D^e] + [D^p]) * [d\varepsilon] - [C^{th}]dT = 0 \qquad (4.7)$$

Where σ_{ij} is the stress tensor and b_{ij} is the body force per unit mass. $[D^e]$ is the elastic stiffness matrix, $[D^p]$ is the plastic stiffness matrix, $[C^{th}]$ is the thermal stiffness matrix, $d\sigma$ is the stress increment, $d\varepsilon$ is the strain increment, and dT is the temperature increment. Apart from the basic heat transfer modes, in arc welding, there are physical phenomena like viscous force, buoyancy force, convective flow, and Marangoni effects in the arc pool (Heiple and Burgardt 1985). These effects are neglected in the numerical simulation as they are not significant in terms of residual stresses arising due to thermal strains.

4.2.5 Material properties

The material chosen for this study was DH36 shipbuilding steel (EN10025-2:2004 S355J2+N). Numerical modelling of the welding process requires temperature dependent thermal and mechanical properties of the material involved in the process. The required

material property data of DH36 were obtained from experimental measurement and literature surveys (Fu et al. 2014). In terms of hardening behaviour, isotropic hardening behaviour is assumed in both weld and parent material in this work. Isotropic hardening assumes that the yield surface does not move but can expand in size uniformly in all directions, essentially enabling strain hardening in tension and compression to the same level.

Phase transformation effects were not considered in the weld simulation. The yield strength of the weld material at ambient temperature was considered to be slightly higher than the base material to consider overmatching during welding. For both parent and weld metals, the same values of material properties were used apart from yield strength which are different as determined from the mechanical testing presented in Chapter 3. The material property data used are listed in Tables 4.1 to 4.6.

Table 4.1: Temperature-dependent material conductivity data used in weld simulations.

Temperature (°C)	Conductivity (W/m°C)
4	45.72
58	45.13
134	45.01
206	43.70
360	40.49
443	39.19
530	36.46
664	30.16
794	23.39
913	24.58
1015	25.53
1373	29.69
1461	30.76
1523	51.78
1583	100.10
1731	99.88

Table 4.2: Temperature-dependent specific heat capacity data used in weld simulations.

Temperature (°C)	Specific heat (J/ Kg°C)
2	425.83
56	464.76
114	500.15
278	568.56
380	596.87
480	636.98
584	692.42
684	771.45
783	849.31
858	684.16
1042	572.10
1350	612.21
1507	629.90
1977	658.21

Table 4.3: Temperature-dependent material thermal expansion coefficient data used in weld simulations.

Temperature (°C)	Thermal expansion coefficient, α
17	1.14E-05
67	1.18E-05
115	1.20E-05
178	1.24E-05
244	1.29E-05
309	1.32E-05
380	1.35E-05
443	1.37E-05
511	1.39E-05
581	1.40E-05
662	1.41E-05
757	1.42E-05
847	1.42E-05
938	1.42E-05
1037	1.42E-05
1131	1.42E-05
1225	1.42E-05
1487	1.42E-05

Table 4.4: Temperature-dependent material elastic modulus and Poisson's ratio data used in weld simulations.

Temperature (°C)	Youngs modulus (GPa)	Poisson's ratio, ν
20	210	0.3
191	200	0.3
273	190	0.3
399	175	0.3
467	161	0.3
575	139	0.3
689	109	0.3
748	93	0.3
890	50	0.3
978	21	0.3
1098	6	0.3
1179	3.3	0.3
1260	1.2	0.3
1388	1	0.3
1475	0.9	0.3

Table 4.5: Temperature-dependent material conductivity data used in weld simulations.

Temperature (°C)	Plastic strain	Yield strength-Parent (MPa)	Yield strength-Weld (MPa)
20	0	360	420
20	0.1	619	659
100	0	330	330
100	0.1	527	527
200	0	258	258
200	0.1	432	432
300	0	230	230
300	0.12	414	414
400	0	210	210
400	0.094	377	377
500	0	187	187
500	0.11	380	380
700	0	77	77
800	0	75	75
900	0	44	44
1056	0	23	23
1180	0	11	11
1300	0	4	4

Table 4.6: Temperature-dependent material mass density data used in weld simulations.

Temperature (°C)	Mass density (kg/mm^3)
0	7.78E-09
92	7.74E-09
168	7.70E-09
266	7.64E-09
366	7.61E-09
466	7.57E-09
560	7.50E-09
674	7.45E-09
773	7.42E-09
860	7.38E-09
952	7.34E-09
1153	7.25E-09
1260	7.19E-09
1353	7.12E-09
1432	7.09E-09
1480	7.08E-09

4.3 Simulation of residual stresses in Butt-welded plates

The section below explains the implementation of the numerical simulation of butt-welded plates manufactured in two different orientations, one with a long weld and one with a short weld, with the nomenclature used here as butt-welded plate with long weld and butt-welded plate with short weld.

4.3.1 Butt-welded geometry

Weld cross section macrographs were obtained from positions x=60mm and x=200mm based on a coordinate system illustrated in Figure 3.17a and 3.17b respectively in the cross-sectional view of the plates. A multi-pass arc welding with a single V-groove consisting of a root pass, a fill pass and two cap passes (with weld crown) was implemented on both models. The weld geometry has been made in an effort to represent the actual weld profile as closely as possible. However, the simplifications are introduced in the geometry to reduce any potential complexity in sketching and meshing. Moreover, as the welding parameters were the same for both plates (the only difference being in the weld plate dimensions) an average sketch dimension from both Figure 4.1a and 4.1b is employed in the FEA weld cross section. Figure 4.1c shows the modelled weld zone with created partitions for each pass (root, fill, cap 1 and cap 2) which considered the HAZ

region as well as the material overlap effect between every two sequential passes. Two sets of the materials, the parent metal and the weld metal, were defined as shown in Figure 4.1c. The details of the material properties used in this analysis are given in Section 4.2.5.

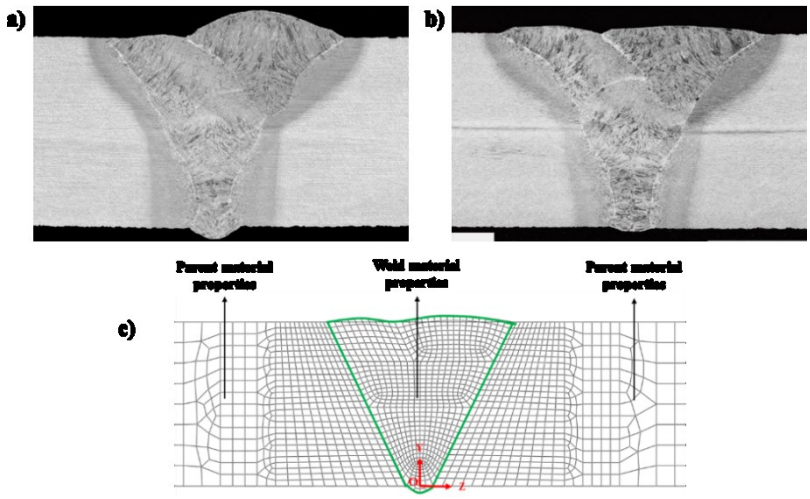

Figure 4.1: Weld cross section macrographs from butt welded plates: a) Butt-welded plate with the short weld, b) butt welded plate with the long weld and, c) weld cross section used in the FEA model.

Two separate 3D finite element models of rectangular plates of dimension $140\times400\times12.7mm^3$ and $140\times380\times12.7mm^3$ were modelled to use in the simulations in which one plate has a short weld and the other plate has a long weld (Figure 4.2).

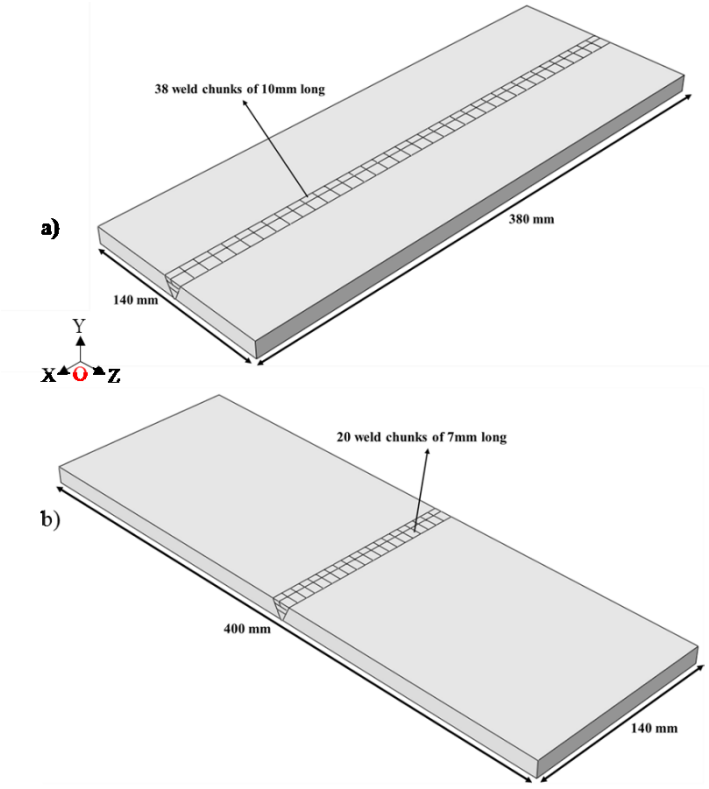

Figure 4.2: Butt weld model geometry used in weld simulations: a) Plate with the long weld, and b) plate with the short weld.

In the FE model, the butt welds were designed by partitioning each weld pass into smaller weld chunks as shown in Figure 4.2a and 4.2b. In the case of the butt-welded plate with the long weld, each pass was partitioned into 38 weld chunks of 10mm long (Figure 4.2a). For the butt-welded plate with the short weld, each pass was partitioned into 20 weld chunks of 7mm length (Figure 4.2b).

4.3.2 FEA element type and mesh design

The mesh details for both thermal and mechanical analysis were the same and consisted of 736733 and 654755 elements with varying size on the long weld plate and the short weld plate respectively. An element size of about 0.3 × 0.3 × 0.3 mm^3 was used in the weld and HAZ region based on an initial mesh sensitivity analysis under heat transfer mode. The element size was also controlled in order to choose a suitable time increment based on R6 section III equation as below;

$$\Delta t > \frac{\rho C_p}{6K}\Delta l^2 \qquad (4.8)$$

where Δt is the minimum time increment in the FE model and Δl is the minimum size of the mesh.

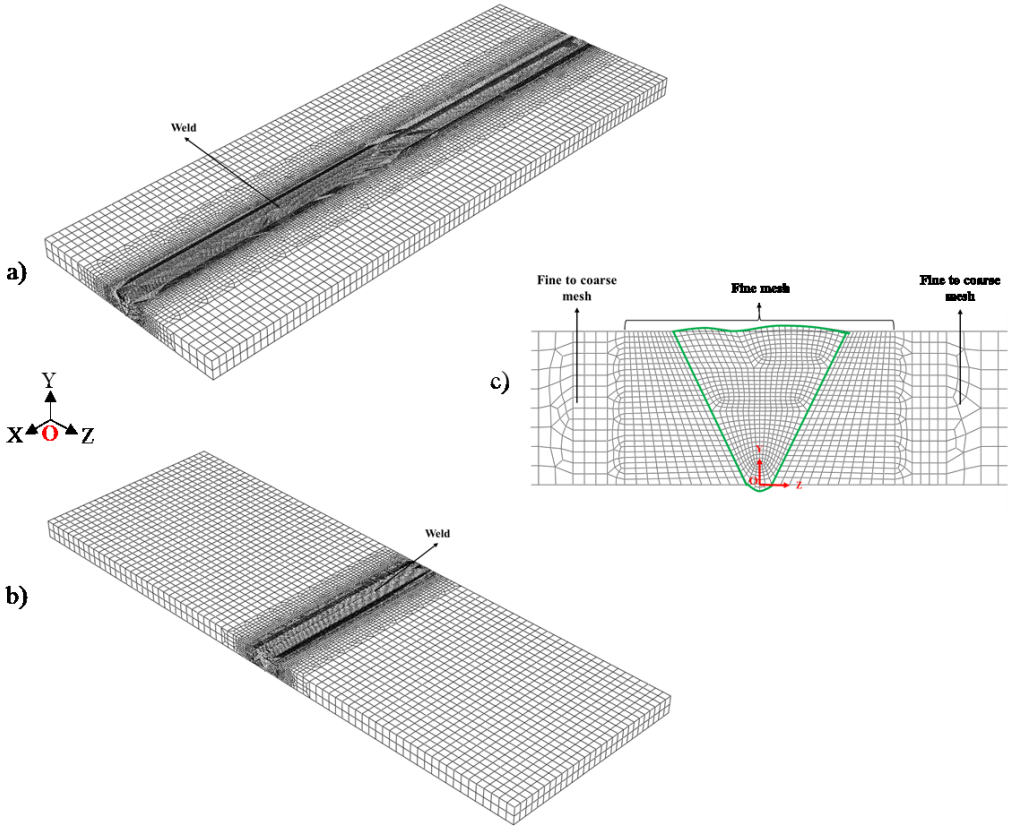

Figure 4.3: Mesh details showing fine to coarse transition in the butt weld model: a) Butt welded plate with the long weld, b) butt welded plate with the short weld, and c) weld cross section in both models.

In this FE model, first order 8-node heat transfer elements (DC3D8) and first order 8-node 3D stress elements with reduced integration (C3D8R) were used for thermal and mechanical simulations respectively (O'Meara, Smith and Francis 2015). Reduced integration elements were used for mechanical analysis because the welding process may introduce high level of plastic strain which can result in element-locking in fully integrated elements (McDill, Runnemalm and Oddy 2001). Figure 4.3 show the mesh details used for the butt-welded plates.

A high degree of mesh refinement at the fusion zone (FZ) and heat affected zone (HAZ) was implemented to assist the high-temperature gradient and non-uniform thermal strain. A coarse mesh was employed away from the weld to improve the computational efficiency.

4.3.3 Heat transfer analysis of butt welding

As mentioned before, each weld pass in the model was divided into smaller weld chunks. Weld zone materials experienced a sequence of heating and cooling during the process, which was modelled in the STEP module of ABAQUS (Abaqus Manual 2013). Heating and cooling steps were created with values assigned according to the heat flux and heating time calculated using Equations 4.3 and 4.4 and cooling time recorded during the actual welding process.

Table 4.7: Step module details for butt weld simulations of the short and the long weld.

Step name	**Short weld**		**Long weld**	
	Number of steps	Time period (sec)	Number	Time period (sec)
Step 1: (No weld deposited)	1	1	1	1
Root pass	20	1.75 each	38	2.5 each
Cool-1	1	170	1	96
Fill pass	20	1.75 each	38	2.5 each
Cool-2	1	210	1	380
Cap-1 pass	20	1.75 each	38	2.5 each
Cool-3	1	230	1	200
Cap-2 pass	20	1.75	38	2.5 each
Cool-4	1	50	1	50

The details of each step used in these analyses are given in Table 4.7. All the elements in the weld region were deactivated before adding any heat into the model. The filler material deposition was modelled by element activation. The first step in both FE models represented the unwelded plates with deactivated weld material elements.

For the butt-welded plate with the short weld, the first step was followed by 20 root pass steps, and for the butt welded plate with the long weld, the first step was followed by 38 root pass steps. Fill and cap passes were introduced after the root pass in the FE models. Between each pass, a cooling step was introduced which had time obtained from the actual welding process. The weld travel speed in the actual welding process was 4mm/s.

Thermal loads were modelled with a distributed body heat flux which assumed that the heat was instantaneously applied to each weld chunk in each weld pass. As mentioned in Section 4.2.3, an effective heat input as per equation 4.3 and 4.4 was calculated based the volume of each weld chunk. The volume of each weld chunk was estimated for each weld pass from the corresponding weld pass cross-section and the length of the weld chunk.

Both convection and radiation were considered as the heat transfer analysis boundary condition. A heat transfer coefficient of 0.025 ($W/mm^2{}^oC$) was applied on the surface of the FE model. Radiation heat transfer was dominant at high temperature near the welds and convective heat transfer was dominant for the near surface during the cooling period. Since the loss of heat input was already considered in the heat flux equation using an effective efficiency of the arc, the effect of radiative heat losses was excluded during weld metal deposition. Thermal boundary conditions were applied to all boundaries of the plates as well as the new boundaries created for each new pass. The initial temperature, in this case, was taken as 30 ºC, the same as the actual welding condition.

4.3.4 Mechanical stress analysis of butt welding

After establishing a heat transfer analysis, a mechanical model was created with the same features. In a mechanical model, the weld geometry and material property must be identical to that of the heat transfer model. Also, features like step type, load and boundary conditions and element type are different from the previous heat transfer model. The step type was changed from heat transfer (in the heat transfer analysis) to a general static step (a static stress procedure is one in which inertia effects are neglected) to obtain a history of stresses and strains.

In the mechanical model, the number of steps and each step time were created as the same as that of the heat transfer model. Filler material deposition was employed using deactivation/activation of the weld beads. The load was applied in terms of stress/strains generated from thermal history data obtained from heat transfer analysis. There was no external load applied on the plates. The plates were constrained in all three directions on the top surface of the plate 50mm away from both sides on the weld centre line to represent a fully restrained welding process as in the case of the actual process.

The temperature output data from the heat transfer analysis were used in the stress analysis for the prediction of residual stresses. This was achieved by predefining the temperature history to the corresponding step to obtain the stress output for that step.

4.4 Simulation of residual stresses in Fillet-welded plates

The following section explains the FEA implementation of the fillet-welded plates manufactured in two different orientations, one with a longer weld and one with a shorter weld, herein termed the fillet-welded plate with the long weld and the fillet-welded plate with the short weld. The methodology adopted was similar to the butt-welding simulations. Hence the fillet weld simulation methodology only explains aspects deviating from the butt weld.

4.4.1 Fillet-weld geometry

Weld cross section macrographs were obtained from the fillet weld plate as shown in Figure 4.4a. Figure 4.4b shows the modelled weld zone with created partitions for each pass (weld pass 1 and weld pass 2).

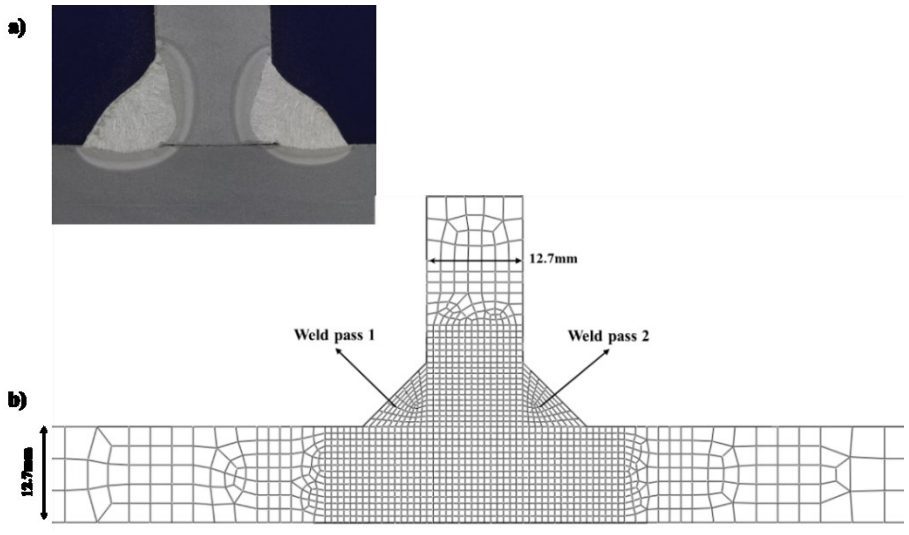

Figure 4.4: Weld cross section macrographs from fillet welded plate: a) Photograph of the macrograph and, b) weld cross section used in the FEA model.

Two sets of materials, the parent metal and the weld metal, were defined as shown in Figure 4.4b. Two separate 3D finite element models of rectangular plates of dimension 140×385×12.7mm^3 and 136×400×12.7mm^3 were designed. The FE geometry design of the fillet welded plate with the long weld and the short weld are shown in Figure 4.5a and 4.5b respectively.

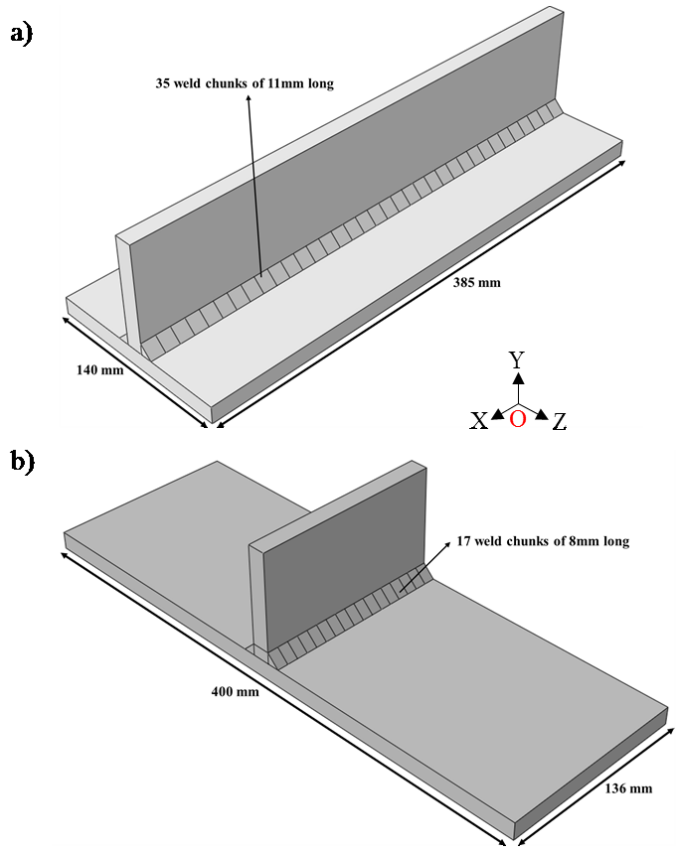

Figure 4.5: Fillet weld model geometry used in weld simulations: a) Fillet welded plate with the long weld and, b) fillet welded plate with the short weld.

In the FE models, in the case of the fillet-welded plate with long weld, each pass was partitioned into 35 weld chunks of 11mm long (Figure 4.5a) and the fillet-welded plate with the short weld, each pass was partitioned into 17 weld chunks of 8mm length (Figure 4.5b).

4.4.2 FEA element type and mesh design

The mesh details for both thermal and mechanical analysis were the same and consisted of 520008 and 227150 elements with varying size on the fillet weld with the long weld and the short weld respectively. The element types used are detailed in Section 4.3.2. An element size of about 0.5 × 0.5 × 0.5 mm^3 was used in the weld and HAZ region based on an initial mesh sensitivity analysis in conjunction with equation 4.8. There was a high degree of mesh refinement at the fusion zone (FZ) and HAZ as shown in Figure 4.6.

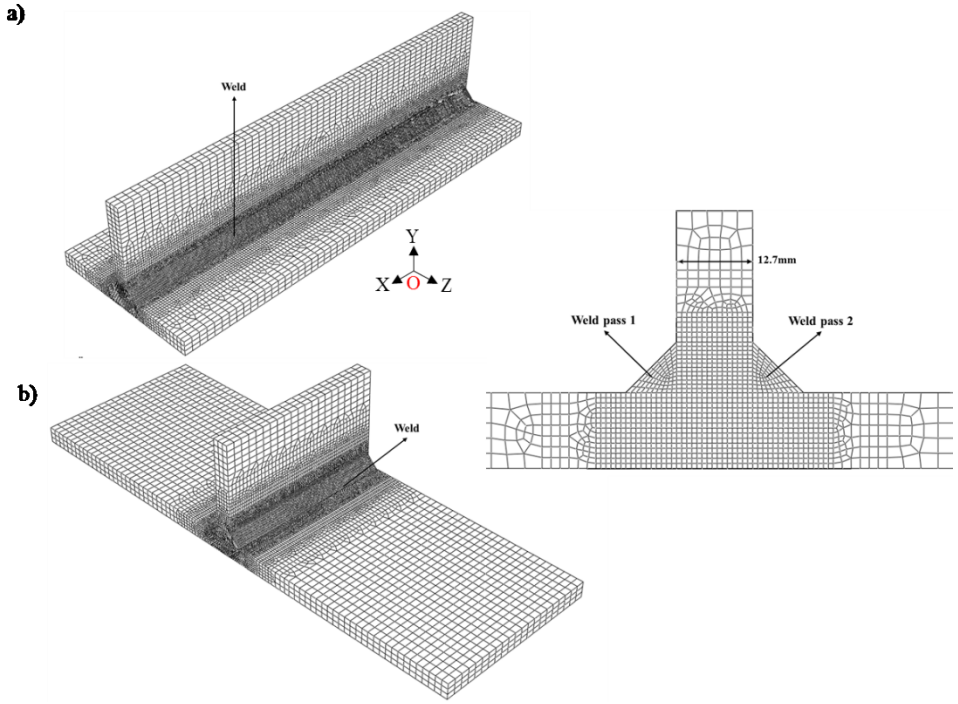

Figure 4.6: Mesh details showing fine to coarse transition in the fillet weld model: a) Fillet welded plate with the long weld and, b) fillet welded plate with the short weld.

4.4.3 Heat transfer analysis of fillet welding

The heat transfer analysis implementation was similar to the butt-welding simulations. The details of each step used in these analyses are given in Table 4.8 for both the fillet-welded plate with the long weld and the fillet-welded plate with the short weld. In the case of the fillet welded plate with the short weld, the first step was followed by 17 "weld pass 1" steps and in the case of the fillet welded plate with the long weld, the first step was followed by 35 "weld pass 1" steps. After completing weld pass 1, a cooling step was added prior to adding weld pass 2 based on the actual welding process. The weld travel speeds in the actual welding process were 3.2mm/s and 2.5mm/s for the fillet welded plate with short weld and long weld respectively.

Table 4. 8: Step module details for fillet weld simulations.

Step name	**Fillet Short weld**		**Fillet Long weld**	
	Number of steps	Time period (sec)	Number	Time period (sec)
Step 1: (No weld)	1	1	1	1
Weld pass 1	17	2.5 each	35	4.4 each
Cool-1	1	40	1	129
Weld pass 2	17	2.5 each	35	4.4 each
Cool-2	1	100	1	100

Thermal loads were modelled similar to the butt-welded specimens as described in section 4.3.3. A heat transfer coefficient of 0.025 (W/mm^{2}°C) was applied on the surface of the FE model. The initial temperature was considered as 30 °C, as measured from the actual welding condition.

4.4.4 Mechanical stress analysis of fillet welding

After establishing a heat transfer analysis, a mechanical model was created with the same features. Mechanical stress models were modelled similar to the butt-welded specimens as described in section 4.3.4. The plates were constrained in all three directions on the edges of the horizontal plate to capture the effects of the strong backs tack welded on the horizontal plate. The model is then considered fully restrained as in the case of the actual process.

4.5 Thermal field results

The temperature output data from each heat transfer analysis are discussed in this section. The thermal history at selected locations is validated against the thermocouple data obtained from the actual welding process.

A comparison was made between the measured and simulated thermal cycles, i.e. the transient temperatures of heating and cooling cycles at specific locations where thermocouples were installed on four weld specimens (Figure 4.7 to Figure 4.10). The thermal history shows good agreement in which the prediction had a similar trend, and the values were within an average ±50 °C with respect to the experimental values. Any deviations from the experimental values are noted below.

On the butt-welded plate with the short weld (Figure 4.7), temperatures were measured from thermocouples close to the weld groove edge at 4mm, 7mm and 20mm. At 4mm away from the weld groove, the experimental values obtained were very high as the final cap pass was very close to the location of thermocouple and it might have caused this sudden increase in the temperature. Also, the FEA underpredicted the temperature at 4mm and 7mm during the third pass (first cap pass). This may be attributed to the location of the first cap pass, which was closer to the opposite weld groove with respect to the thermocouple position. Further away from the weld centre, recorded thermal cycles at 20mm away were in good agreement with those simulated.

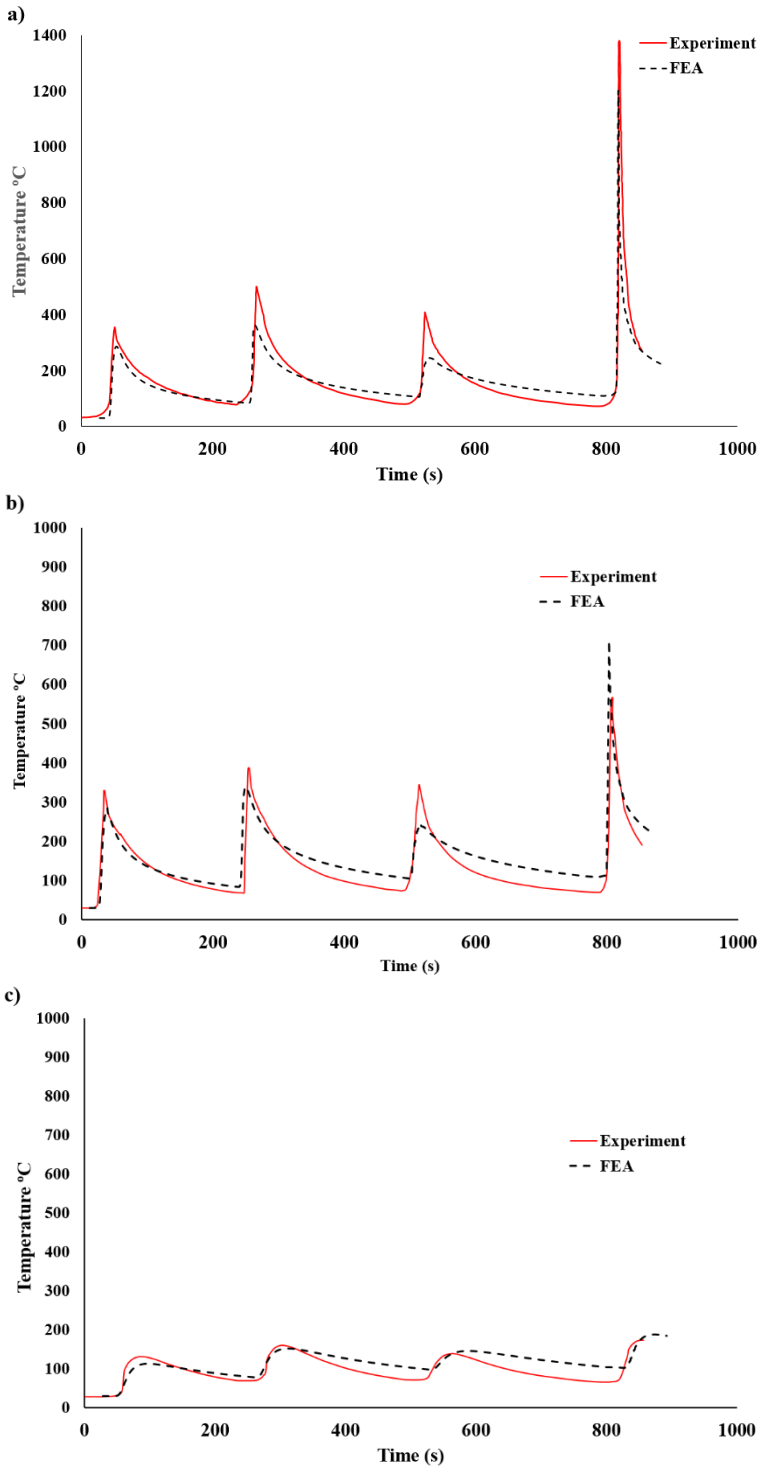

Figure 4.7: Comparison between simulated and measured transient temperatures on butt welded plate with the short weld; a) Thermocouple 4 mm away from the weld, b) Thermocouple 7 mm away from the weld and c) Thermocouple 20 mm away from the weld

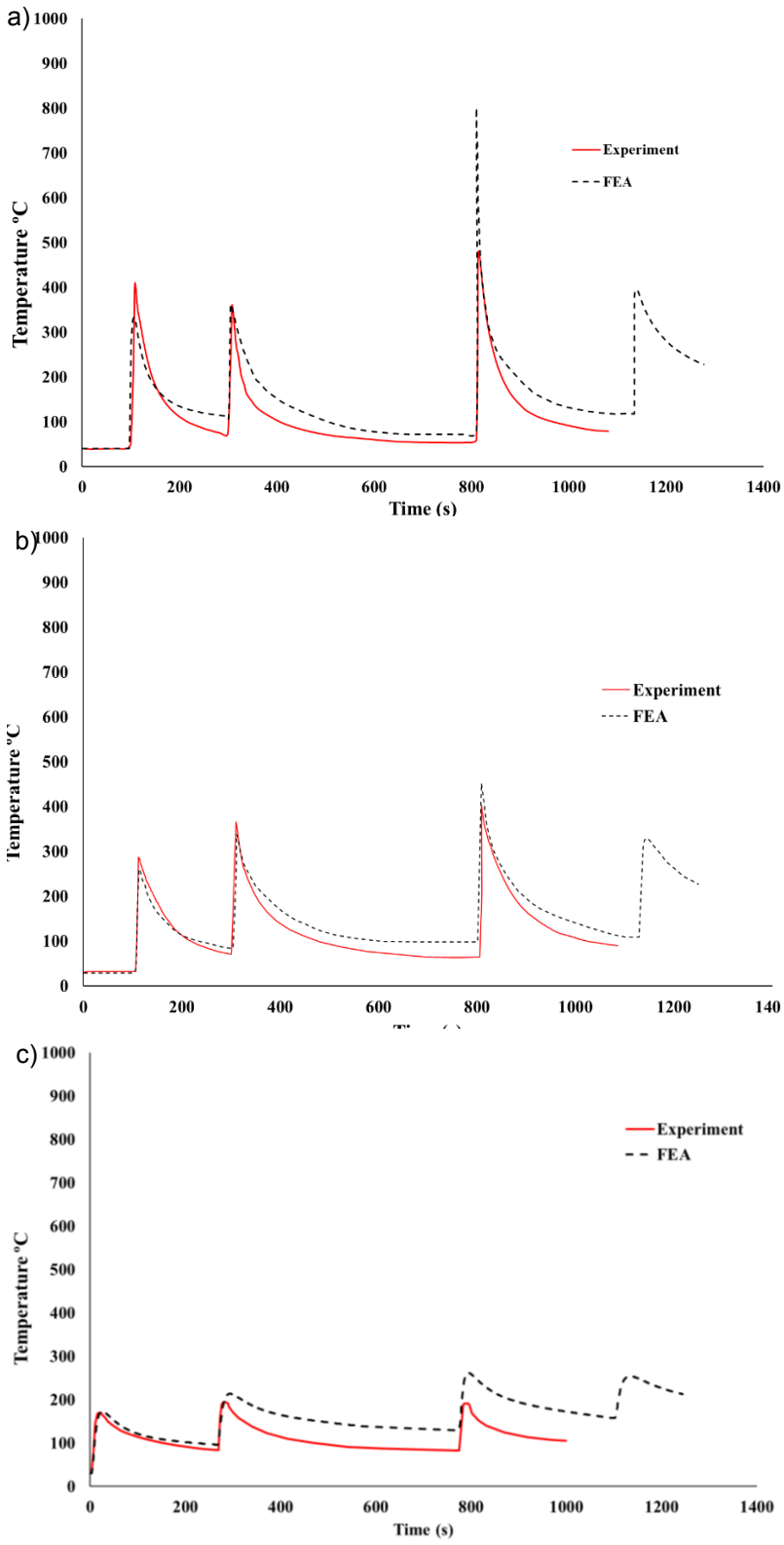

Figure 4.8: Comparison between simulated and measured transient temperatures on Butt welded plate with the long weld; a) Thermocouple 4 mm away from the weld, b) Thermocouple 7 mm away from the weld and c) Thermocouple 15 mm away from the weld

On the butt-welded plate with the long weld (Figure 4.8), the temperatures were measured from thermocouples close to the weld groove edge (4mm, 7mm,15mm) and compared with FE simulations. The comparison is only made up to three passes as the experimental set-up could not capture thermal histories after the third pass. As seen in Figure 4.8a at 4mm, the peak temperatures predicted were much higher than the experimental data. The high values obtained from the thermocouple could be due to the molten weld metal spatter close to the fusion line, which is not considered in the FE model.

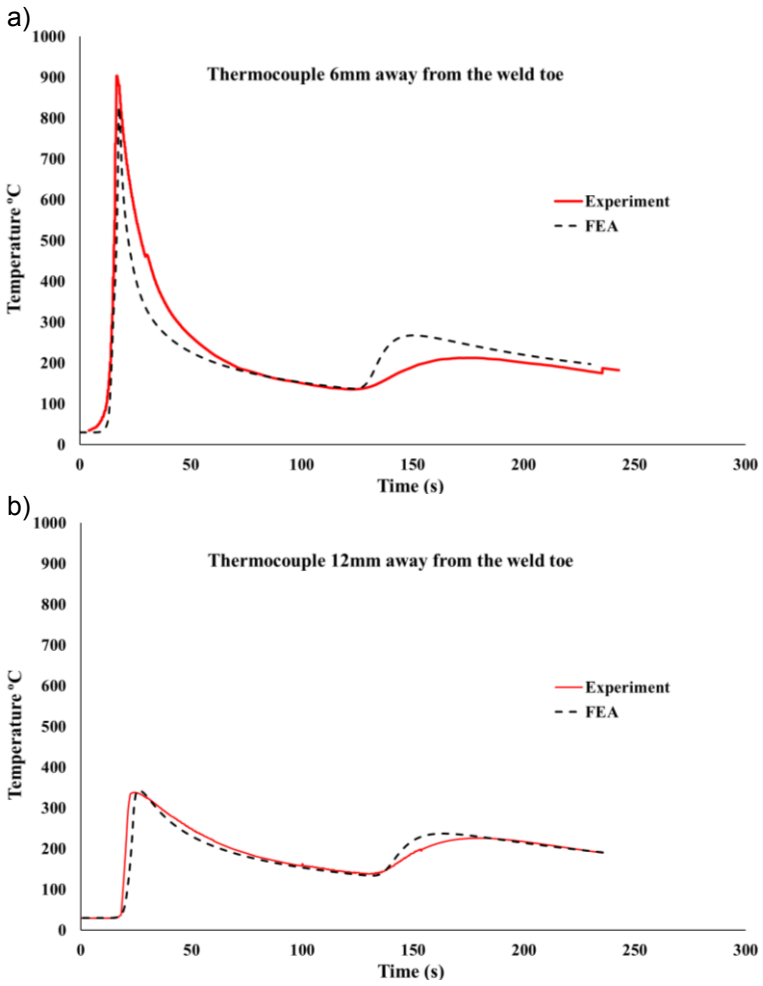

Figure 4.9: Comparison between simulated and measured transient temperatures on fillet welded plate with the short weld; a) Thermocouple 6 mm away from the weld toe and, b) Thermocouple 12 mm away from the weld toe

On the fillet-welded plate with the short weld (Figure 4.9), the temperatures measured from thermocouples close to the weld toe at 6mm and 12mm (position of thermocouples with respect to the weld toe was measured after welding) are compared with FE simulations. The FE simulation slightly over-predicted the maximum temperature at 6mm away from the weld toe. The predictions at 12mm away from the weld toe agrees very well with the experimental measurements.

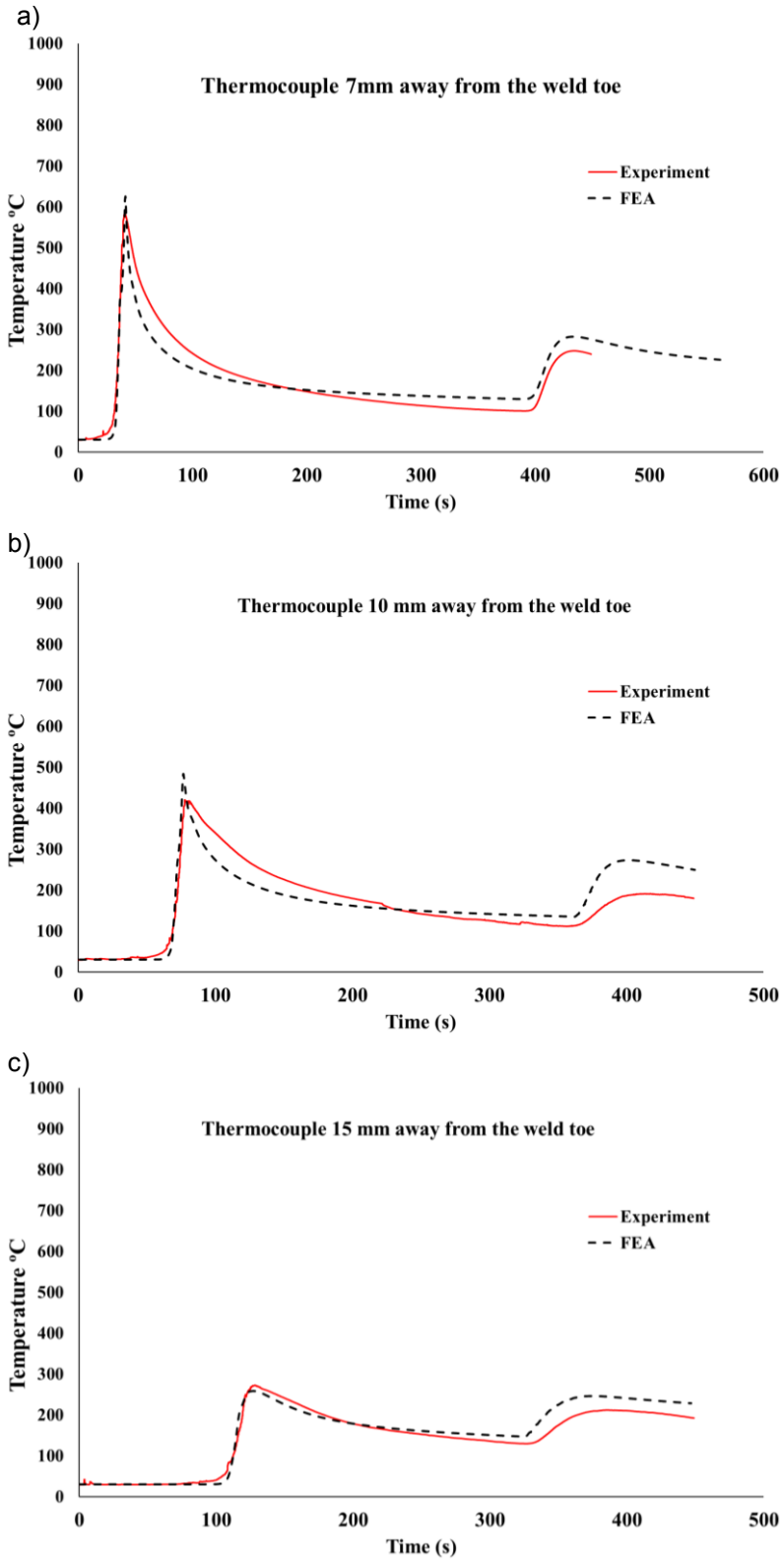

Figure 4.10: Comparison between simulated and measured transient temperatures on fillet welded plate with long weld; a) Thermocouple 7 mm away from the weld toe, b) Thermocouple 10 mm away from the weld toe, and, c) Thermocouple 15 mm away from the weld toe

On the fillet-welded plate with the long weld (Figure 4.10), the temperatures measured from thermocouples close to the weld toe at 7mm, 10mm and 15mm are compared with the FE simulations. The FE simulation slightly over-predicted the maximum temperature at 7mm and 10mm away from the weld toe. The predictions at 15mm away from the weld toe agree very well with the experimental measurements.

4.6 Simulation of EDM cutting

Following thermal history validation of each weld simulation, the mechanical model was run with the corresponding boundary conditions obtained from the experiments. As mentioned in Chapter 3, the welded specimens were subjected to EDM cutting to prepare for mechanical loading before residual stresses in the plates were measured. In order to capture the effect of EDM cutting as well in the as-welded residual stress, an additional simulation of EDM cutting was performed on the mechanical weld simulation models of each specimen. 3D 8-node linear brick elements were used in this analysis. To implement EDM cutting in the numerical model, a separate model was developed in which the stress data obtained from the weld model were fed to the new FE model. There are three points to be noted in the case of these simulations:

I. The cutting was simulated by FEA using the element removal technique: - The cutting process was simulated using the model change capability in ABAQUS where the elements corresponding to the cut region were deactivated in a controlled manner. The sequence of element removal was obtained from the actual EDM cutting. The boundary conditions in each simulation were based on the clamping arrangement that existed during EDM cutting.
II. The mesh used for EDM cutting is different from the mesh details used in the mechanical weld model analysis: - In order to introduce element removal in the model, the mesh details need to be changed due to the required extra partitioning when compared to the weld simulation model. The partitioning and resulting regions to be removed for both the fillet and the butt-welded specimens are shown in Figure 4.11. Each of the regions shown in Figure 4.11 was removed in a series of steps. The resulting geometry of the FE model after EDM cutting for each specimen is shown in Figure 4.12.

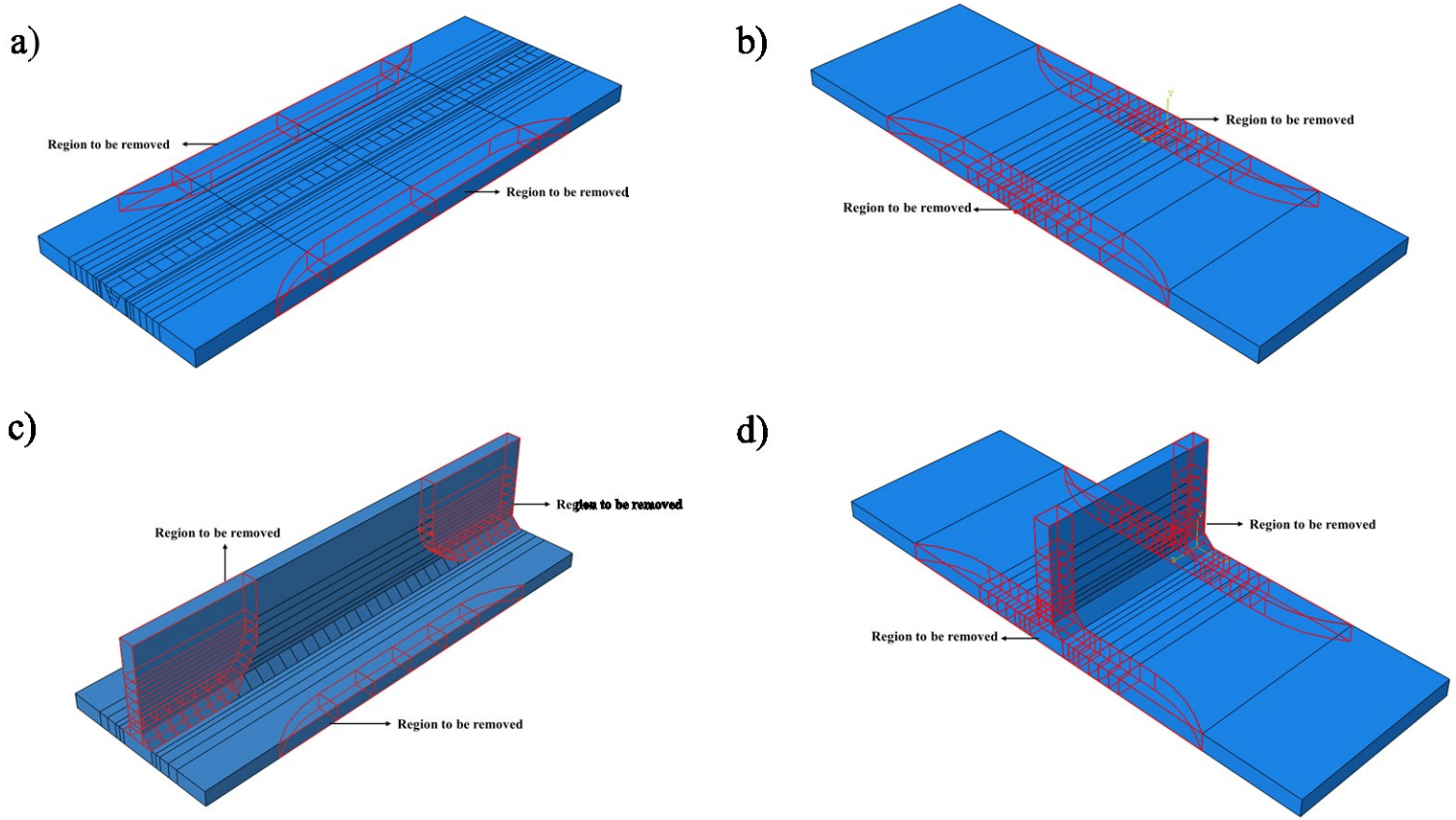

Figure 4.11: Partitioning and cutting region in the welded plate model for the simualtion of EDM cutting: a) Butt welded plate with the long weld, b) butt welded plate with the short weld, c) fillet welded plate with the long weld and, d) fillet welded plate with the short weld.

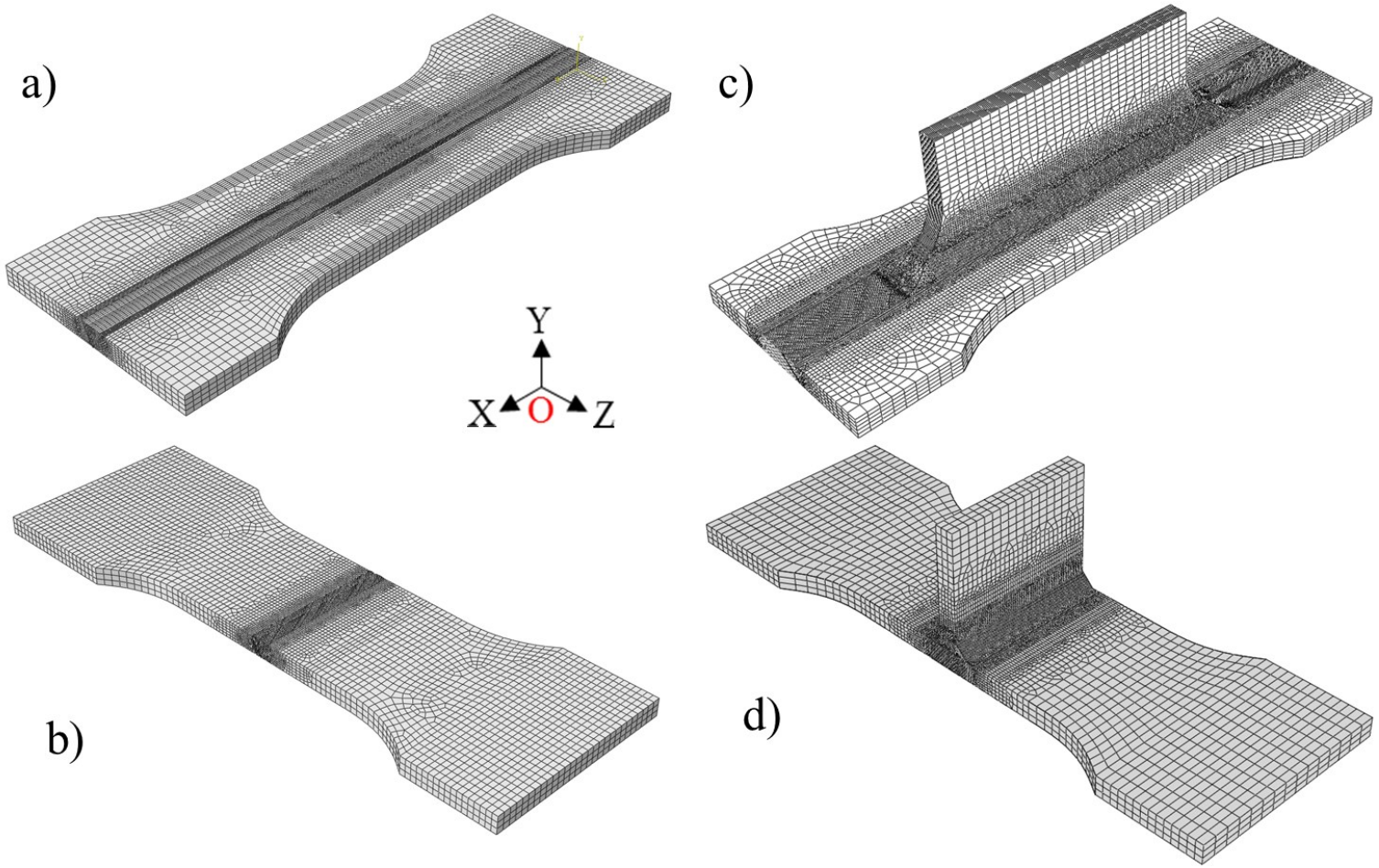

Figure 4.12: Model geometry after implementing EDM cutting simulation on the mechanical weld simulation model: a) Butt welded plate with long weld, b) butt welded plate with short weld, c) fillet welded plate with long weld and, d) fillet welded plate with short weld.

III. The as-welded stress data were mapped onto the newly meshed EDM cut model using solution a mapping technique: - Prior to cutting simulation in the mechanical weld model, in order to simulate the relaxation in residual stress (if any) during cutting, the as-welded residual stress data from the previous weld model should be mapped onto the new model. Mapping a solution from one mesh to another was possible with ABAQUS using a map solution technique. The map solution technique works well, provided that the meshes are sufficiently fine. Here the solution was mapped by interpolating the solution onto the new mesh from the output databases generated with the old mechanical weld model mesh. An initial step called an equilibrium step, is included to allow Abaqus to check for equilibrium after this interpolation has been done. By default, Abaqus/Standard resolves the stress unbalance linearly over the step.

4.7 Predicted and measured residual stress

Predicted welding residual stresses in the longitudinal and transverse directions at the measurement plane as defined in Chapter 3 for each specimen were validated with the stress profiles obtained from the neutron diffraction measurement in this section.

4.7.1 Residual stresses in the butt welded plates

As mentioned in Chapter 3, residual stress components in three orthogonal directions with respect to the butt welded plates were measured on the plane shown in Figure 3.17a and 3.17b. Numerical predictions of the transverse and longitudinal residual stress values from the weld model at the same locations as the neutron diffraction measurements (y = 10.2 mm and y = 2.5 mm) were compared with the experimental values determined from neutron diffraction.

4.7.1.1 The butt-welded plate with the short weld

Figure 4.13a and 4.13b compares the longitudinal and transverse residual stresses in the line scan ay Y=10.2 and 2.5 mm from experimental measurements and numerical model in the butt-welded plate with the short weld. The longitudinal residual stress predicted in the weld model follows a similar trend to the experimental measurements. However, the predicted values from the weld model were compressive away from the weld centre when compared to the near zero and slightly tensile values determined from the experiments. Similarly, the transverse residual stress predicted in the weld model follows a similar trend to the experimental measurements. The transverse stresses at y=10.2mm were

underpredicted by about 70MPa and the stresses at y=2.5mm were in very good agreement with the experimental values.

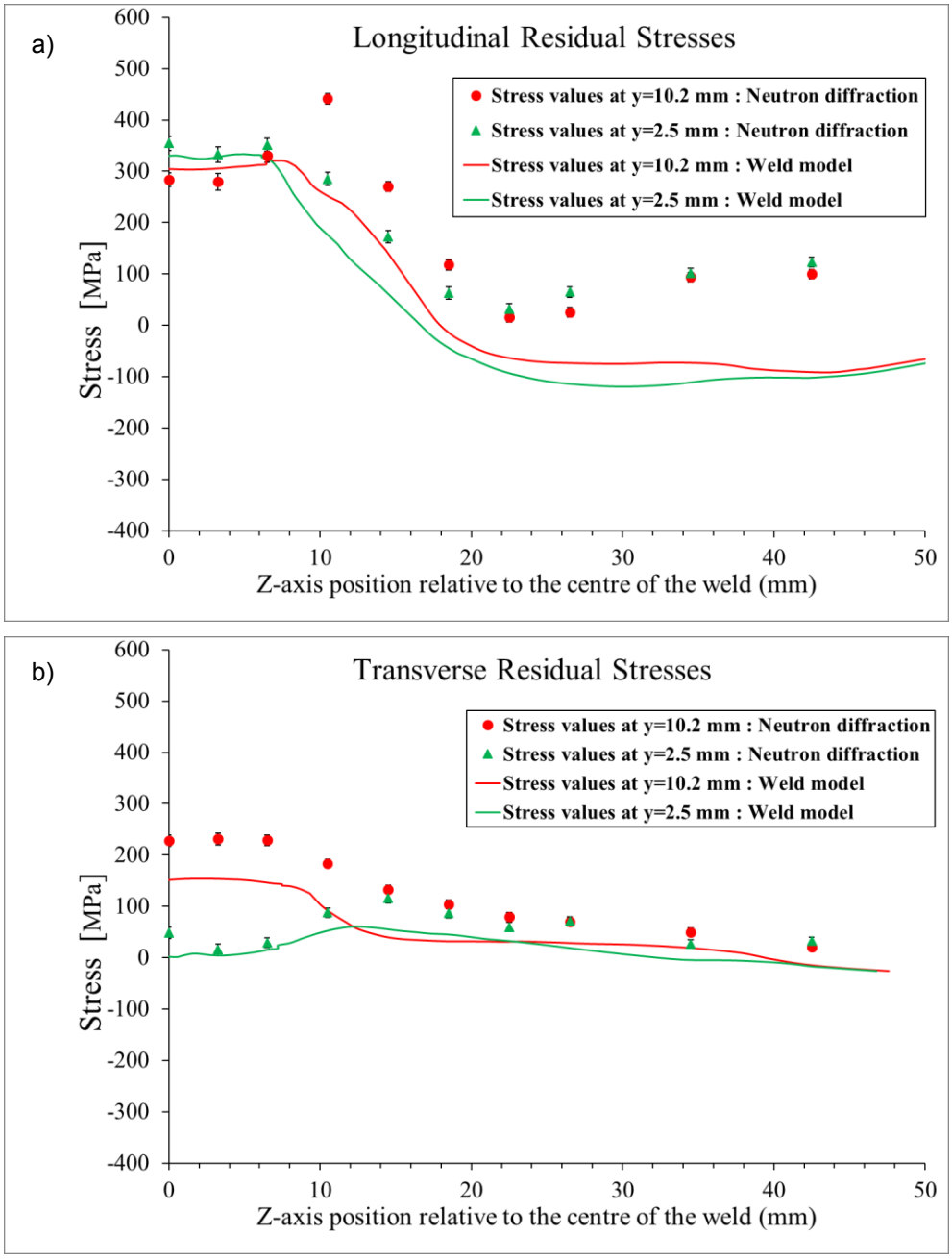

Figure 4.13: Comparison between predicted residual stresses and residual stress measured from Neutron diffraction in butt-welded plate with short weld: a) Longitudinal residual stress, and b) transverse residual stress.

4.7.1.2 *The butt-welded plate with the long weld*

Figure 4.14a and 4.14b compare the longitudinal and transverse residual stresses in the line scan at Y=10.2 and 2.5 mm from experimental measurements and numerical model in the butt-welded plate with the long weld.

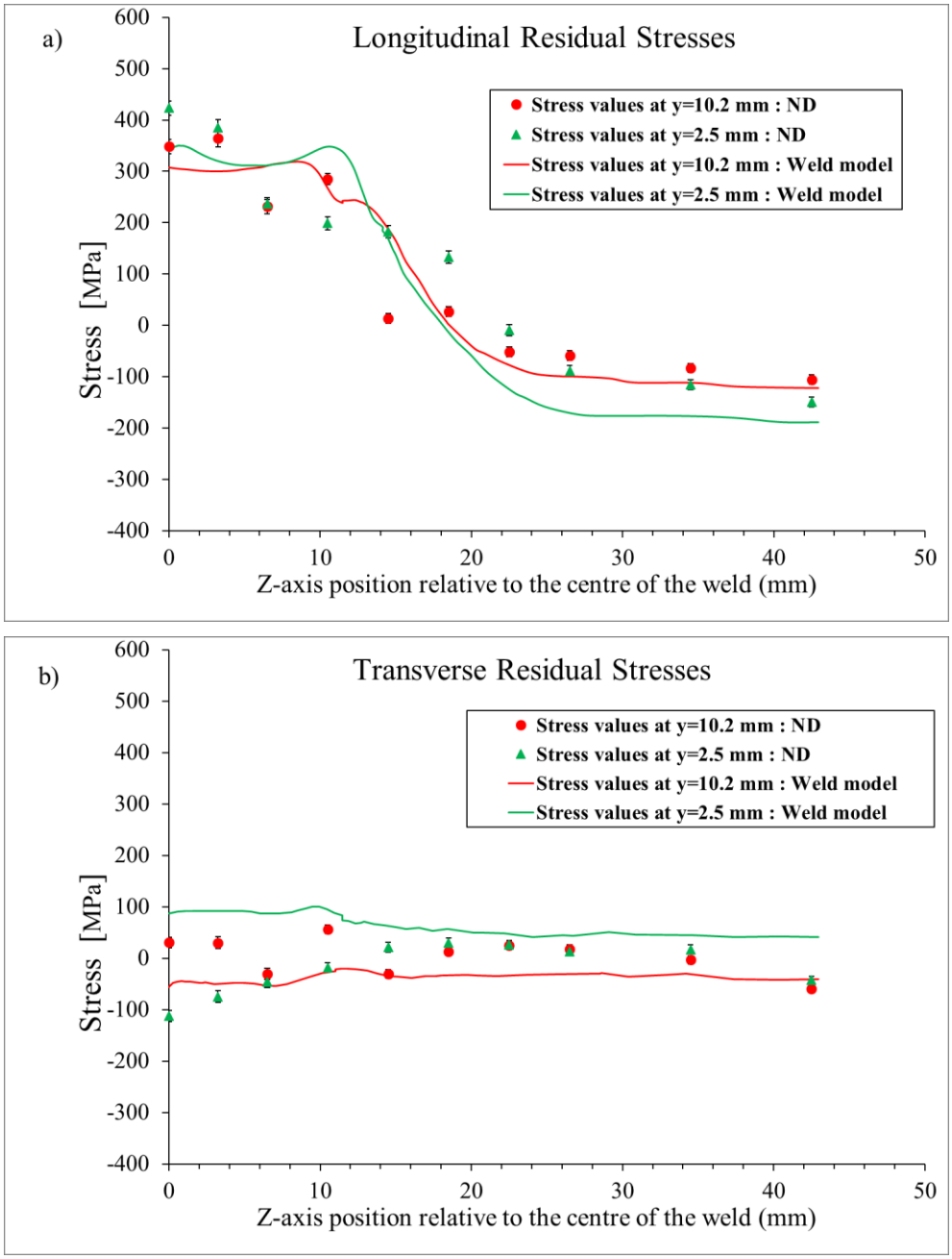

Figure 4.14: Comparison between predicted residual stresses and residual stress measured from Neutron diffraction in butt-welded plate with long weld, a) Longitudinal residual stress, and b) transverse residual stress

Residual stresses from butt-welded plate with the long weld (Figure 4.14) shows a similar pattern when compared to the butt-welded plate with the short weld (Figure 4.13). The differences between the butt-welded plates with the short and long weld was in geometric features and boundary conditions. The welding parameters were the same in both cases. The longitudinal residual stress predicted in the weld model agreed well with the experimental measurements. However, the transverse stresses predicted at y=10.2mm slightly overpredicted the stresses in the weld and HAZ zone and stresses at y=2.5mm were predicted to be completely compressive.

4.7.2 Residual stresses in fillet welded plates

Fillet welded plates consisted of a horizontal plate and a vertical plate as defined in Section 3.7.2. Residual stress components in three orthogonal directions with respect to the horizontal and the vertical plates were measured on the plane shown in Figure 3.21a and 3.21b. Numerical predictions of the transverse and longitudinal residual stress values from the weld model at the same locations as the neutron diffraction measurements were compared with the experimental values determined from neutron diffraction (Figure 4.15 to 4.18). The locations y=2.5 and y=10.2mm were considered in the horizontal plate and y=15.2 and y=25.2mm were considered in the vertical plate.

The as-welded residual stresses determined from neutron diffraction in both longitudinal and transverse directions did not have a definite pattern as in the case of the butt-welded plates.

4.7.2.1 Fillet welded plate with short weld

Figure 4.15a shows the longitudinal residual stresses measured from neutron diffraction and predicted by the weld model at line scans y=10.2 and 2.5mm. The longitudinal residual stress in the horizontal plate below the weld toe on both sides (y =10.2, z = –15 and z = +15mm) was tensile (Figure 4.15a). Particularly at z = –15mm, tensile stress as high as the yield strength was determined from neutron diffraction (Figure 4.15a). High tensile stresses were also noted on the second line scan (y = 2.5mm) at z = –15mm and z = –9mm. However, in the line scan at y=15.2mm, high tensile stress of about 270MPa was calculated at z= 9mm, and for the line scan corresponding to y = 25.2mm, high tensile stress of about 260MPa was determined at z= 4mm (Figure 4.15b).

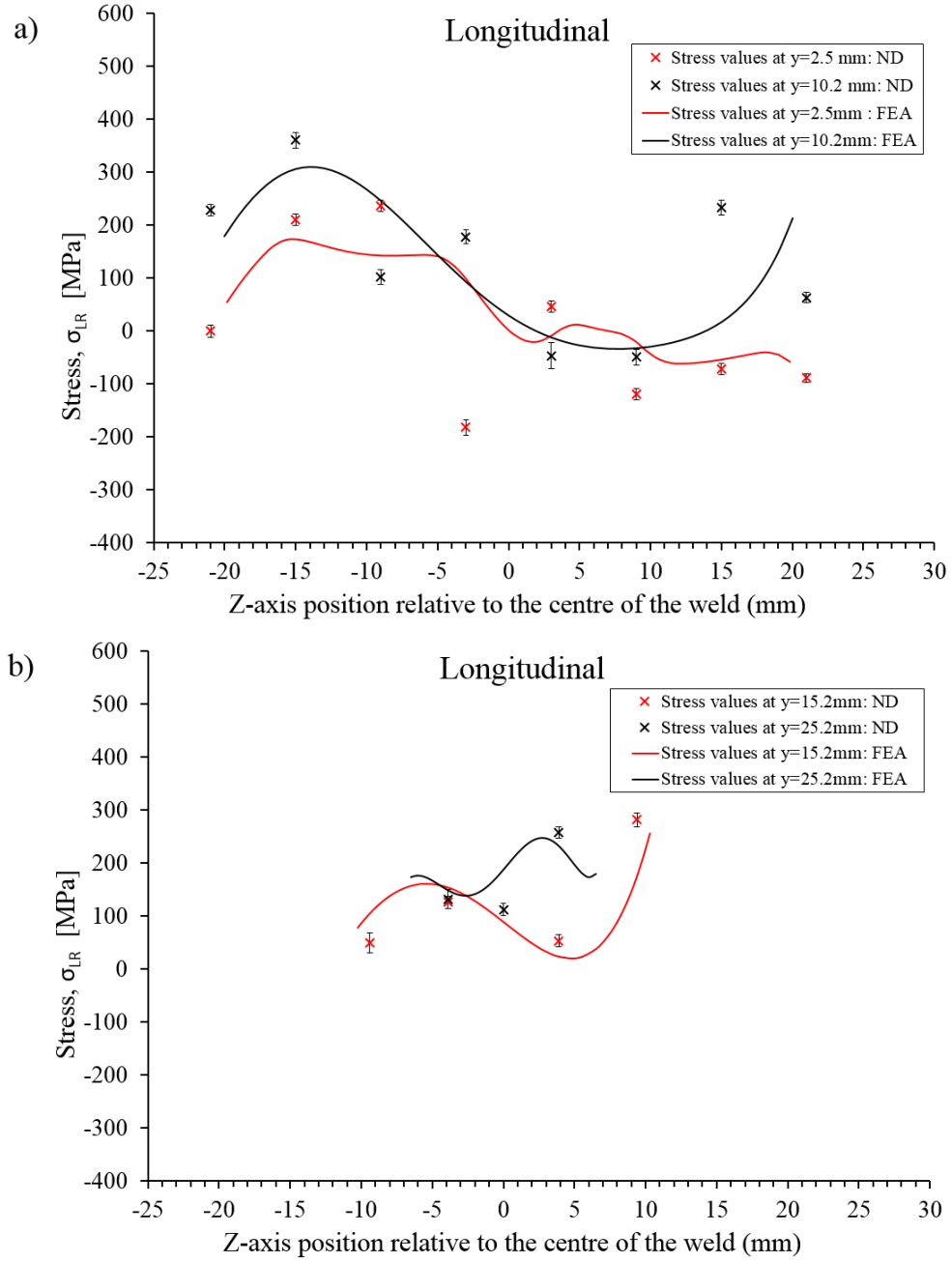

Figure 4.15: Comparison between predicted stresses and residual stress measured from neutron diffraction in fillet welded plate with short weld, a) Longitudinal residual stress in the horizontal plate, and b) longitudinal residual stress in the vertical plate.

Figure 4.16a shows the transverse residual stresses measured from neutron diffraction and predicted by the weld model at line scans y=10.2 and 2.5mm. The transverse residual stress on the horizontal plate was calculated as fully tensile in the line scan corresponding to y=10.2mm. At y=10.2mm, a peak tensile residual stress of about 310MPa was observed at z= –21mm and z = –15mm. In the line scan corresponding to y=2.5mm, a maximum of 190MPa was observed with the majority of the points being only slightly tensile. On the vertical plate, in the line scan corresponding to y=15.2, only slightly tensile (below

90 MPa) stresses were noted and in the line scan corresponding to y=25.2, compressive stresses were calculated (Figure 4.16b).

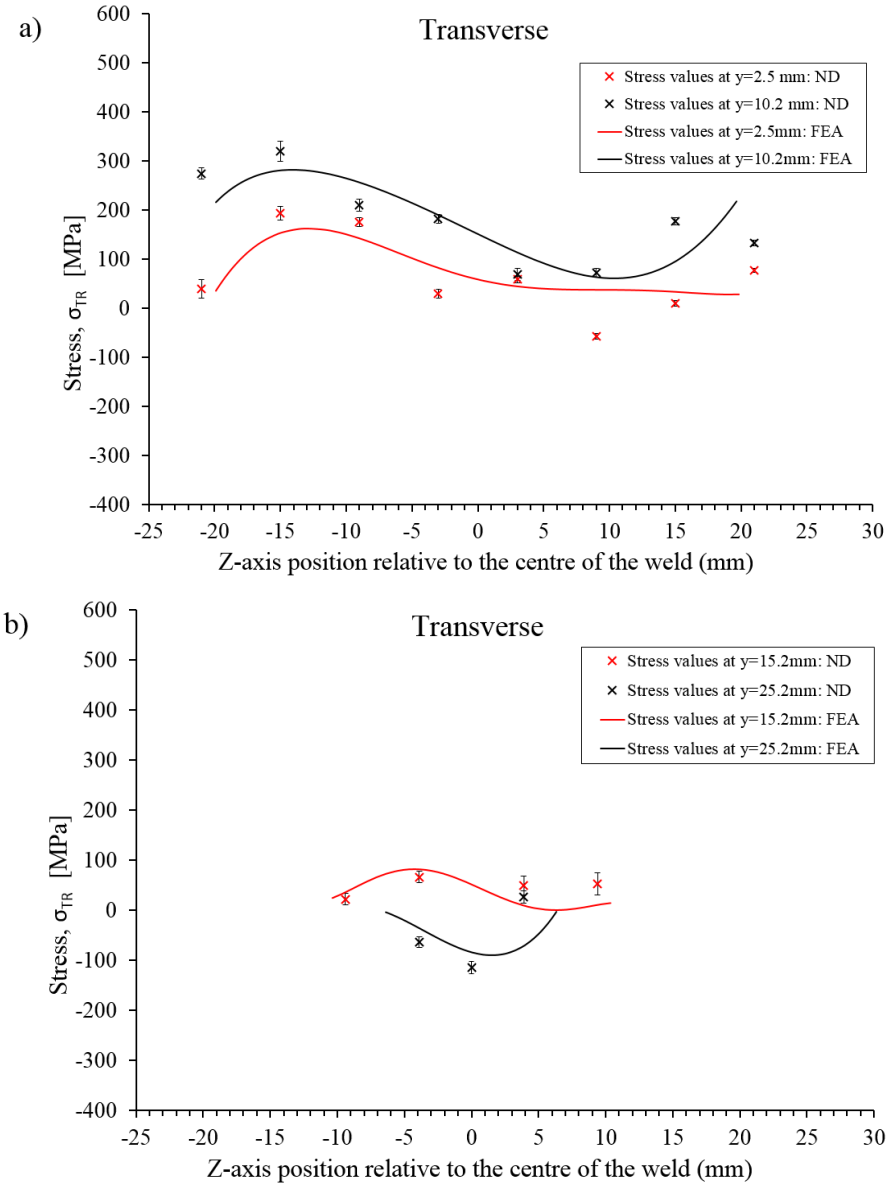

Figure 4.16: Comparison between predicted residual stresses and residual stress measured from Neutron diffraction in fillet welded plate with short weld: a) Transverse residual stress in the horizontal plate and, b) transverse residual stress in the vertical plate.

The fillet weld simulation captures the trend of residual stress distribution well. Predicted longitudinal and transverse residual stress in the fillet welded plate had a non-symmetric residual stress profile as shown in Figure 4.15 and 4.16. The comparisons of the predicted residual stress profiles with the measured values had a trend, passing through the vicinity of the measured values, however, there exist a few exceptions (a compressive longitudinal stress value of about 170MPa at z = –3mm and a tensile longitudinal stress value noted at z = 15.5 mm) that were away from the predicted values.

4.7.2.2 *Fillet welded plate with long weld*

Figure 4.17a shows the longitudinal residual stresses measured from neutron diffraction and predicted by the weld model at line scans y=10.2 and 2.5mm. The longitudinal residual stress measured on the horizontal plate in the line scan corresponding to y = 10.2mm were predominantly compressive with the exception at z = –9mm and z = +15mm where a tensile stress of about 120MPa was calculated. In the line scan corresponding to y=2.5mm, all calculated values were compressive. On the vertical plate, all the measured values were tensile with a peak tensile value of 270MPa in both y=15.2 and y=25.2mm line scans.

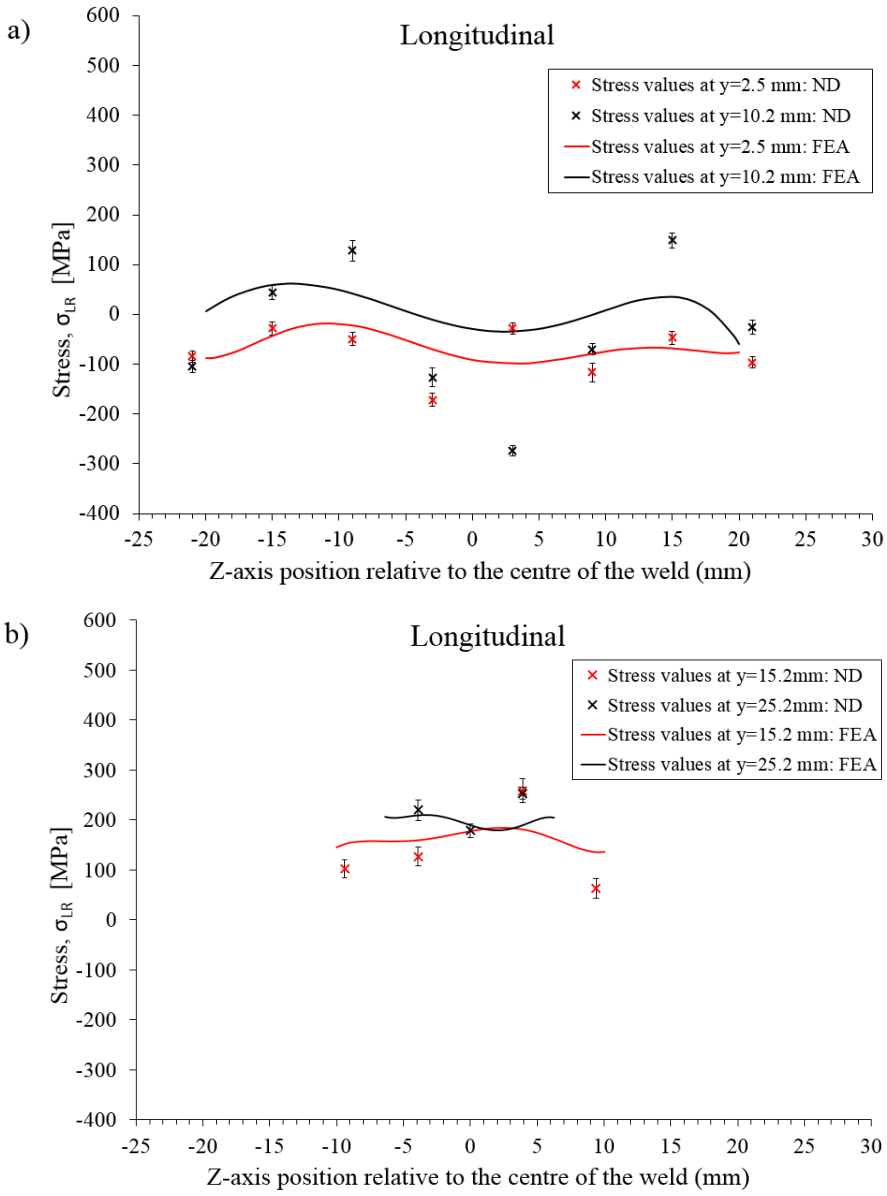

Figure 4.17: Comparison between predicted residual stresses and residual stress measured from Neutron diffraction in fillet welded plate with long weld: a) Longitudinal residual stress in the horizontal plate, b) longitudinal residual stress in the vertical plate.

Figure 4.17b shows the transverse residual stresses measured from neutron diffraction and predicted by the weld model at line scans y=10.2 and 2.5mm. The transverse residual stress on the horizontal plate was calculated as fully compressive in both line scans (y=10.2mm and y=2.5mm). A peak compressive residual stress of about –200MPa was observed at z= –21mm and z = –15mm. On the vertical plate, in the line scan corresponding to y=15.2, only slightly tensile (a peak value of 100 MPa) stresses were noted, and in the line scan corresponding to y=25.2, a peak tensile value of 180MPa was calculated at z=+4mm.

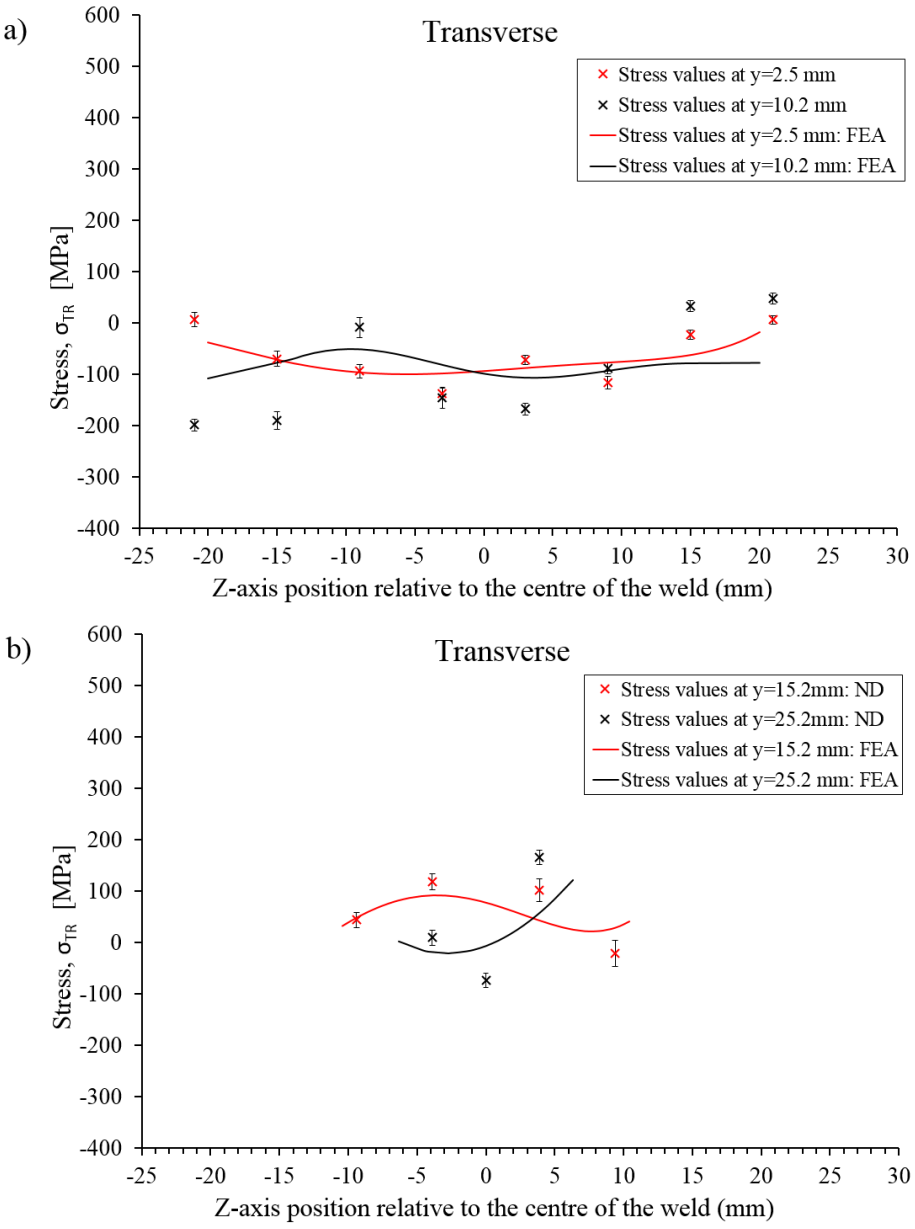

Figure 4.18: Comparison between predicted residual stresses and residual stress measured from Neutron diffraction in fillet welded plate with long weld: a) Transverse residual stress in the horizontal plate and, b) transverse residual stress in the vertical plate.

Similar to the fillet welded plate with the short weld, the predicted longitudinal and transverse residual stress in the fillet welded plate had a non-symmetric residual stress profile as shown in Figure 4.17 and 4.18. The predicted residual stresses in the same location as the measurement line scans agree well with the trend of residual stress values from neutron diffraction. The comparisons of the predicted residual stress with the measured values had a profile passing through most of the measured longitudinal and transverse residual stresses.

4.8 Discussions

4.8.1 Heat transfer analysis

Numerical prediction of the thermal history of the welding process in a weld model is essential in achieving a good residual stress prediction. To enable an accurate thermal analysis, parameters of the welding process such as voltage, current, inter-pass temperature and torch travel speed were noted during the actual welding process in each specimen. These parameters determined the amount of heat input and cooling period in each pass.

Thermocouples spot welded at various locations enabled the validation of the thermal history in the same positions in the FEA model. However, due to the spatter from the weld pool, welding chamber atmosphere and inevitable and/or unexpected set-up errors, there were some undesirable results in terms of a few wrong data from the thermocouples. In each specimen, multiple thermocouples at the same distance away from the weld but at different longitudinal positions were employed. The validation of thermal cycles in this work has been carried out with the best thermal history obtained from the experiment. Particularly, in the case of thermocouples close to the weld fusion line, molten spatter was expected to fall on the thermocouples. Placement of thermocouples at the same distance away from the weld at multiple longitudinal positions aided at least one result from at least one location away from the weld.

In this work, the thermal cycle predicted from the FEA model was in a good agreement with the measurement results away from the welds. However, near-weld values did not match well with those measured using thermocouples. It was found that the R-type thermocouples were not well installed. At locations 10mm and further away from the weld, there are better agreements between the results of measurement and simulation.

The input heat flux applied on each specimen was slightly revised in order to achieve a similar weld cross section as the macrographs obtained from the weld plates.

Although welding process parameters were all recorded, enabling a good approximation of heat flux, it was still challenging to achieve precise thermal solutions due to the influence of temperature-dependent material properties.

4.8.2 Mechanical stress analysis

As mentioned in the preceding sections, the temperature-dependent material properties used for the mechanical analysis were not entirely accurate. The material data for DH 36 was obtained for DH 36 material, and the weld material was assumed to have the same properties except for the yield strength, which was determined from experiments.

As the numerical modelling of the welding process is not the main objective of this work, instead the process simulation was the best route towards achieving a full stress field in the FE models for the elastic shakedown and residual stress redistribution analysis, so phase transformation was ignored, and a simple isotropic strain hardening mechanism was considered.

During welding, a sequence of repeated sudden heating and cooling is introduced into the weld plate. The thermal gradient, as a result, acts as cyclic tensile and compressive loading to the material and induces stress-strain behaviour with plastic deformation and hence strain hardening. An isotropic hardening model tends to overpredict residual stresses (RW.ERROR - Unable to find reference:292; L. Wei and M. Gallegillo 2012; Smith et al. 2012; Yaghi et al. 2010). It is suggested that a combined isotropic-kinematic strain hardening model is more applicable for the actual hardening behaviour of the material (Smith et al. 2012). However, due to lack of material data and the complexity involved, this hardening behaviour was not modelled in this work.

The residual stress prediction is also affected by the phase transformation due to the temperature history (Hamelin et al. 2014). For DH 36, a ferritic steel studied in this work, the residual stress field, especially the transverse residual stress component can have influence from volume changes during the phase transformation from austenite to bainite/martensite (Deng and Murakawa 2006; O'Meara, Smith and Francis 2015).

Although assumptions and approximations were introduced in the weld process simulations, the overall trend of stress profiles predicted from the FEA model were in good agreement with the measured results. The minor difference between the results

predicted using welding simulation and experimental measurement may be due to the reasons stated above along with experimental errors, including those arising from the EDM cutting and neutron diffraction set-up.

4.9 Residual stress mapping

Over the last few decades, with the advancement in computational capacity, there have been hundreds of papers on arc weld modelling, mainly to predict residual stresses and hence to optimise welding process parameters. Weld modelling essentially helps to replace, to an extent, the experimental work required in the development of new welding procedures. However, fracture and fatigue assessments, which require accurate weld residual stresses over a relatively small region of interest, often require welding process simulations, which can be complicated and consume huge computational resource.

A residual stress mapping method was implemented which is expected to reduce computation time while preserving the accuracy in determining the stress state in the region of interest. The technique was demonstrated on the butt-welded plate with the short weld.

4.9.1 Background on residual stress mapping

On top of the experimental methods and deformation process modelling approach, another method for determining residual stress is to use a predictive method based on extracting a distribution of eigenstrain or inherent strains, as introduced by Mura (Mura 1987), based on experimental measurements. The term eigenstrains as used by Mura consists of all inelastic strains formed in a body due to various mechanisms such as phase transformation, purely-plastic flow and thermal expansion. Reißner (Reißner 1931) was the first to use such inelastic strains to discuss misfit strains. Recently, Lee et al. (Lee et al. 2018) used a simpler definition based on elastic energy, since residual stresses are formed due to the external and/or internal constraints in the eigenstrain region. One example of the application of the eigenstrain technique is the inverse eigenstrain method used by Jun et al. (Jun and Korsunsky 2010) in which eigenstrains were estimated by analysing limited measurements. An eigenstrain distribution can be determined from an incomplete residual stress distribution in such a way that it is represented by a set of basic functions, which is called the inverse problem. (Korsunsky 2009) performed finite element (FE) analysis in conjunction with minimisation of error with respect to experimental values and determined the complete eigenstrain distribution. Kartal et al.

(Kartal et al. 2008) used displacement measured from multiple cuts during contour measurements to reconstruct residual stress using eigenstrain approach. A similar technique derives stress profiles that are analytically determined using both Airy's stress functions and experimental measurements. Farrahi et al. (Farrahi, Faghidian and Smith 2009) used this method to reconstruct residual stresses in an axisymmetric cylinder. Later, Farrahi et al. (Farrahi, Faghidian and Smith 2010) extended this study to reconstruct residual stresses in a welded plate and Faghidian et al. (Faghidian et al. 2012) reconstructed residual stresses introduced in a steel beam by elastic-plastic bending.

Ficquet (Ficquet 2007) introduced an iterative mapping procedure using predefined stress values in the FE analysis to estimate the complete residual stress field in a butt-welded plate with limited measurement values. Later, Do et al. (Do, Serasli and Smith 2013) mapped residual stresses on welded components where residual stresses were experimentally determined from deep-hole drilling measurements. This technique was also used by Coules et al. (Coules et al. 2014) for a geometry in which the incompatibility is confined in a small portion. They noted that the stress function method and inverse problems are most helpful if the residual stress or eigenstrain distributions can be parametrised accurately. However, the stress values mapped in these studies can lead to non-unique solutions in an FE solver due to the imbalance introduced with the stresses of a small area. One of the inherent properties of residual stresses is that they should be self-balanced in the absence of any external loads. In almost every residual stress measurement experiment, an area with high residual stress is prioritised more than the areas with low residual stress. Therefore, the measurement data are usually incomplete. This leads to an unbalanced stress field if the data from the measurement are input into an FE model. The effect of incomplete residual stress measurements on the evaluation of stress intensity factor has been studied by Bao et al. (Bao, Zhang and Yahaya 2010).

4.9.2 Governing equations in residual stress mapping

In contrast to most earlier studies, this work estimates a distribution by fitting experimental measurements of residual stresses for butt joints based on a profile introduced by (Masubuchi and Martin 1966) which is given below.

$$\sigma_{res} = \sigma_m[1 - (\frac{z}{f_1})^2][e^{-0.5\,(\frac{z}{f_2})^2}] \qquad (4.9)$$

where σ_{res} is the residual stress component, σ_m is the maximum residual stress (as high as the yield strength of the weld material in some cases). The parameters f_1 and f_2 define

the width of the tension zone and compression zone of the residual stress component. Equation 4.9 in its original form as introduced by (Masubuchi and Martin 1966) has $f_1 = f_2 = f$. Figure 4.19 shows the butt-welded specimen model. The coordinate z is defined as the distance across the weld as shown in Figure 4.19a. A residual stress profile was estimated based on experimentally measured residual stress values across the weld by solving f_1 and f_2 such that the estimated profile represents the measured values. Here it is assumed that the transverse and longitudinal components of residual stress are independent of the through-thickness axis of the plate.

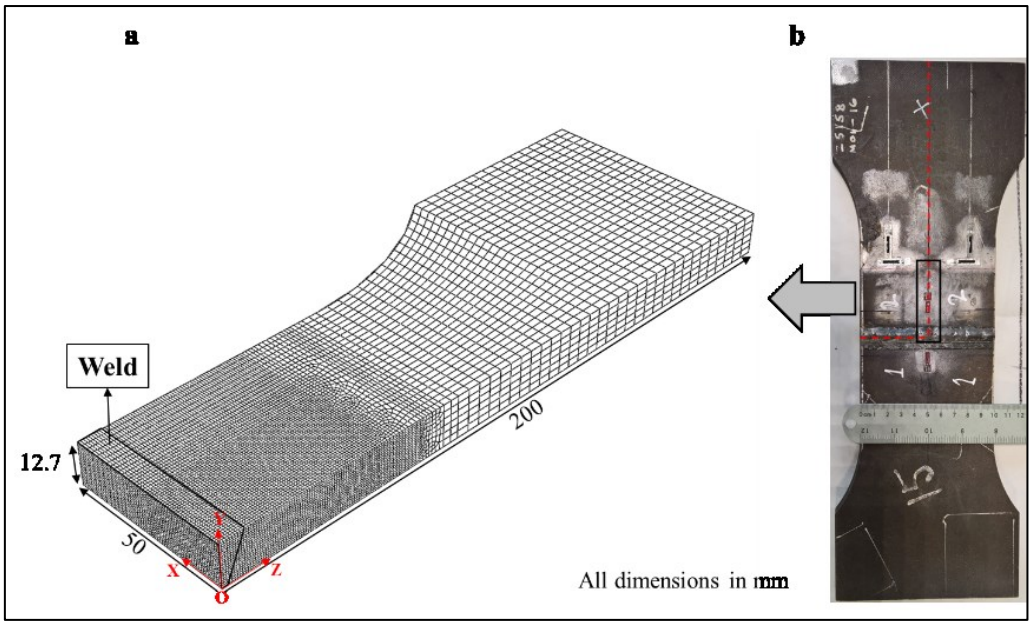

Figure 4.19: The butt-welded specimen design used in residual stress mapping FEA: a) Quarter Finite Element (FE) model showing the dimension and meshing used for all iterations, and b) photograph of the butt-welded plate.

For a body containing residual stresses to be in equilibrium, based on small deformation theory, the body must satisfy the small-strain incompatibility condition. In the small deformation approximation, the total strain can be represented as the sum of elastic strain ($\boldsymbol{e}$) and eigenstrain (ε^*) as given below:

$$\varepsilon = e + \varepsilon^* \qquad (4.10)$$

Hence, in a linearly elastic material, the incompatibility introduced by eigenstrains can be defined as (Korsunsky 2009):

$$\frac{\partial^2 e_{xx}}{\partial y^2}+\frac{\partial^2 e_{yy}}{\partial x^2}-2\frac{\partial^2 e_{xy}}{\partial x\partial y}=\Xi_1=-\frac{\partial^2 \varepsilon^*{}_{xx}}{\partial y^2}-\frac{\partial^2 \varepsilon^*{}_{yy}}{\partial x^2}+2\frac{\partial^2 \varepsilon^*{}_{xy}}{\partial x\partial y}$$

$$\frac{\partial^2 e_{yy}}{\partial z^2}+\frac{\partial^2 e_{zz}}{\partial y^2}-2\frac{\partial^2 e_{yz}}{\partial z\partial y}=\Xi_2=-\frac{\partial^2 \varepsilon^*{}_{yy}}{\partial z^2}-\frac{\partial^2 \varepsilon^*{}_{zz}}{\partial y^2}+2\frac{\partial^2 \varepsilon^*{}_{yz}}{\partial z\partial y}$$

$$\frac{\partial^2 e_{zz}}{\partial x^2}+\frac{\partial^2 e_{xx}}{\partial z^2}-2\frac{\partial^2 e_{xz}}{\partial x\partial z}=\Xi_3=-\frac{\partial^2 \varepsilon^*{}_{zz}}{\partial x^2}-\frac{\partial^2 \varepsilon^*{}_{xx}}{\partial z^2}+2\frac{\partial^2 \varepsilon^*{}_{xz}}{\partial x\partial z} \qquad (4.11)$$

$$\frac{\partial^2 e_{xx}}{\partial y\partial z}+\frac{\partial}{\partial x}\left(-\frac{\partial e_{yz}}{\partial x}+\frac{\partial e_{zx}}{\partial y}+\frac{\partial e_{xy}}{\partial z}\right)=\Xi_4=-\frac{\partial^2 \varepsilon^*{}_{xx}}{\partial y\partial z}-\frac{\partial}{\partial x}\left(-\frac{\partial \varepsilon^*{}_{yz}}{\partial x}+\frac{\partial \varepsilon^*{}_{zx}}{\partial y}+\frac{\partial \varepsilon^*{}_{xy}}{\partial z}\right)$$

$$\frac{\partial^2 e_{yy}}{\partial x\partial z}+\frac{\partial}{\partial y}\left(\frac{\partial e_{yz}}{\partial x}-\frac{\partial e_{zx}}{\partial y}+\frac{\partial e_{xy}}{\partial z}\right)=\Xi_5=-\frac{\partial^2 \varepsilon^*{}_{yy}}{\partial y\partial z}-\frac{\partial}{\partial y}\left(\frac{\partial \varepsilon^*{}_{yz}}{\partial x}-\frac{\partial \varepsilon^*{}_{zx}}{\partial y}+\frac{\partial \varepsilon^*{}_{xy}}{\partial z}\right)$$

$$\frac{\partial^2 e_{zz}}{\partial x\partial y}+\frac{\partial}{\partial z}\left(\frac{\partial e_{yz}}{\partial x}+\frac{\partial e_{zx}}{\partial y}-\frac{\partial e_{xy}}{\partial z}\right)=\Xi_6=-\frac{\partial^2 \varepsilon^*{}_{zz}}{\partial x\partial y}-\frac{\partial}{\partial z}\left(\frac{\partial \varepsilon^*{}_{yz}}{\partial x}+\frac{\partial \varepsilon^*{}_{zx}}{\partial y}+\frac{\partial \varepsilon^*{}_{xy}}{\partial z}\right)$$

where $\Xi = [\Xi_1, \Xi_2, \Xi_3, \Xi_4, \Xi_5, \Xi_6]^T$ is the forcing term which represents the incompatibility or residual stress in the object. In a fully compatible body, the forcing term, Ξ, is equal to zero. For a residually stressed body, in the absence of external loading, equilibrium can be defined as:

$$div\ \sigma = 0 \qquad (4.12)$$

where σ is the stress tensor. For a linear-elastic material of stiffness tensor C, stress tensor can be defined using Hooke's law:

$$\sigma = C : e \qquad (4.13)$$

Equation 4.13 implies that the residual stress fields in a solid body can be determined using the eigenstrain distribution and the elastic properties. Combining Hooke's law and the compatibility equations in conjunction with the known stress field, the forcing term Ξ can be determined. Considering the first compatibility equation, for an isotropic and linearly elastic material, the forcing term can be defined as:

$$\Xi_1=\frac{1}{E}\left|\frac{\partial^2}{\partial y^2}\left(\sigma_{xx}-v(\sigma_{yy}+\sigma_{zz})\right)+\frac{\partial^2}{\partial x^2}\left(\sigma_{yy}-v(\sigma_{zz}+\sigma_{xx})\right)-2(1-v)\frac{\partial^2 \tau_{xy}}{\partial x\partial y}\right| \qquad (4.14)$$

where E is Young's modulus of the material, and v is Poisson's ratio. From Equation 4.14, it can be concluded that the stress distributions from the experiment can be used directly in the FE model instead of eigenstrain distribution to generate a complete stress field.

4.9.2.1 Target residual stress field from measurements

Measured residual stresses were used to estimate a stress distribution based on Equation 4.9. These distributions were used for the stress field reconstruction on the quarter FE model of the specimen shown in Figure 4.19a. Varying parameters in Equation 4.9 and minimising error against the measured values the residual stress distribution was estimated for both longitudinal and transverse residual stress. The stress distributions presented below are estimated as the profile of the measured longitudinal (σ_{LR}) and transverse (σ_{TR}) residual stresses, respectively.

$$\sigma_{LR} = 450\left[1-\left(\frac{z}{16}\right)^2\right]exp\left[-\frac{1}{2}\left(\frac{z}{15}\right)^2\right] \quad (4.15)$$

$$\sigma_{TR} = 230\left[1-\left(\frac{z}{22}\right)^2\right]exp\left[-\frac{1}{2}\left(\frac{z}{13}\right)^2\right] \quad (4.16)$$

where σ_{LR} and σ_{TR} are the estimated longitudinal and transverse residual stresses which are shown in Figure 4.20 and 4.21 respectively in the following section.

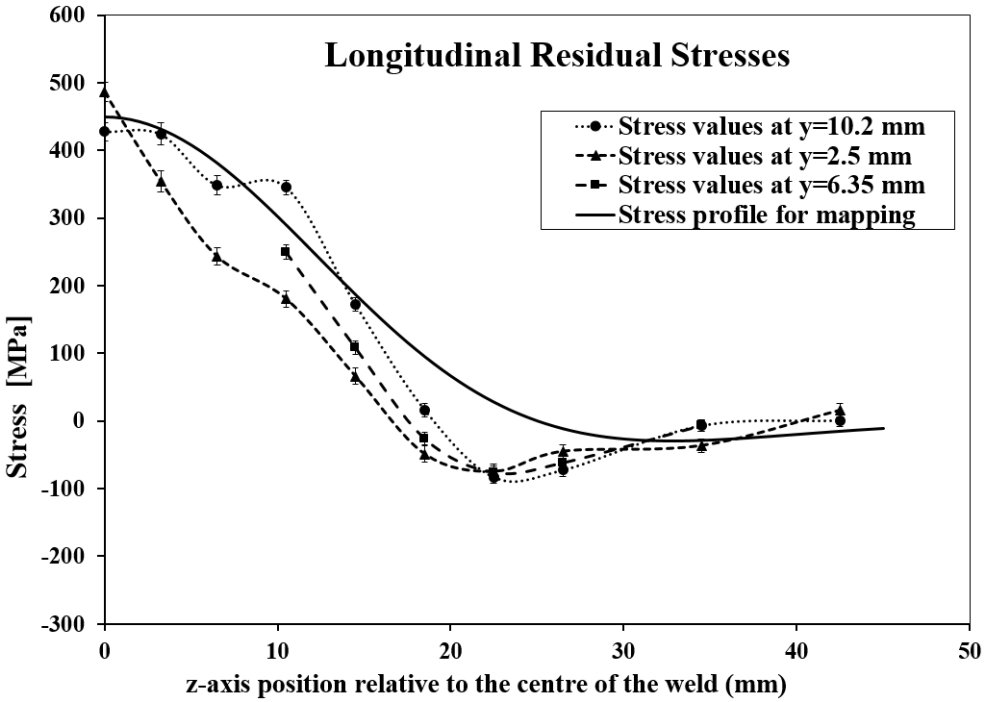

Figure 4.20: Longitudinal residual stress determined from neutron diffraction, and the stress profile used for mapping in the FE model determined using experimental data as per Equation 4.15.

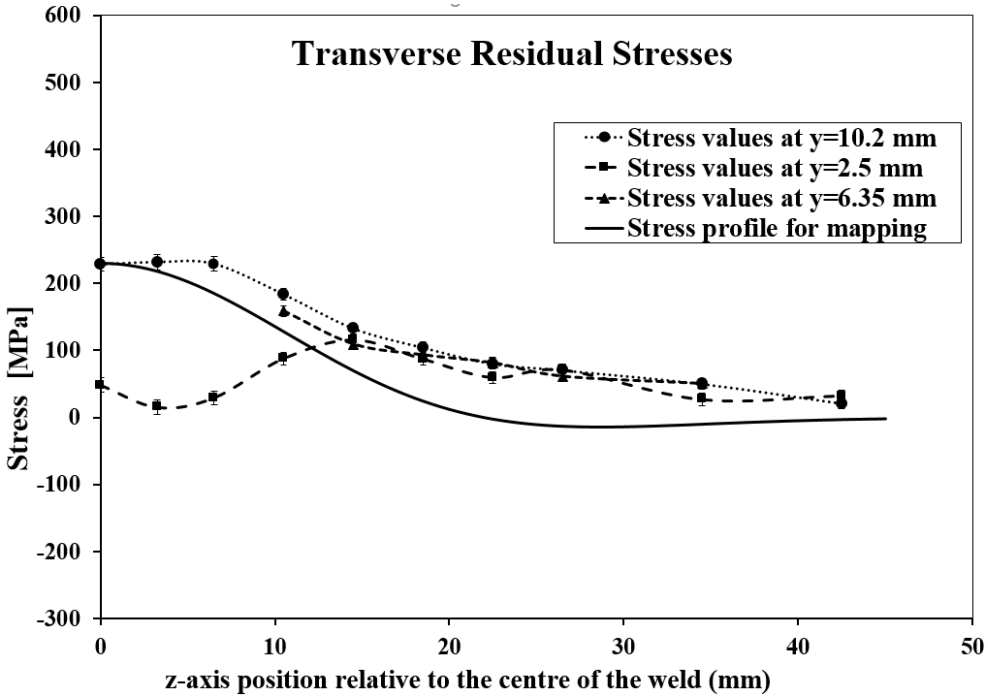

Figure 4.21: Transverse residual stress determined from neutron diffraction, and the stress profile used for mapping in the FE model determined using experimental data as per Equation 4.16.

4.9.3 Iterative technique implementation

The estimated stress profile was mapped from x=0 to 25mm, y=0 to 12.7mm and z=0 to 45mm. A very fine mesh was used in the area where stresses are mapped. Based on a mesh sensitivity study, an element size of about $0.5 \times 0.5 \times 0.5$ mm^3 was used in the stress mapping zone. The size of the meshing was also defined by the mapping resolution.

The mesh consisted of 83976, 20-node quadratic brick, reduced-integration elements. Routine scripts in Python code were used to write an input file for the solver in each iteration. The implementation of FE analysis with the help of Python subroutine is shown in the flow chart illustrated in Figure 4.22.

For computational efficiency, a quarter FE model was implemented. In the first iteration, measured stresses were fitted based on Equation 4.15 and 4.16 to obtain input, σ_{input}. The σ_{input} was pre-defined at the appropriate node locations (measured locations). An equilibrium step was run following initial stress pre-definition. In postprocessing, the stress distribution in the measured location, σ_{output} was extracted. The extracted output stresses were compared with the input stresses after each iteration. The initial few iterations were expected to redistribute the mapped stress to maintain equilibrium in the system because the mapping was only on a small region of the entire plate. In the first iteration, as a result of redistribution of stresses in the measurement locations following

equilibrium step, residual stresses were generated on the area around the measurement location. If the input stresses, σ_{input} at the measurement location are seen redistributed, next iteration is run by re-inputting σ_{input} at the appropriate nodes while keeping the newly generated residual stress in the rest of plate as same as the last iteration. With each iteration, the deviation between input stress and output stress was decreasing. The analysis involved 75 iterations until the output stresses in the measurement locations were same as the input stresses.

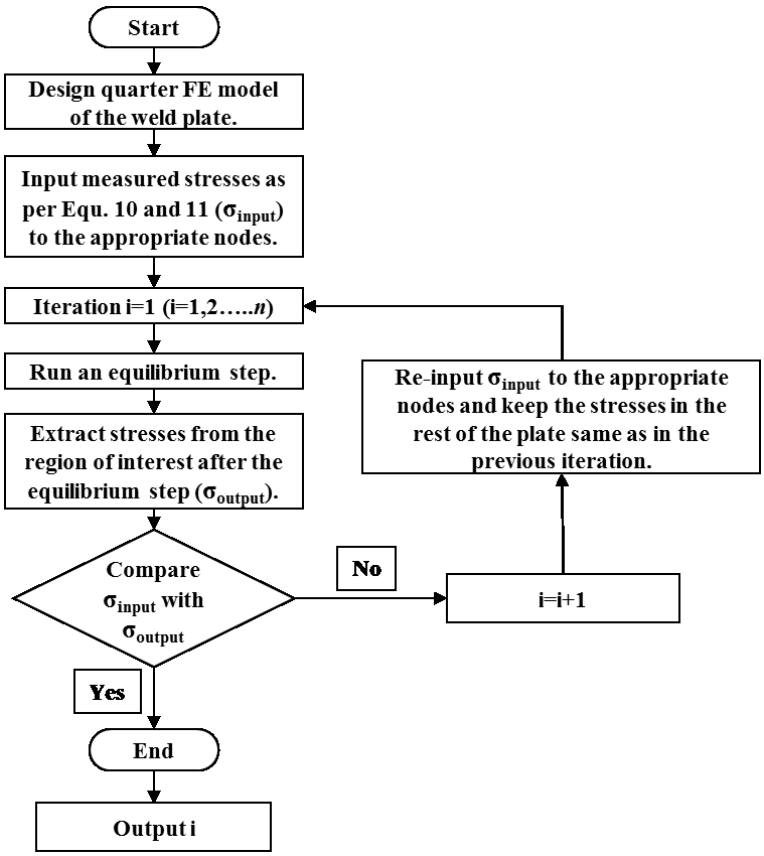

Figure 4.22: Flow chart illustrating the iterative finite element analysis for residual stress mapping from limited number of experimental measuremnts.

Each iteration analysis consisted of two steps. In the initial step, all the measured stresses were predefined in the FE model. The second step was an equilibrium step in which the FE solver equilibrated the stress throughout the specimen. For each iteration, the Python routine created a new solver file consisting of all the predefined stresses in the target zone and the stresses around the target area extracted from the previous iteration. The mesh throughout all iterations was not modified. In the case of all pre-definitions of the stress field, the averaged data were imposed element-wise at the integration points.

4.9.4 Residual stress mapping results and discussions

Stress mapping model was iterated 75 times until residual stress mapped were matching the estimated stress based on Equation 4.15 and 4.16 and a stable residual stress profile was achieved overall. Figure 4.23 shows the longitudinal residual stress contour plot of the FE model after 75 iterations.

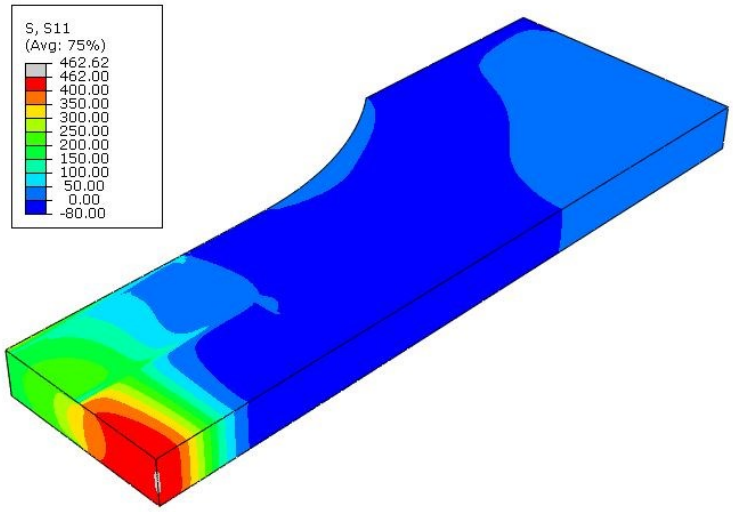

Figure 4.23: Reconstructed longitudinal residual stress contour obtained from residual stress mapping FE model after 75 iterations.

The stress field in the mapped area is completely reconstructed after the iterations, and Figure 4.24 and 4.25 shows the comparison between longitudinal and transverse stress distribution in the measurement plane at y=6.35mm after the 1st and 75th iterations against the mapped stress profile. From the graphs, it can be noted that the stress mapping on the mapping plane matches with the required stress very well.

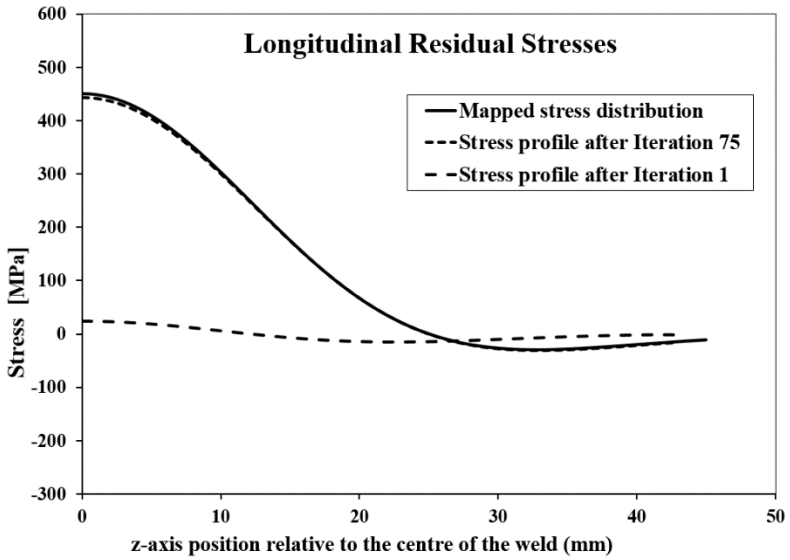

Figure 4.24: Comparison of input longitudinal residual stresses with stress mapping FE model output stresses after 1st and 75th iterations.

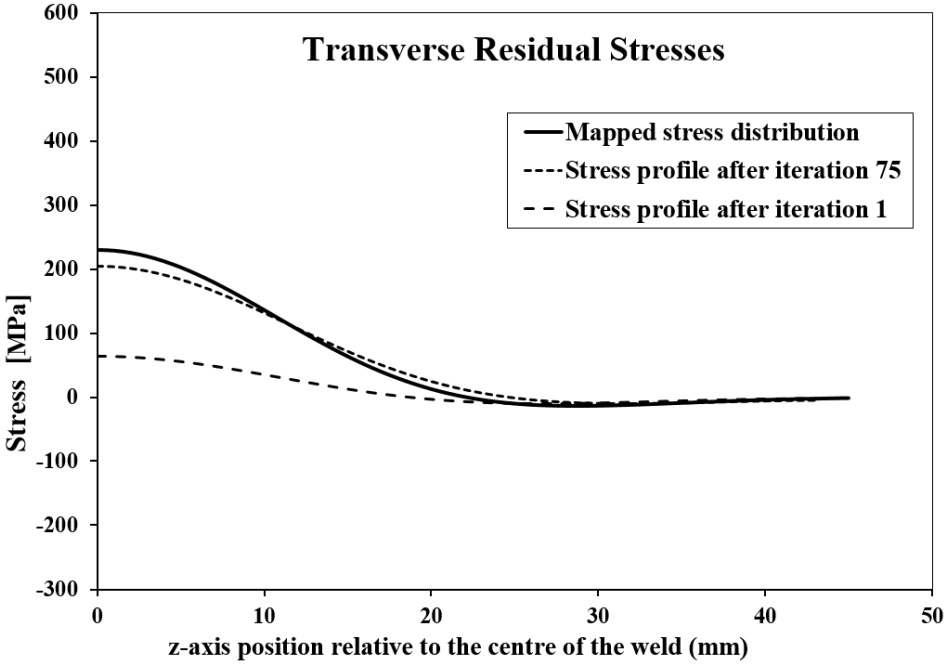

Figure 4.25: Comparison of input transverse residual stresses with stress mapping FE model output stresses after 1st and 75th iterations.

Figure 4.26 and 4.27 shows the comparison of longitudinal and transverse stresses obtained from neutron diffraction, weld model and residual stress mapping

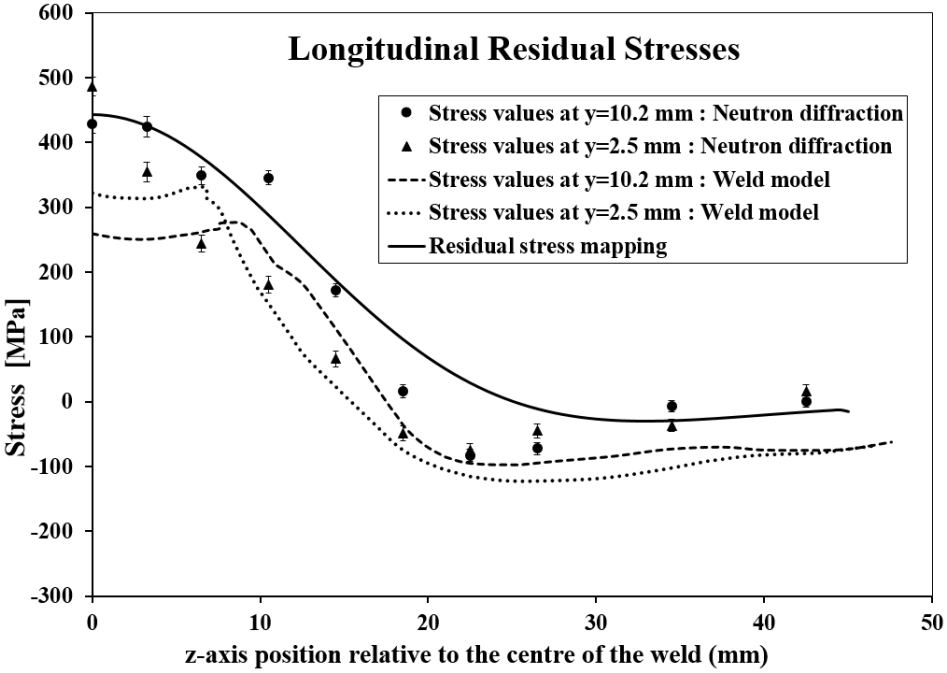

Figure 4.26: Comparison of longitudinal residual stress from experimental data, stress mapping FE model, and welding process simulation.

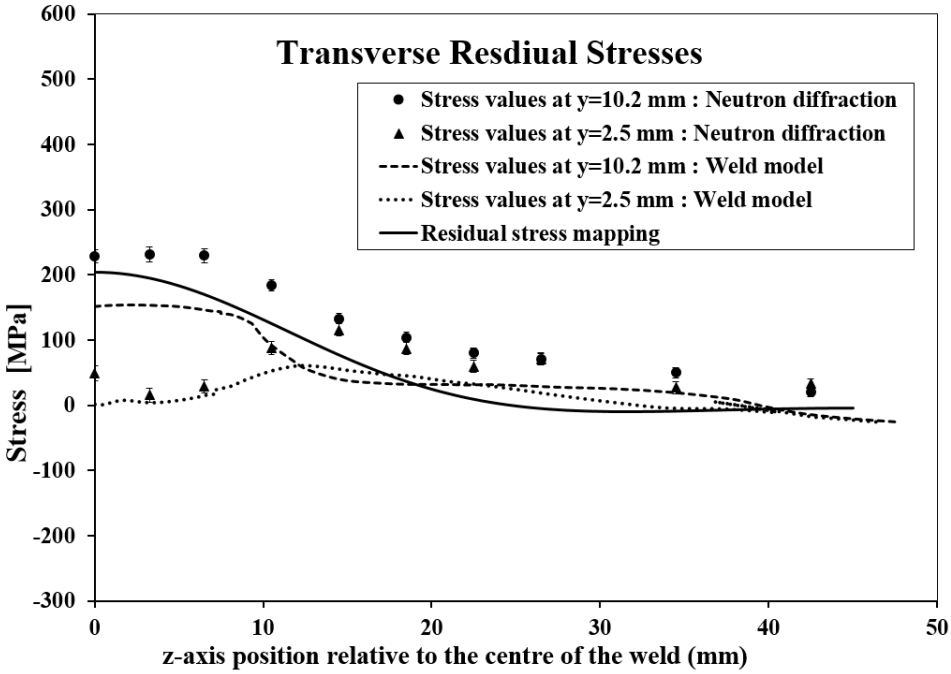

Figure 4.27: Comparison of transverse residual stress from experimental data, stress mapping FE model, and welding process simulation.

It is worth noting that this technique of residual stress field mapping is most accurate when the strain incompatibility is confined to a relatively small region such as a small weld. However, this method can be successfully employed in studies like engineering failure assessment in which accurate residual stress details are required on a small region such as around a crack in a weld zone (fusion zone or heat affected zone). In cases where the focus is on the crack propagation, if the stress intensity factor due to residual stress can be determined correctly, the conservatism in the engineering critical assessment can be reduced. In the present study, longitudinal and transverse residual stresses are represented as a stress distribution function to determine stress values at locations between two measurement points so that unique values are mapped on to a set of elements in the FE model. Therefore, it is emphasised that the stress values measured need be represented in a distribution function. Residual stress measurement of locations on a line scan with very small increments are often prohibitively expensive and time-consuming. This suggests that the residual stress measurement experiments can be planned in such a way that more of the measurement locations contain the inherent strains.

Also, this method is dependent on the number of stress components being mapped. In this work, only two orthogonal stress components, longitudinal and transverse components, were used. The third orthogonal component in the through-thickness direction in a plate is usually fairly low.

4.10 Summary

In this work, a 3D model was created to simulate welding process and predict residual stresses in the butt and the fillet welded DH 36 plates. Predicted residual stress components were compared with residual stress measurements determined using neutron diffraction. Residual stress mapping in the butt-welded plate with the short weld using a limited number of stress data measured using neutron diffraction was achieved using a self-balancing stress distribution in a finite element model. Comparison is drawn between the predicted residual stresses from the corresponding 3D analytical weld model and the mapped stresses. The following conclusions can be drawn:

I. Heat transfer analysis implemented by the application of a volume heat flux (based on recorded arc voltage and current) to small weld chunks was used to simulate the thermal history of the welding process. In the FEA models, with the predicted effective heat input and heating time, temperatures at certain locations in the parent metal were in good agreement with the measurement results recorded from thermocouples. Macrograph of the weld cross section of the butt and fillet welded plates revealed weld fusion lines so that the heat input could be adjusted to obtain a thermal history practically matching the thermocouple data. The cooling rate as predicted by FEA was slightly lower than the thermocouple data which could be due to the high heat conduction from the metal fixture setup in the actual welding process.

II. EDM cutting was successfully implemented in the weld process simulation of each specimen.

III. Residual stress profiles obtained from the FEA model show a similar trend with most of the line scans measured using neutron diffraction. Also, the magnitudes, at the region of interests, showed reasonable agreement with the measurement values. Poor agreement occurred in a few locations. Factors such as accurate material mechanical properties and material final stage phase transformation can be the reasons for inaccurate prediction.

IV. As the primary objective of the welding process simulation is to introduce a reasonably accurate residual stress field into the model of the specimens under study, assumptions and approximations were used to balance accuracy and computation efficiency. Overall the results are considered suitable for further residual stress redistribution and elastic shakedown analysis.

V. Analytical weld modelling is still one of the best methods to generate the complete stress field on a weld plate. However, the computational efficiency of the residual stress mapping technique was much better than the full welding process modelling. For fracture or fatigue analysis of welded structures, in which the area of potential crack initiation is identified, the mapping technique can increase the computational efficiency considerably without losing accuracy.

VI. Self-balancing stress equations can play an important role in supporting residual stress mapping techniques such as neutron diffraction, where data are typically obtained from a relatively small region of interest only.

VII. The as-welded residual stresses as recommended by BS 7910 are at the yield strength of the base plate. This is hence considered conservative. An upper-bound residual stress distribution can be estimated to implement in a finite element model using the residual stress mapping technique in this paper. This increases efficiency and reduces the complexity of modelling. By using an upper bound distribution based on measured residual stresses, the conservatism in the stress will be secure.

CHAPTER 5.REDISTRIBUTION OF RESIDUAL STRESSES

5.1 Introduction

This chapter describes the residual stress redistribution following a limited number of loading cycles in the welded specimens. Initially, the residual stress measurements obtained from neutron diffraction on the butt welded and the fillet welded specimens are presented. Next, the methodology and implementation of the numerical simulation of residual stress redistribution in each specimen are explained. The resulting numerical predictions of residual stress simulations are then compared with the experimental measurements. The experimental procedure performed in this study is described in Chapter 3 in detail. For continuity, the following sections will briefly introduce the experiments conducted with reference to Chapter 3. Finally, a discussion on the effect of the elastic shakedown on the redistribution of residual stress is presented.

5.2 Experimental procedure

Residual stress measurements were conducted on four specimens, the butt-welded plates with the long weld, the butt-welded plates with the short weld, the fillet welded plate with the short weld, and the fillet welded plate with the long weld as shown in Figures 3.7 and 3.8. A limited number of loading cycles were applied as discussed in Section 3.6. The load levels discussed in Section 3.6 were selected based on the request of Lloyd's register marine to accurately represent the maximum design loads in typical container ships. The methodology used for the measurement of residual stresses in the butt-welded specimens, in the as-welded condition and after one, three and ten load cycles, and in the fillet welded specimens in the as-welded condition, and after one and three load cycles, using neutron diffraction measurements, are presented in Section 3.7. The load levels were selected based on preliminary shakedown limit analysis and typical load levels experienced in the load-bearing members of a container ship.

5.3 Residual stress redistribution in butt-welded plates

The as-welded residual stress redistributions determined for the butt-welded plates are presented in Figure 5.1 to 5.6. In each figure longitudinal (along the weld), transverse (across the weld) and normal stress (through thickness) components obtained from the neutron strain measurements are plotted separately. In both butt-welded plates, Y=10.2mm, 6.35 and 2.5mm represent the line scan near the top surface, mid-thickness, and near the bottom surface of the weld plate respectively.

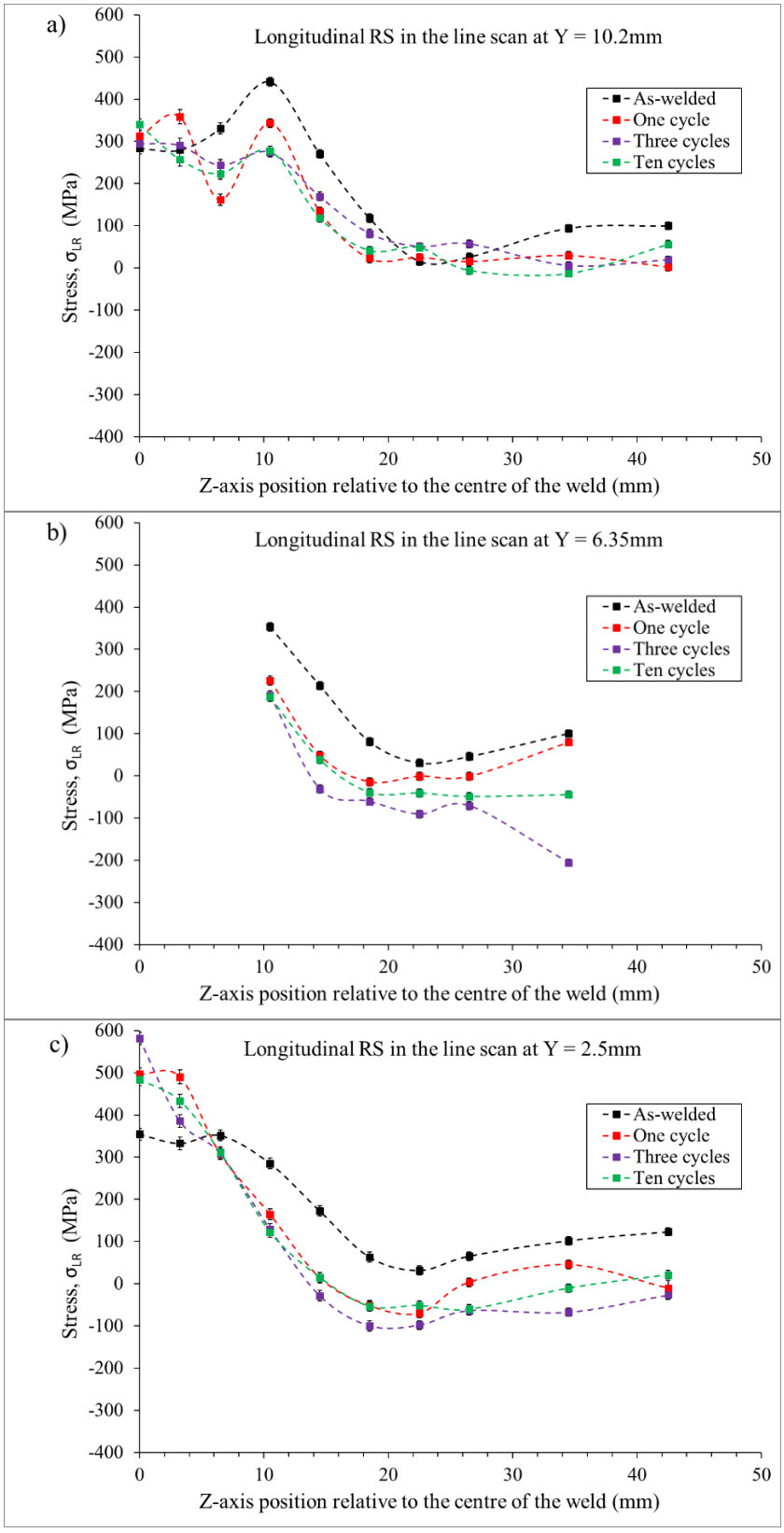

Figure 5.1: Longitudinal residual stress redistribution measured using neutron diffraction in the butt-welded plate with the short weld: a) The line scan at y=10.2mm, b) the line scan at y=6.35mm and, c) the line scan at y=2.5mm.

The three-line scans were considered for the investigation primarily to see the variation of the weld residual stresses through-the-thickness at the same time to avoid any overlaps in the gauge volume used in the neutron diffraction experiment.

The redistribution of residual stress was measured in most of the line scans. Some of the line scans were measured as relaxed after the application of a few cycles. The percentage of relaxation after N load cycles was calculated using equation 6.1 as below.

$$S\ (\%) = \frac{Initial\ RS - RS\ at\ Nth\ Cycle}{Initial\ weld\ stress} \times 100 \qquad (5.1)$$

5.3.1 Butt welded plate with the short weld

In the butt-welded plate with the short weld, the cyclic load was applied along the transverse direction. Figure 5.1 shows the longitudinal residual stress redistribution at three line scans in this weld plate. In all three-line scans, away from the weld centre line (Z=18 to 16 mm as defined in Figure 3.17a), residual stresses were measured as slightly tensile or compressive after ten load cycles and were not considered significant in terms of redistribution/relaxation. It was not considered significant because of the relaxation in the regions slightly away from the weld.

Literature (Morrow J 1958) from previous studies have concluded that the load cycles perpendicular to the residual stress component has little or no effect on the relaxation of that component. However, it should be noted that the plasticity which is the primary reason for the relaxation is not direction dependent. Hence, even though the weld and HAZ regions had little redistribution over ten load cycles in the longitudinal component because the load was applied perpendicular to this direction (Figure 5.1a and 5.1c), the slight redistribution is attributed to the plasticity effects. However, in this work, in the line scan at Y=10.2mm, from Z=10 to 15mm, an average of 37% relaxation is noted over the ten cycles. In both Y=6.35 and 2.5 mm line scans, a relaxation of about 50% was noted at Z=10mm, and Z=14mm had tensile residual stress reversed to compressive stress over ten load cycles. It is important to note that the amount of relaxation/redistribution is predominant after the first cycle. However, this was not expected due to the applied load direction. The bending induced relaxation during the first load cycle because of the yield-strength-level as-welded residual stresses and the initial distortion (though very small) could be a reason for the redistribution after the first cycle in the longitudinal component.

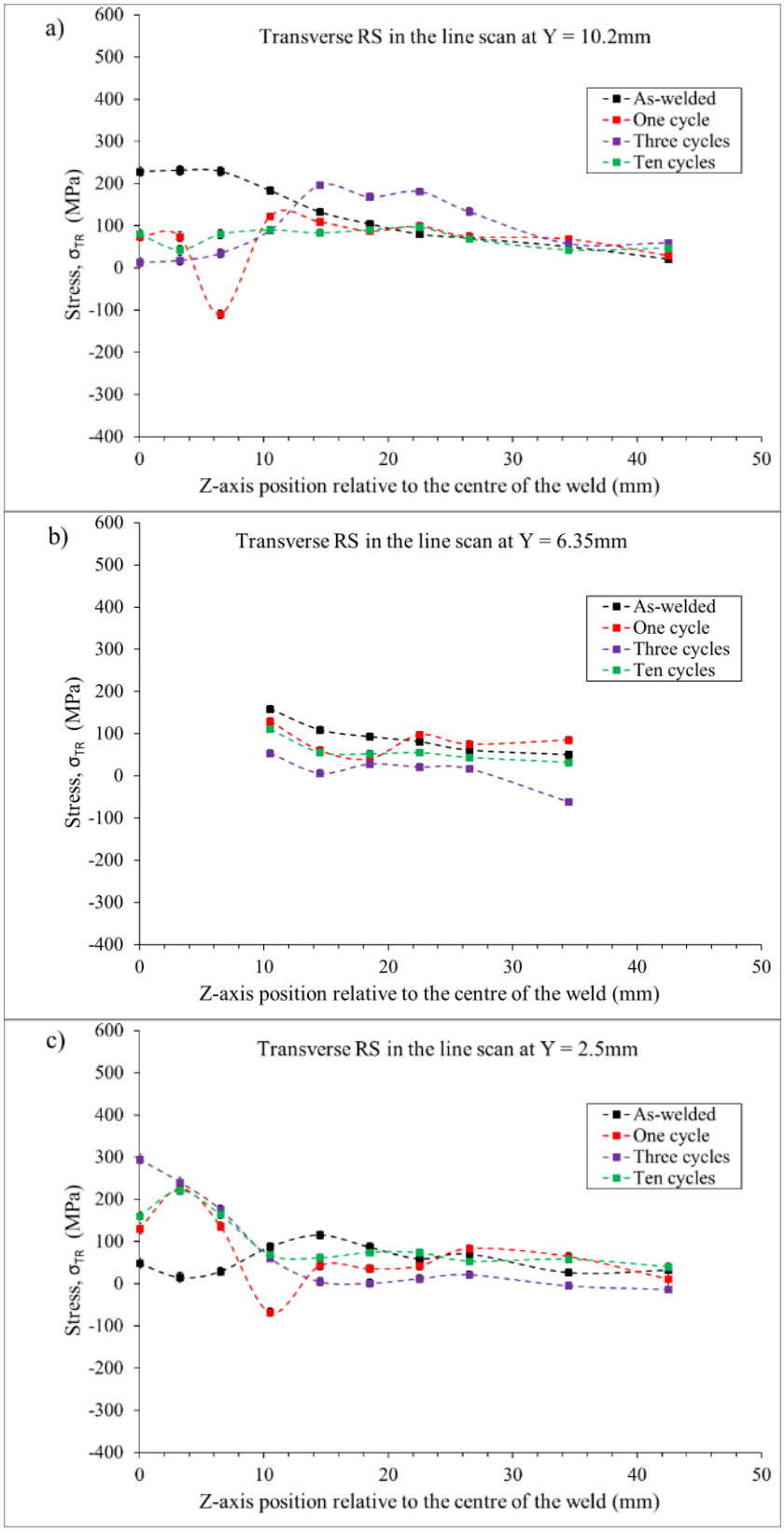

Figure 5.2: Transverse residual stress redistribution measured using neutron diffraction in the butt-welded plate with the short weld: a) The line scan at y=10.2mm, b) the line scan at y=6.35mm and, c) the line scans at y=2.5mm.

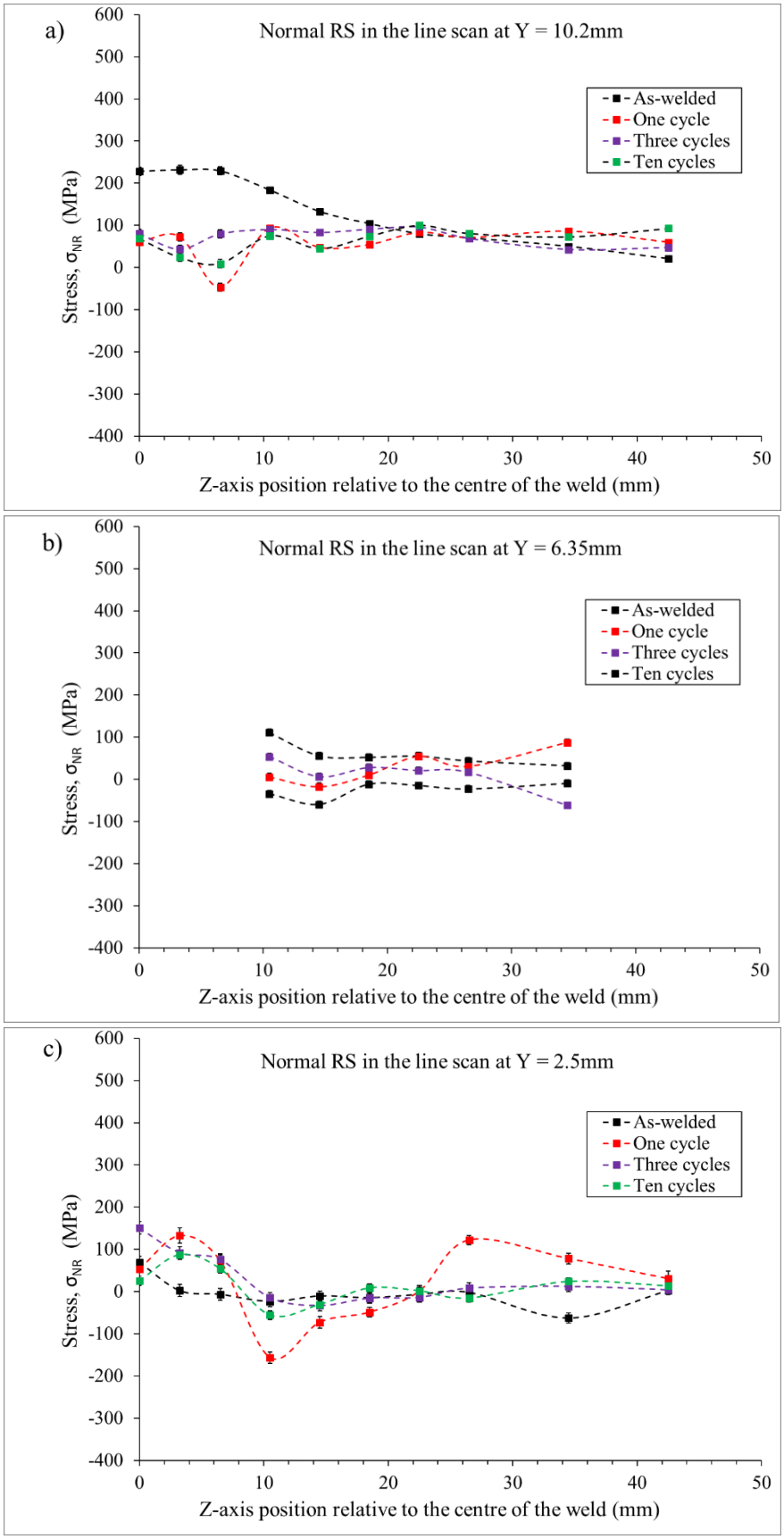

Figure 5.3: Normal residual stress redistribution measured using neutron diffraction in the butt-welded plate with the short weld: a) The line scan at y=10.2mm, b) the line scan at y=6.35mm and, c) the line scan at y=2.5mm.

Figure 5.2 shows the transverse residual stress redistribution at three-line scans. In the line scan at Y=10.2mm, after ten load cycles, experimental measurements showed about 90% relaxation in the weld and HAZ (Figure 6.2a). Also, an insignificant tensile residual stress away from the weld is noted after ten load cycles in the line scan at Y=10.2mm. The line scan at Y= 6.35mm shows a steady relaxation to near zero levels following ten load cycles (Figure 5.2b). On the other hand, the line scan at Y=2.5mm, which is near to the bottom of the plate, has moved significantly to the tensile zone after the first cycle and stayed in the tensile zone over the ten load cycles (Figure 5.2c). This increase in tensile stresses at the line scan near the bottom of the plate was not expected and could be as a result of the variation of transverse stresses through the thickness of the specimen to maintain equilibrium following the relaxation in the line scans above.

Figure 5.3 shows the normal residual stress redistribution for three line scans. The normal residual stresses did not see any significant redistributions as the as-welded stress levels were low and the applied loads were not expected to cause any significant effect in this direction.

5.3.2 Butt welded plate with the long weld

In the butt-welded plate with the long weld, the cyclic load was applied along the longitudinal component. Figure 5.4 shows the longitudinal residual stress redistribution at three-line scans in this weld plate. Similar to the butt-welded plates with the short weld, in all three-line scans, farther away from the weld (Z=18 to 16mm as defined in Figure 3.17b), residual stresses have stayed slightly tensile (below 100MPa) or compressive after ten load cycles and were not considered as showing significant redistribution/relaxation.

In the weld and HAZ region (Z=0 to 6 mm) significant relaxation was measured in all three line scans over the ten load cycles. In all line scans, the relaxation was predominant in the first cycle. In the bottom scan at Y=2.5mm, a relaxation of 60% was noted after the first cycle (Figure 5.4c). Overall, after ten cycles an average of about 50% relaxation was noted in the weld and HAZ. Also, it should be noted that after the initial cycle, the trend of the stress profile was seen relatively stable up to ten cycles. However, there were a few locations where the measurements had a deviation from the general trend. Moreover, the initially compressive stresses in the base plate away from the weld because slightly tensile after ten load cycles. This could also be due to the global redistribution in the plate.

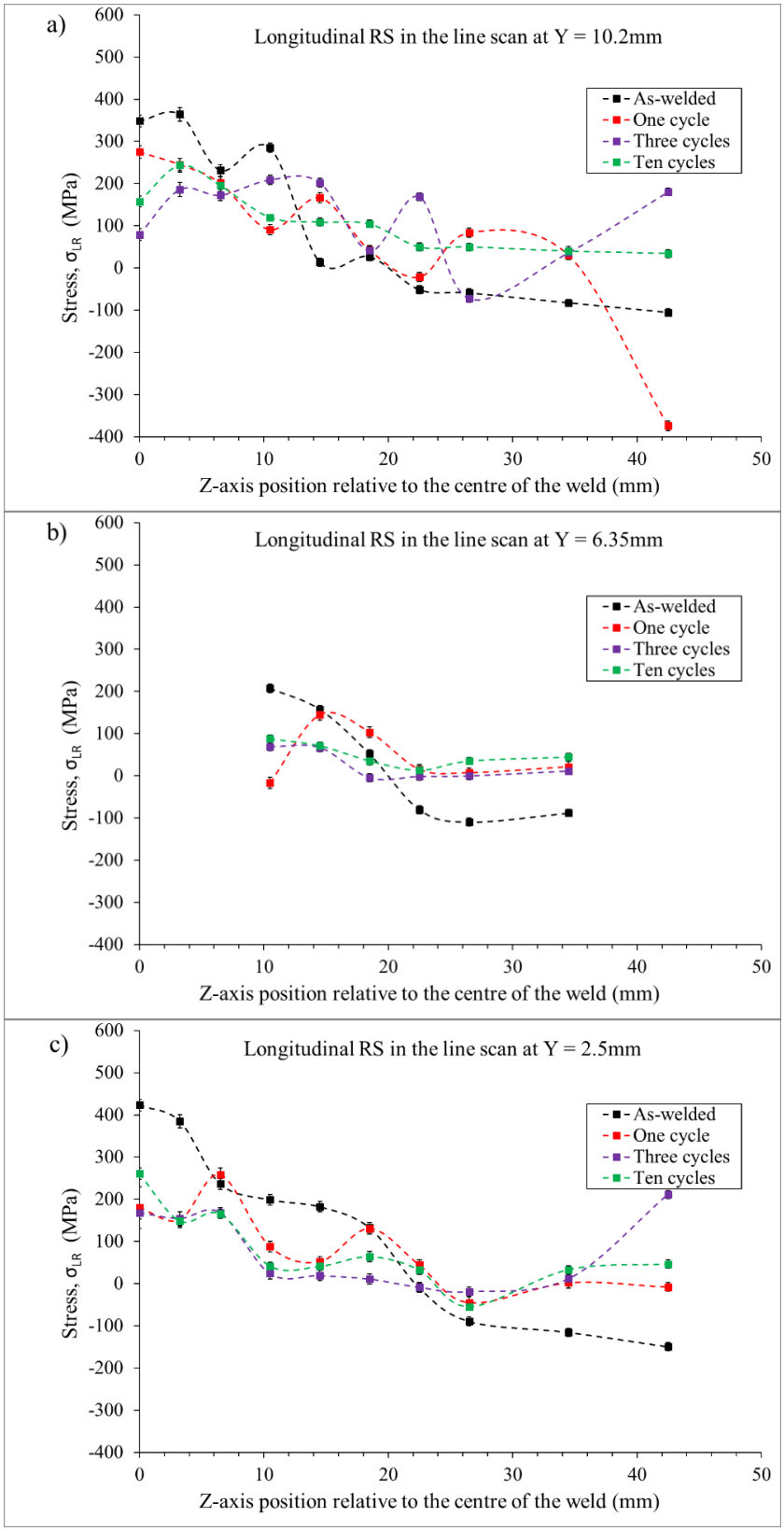

Figure 5.4: Longitudinal residual stress redistribution measured using neutron diffraction in the butt-welded plate with the long weld: a) The line scan at y=10.2mm, b) the line scan at y=6.35mm and, c) the line scan at y=2.5mm.

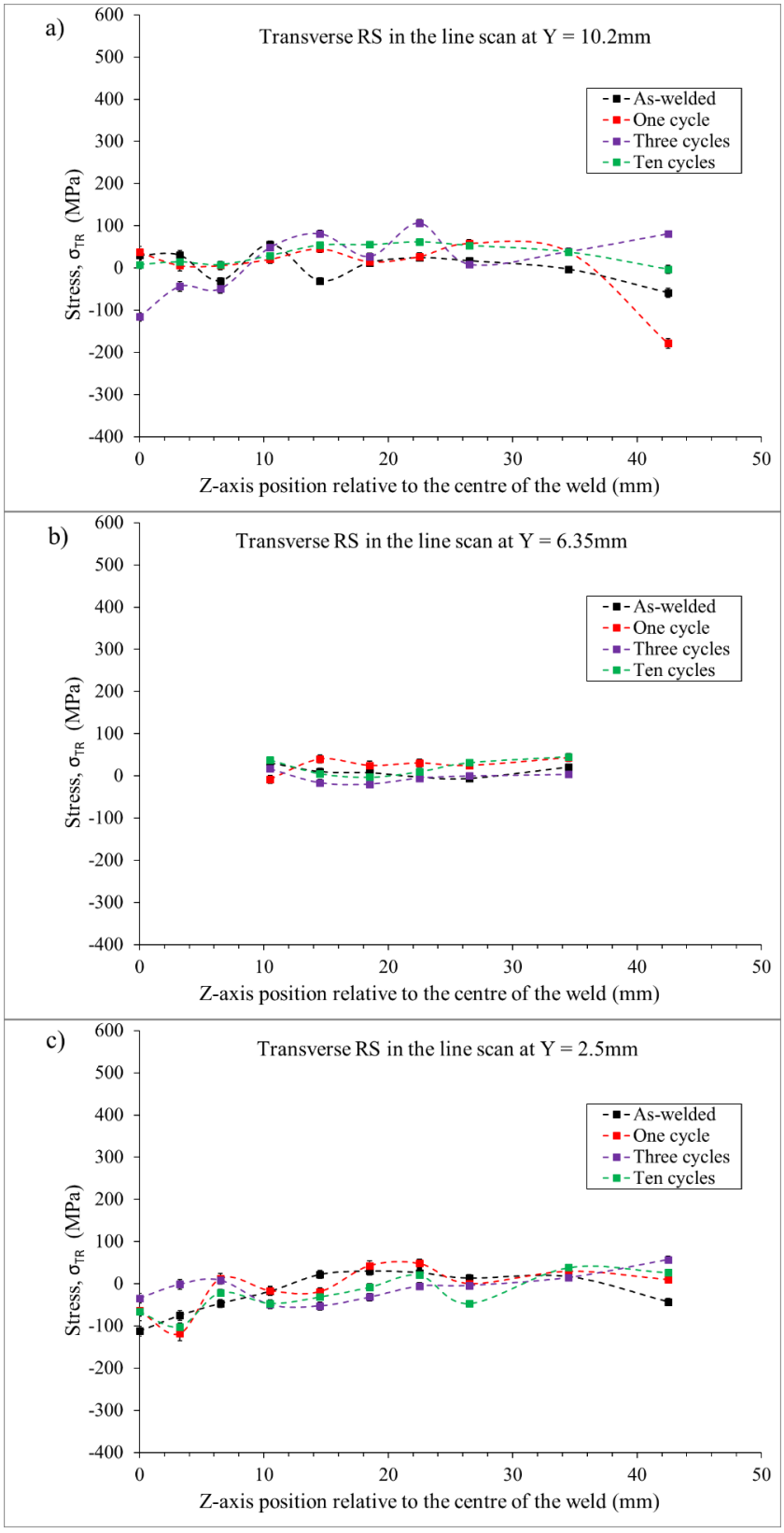

Figure 5.5: Transverse residual stress redistribution measured using neutron diffraction in the butt-welded plate with the long weld: a) The line scan at y=10.2mm, b) the line scan at y=6.35mm and, c) the line scan at y=2.5mm.

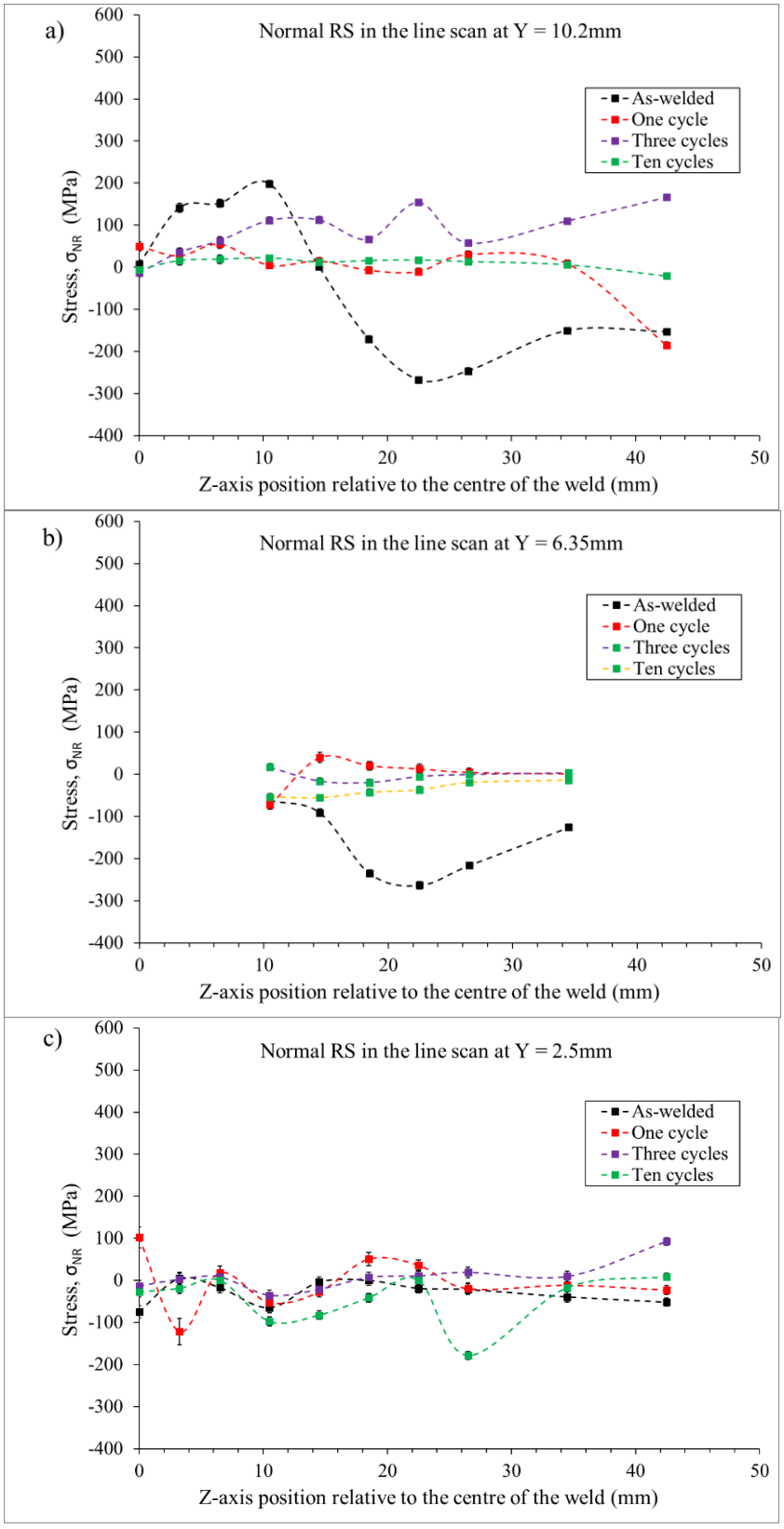

Figure 5.6: Normal residual stress redistribution measured using neutron diffraction in the butt-welded plate with the long weld: a) The line scan at y=10.2mm, b) the line scan at y=6.35mm and, c) the line scan at y=2.5mm.

Figure 5.5 shows the transverse residual stress redistribution in the long-welded plate at three-line scans. The measured stresses in all three-line scans had little or no redistribution after ten load cycles. This is simialr to the case of the butt-welded plate with the short weld. However, the magnitude of as-welded longitudinal residual stresses in the butt-welded plate is significantly higher than the level of as-welded transverse residual stresses.

Figure 5.6 shows the normal residual stress redistribution in all three line scans. The as-welded compressive normal residual stresses were measured tensile or about zero level after the application of load cycles.

5.4 Residual stress redistribution in fillet welded plates

The as-welded residual stress redistribution determined for the fillet-welded plates in the line scan locations shown in Figure 5.7 are presented in Figures 5.8 to 5.17. Unlike the butt-welded plates, for ease of interpretation, in both fillet-welded plates, the figures are presented separately for the horizontal and the vertical plate. The line scans at Y=2.5, 6.35 and 10.2mm are near the top surface, mid-thickness and bottom surface respectively in the horizontal plate. The line scans at Y=15.2mm represent the line scan from one side of the weld to the other side through the vertical plate. The line scans at Y=20.2 and 25.2mm represent locations in the vertical plate. The coordinates were defined as shown in Figure 5.7.

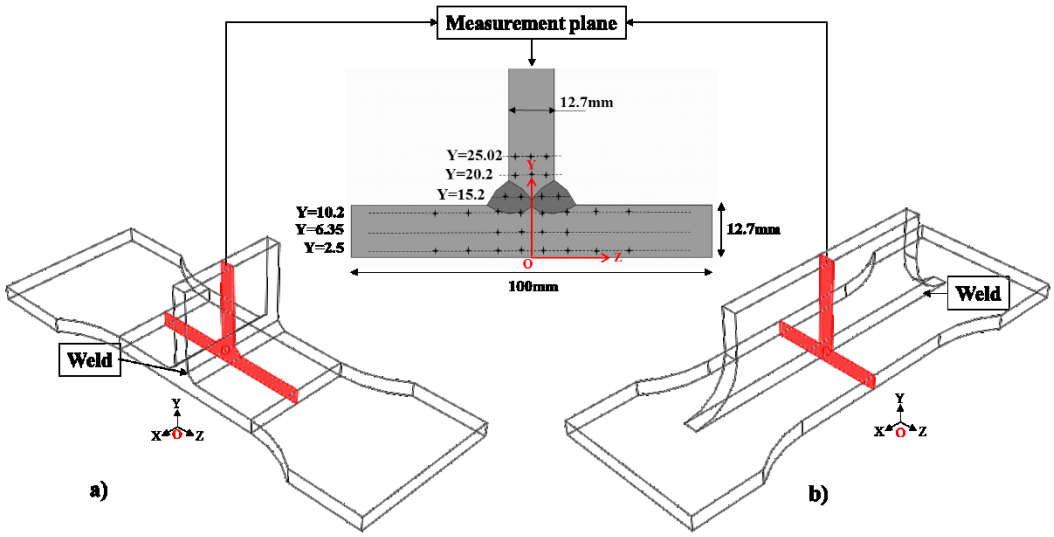

Figure 5.7: Measurement locations in fillet welded specimens: a) Fillet welded plate with the short weld, and b) fillet welded plate with long weld

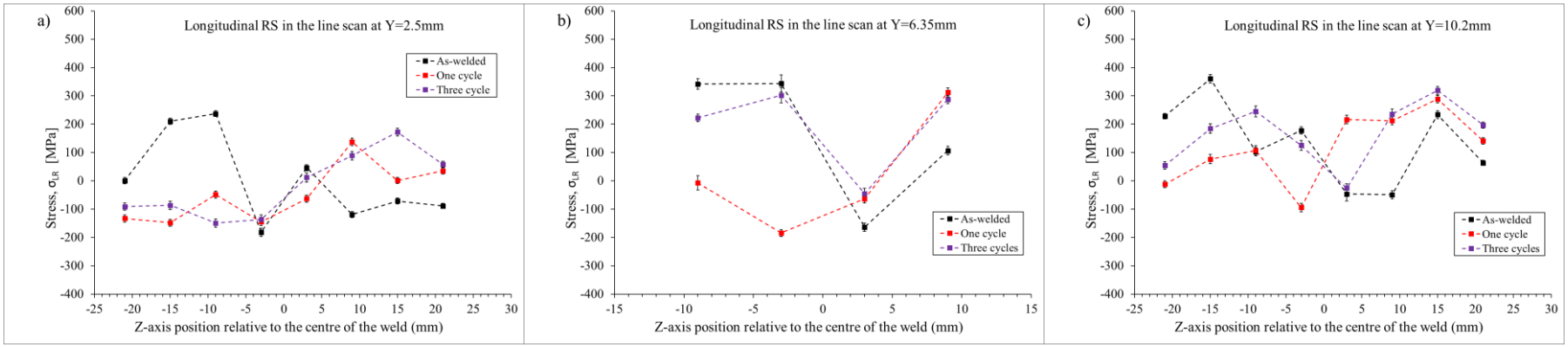

*Figure 5.8: Longitudinal residual stress redistribution measured using neutron diffraction in the **horizontal** plate of the fillet-welded plate with the short weld: a) The line scan at y=2.5mm, b) the line scan at y=6.35mm and, c) the line scan at y=10.2mm.*

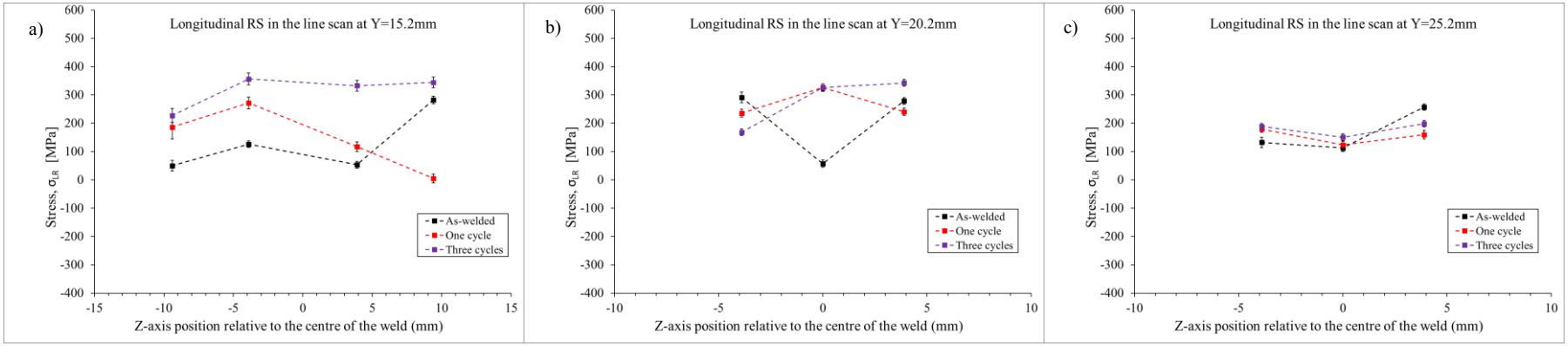

*Figure 5.9: Longitudinal residual stress redistribution measured using neutron diffraction in the **vertical** plate of the fillet-welded plate with the short weld: a) The line scan at y=15.2mm, b) the line scan at y=20.2mm and, c) the line scan at y=25.2mm.*

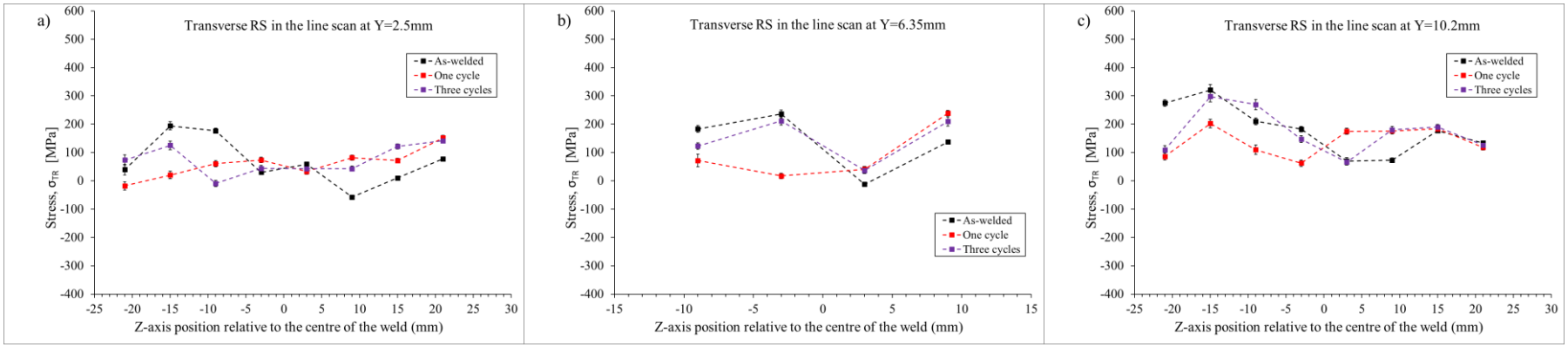

*Figure 5.10: Transverse residual stress redistribution measured using neutron diffraction in the **horizontal** plate of the fillet-welded plate with the short weld: a) The line scan at y=2.5mm, b) the line scan at y=6.35mm and, c) the line scan at y=10.2mm.*

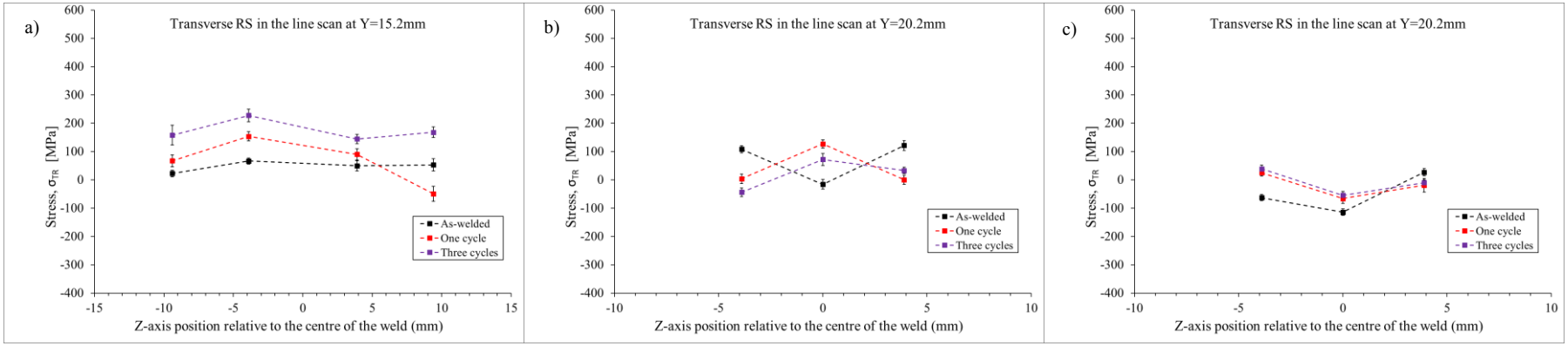

*Figure 5.11: Transverse residual stress redistribution measured using neutron diffraction in the **vertical** plate of the fillet-welded plate with the short weld: a) The line scan at y=15.2mm, b) the line scan at y=20.2mm and, c) the line scan at y=25.2mm.*

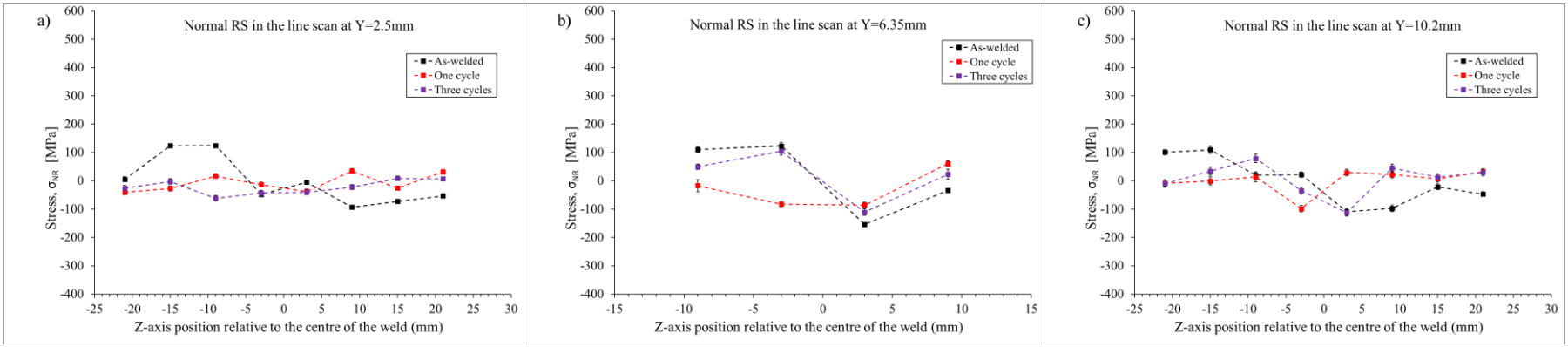

*Figure 5.12: Normal residual stress redistribution measured using neutron diffraction in the **horizontal** plate of the fillet-welded plate with the short weld: a) The line scan at y=2.5mm, b) the line scan at y=6.35mm and, c) the line scan at y=10.2mm.*

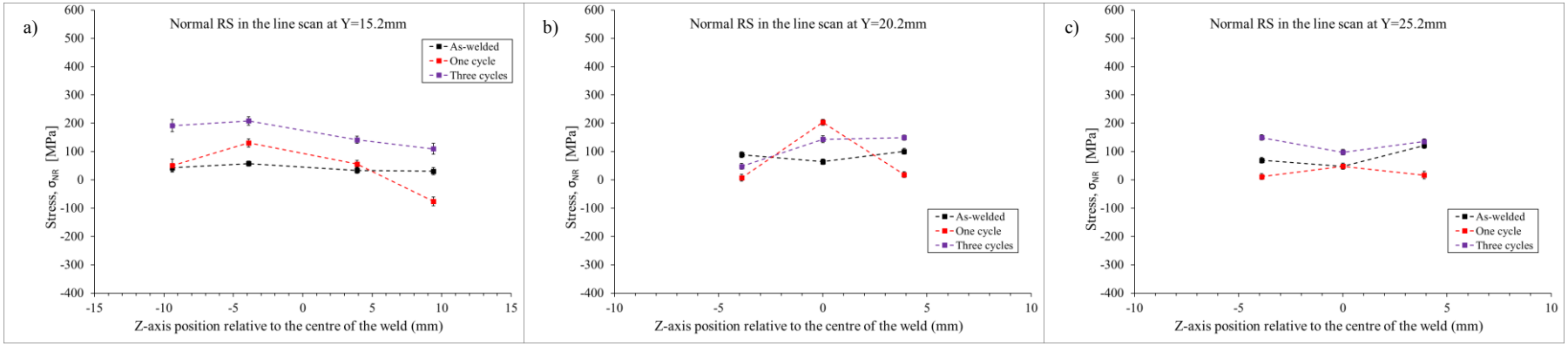

*Figure 5.13: Normal residual stress redistribution measured using neutron diffraction in the **vertical** plate of the fillet-welded plate with the short weld: a) The line scan at y=15.2mm, b) the line scan at y=20.2mm and, c) the line scan at y=25.2mm.*

5.4.1 Fillet welded plate with the short weld

In the fillet-welded plate with the short weld, the cyclic load was applied along the transverse direction. Figure 5.8 shows the longitudinal residual stress redistribution in three-line scans in the horizontal plate of this specimen. Unlike the butt-welded plates, the residual stress values measured were very discontinuous and non-symmetrical on both sides of the weld. In the line scan at Y=2.5mm, a significant relaxation was measured at Z= –21, –15 and –9mm after the first load cycle (Figure 5.8a). On the other hand, the longitudinal stresses at Z=+9 to Z=+21mm were seen become tensile from a compressive as-welded value. The values observed in the middle of the plate at Y=2.5 mm were not redistributed.

In the line scan at Y=6.35mm (Figure 5.8b), longitudinal stress values measured after the first load cycle showed significant relaxation on the weld on one side. However, after three cycles the relaxed cycles were increased again to the as-welded stress state. Figure 5.9 shows the longitudinal residual stress measured in the vertical plate of the fillet welded plate with the short weld. In both line scans at Y=15.2 and 20.2mm, the stresses were highly tensile and after three load cycles have stayed tensile (Figure 5.9a and 5.9b). At Y=2.5mm an increase in tensile values was measured following three load cycles (Figure 5.9a). The line scan at Y=25.2mm had no or little redistribution which may be because the load was applied only on the horizontal plate and there was minimal load transfer to the vertical plate at Y=25.2mm.

Figure 5.10 shows the transverse residual stress measured on the horizontal plate in the fillet welded plate with the short weld. In the line scan at Y=2.5mm, at Z= –21 to –9mm, measured values showed relaxation whereas at Z=+9 to +21mm showed an increase in residual stress after three cycles. However, the trend in this line scan was observed as similar to the as-welded stresses.

Figure 5.11 shows transverse residual stress measured on the vertical plate in this specimen. In the vertical plate, the as-welded stresses were noted as near zero at Y=15.2mm. However, an increase in tensile stresses was observed following three load cycles. The Y=15.2mm line scan was across the weld on both sides, and this redistribution for residual stress may be because of the plasticity effects at the weld toe. The plasticity at the weld toe will relax residual stresses at the weld toe, however, can potentially redistribute the residual stresses in the nearby region. At Y=20.2 and 25.2mm, the stresses stayed near zero or compressive after three load cycles.

Figure 5.12 and 5.13 shows the normal residual stress redistribution in horizontal and vertical plates respectively. The as-welded normal stresses were low when compared to other components. However, a similar redistribution trend to that of transverse stresses was noticed. As mentioned before, the plasticity which is direction independent at the weld toe may be the reason for the stresses redistributed to a tensile level after three load cycles at Y=15.2mm, (Figure 5.13). On the horizontal plates, normal stresses were observed as compressive after three load cycles (Figure 5.12).

5.4.2 Fillet welded plates with the long weld

In the fillet-welded plate with the long weld, the cyclic load was applied along the longitudinal direction. Figure 5.14 shows the longitudinal residual stress redistribution in three-line scans in the horizontal plate in this specimen. The line scan at Y=2.5mm did not measure any significant redistribution which could be due to a low level of as-welded residual stress (Figure 5.14a). At Y=10.2mm, as welded compressive residual stresses had changed to tensile after three load cycles (Figure 5.14c).

Figure 5.15 shows the redistribution of longitudinal stresses in the vertical plate in this specimen. The as-welded longitudinal residual stresses in the vertical plate were significantly tensile (Figure 5.15b and 5.15c). Like the fillet welded plate with the short weld, there was a significant increase in the tensile stress in the line scan at Y=15.2mm after three load cycles (Figure 5.15a). The line scans at Y=20.2, and 25.2mm had little redistribution.

Figure 5.16 and 5.17 shows transverse residual stress measured on the horizontal plate and the vertical plate respectively. In the horizontal plate at Y=2.5 and 6.35mm, stress redistribution was minimal. However, in the case of Y=10.2mm, the compressive as-welded residual stress has changed to tensile residual stresses after three load cycles (Figure 5.16c). In the vertical plate, the as-welded stresses were slightly tensile at Y=15.2mm had similar levels after three load cycles (Figure 5.17). However, an increase in tensile stresses was observed following the first load cycle.

Figure 5.18 and 5.19 shows the normal residual stress redistribution in the horizontal and the vertical plates respectively. The as-welded normal stresses were near zero or slightly compressive on all line scans expect at Y=20.2mm, Z=0mm (Figure 5.19b). Moreover, the redistribution observed on these line scans were still near zero or compressive.

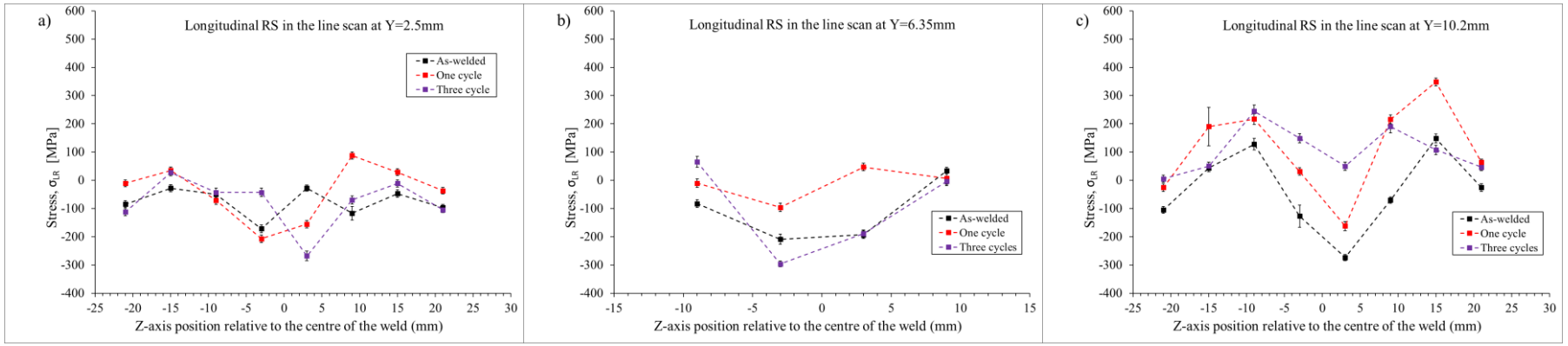

*Figure 5.14: Longitudinal residual stress redistribution in the **horizontal** plate of the fillet-welded plate with the long weld in the line scan at a) y=2.5mm, b) y=6.35mm and, c) y=10.2mm.*

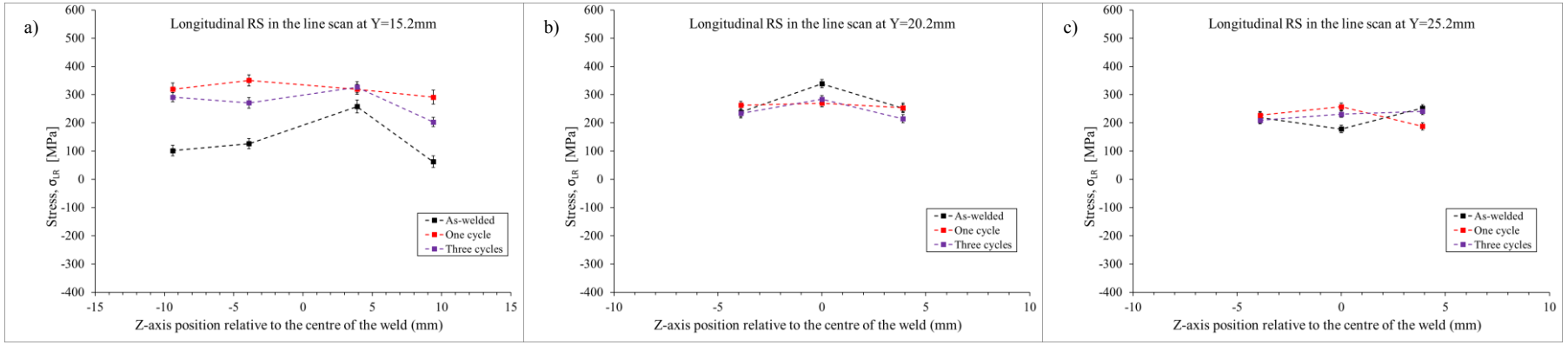

*Figure 5.15: Longitudinal residual stress redistribution measured using neutron diffraction in the **vertical** plate of the fillet-welded plate with the long weld: a) The line scan at y=15.2mm, b) the line scan at y=20.2mm and, c) the line scan at y=25.2mm.*

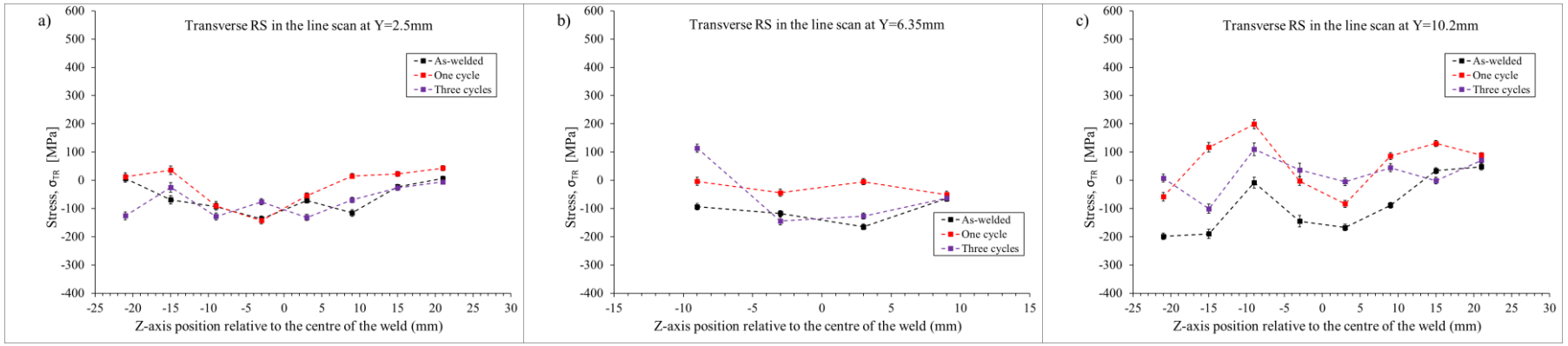

*Figure 5.16: Transverse residual stress redistribution measured using neutron diffraction in the **horizontal** plate of the fillet-welded plate with the long weld: a) The line scan at y=2.5mm, b) the line scan at y=6.35mm and, c) the line scan at y=10.2mm.*

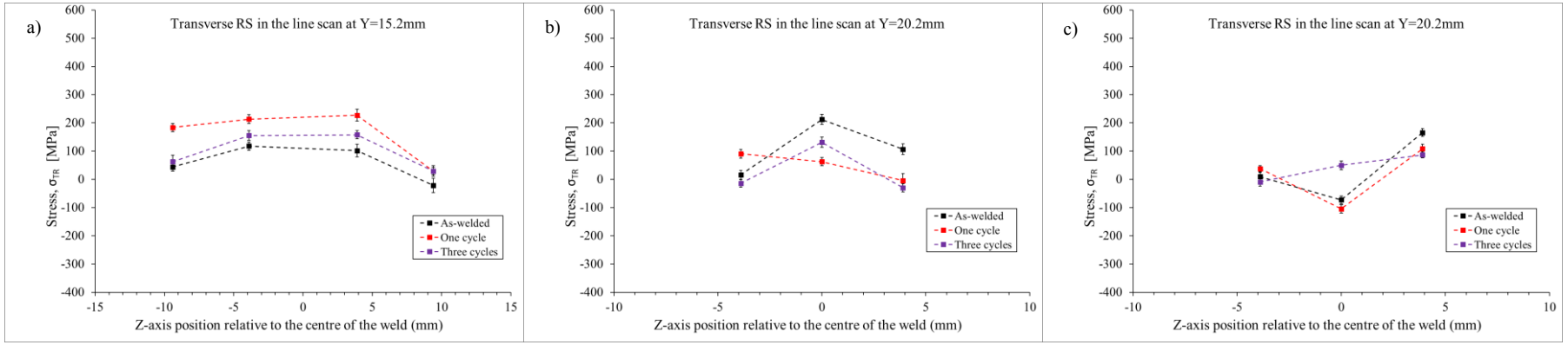

*Figure 5.17: Transverse residual stress redistribution measured using neutron diffraction in the **vertical** plate of the fillet-welded plate with the long weld: a) The line scan at y=15.2mm, b) the line scan at y=20.2mm and, c) the line scan at y=25.2mm.*

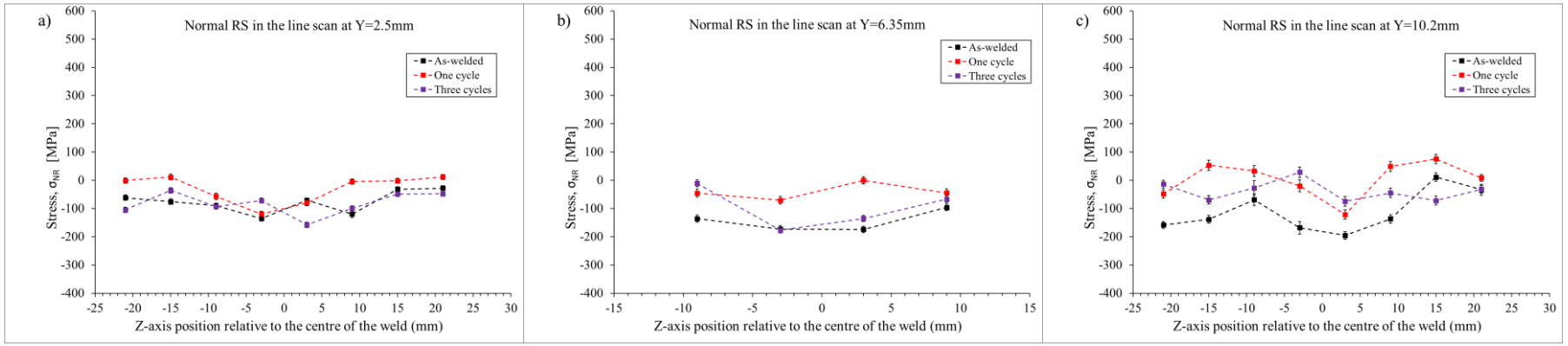

*Figure 5.18: Normal residual stress redistribution measured using neutron diffraction in the **horizontal** plate of the fillet-welded plate with the **long** weld in the line scan at a) the line scan at y=2.5mm, b) the line scan at y=6.35mm and, c) the line scan at y=10.2mm.*

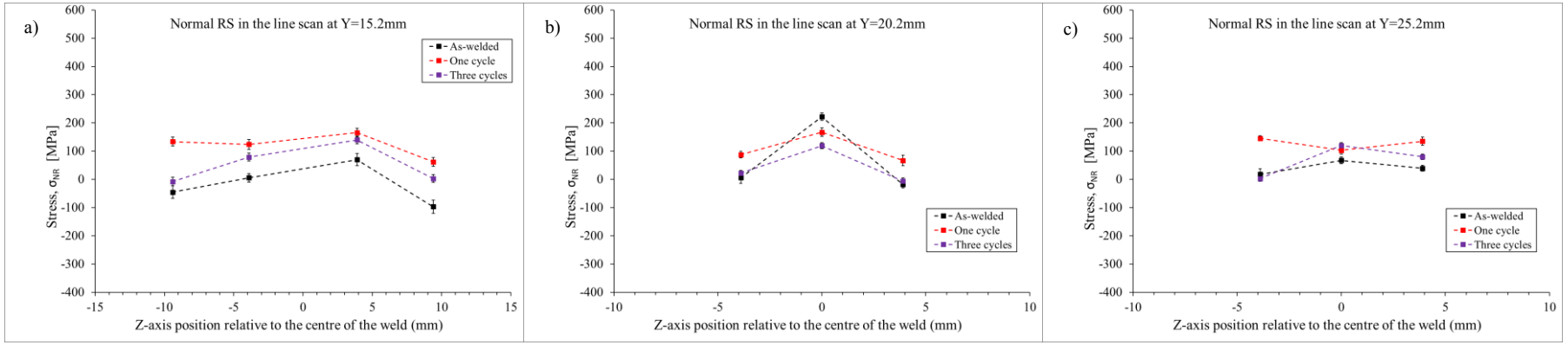

*Figure 5.19: Normal residual stress redistribution measured using neutron diffraction in the **vertical** plate of the fillet-welded plate with the **long** weld: a) the line scan at y=15.2mm, b) the line scan at y=20.2mm and, c) the line scan at y=25.2mm*

5.5 Discussion on residual stress redistribution

The state of residual stress at any given time on a critical structure is an important parameter to consider in structural integrity assessment (API 579-1 2016; BSI 2015; R6 Revision 4 2015). However, the influence of welding residual stress on structural integrity during fatigue depends strongly on the stability of the residual stresses during cyclic loading. The fact that fatigue crack initiations occur on the surface of the component has typically limited research on residual stress redistribution to focus only on the surface residual stress behaviour under cyclic loading (Cho and Lee 2016a; Farajian-Sohi, Nitschke-Pagel and Dilger 2009; Hao et al. 2015b; M. Farajian and T. Nitschke-Pagel 2012; Morrow J 1958).

On an ideal weld plate with zero distortion, uniaxial loading and no notch like discontinuity, the relaxation should be uniform across the loading cross-section. However, in real structures, the welded components experience both distortion and discontinuities due to the weld geometry, in which case a load across the cross-section could introduce bending stresses in addition to the membrane stress. In welded components in applications like offshore, since residual stresses are self-balancing internal stresses, a relaxation of residual stress measured on the surface of a plate following a load cycle could mean a redistribution of residual stress in the mid-thickness or below the top surface to become tensile. The residual stress values measured through the thickness determined using neutron diffraction after a limited number of load cycles have provided valuable information on the behaviour of residual stress inside the plate under cyclic load.

In this work, the specimens were manufactured in terms of welding procedure and the dimensions in line with shipbuilding practice. The load levels considered in the experiments were also chosen as the largest quasi-static loads that load bearing members such as stiffeners and transverse members will experience in its lifetime (Erny et al. 2012). This was to consider the change in residual stress during these overloads because it was expected to introduce the highest level of redistribution.

It is worth noting that the modern structural integrity codes consider highly conservative residual stress levels in welded components (API 579-1 2016; BS 7910:2013+A1:2015 2013; R6 Revision 4 2015). Even though stress in the weld is often as high as the yield strength in butt-welded specimens, it is often lower in fillet welded specimens.

In this work, residual stress redistribution in butt-welded specimens was consistent with some of the predictions found in previous literature. However, it was noted that a load applied perpendicular to the residual stress component under study still redistributes as a result of relaxation/redistribution in the residual stress along the load direction. It is, therefore, concluded that the geometry of the plate under study affects the way residual stresses relax/redistribute. One of the objectives of this work is to include the effect of geometry in the case of residual stress relaxation or redistribution problems. This work proposes a numerical model for the shakedown limit analysis described in the previous chapter which determines a lower bound shakedown limit of the specimens under study based on the geometry, material and load detail considered.

On fillet welded specimens there are little or no reported results on the residual stress measurements. The bulk of research data available regarding residual stress redistribution in fillet welded joints are mostly limited to numerical simulations or the surface of the specimens in the case of experimental work (Deng, Liang and Murakawa 2007; Gannon et al. 2013; Mahapatra, Datta and Pradhan 2006). The primary reason for the lack of data on residual stress measurements in fillet welded plates could be the difficulty in accessing locations near the weld using the existing non-destructive techniques (NDT is required to study redistribution of residual stress). Surface measurement techniques such as XRD often have limited access to the weld toe region on a fillet welded plate due to the limited access by the web plate. In this work, XRD was not able to measure any points close to the weld as the vertical plate was limiting access to the required locations. On the other hand, much research has been conducted on the residual stress prediction in fillet welded plates using welding process simulation. A few have been validated against surface residual stresses, but many in the literature only consist of experimental validation in terms of thermal analysis, not the validation of predicted residual stresses.

Neutron diffraction was used to measure residual stresses in six line scans in the mid-thickness of two fillet welded plates, and the results were presented. A recent study was conducted by Justin Mach et al. which studied the as-welded residual stresses in fillet welded plates (Justin Mach et al. 2019). They found that the residual stress distribution through the mid-section thickness was tensile on both sides of the web plate and compressive at the mid thickness of the plate. This latest result published in April 2019 is consistent with the results obtained for fillet welds in this study.

5.6 Numerical modelling of residual stress redistribution

Before the numerical modelling of residual stress redistribution, a 3D FE simulation of the welding process was performed on both butt and fillet welded plates. The welding process simulation was followed by an EDM cutting simulation to simulate the mechanical loading specimen manufacturing. The welding and EDM cutting simulation was validated, and the results were presented in detail in Chapter 4. Predicted as-welded residual stresses were used to define residual stress field in the residual stress redistribution model. The final models after the EDM cutting simulations are shown in Figure 4.12.

5.6.1 Material model

Since the redistribution of residual stresses is a result of shakedown, a clear partition between cyclic hardening or softening in kinematic and isotropic hardening should be considered (Wang and Liu 2017). The numerical modelling of residual stress redistribution was established on an elastic-plastic model initially developed by Lemaitre and Chaboche (Lemaitre and Chaboche 1994). A constitutive model for cyclic plasticity based on the unified Chaboche formulation is accurate enough to simulate both elastic and plastic shakedown (R5 2014). The redistribution or relaxation following cyclic loading is predominantly due to either elastic or plastic shakedown. The concept of the Chaboche constitutive model is presented in Section 3.5.1. An experimental programme detailed in section 3.5.2 was implemented to determine the required parameters. The material parameters obtained for DH36 base material and weld material are shown in Table 3.3.

5.6.2 Predefinition of as-welded residual stress

With the complete as-welded residual stresses identified in each specimen, a 3D elastic-plastic FE analysis of residual stress redistribution under cyclic loading was continued from the EDM cutting simulation output database. This required the transfer of all the output data from the EDM simulation analysis to be defined as the initial states in the new model.

One way to import residual stresses into the FE model is by using the eigenstrain method, where the strain incompatibility found initially in the model is used to determine corresponding stresses. Another way in ABAQUS is by using the SIGINI Fortran subroutine to introduce the initial conditions. In both these techniques, the as-welded

plastic strain information is left behind, and only residual stresses are imported. This is then considered not accurate for any further relaxation or redistribution analysis as the material properties are no longer accurate. Moreover, defining stresses in all three directions using these techniques is complicated and hence importance is given only to those components parallel to the load direction. This is also considered not accurate enough to simulate residual stress redistribution. However, these techniques have been used by many researchers, and often under the assumption that the stress distribution along the weld centre line is constant, which is not accurate (Lei, O'dowd and Webster 2000; Liljedahl et al. 2010; Smith et al. 2001).

In this work, the residual stress results obtained from the previous analysis were imported to redistribution analysis using the ABAQUS mesh-to-mesh solution mapping capability. This enables the transfer of all variables from the previous analysis to a new analysis. Moreover, this technique can be used in two different meshes, where ABAQUS will interpolate/extrapolate the stress from the previous nodes to the new nodes (the part dimension should be exact). This technique has been used in recent years by several teams (Cho and Lee 2016b; Lee, Chang and Van Do 2015; Wang et al. 2017a; Xie et al. 2017).

The “Restart Requests” command was used in the EDM cutting simulation to assist the import of stress results for the redistribution analysis with the stress, strain components and accumulated plasticity obtained after EDM cutting analysis. Following the import of initial residual stresses, a static step was defined for the numerical solver to establish an equilibrium state in the FE model before commencing cyclic load application.

5.6.3 Implementation of residual stress redistribution models

A complete 3D FE model was considered on all four weld specimens. The residual stress output from the EDM cut simulations was predefined using the Map solution keyword to the loading model. The load cycles were applied axially along the weld plate longer direction as presented in Table 5.1.

Table 5. 1: Applied load cycle details in each model

Specimen	Load direction	Maximum Load	Number of cycles
Butt welded plate with the short weld	Across the weld	370kN	Ten
Butt welded plate with the long weld	Along the weld	370kN	Ten
Fillet welded plate with the short weld	Across the weld	310kN	Three
Fillet welded plate with the long weld	Across the weld	400kN	Three

In the FE model, the gripping end of the weld plate was fixed on both top and bottom surfaces. Figure 5.20 shows the boundary conditions and load application implemented in the fillet welded plate with the short weld. The load was applied on a reference point which was coupled to the top and bottom surface of the load application side. A load amplitude precisely the same as the one collected from the stress rig was used for the load application. The time increment in each step was selected such that it captures all the points in the load amplitude defined in the FE model. The load cycles applied were tensile (R-ratio=0) sine wave cycles with 0.25Hz frequency.

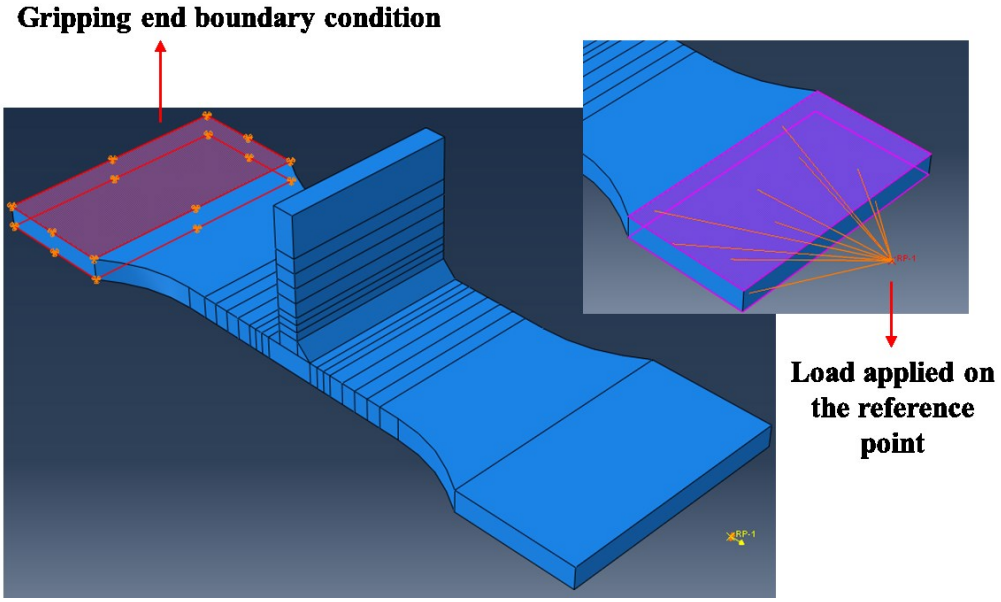

Figure 5.20: Loading and boundary conditions applied in the FEA simulating residual stress redistribution analysis on the fillet welded plate with the short weld.

3D-stress eight-node linear brick elements were used in the FE analysis. A fine mesh was employed on the gauge area, and a smooth transition was ensured from the fine mesh to the coarse mesh which was away from the gauge area as shown in Figure 4.12.

Residual stress values in longitudinal and transverse directions from corresponding measurement line scan locations in the butt and fillet welded specimens were extracted from the FE models after one, three and ten cycles. The comparison between the residual stress redistribution predictions obtained from the FE model and the experimental values obtained from neutron diffraction is presented in the following section.

5.7 Residual stress redistribution predictions

The predicted residual stress values were extracted from paths created through the measurement line scans and are obtained as an average value from the integration points of the elements inside the gauge volume. For conciseness, normal residual stresses were not compared as these were not significant in the loading direction considered in this work. The thickness and weld specification of the plate is selected based on the flat bar stiffener member in the bottom deck of a ship structure. Since the capacity of the in-situ loading rig at ENGIN-X is not enough to introduce residual stress shakedown, loading was performed at TWI Ltd, between neutron measurements. Even though care was taken during the set-up, small errors were expected in consequence.

5.7.1 Residual Stress redistribution predictions in butt-welded plates

In the case of the butt-welded plates, the line scans at Y=2.5mm and Y=10.2mm were compared with the corresponding measurement values. Here the measurement values obtained as-welded, and after one and ten load cycles, are compared with the FE model.

5.7.1.1 Butt welded plate with the short weld

Figure 5.21 compares the redistribution of longitudinal stress components from neutron diffraction measurements, and from the numerical model after the application of ten load cycles in the line scans at Y=10.2 and 2.5mm. As mentioned earlier, the applied load is along the transverse residual stress direction; hence little relaxation on the longitudinal stress component is observed in the FE model when compared with the experimental values. In the numerical results, a slight relaxation of about 100 MPa was noticed in the line scan at Y=10.2mm near the weld toe moving away from the weld centre.

Figure 5.22 compares the redistribution of transverse stress components from experimental measurement and numerical model after the application of ten load cycles in the line scan at Y=10.2 and 2.5mm. Although the transverse residual stress following three load cycles shows redistribution, this was noted to be different in the case of each line scan at different locations through the thickness. In the line scan at Y=10.2mm, after three load cycles, numerical results showed about 70% relaxation in the weld toe region compared with 90% relaxation from experimental measurements. This can be attributed to the underprediction of the initial weld residual stresses which is an influencing factor in the amount of relaxation.

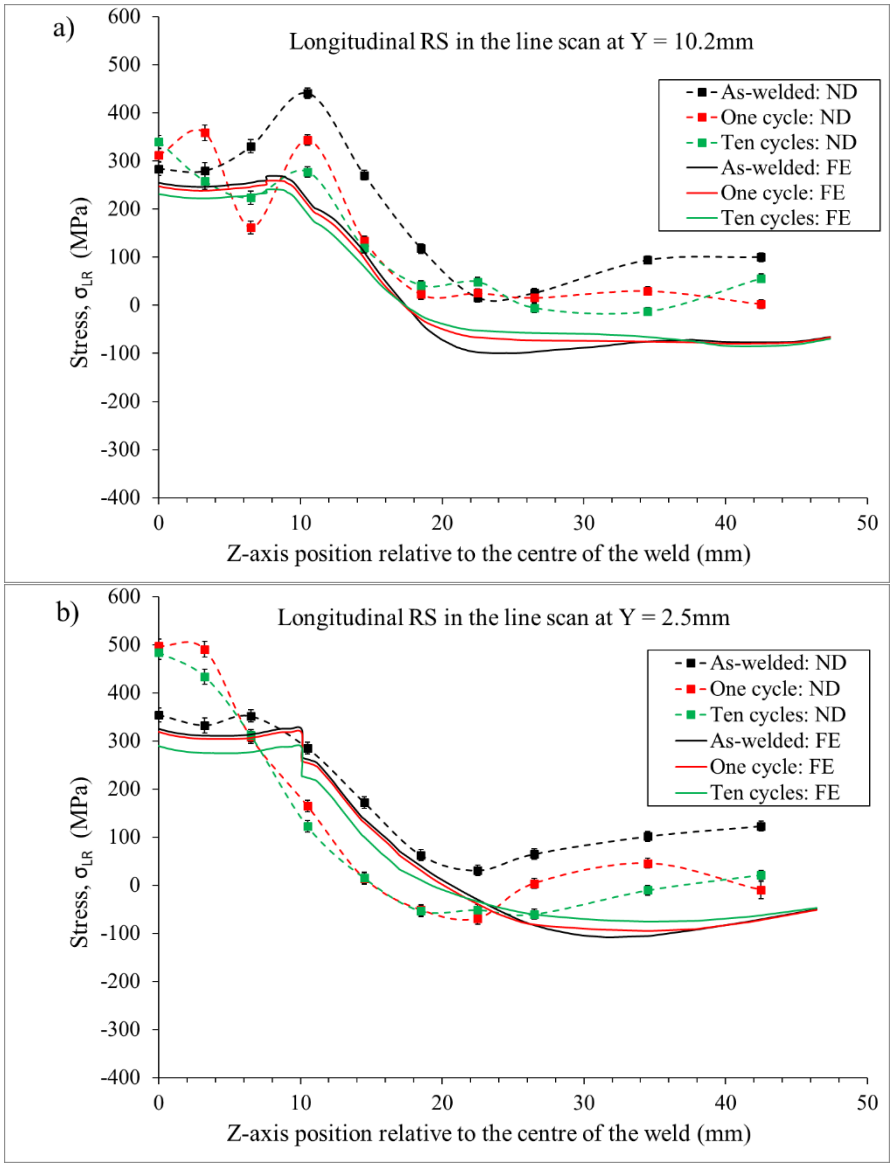

Figure 5.21: Comparison of longitudinal residual stress between experimental measurements and FE model data from the butt-welded plate with the short weld: a) Residual stress in the line scan Y=10.2mm and, b) residual stress in the line scan at Y=2.5mm.

Additionally, the amount of redistribution is a maximum after the first load cycle as shown in Figure 5.22a. On the other hand, the line scan at Y=2.5mm of the transverse component has shifted more into the tensile zone than the as-welded state after the application of three load cycles. This small increase could be the variation of the transverse component through the thickness to maintain internal equilibrium following a relaxation in the scan at Y=10.2mm. There also exists a tensile region with a maximum stress of 90MPa at the mid-thickness following redistribution in a line scan at Y=6.35mm (not shown in the graphs). It is noted that preloading weld plates for relieving tensile stresses can be useful on the top surface or weld toe of the plate (which is considered as detrimental), but it can also introduce tensile stresses through the thickness.

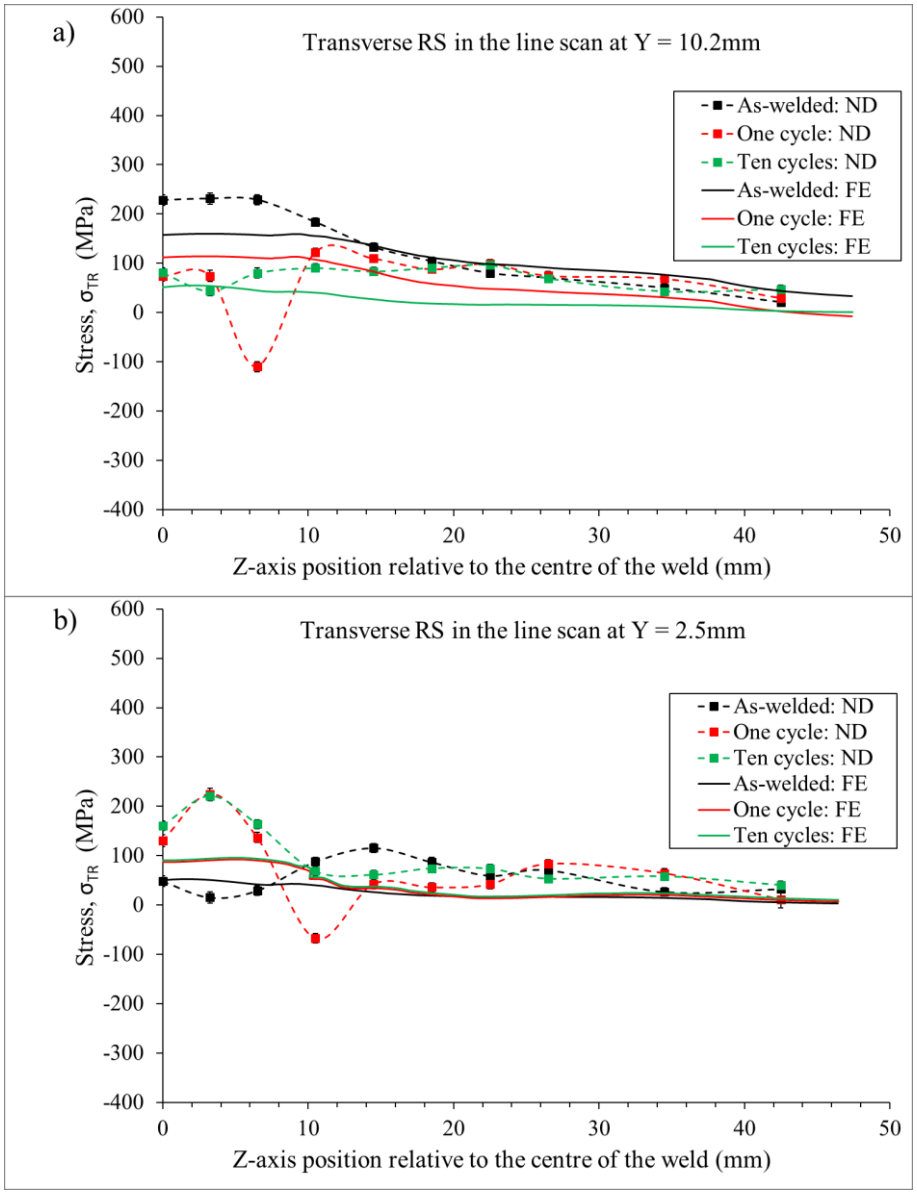

Figure 5.22: Comparison between experimental measurements and FE model of the butt-welded plate with the short weld along the transverse residual component: a) Residual stress in the line scan Y=10.2mm and, b) residual stress in the line scan at Y=2.5mm.

5.7.1.2 Butt welded plate with the long weld

Figure 5.23 compares the redistribution of longitudinal stress components from neutron diffraction measurements, and from the numerical model after the application of three load cycles in the line scans at Y=10.2 and 2.5mm.

As mentioned earlier, the applied load is along the transverse residual stress direction; hence little relaxation on the longitudinal stress component is observed in the FE model when compared with the experimental values. In the numerical results, a slight relaxation of about 100MPa was noticed in the line scan at Y=10.2mm near the weld toe moving away from the weld centre.

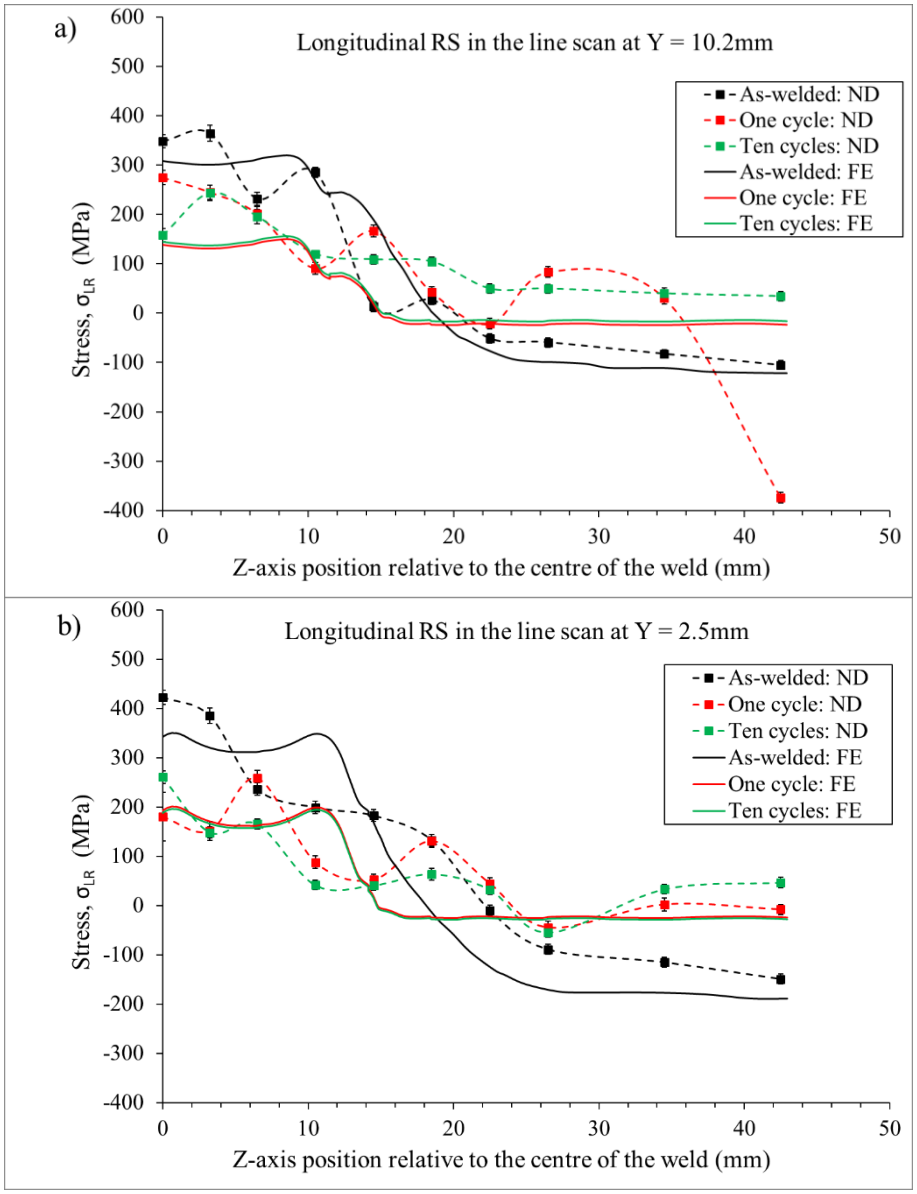

Figure 5.23: Comparison between experimental measurements and FE model of the butt-welded plate with the long weld along the longitudinal residual component: a) Residual stress in the line scan Y=10.2mm and, b) residual stress in the line scan at Y=2.5mm.

Figure 5.24 compares the redistribution of transverse stress components from experimental measurement and numerical model after the application of ten load cycles in the line scan at Y=10.2 and 2.5mm. Although the transverse residual stress following three load cycles shows redistribution, this was noted to be different in the case of each line scan at different locations through the thickness. In the line scan at Y=10.2mm, after three load cycles, numerical results showed about 70% relaxation in the weld toe region compared with 90% relaxation from experimental measurements. This can be attributed to the underprediction of the initial weld residual stresses which is an influencing factor in the amount of relaxation.

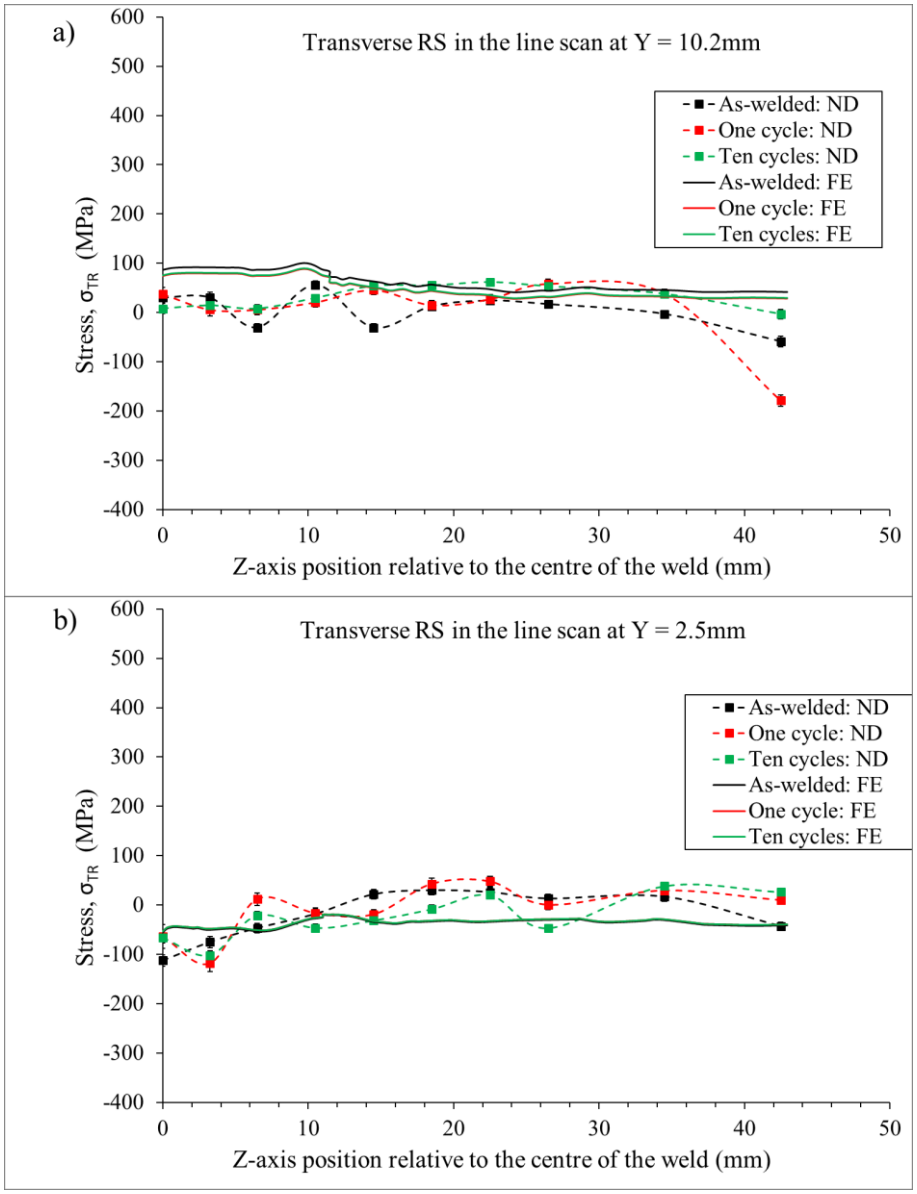

Figure 5.24: Comparison between experimental measurements and FE model of the butt-welded plate with the long weld along the transverse residual component: a) Residual stress in the line scan Y=10.2mm and, b) residual stress in the line scan at Y=2.5mm.

Additionally, the amount of redistribution is a maximum after the first load cycle as shown in Figure 5.22a. On the other hand, the line scan at Y=2.5mm of the transverse component has shifted more into the tensile zone than the as-welded state after the application of ten load cycles. This small increase could be the variation of the transverse component through the thickness to maintain internal equilibrium following relaxation in the top scan. There also exists a tensile region with maximum stress of 90MPa at the mid-thickness following redistribution in a line scan at Y=6.35mm (not shown in the graphs). It is noted that preloading weld plates for relieving tensile stresses can be useful on the top surface or weld toe of the plate (which is considered as detrimental), but it can also introduce tensile stresses through the thickness.

Overall, the FE predictions of the residual stress redistribution were in good agreement with the trend of the measurement values. The deviation in magnitude could be due to the underprediction of the as-welded residual stress and the scatter in the residual stress measured between each weld. Beyond underprediction of the as-welded stresses, various factors such as the material response, loading, boundary conditions and inevitable experimental errors can also affect the results.

5.7.2 Residual Stress redistribution predictions in fillet welded plates

In the case of the fillet welded plates, the line scans only close to the weld at Y=10.2, 15.2 and 20.2mm were considered for comparisons with experimental values. Here the measurement values from as-welded, after one and three load cycles were compared with the FE model data.

5.7.2.1 Fillet welded plate with the short weld

Figure 5.25 compares the redistribution of longitudinal stress components from neutron diffraction, and from the numerical model over three load cycles in the line scans at Y=10.2, 15.2 and 20.2mm. Overall the redistribution in the longitudinal residual stresses seen from the numerical model is very small in the horizontal plate as shown in figure 5.25a. However, in the line scans at Y=15.2 and 20.2mm, there was significant redistribution in the first cycle, and little or no effect was seen after three cycles (Figure 5.25b and 5.25c).

Figure 5.26 compares the redistribution of transverse stress components from neutron diffraction and from the numerical model over three load cycles in the line scans at Y=10.2, 15.2 and 20.2mm. The horizontal plate had a higher magnitude of as-welded stresses when compared with the values measured in the vertical plate. The redistribution of transverse stresses was seen in the FE model after the application of three load cycles. The numerical model was able to capture the trend in the measured stress in terms of redistribution. For example, in the case of the line scans at Y=15.2 and 10.2mm, the stress profile has shifted more into tension after three cycles and was seen similarly in the numerical model (Figure 5.24a and 5.24b). Interestingly, the near-zero as-welded stresses at Y=15.2mm have increased to about 100MPa after three cycles. In the case of the line scan at Y=20.2mm, no change in residual stress was noticed following three load cycles.

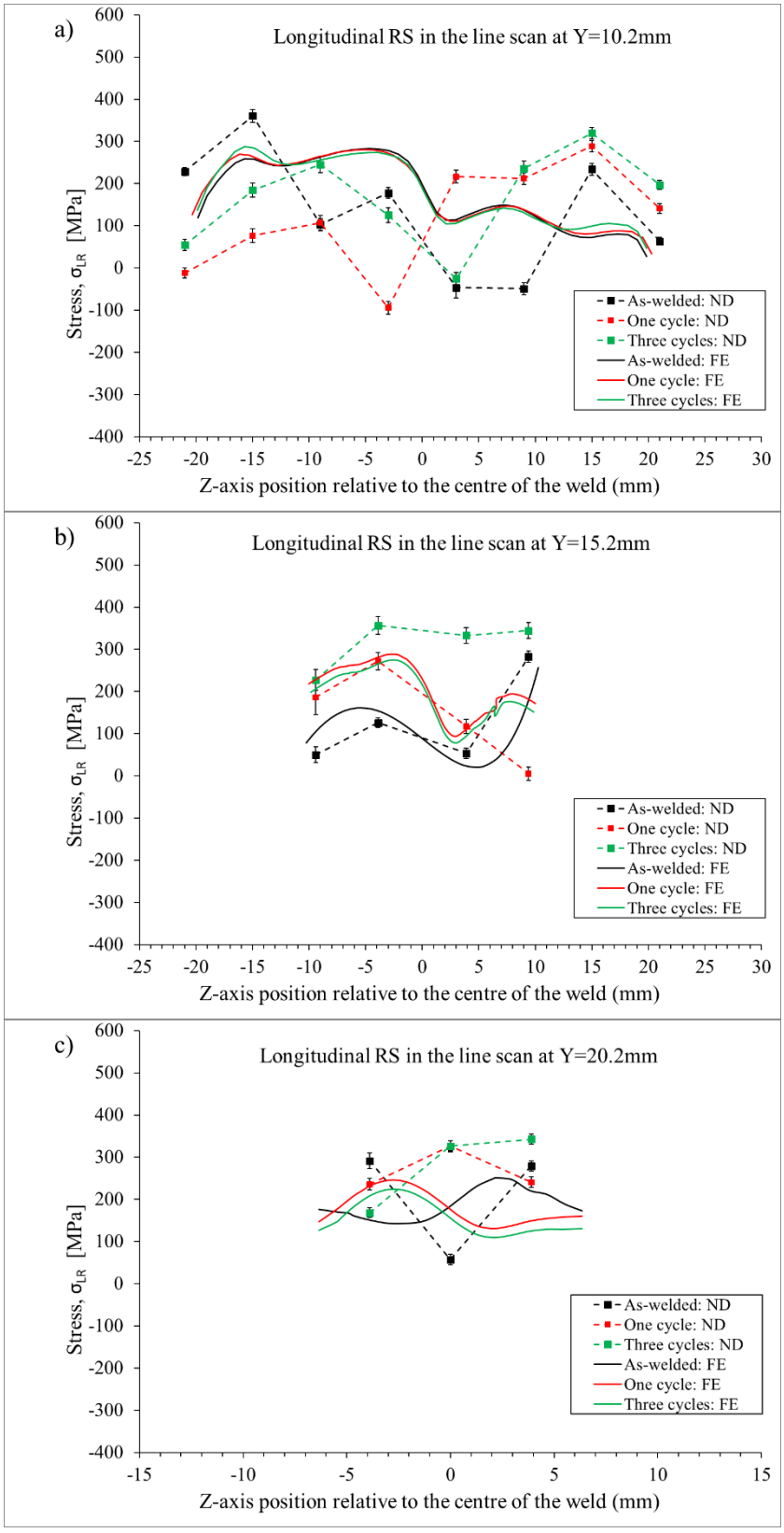

Figure 5.25: Comparison between experimental measurements and FE model of the fillet welded plate with the short weld along the longitudinal component: a) Residual stress in the line scan Y=10.2mm, b) residual stress in the line scan at Y=15.2mm, and c). Residual stress in the line scan Y=20.2mm.

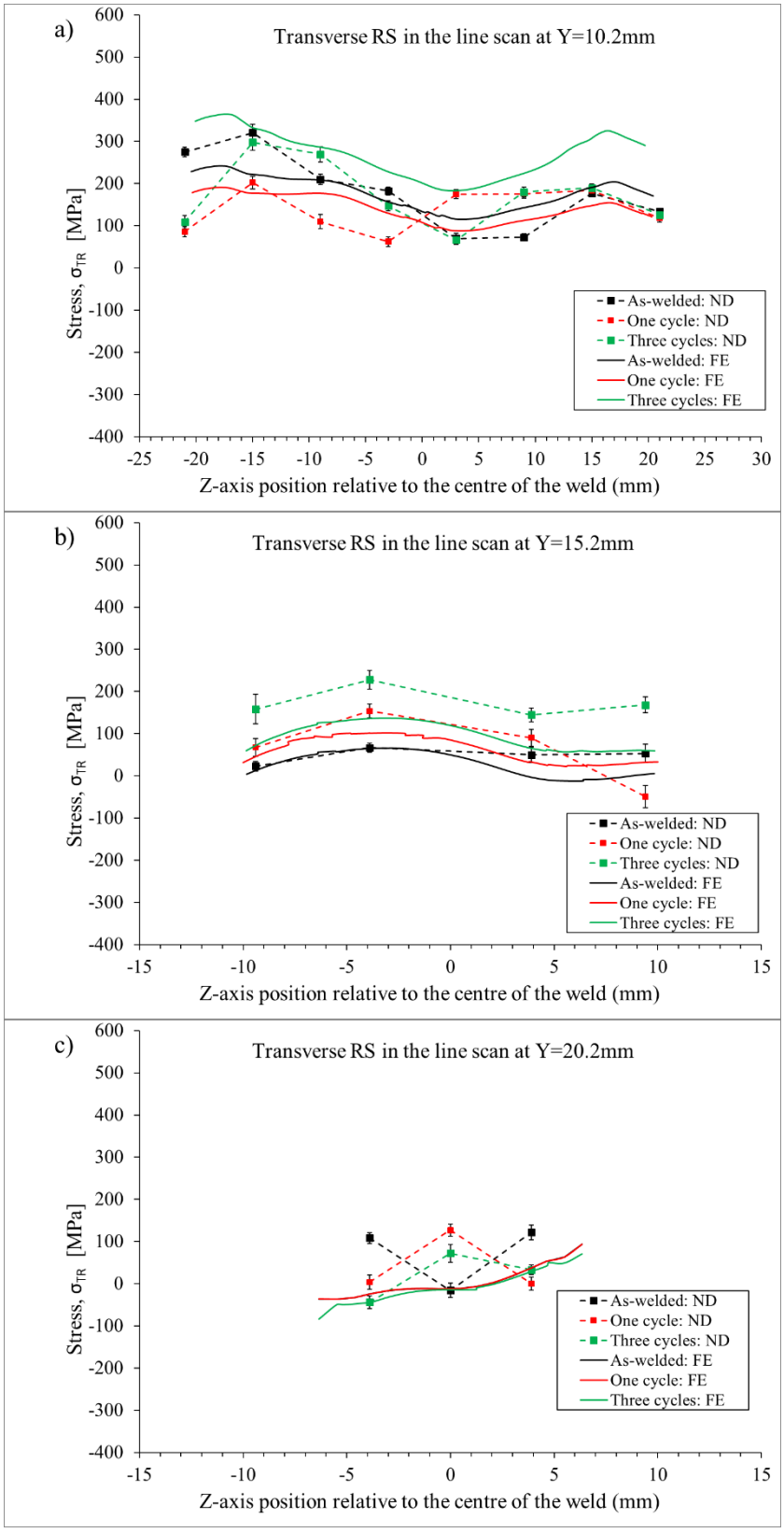

Figure 5.26: Comparison between experimental measurements and FE model of the fillet welded plate with the short weld along the transverse component: a) Residual stress in the line scan Y=10.2mm, b) residual stress in the line scan at Y=15.2mm, and c). Residual stress in the line scan Y=20.2mm.

5.7.2.2 Fillet welded plate with the long weld

Figure 5.27 compares the redistribution of longitudinal stress components from neutron diffraction, and the numerical model over three load cycles from the fillet welded plate with the long weld at Y=10.2, 15.2 and 20.2mm. At both Y=10.2 and 15.2mm, longitudinal residual stresses were measured to be tensile from an initial low value of as-welded residual stresses, just after one cycle and there was no redistribution after the first cycle (Figure 5.27a and 5.27b). Moreover, there was a significant relaxation in the longitudinal residual stress in the line scan at Y=20.2mm measured on the vertical plate of the specimen. In all line scans the relaxation or redistribution was predominant in the first cycle and was seen as the same in the numerical model under further load application.

Figure 5.28 compares the redistribution of transverse stress components from neutron diffraction and the numerical model. The transverse stresses had a similar pattern to that of longitudinal residual stress redistribution in the FE model. The as-welded transverse residual stresses were very low in the line scans at Y=10.2 and 15.2mm. However, longitudinal residual stresses were measured as tensile from an initial low value of as-welded residual stress, just after one cycle and there was no redistribution after the first cycle (Figure 5.28a and 5.28b). Also, there was relaxation in the longitudinal residual stress in the line scan at Y=20.2mm measured on the vertical plate of the specimen.

The numerical model was able to capture the trend in the measured stress in terms of redistribution. In the case of the line scans at Y=15.2 and 10.2mm, the stress profile has shifted more into tension after one load cycle and was seen similarly in the numerical model (Figure 5.27 and 5.28). Interestingly, the near-zero as-welded longitudinal residual stresses at Y=15.2mm is seen increased to about 200MPa after one load cycle.

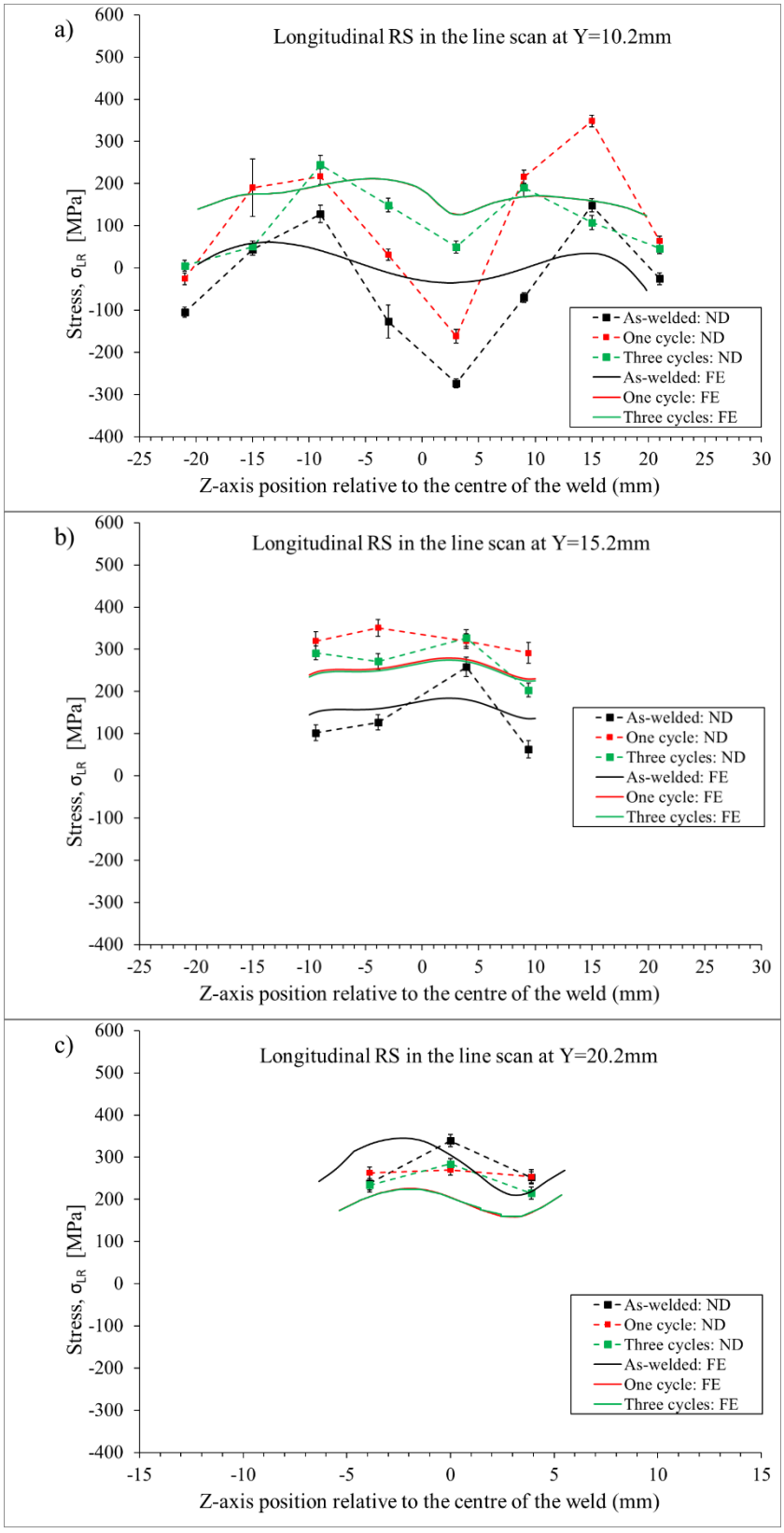

Figure 5.27: Comparison between experimental measurements and FE model of the fillet welded plate with the long weld along the longitudinal component: a) Residual stress in the line scan Y=10.2mm, b) residual stress in the line scan at Y=15.2mm, and c). Residual stress in the line scan Y=20.2mm.

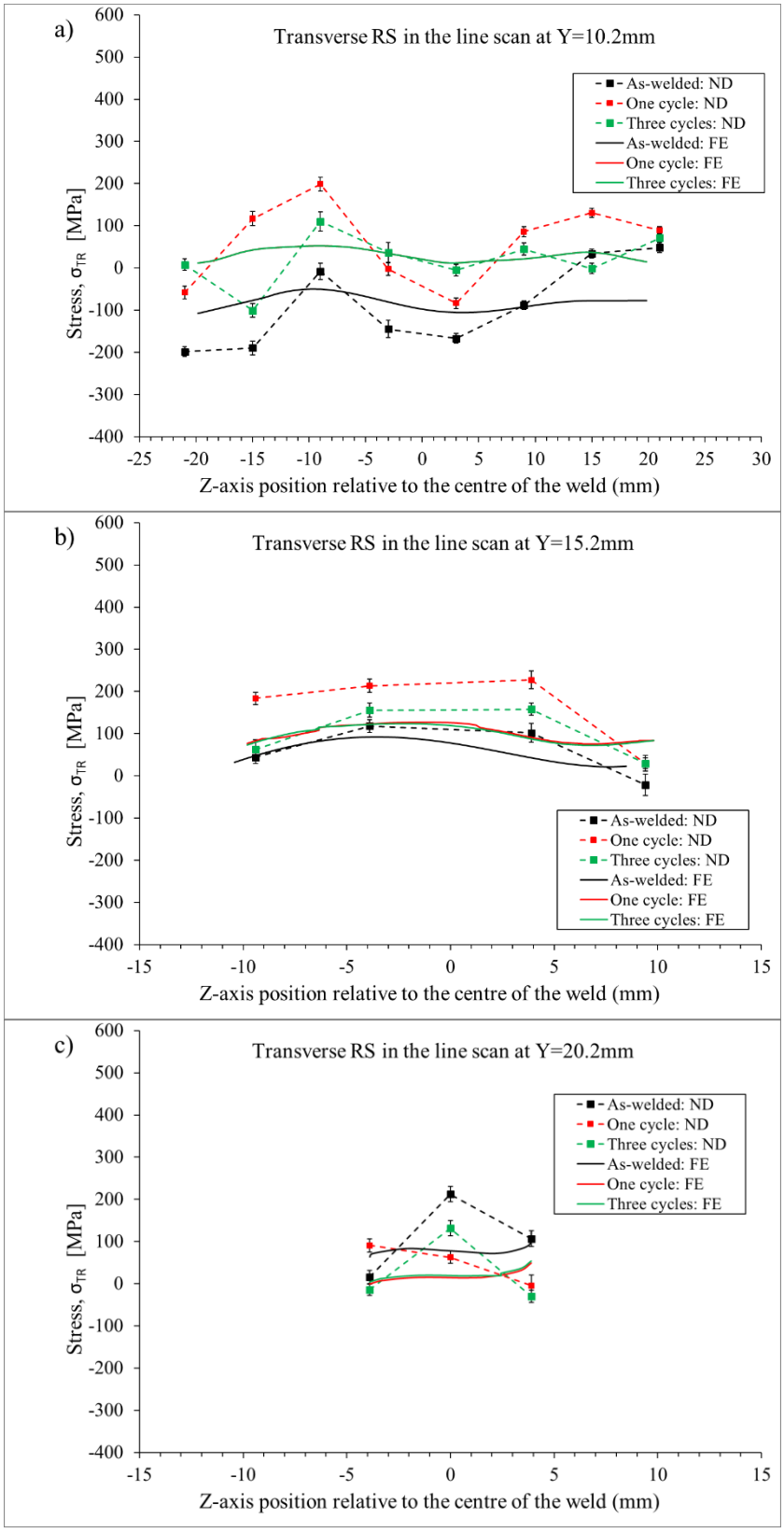

Figure 5.28: Comparison between experimental measurements and FE model of the fillet welded plate with the long weld along the transverse component: a) Residual stress in the line scan Y=10.2mm, b) residual stress in the line scan at Y=15.2mm, and c). Residual stress in the line scan Y=20.2mm.

5.8 Summary

This chapter presented the redistribution of as-welded residual stresses in butt and fillet welded plates. Experimental methods were implemented to apply a few cyclic loads on the welded mechanical test specimens. The residual stress values in selected measurement planes were determined using neutron diffraction in the as-welded condition, and after one, three and ten cycles. A numerical model was implemented for the numerical simulation of residual stress redistribution under cyclic loading in the specimen under study. The resulting residual stress measurements from the experiment and the predictions were discussed and compared against the experimental values obtained from neutron diffraction.

CHAPTER 6.NUMERICAL SIMULATION OF ELASTIC SHAKEDOWN IN WELDED PLATES

6.1 Introduction

A 3D numerical simulation of the shakedown limit analysis of weld plates under uniaxial mechanical loading is presented in this chapter. An elastic-plastic material model considering a mixed kinematic and isotropic hardening material behaviour was adopted. An incremental FEA technique coupled with reduced basis technique and energy method was implemented to solve the discretised shakedown problem numerically. This chapter describes the underlying principle of shakedown limit analysis performed on the weld specimens under study. Initially, the governing equations for the shakedown limit analysis and their implementation in ABAQUS software are described.

Further, the shakedown limit obtained for each welded specimen is discussed. Finally, a shakedown regime is defined based on the obtained shakedown limit and normalised residual stresses. The shakedown regime is used to investigate the redistribution of residual stresses in four critical locations in each specimen.

6.2 Micromechanics during shakedown

All metals contain distributions of dislocations which are linear lattice defects responsible for nearly all aspects of the plastic deformation (Dieter and Bacon 1986). Under a cyclic stress, dislocations will rearrange themselves within each grain and subgrain. Residual stress in a material is a result of external/internal constraints within the material storing elastic energy in atomic bonds. Application of external load on a residually stressed body facilitates dislocation movements, to resulting in residual stress relaxation. As this relaxation is due to plastic flow, this usually results in strain hardening

Strain hardening is caused by the interaction of dislocations with barriers which hinder their motion through the crystal lattice. One of the earliest concepts of dislocations to explain strain hardening is better explained using the concept of a back stress due to dislocation pile up on slip planes at barriers (Dieter and Bacon 1986). The back stress opposes the applied stress on the slip plane, so increasing the yield stress of the material. A crystal under loading in one direction up to yield and then reversing the loading to the opposite direction yields at a lower stress. This is because the back stress developed during the first loading cycle helps the dislocation movement in the opposite direction of

slip. Since dislocations of opposite sign attract and cancel out each other, effectively resulting in a further softening of the lattice, this explains the lower yield strength in the second load direction when compared to continued flow in the first load direction. The lowering of the yield stress when deformation in one direction is followed by deformation in the opposite direction is called the Bauschinger effect.

During shakedown in structures where residual stresses are not uniform, the structure undergoes yielding at some part of the structure due to dislocation movement aided by increased elastic energy in the system. As this yielding is localised, a redistribution of stresses takes place. This local yielding can be considered as a plastic zone embedded in an elastic region (Stein, Zhang and Mahnken 1993). The region which underwent yielding may have undergone strain hardening. Also, under alternating stress field Bauschinger effect can also take place.

6.3 Application of energy method during shakedown

In energy method, the deformation, displacement and the internal force associated with the deformation is determined using the amount of work done (Young 1981). Consider a deformable body in which an external body force is applied anywhere on its volume, and assume the applied load is sufficient to introduce a finite amount of deformation on the body. This means a finite amount of work was done on the deformable body as a result of the applied external force. The energy associated with the external force or the work done is absorbed by the deformable body to undergo deformation. Up to the elastic limit, the deformable body deforms elastically as a result of the force. The energy associated with the force is also lost when the external force is removed. Here the stress and strain have a linear relation as defined by Hooke's law. This is usually the case when the applied load levels are below the elastic limit. When the applied load is above the elastic limit of the material, the material will undergo permanent deformation at the expense of the energy from the external load. As a result, the stress-strain correspondence becomes nonlinear. A residual plastic deformation energy is consumed by the deformable body under external load in order to undergo permanent deformation. Hence, permanent plastic deformations are irreversible. Upon the release of all external load after permanent deformation, the remaining elastic energy is released.

In most materials, on a microscopic level, the dislocation configuration tends to be more stable to result in hardening at the expense of internal energy in the material. The plastic deformation energy absorbed as a result of loading above yield strength results in strain

hardening. In the case of cyclic loading, this results in cyclic hardening. Due to cyclic hardening, the material's deformation resistance is increased as a result of increased dislocation density. If the resulting elastic limit after cyclic hardening is above the external load levels, the structure will respond elastically in the subsequent cycles. In this condition, the structure is considered to have achieved a shakedown state.

In the theory of thermodynamics, no system can absorb energy indefinitely. In physical terms, if an external load is applied indefinitely such that there exists a finite amount of energy absorption due to plastic deformation throughout the period of the external load, the structure will ultimately fail due to plastic collapse (Zouain et al. 1993). Therefore, if a structure reaches a shakedown state, that means a definite amount of energy was absorbed as a result of external loading.

In this work, a numerical method based on the irreversible plastic deformation energy in terms of the amount of plastic work done on the specimen over an applied external load was used as a criterion to check for a shakedown state.

6.4 Shakedown limit analysis

In theory, the material shakes down to elastic response after the first few load cycles when the applied load is below the elastic shakedown limit. If the elastic shakedown limit is exceeded, plastic shakedown or ratcheting could occur as discussed in Chapter 2. One is shakedown state if the applied load is below the shakedown limit in which, after a few numbers of load cycles, plastic deformation tends to saturate, and the response becomes purely elastic for subsequent load cycles. The second is if the applied load cycles are above the shakedown limit, in which case, a definite plastic flow continuously advances until the structure collapse (ratcheting) or alternating plastic deformations lead to low cycle fatigue and fracture finally.

6.5 Reduced basis technique

Consider a general load domain Ω in which any point in this load domain can be assumed to be a set of external loads, applied in any sequence. For *m* number of independent generalised loads, *P* (volume forces, surface tractions, temperature changes or combinations), the load domain Ω will represent an m-dimensional polyhedron (Groβ-Weege 1997). The load domain Ω can then be defined as;

$$\Omega = [P_1, P_2, \dots \dots \ P_m]^T \qquad (6.1)$$

Resolving a common amplification factor μ, the load domain can be represented as;

$$\Omega = \mu[\lambda_1 p_1, \lambda_2 p_2, \dots \dots \ \lambda_m p_m]^T = \mu\{\lambda_m p_m\}, \lambda_m^- \leq \lambda_m \leq \lambda_m^+ \qquad (6.2)$$

Where p_m represents the limit below which no plastic deformation occurs and λ_m are the scalar multipliers which denote the amplification coefficient of p_m with upper and lower bounds λ_m^+ and λ_m^-, respectively. In the load domain defined above, each polyhedron corner defines individual loading representing primary or secondary loads in the load domain in any different direction and combination. In this work, only uni-axial primary tensile load cycles in one direction were considered. This simplifies the load domain to a line vector with one vertex as below:

$$\Omega = \mu[\lambda_1 p_1]^T = \{\mu p\}, 0 \leq \mu \leq \mu^+ \qquad (6.3)$$

where the amplification factor μ becomes the ratio of the magnitude of the load to the initial yield strength value in the load application direction. Therefore, the main objective of shakedown limit analysis in this work is simplified to solve for the amplification factor μ.

In welded plates, due to geometric discontinuities as a result of notch effects from the weld toe, under an external load, hot-spot stresses can arise which will then complicate the elastic limit defined in the plate (Hobbacher 2009). Hence the average stress values from the integration points of an element slightly away from the plane were chosen, and the corresponding load was considered as *p* in equation 6.3.

6.5.1 Governing equations in shakedown limit analysis

Now that the load domain is reduced to the specific problem in this work, this section presents the formulation of shakedown criterion using the energy method. Consider a component subjected to any numbers of cyclic loading, if the load levels are such that it plastically deforms the component, the plastic strain increment, $\Delta\varepsilon_{ij}^p$, associated with each

load cycles extracted at the end of each load cycle over a time interval $n \times t$ to $(n+1) \times t$ can be expressed as:

$$\Delta\varepsilon_{ij}^{p} = \int_{nt}^{(n+1)t} \dot{\varepsilon}_{ij}^{p} dt \qquad (6.4)$$

Where n is cycle count number, t is time period of each cycle and $\dot{\varepsilon}_{ij}^{p}$ is the plastic strain rate. With each load cycle applied on a deformable body having a volume V resulting in a generalised displacement, ΔU, the total work done W^{t}, can be defined as:

$$\int_{nt}^{(n+1)t} P\,\dot{U} dt = W^{e} + W^{p} \qquad (6.5)$$

$$W^{e} = \int_{nt}^{(n+1)t} dt \int_{nt}^{(n+1)t} \sigma_{ij} \dot{\varepsilon}_{ij}^{e} dV \qquad (6.6)$$

$$W^{p} = \int_{nt}^{(n+1)t} dt \int_{nt}^{(n+1)t} \sigma_{ij} \dot{\varepsilon}_{ij}^{p} dV \qquad (6.7)$$

where W^{e} and W^{p} are the elastic and plastic work done respectively, P is the generalised load and σ_{ij} is the Cauchy stress tensor. With a set of load cycles applied on the structure under study which can introduce plasticity in the structure, the plastic strain increment and the rate of plastic strain after a number of cycles, can result in the following (Abdel-Karim 2005).

1- $\Delta\varepsilon_{ij}^{p} \neq 0$ and $\dot{\varepsilon}_{ij}^{p} \neq 0$

The elastic strain in each cycle will stabilise with load cycle increments to a constant value. Hence the elastic work done will be zero (Equation 6.6 becomes zero). However, with a finite amount of plastic strain increment and plastic strain rate, the plastic work done (Equation 6.7) will always be greater than zero and the structure, if cycled indefinitely, cannot sustain the load and ultimately fails due to incremental plasticity. In this condition, the structure will not achieve a shakedown state.

2- $\Delta\varepsilon_{ij}^{p} = 0$ and $\dot{\varepsilon}_{ij}^{p} \neq 0$

If the change in plastic strain is zero and the rate of plastic strain is not zero, the structure is alternating between a constant plastic deformation. Here the displacement, displacement rate and the plastic strain rate are all cyclic. This condition is usually called alternating plasticity or reverse plasticity. If cycled indefinitely, the failure of the structure will ultimately occur due to low-cycle fatigue. In this condition also, the structure will not achieve a shakedown state.

3- $\dot{\varepsilon}_{ij}^{p} = 0$

If the rate of plastic strain is zero between each load cycle, the plastic work done (Equation 6.7) will become zero. Also, upon unloading the elastic strain will be removed and as a result, the elastic work done will also be zero. Here, as a result of initial plastic deformation in the structure, plasticity induced residual stress, ρ_{ij} will exist in the structure. However, due to no further work done in the system, the residual stress field will be time-independent and will be formed simply based on the plastic deformation in the initial few load cycles. Therefore, it can be said that the structure responds elastically to the applied load and satisfies Melan's lower bound theorem (Melan 1938a). The structure has now achieved shakedown state as the accumulated plasticity or cumulative dissipated energy in the structure is restricted within limits over time.

It can be seen that in all three conditions, plastic work done indicates the state of the response of the structure after each cycle. Considering an FE model with N number of elements, and a volume of V^e for each element, by combining equations 5.5 and 5.8, the plastic work done becomes:

$$W^p = \sum_{i=1}^{N} \int_{V^e} \sigma_{ij} \Delta\varepsilon_{ij}^{p} dV^e \qquad (6.8)$$

Hence it is concluded that W^p defined in equation (6.8) can be used as a shakedown criterion in the following FE models.

6.6 FE implementation

The FE model for determining the shakedown limit was developed on the final EDM cut specimens to capture all of the geometric features on each specimen. Shakedown limit analysis on all weld geometries was performed without considering the as-welded residual stress field. Let $\mu_i (i = 1, \ldots\ldots n)$ be load factors where n is the number of increments from the initial elastic limit. The largest value of μ_i will be the load at which the structure can achieve shakedown with imposed boundary conditions.

A Python script was used with the FE package ABAQUS to implement the procedure. With the modern computation capabilities, the shakedown limit was implemented using a step-by-step iterative procedure illustrated in Figure 6.1. The step-by-step procedure is further explained in detail below.

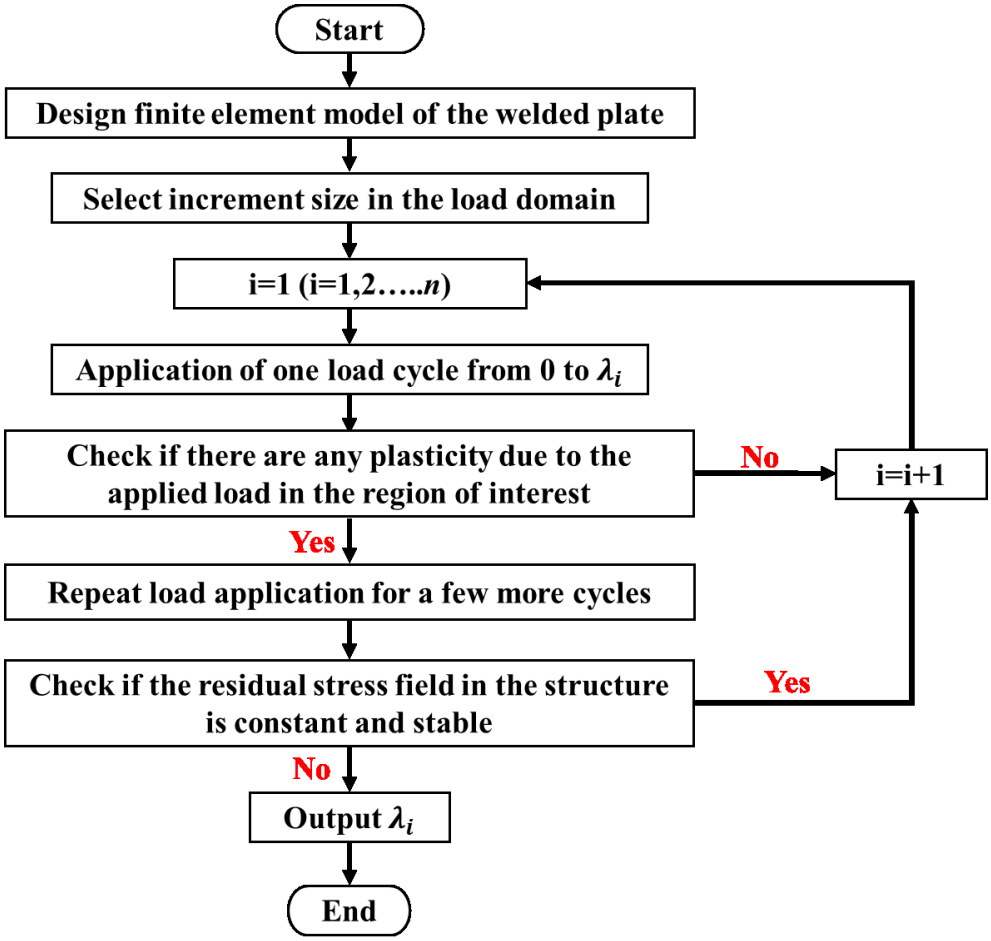

Figure 6.1: Flow chart of the procedure used in the FEA to implement shakedown limit analysis.

I. The first step is to design the structure under study considering all the geometric features. Also, the material properties used in the analysis play an important role as the plastic strain response and the cyclic hardening results are obtained as a result of the material behaviour.

II. To define a load domain which represents the actual problem. For example, for a problem considering a bi-axial load with secondary thermal stress, a triangular load domain (three vertices) should be considered. In this work, only one vertex was considered for the load domain as explained in the section above. It should be noted that in an n-dimensional polyhedron, with the increase in the number of vertices, the accuracy of the solution will be better, but it would mean higher computational demand.

III. During the application of the initial load level, μ_1, at first, the FE model was subjected to a load from 0 to μ_1 and then unloaded to 0, which constitutes a load cycle. The output results from a single load cycle were investigated for any plastic zone formed using a python script. If there were no plasticity found in the plates, then the applied

load levels were increased to the next increment at μ_2. If a plasticity exists in the plate, the same load is applied for a few more cycles, and any time-independent stable residual stress field, ρ_{ij} in the FE model was checked. The residual stress mentioned here is not the weld residual stress, but the residual stress generated in the plate as a result of plastic flow.

IV. After the application of 50 load cycles, if stable residual stress was not found, then the previous load levels at μ_{i-1} and associated load multiplier factor was considered as the shakedown limit. Otherwise, the structure was subjected to the next load point at μ_{i+1}.

V. By iterating the procedure described in (c) and (d), the maximum load applied to achieve shakedown state, and the corresponding shakedown limit was obtained as an output.

During the iterative process, at each condition checkpoints in the flow chart, the plastic work done according to Equation 6.7 was calculated after each load cycle. The cumulative plastic work done over a range of load cycles performed was then determined. A condition for the same cumulative work done between two successive load cycles was checked, and if they were equal, it was considered that the rate of plastic strain, $\dot{\varepsilon}_{ij}^{p} = 0$ and the rate of change of residual stress, $\dot{\rho_{ij}} = 0$. The analysis was then considered as having achieved shakedown as the cumulative energy dissipation is bounded.

In this work, when solving the shakedown limit analysis, a linear loading path from 0 was chosen. This is not expected to decrease the accuracy of the solutions as the plasticity behaviour mainly depends on the history of the maximum load when compared to the load path.

6.7 Model geometry, material model and boundary conditions

As mentioned earlier the specimen after EDM cutting was designed for the shakedown limit analysis. The dimensions of the plates were chosen exactly as the dimension of the manufactured specimens presented in Chapter 3. Weld dimensions were obtained from a macrograph of the weld bead. Both weld crown and the root pass was modelled in the butt welded plates to consider plasticity at the stress concentration areas of the geometry. The same boundary condition as to the load application of fatigue loads was applied to the model.

The Chaboche mixed hardening model described in section 3.5.1 was implemented to consider plasticity effects in the FE model. In ABAQUS, the definition of the combined hardening model can be implemented without any subroutines.

The mesh was designed in such a way that a very fine mesh was employed in the gauge area of each specimen (Figures 6.2 and 6.3). Shakedown based on plastic work done was checked in the gauge area. Away from the gauge area, a smooth transition was ensured in the geometry, and, a coarser mesh was introduced toward the outer areas of the plates using smooth mesh transition. There was a high degree of mesh refinement at the weld and HAZ. In all FE models, the elements on the weld were $0.75\times0.75\times1mm^3$ in the case of butt-welded plates and $1\times1\times1mm^3$ in the case of fillet welded plates. All four shakedown limit analyses used first-order 8-node 3D stress elements with reduced integration (C3D8R).

For computational efficiency, the butt and fillet welded plates with the short welds were implemented by considering symmetry across the weld. Figure 6.2 shows the mesh details, symmetric plane (along the x-axis), boundary conditions and the loading region used in the shakedown limit analysis of butt and fillet welded plates with short welds. Here the load was applied across the weld. On the other hand, the butt and fillet welded plates with long welds did not have a symmetric plane and hence a complete FE model was implemented.

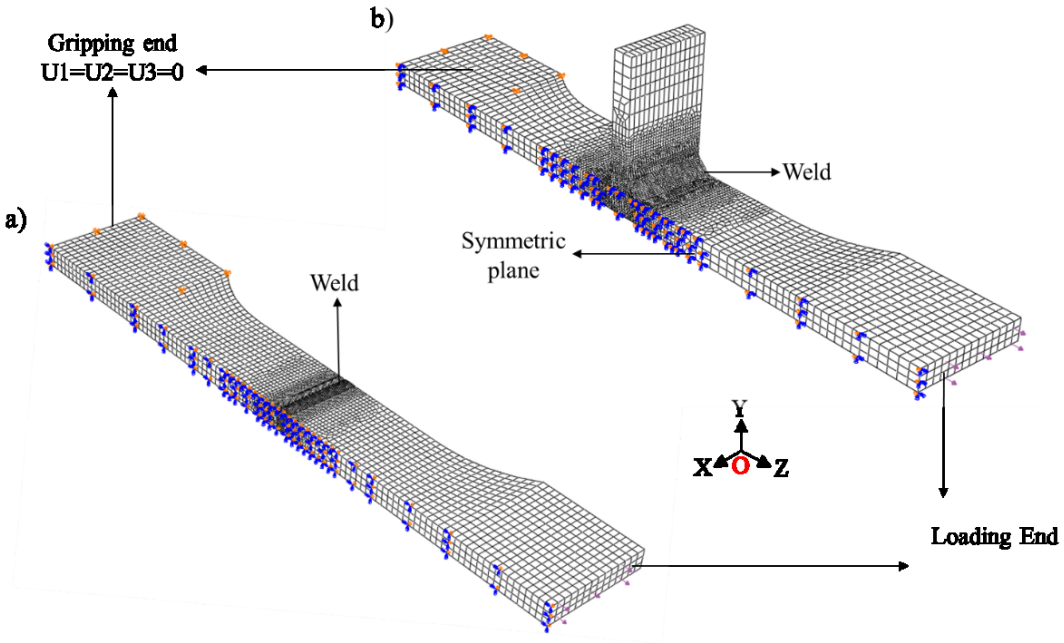

Figure 6.2: FE model details showing boundary conditions and loading end for shakedown limit analysis in Abaqus: a) Butt welded plate with the short weld and, b) fillet welded plate with the short weld.

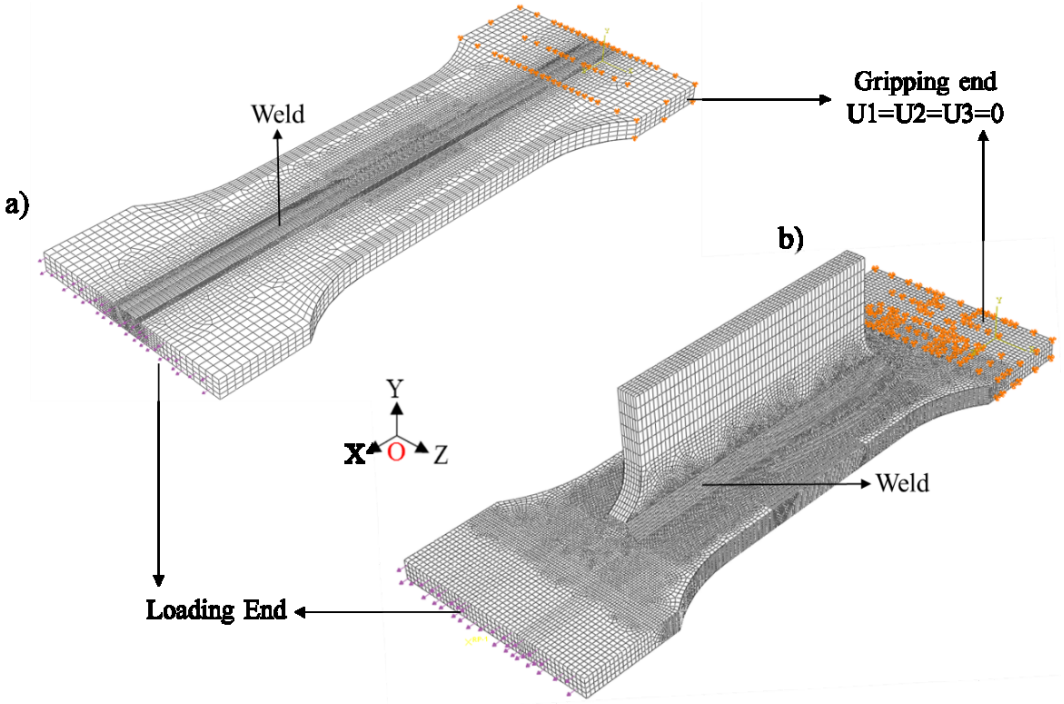

Figure 6.3: FE model details showing boundary conditions and loading end for shakedown limit analysis in Abaqus:a) Butt welded plate with the long weld and, b) fillet welded plate with the long weld.

Figure 6.3 shows the mesh details, boundary conditions and the loading region used in the shakedown limit analysis of butt and fillet welded plates with long welds. Here the load was applied parallel to the weld line.

6.8 Loading details

The focus was on the gauge area, and it was expected to have a uniform stress distribution in the area of interest. However, with the consideration of the weld in the centre of the gauge volume in all specimens, hot-spot stresses were expected. The shakedown limit analysis was performed based on nominal stress extracted from a plane away from geometric discontinuities in the weld plate. The transition region to the loading area, the weld toe and the weld root region was considered as geometric discontinuities in the specimens. However, due to the dog bone design, the transition zone discontinuity was ignored.

Table 6.1 presents the tensile load levels, equivalent to nominal stress of 350MPa at a plane away from the geometric discontinuity and the load increments used in each iteration. For example, in the case of the butt-welded plate with the short weld, the tensile load of 250 MPa applied was equivalent to nominal stress of 350MPa from the plane at Z=50mm (Z= 0 corresponds to the weld centre line). Z=50mm was considered away from any geometric discontinuity. Figure 6.4a shows the plane considered in the butt welded

plate with the short weld. Here the applied stress of 250MPa at Z=200mm plane corresponds to 350MPa at Z= 50mm plane. Similarly, Figure 6.4b shows the plane used for nominal stress consideration in the fillet welded plate with the short weld.

Table 6.1: Load details used in each FEA model during shakedown limit analysis

Specimen	Nominal stress	Location of plane nominal stress	Applied load at the specimen ends	Load Increment
The butt-welded plate with the short weld	350 MPa	Z = 50 mm	250 MPa	1%
The butt-welded plate with the long weld	350 MPa	X = 0 mm	250 MPa	1%
The fillet welded plate with the short weld	350 MPa	Z = 50 mm	250 MPa	1%
The fillet welded plate with the long weld	350 MPa	X = 0 mm	260 MPa	1%

On the other hand, the butt and fillet welded plate with the long weld did not have a notch effect as the applied load was parallel to the weld line. Here the stresses in the weld cross section were uniform. Hence the reference plane for the extraction of nominal stress was from the plane at X = 0mm as shown in Figures 6.5a and 6.5b.

Initially, a tensile load cycle (R-ratio=0) from 0 to 175MPa was applied to see if there are any plasticity zones developed. When the condition for plasticity was satisfied, the analysis was launched with the same load level, up to 50 load cycles. A structure is said to have achieved shakedown when there exists a constant time-independent residual stress in the structure after a few initial cycles (R5 2014). Therefore, the results were analysed for a constant residual stress field after the first few cycles. During the shakedown limit analysis, this was checked by comparing the equivalent plastic strain variation in the analysis. The load level in each iteration was incremented by 1%.

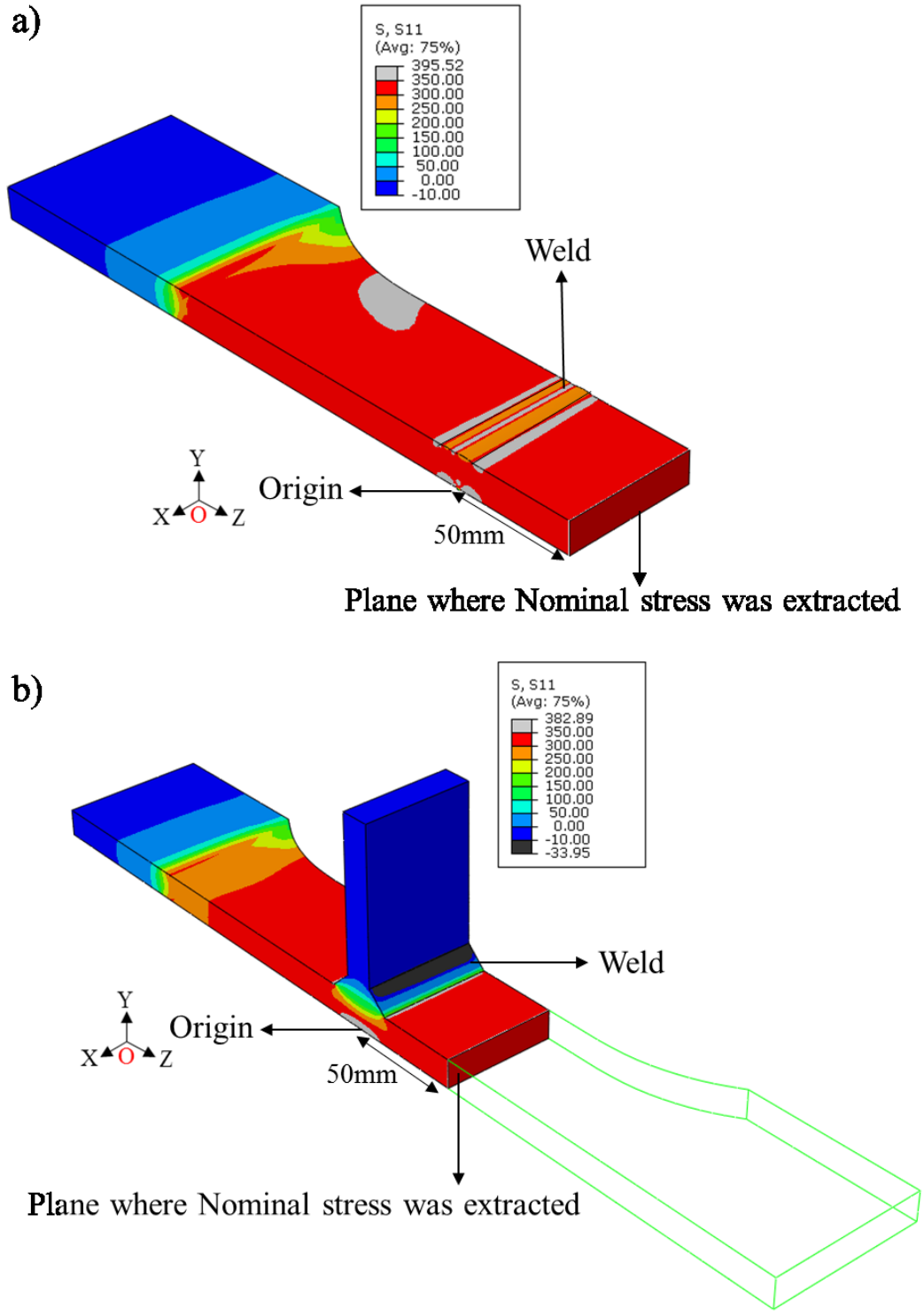

Figure 6.4: Stress contour under static loading prior to shakedown limit analysis showing plane at Z=50mm from which the nominal stress of 350MPa was considered: a) The butt-welded plate with the short weld and, b) the fillet welded plate with the short weld.

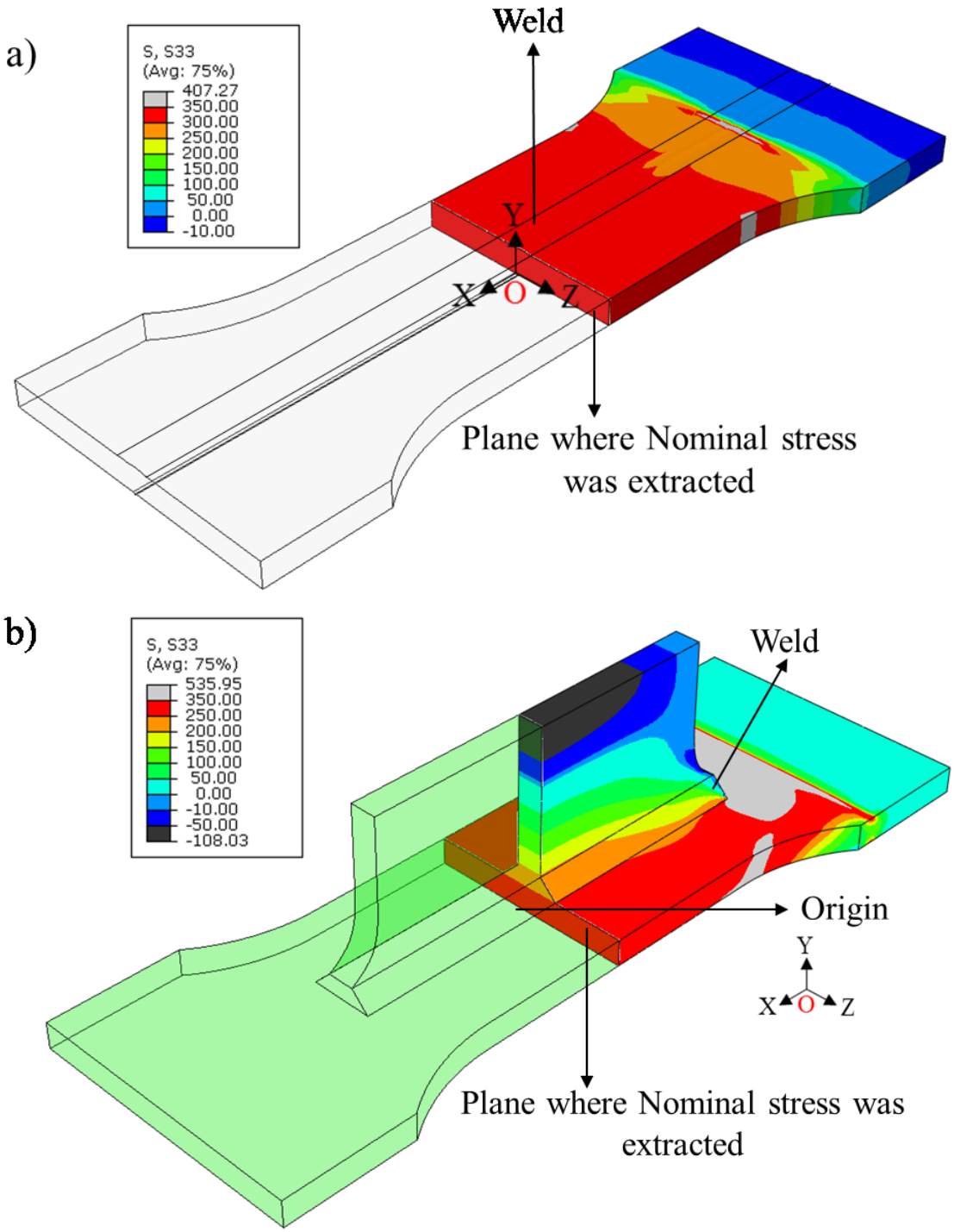

Figure 6.5: Stress contour under static loading prior to shakedown limit analysis showing plane at Z=0mm from which the nominal stress of 350MPa was considered: a) The butt-welded plate with the long weld and, b) the fillet welded plate with the long weld.

6.9 Shakedown limit estimated

The FE model is subjected to increasing loads starting from 50% of the yield strength of the parent material. After each load cycle, the equivalent plasticity at the end of a cycle is used to check the formation of plasticity. Based on a maximum number of 50 iterations, the shakedown limit estimated by the FE model for each specimen is listed in Table 6.2. The butt-welded plate with the short and, the long weld obtained a shakedown limit of $1.17\times\sigma_y$ and $1.22\times\sigma_y$ respectively, where σ_y is the parent material yield strength. Also, the fillet welded plate with the short and, the long weld obtained a shakedown limit of $0.89\times\sigma_y$ and $0.99\times\sigma_y$ respectively.

Table 6.2: The shakedown limit obtained from FEA for each specimen.

Specimen	Shakedown limit as a percentage of yield strength of DH36
The butt-welded plate with the short weld	1.17
The butt-welded plate with the long weld	1.22
The fillet welded plate with the short weld	0.89
The fillet welded plate with the long weld	0.99

The obtained shakedown limit implied that the weld plate could achieve shakedown state operating in the load level defined as per the limit. For example, in the butt-welded plate with the short weld, in the absence of a residual stress field any cyclic load within 1.17 times the yield strength applied in this set-up will achieve a steady state after initial plastic response. It should be noted that the shakedown limit is not an indication of fatigue failure by high cycle fatigue or low cycle fatigue. The shakedown limit analysis implemented in this work was based on the geometry of the specimen, the plastic-hardening model representing DH36 and the load application direction. Even though the procedure was implemented for a particular loading path, the method was applicable in multi-dimensional loading spaces.

The stress-strain response from a reference element close to the weld toe (in both butt and fillet welds) from the FE model was considered. The location of the element chosen for each weld plate is illustrated in Figures 6.6 and 6.7. The reference element closest to the weld is chosen to avoid any influence of the notch effect resulting in a non-linear stress peak due to the weld (Hobbacher 2009).

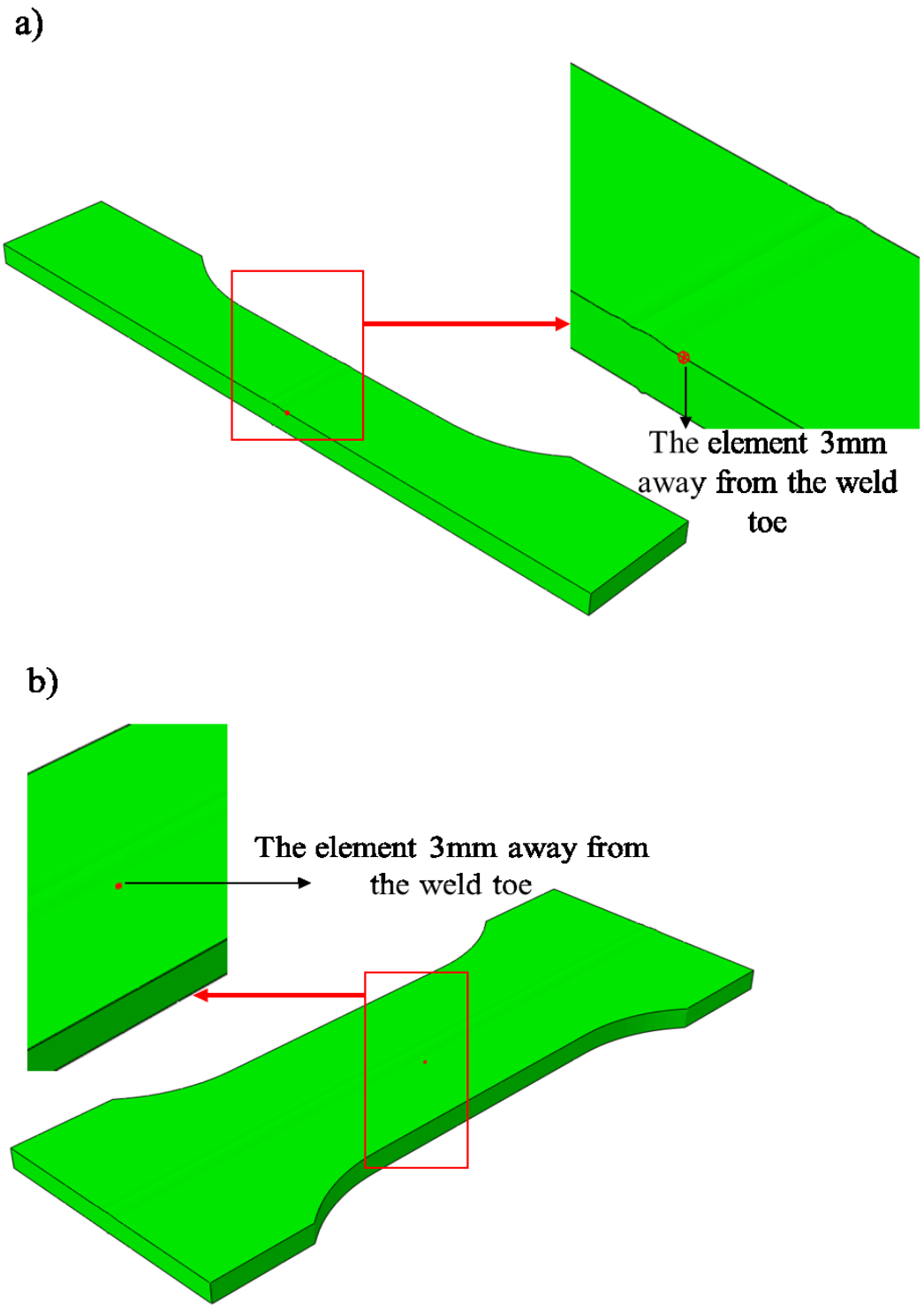

Figure 6.6: Shakedown limit abnalysis FE model detail showing the location of the element from which the shakedown response was extracted: a) The butt-welded plate with the short weld and, b) the butt-welded plate with the long weld.

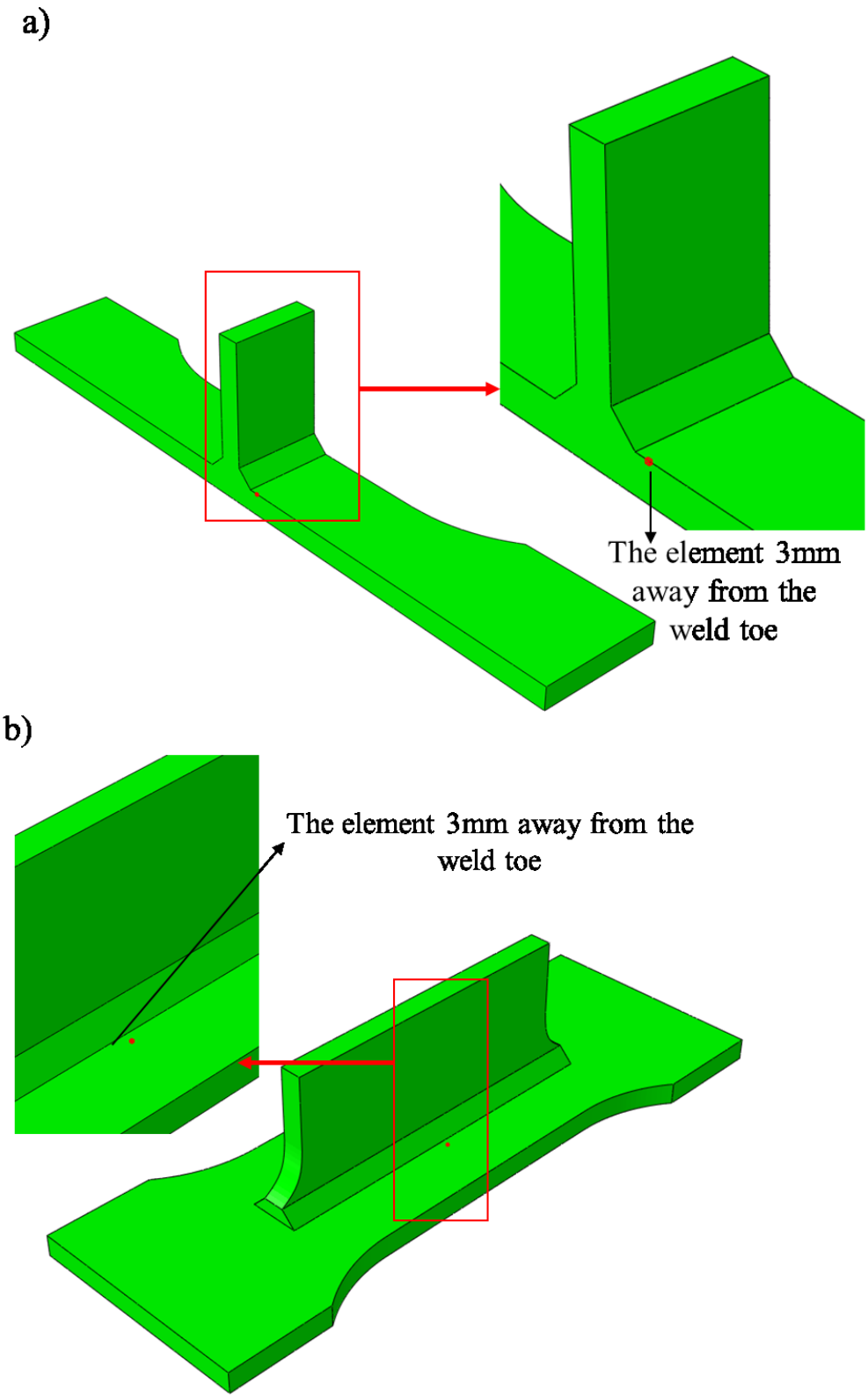

Figure 6.7: Shakedown limit abnalysis FE model detail showing the location of the element from which the shakedown response was extracted: a) The fillet welded plate with the short weld and, b) The fillet welded plate with the long weld.

The shakedown limit determined is slightly different for each specimen. The weld plates considered in the shakedown limit analysis have overmatched welds with a weld material of yield strength 400MPa. As the numerical simulation is defined for a specific load case, the main differences in each of these analyses are the geometric features and applied load direction. For instance, the weld geometry of the butt-welded plate with the short weld and the long weld are of the same detail. However, the plate dimension and the load application are different. Also, the material property defined in all analyses is the same for weld and parent material.

The shakedown limit analysis of the butt-welded plates determined higher shakedown limit when compared to that of the fillet welded plates. This is attributed to the stress concentration factor in the fillet welds due to the weld toe angle. In the case of the fillet welded plate with the long weld, even though the load is applied across the weld toe, the load application was only on the horizontal plate, and hence, the attachment web could introduce a boundary condition along the weld mostly leading to bending stresses.

Also, the shakedown limit determined for both the butt and the fillet welded plates with the short weld had lower shakedown limit compared with the butt and fillet welded plates with the long weld. This is because of the applied load direction which is across the weld line to bring out the effects of stress concentration at the weld toes.

Even though shakedown limits are not covered in standards for applications not concerning high-temperature loads such as stiffeners in ship structures, shakedown limits can be considered as a design against low cycle fatigue. For applications involving low cycle fatigue, it is evident that standards such as BS 7608 (BS 7608 2014), PD 5500 (PD 5500:2018 2018), ASME (ASME BPVC Section VIII.2 2015) and DNV (DNVGL-ST-F101 2017) require a limit on the stresses or stress range that may be considered.

These standards do not explicitly provide guidance on low-cycle fatigue but provide bounds to limit the amount of plasticity that may occur in a member, in turn, circumventing the need to consider low-cycle fatigue. This is because of the difficulty to consider strain life models that can be generalised to be included in design guidelines. It is often very complex and not general to define life models considering significant plastic cycling when compared to the conventional S-N curve method under elastic conditions. The cyclic hardening properties of the material are generally unknown during the design stage of any components, and these properties are proven to hugely affect the low-cycle fatigue life of the component. Though primarily intended for thermal and pipeline

application, in the absence of a specific code defining low cycle fatigue for ship structures, the section following briefly explains various requirements when assessing low-cycle fatigue in welded structures and a comparison with the one estimated in this work.

6.9.1 BS 7608 and PD 5500

BS 7608 design load limits under normal operating conditions are limited at a maximum calculated tensile stress ≤60% of the yield strength. Under extreme loading conditions a maximum calculated tensile stress ≤80% of yield strength is considered. Here the calculated stress to be considered is the maximum membrane stress on the net sectional area away from the geometric discontinuity and also excluding secondary stresses such as weld residual or thermal stresses. Based on a tensile loading (R=0) as applied in this work, the limits becomes stress ranges of 0.6 times yield and 0.8 times yield for normal and extreme conditions respectively. The main objective of these limitations are to limit stress cycling within the elastic range to have consistence with those in the tests used to generate the fatigue design curve. PD 5500 (PD 5500:2018 2018) has the same design SN curves as BS 7608. PD 5500 assumes that shakedown will occur within the static design limits. This enables to use the load-control S-N curves equivalent to strain controlled and hence it can be simply extrapolated into the low-cycle zone.

The obtained shakedown limits on the butt and fillet welded plates are higher than 0.8 times the yield strength as defined by BS 7608. Based on the results in this work, the BS 7608 limits are conservative. This could be because of the material properties considered in this work. BS 7608 does not provide design curves for different materials; instead a general fatigue curve is provided for a weld detail. Earlier studies on the material hardening behaviour and low-cycle fatigue have shown that yield to tensile ratio below 0.7 cyclically harden and above 0.83 will cyclically soften on a wide range of metallic materials (Hirschberg, Manson and Smith 1963; Tanaka et al. 1981). Qian et al. experimentally verified that no significant redistribution of welding residual stresses occurs during 4-point bending for the cyclic softening steel AISI 4142 (Qian et al. 2013).

6.9.2 ASME boiler and pressure vessel code

Unlike BS 7608, the ASME boiler and pressure vessel code (ASME BPVC Section VIII.2 2015) have fatigue design curves for low-cycle fatigue assessments. The local stress amplitude is used with the fatigue curves for assessment.

The ASME code requires limits on the magnitude of various load types including load combinations. These limits are in addition to examining the fatigue life for the applied amplitude against the number of applications of cycle loads, The limits are on the local membrane stress ($\leq 1.5 \times \sigma_m$) and primary plus secondary stress ($\leq 3\sigma_m$ or $2\sigma_y$), where σ_m is the basic code allowable stress for the material grade, and σ_y is the material yield strength. Specifically, the code states that these limits are such that shakedown occurs within the first few cyclic and will be elastic, except in regions containing geometric discontinuities or local thermal stress. Again, these limits are placed in pressure vessel applications undergoing thermal and pressure loads which are critical in terms of shakedown when compared to applications such as load bearing members in ship structures. The limits obtained in this work were higher than the ASME code recommendations for pressure vessel.

In summary, the ASME code provides guidance to avoid ratcheting. This is very important to ensure that a structural component designed to the code do not deviate significantly from the strain-controlled test specimens used to generate the fatigue design curves.

It should be noted that the shakedown requirement is not needed if the yield to tensile strength ratio is ≤ 0.7, suggesting that the risk of ratcheting is considered to be negligible if the Y/T ratio is ≤ 0.7 corresponding to cyclic hardening. This is consistent with the observation from the reviews of (Tanaka et al. 1981) that cyclic softening is unlikely for the materials with Y/T values below this threshold.

6.10 Residual stress relaxation under Shakedown state

Researchers using experimental methods have proposed empirical relations on residual stress relaxation under cyclic loads. FE analysis based on complex elastic-plastic models has aided in the development of these empirical relations. Residual stress relaxation studies on welded specimens are summarised in Table 6.3. Most of the materials listed in the table are steel.

In experimental tests of residual stress relaxation, many researchers (Table 6.3) reported significant relaxation in the initial cycle followed by reduced relaxation in the subsequent load cycles (Farajian-Sohi, Nitschke-Pagel and Dilger 2009; M. Farajian and T. Nitschke-Pagel 2012; Qian et al. 2013).

Various equations and formulas based on experimental and numerical models are used to describe the relaxation of residual stress. For welded plates, Xie et al. (Xie et al. 2017) and Qian et al. (Qian et al. 2013)describe a residual stress relaxation rule in line with the characteristics of a creep equation. Under a cyclic load having amplitude σ_a they proposed an equation for predicting stress relaxation S as given below:

$$S = \left[a\left(\frac{\sigma_a}{\sigma_y}\right)^n + b\right][log(N+1)]^m \qquad (6.9)$$

Taleb (Taleb 2013) was critical of the physical basis of this equation because creep in some ferritic steels is insignificant at ambient temperature. Moreover, as seen in the residual stress redistribution results, the yield stress is not unique for residual stress relaxation prediction as they are dependent on the cyclic hardening of the material. The material hardening will affect yield strength. Moreover, the inherent microstructure heterogeneity in the weld and the geometric features could result in different yield stresses in different locations of a specimen.

Morrow and Sinclair (Morrow J 1958), Zhuang and Halford (Smith et al. 2001; Zhuang and Halford 2001) and Smith et al. (Smith et al. 2001) also proposed empirical relations similar to the equation 6.9. All these prediction formulas are fundamentally developed based on experiments on butt welded plates. However, the results in this work indicate that unlike butt-welded plates, T-joints have much more complex residual stress redistributions under cyclic loading.

Table 6.3: Past research work on residual stress relaxation/redistribution in weld plates.

Investigation method	Authors	Specimen details	Material	Loading details	Finding
Experimental	(Qian et al. 2013)	100 ×50 mm^2 butt welds	AISI 1008, ASTM A572 and AISI 4142	10000 bending cycles at R=0.1	AISI 1008 and ASTM A572 relax significantly in the first cycle itself; AISI 4142 did not relax
	(Farajian-Sohi, Nitschke-Pagel and Dilger 2010)	250 × 60 mm^2 butt joints	S355j2G3	Tensile load in the transverse direction and 1000 cycles at R= –1	Significant relaxation in the first cycle itself
	(Farajian, Nitschke-Pagel and Dilger 2010)	250 × 60 mm^2 butt joints	S355j2G3	Tensile load in the transverse direction and 15000 cycles at R= –1	Significant relaxation in the first cycle itself
	(James et al. 2009)	190 × 150 mm^2 butt joints	Al 5083-H321	R=0,0.1, –1, 10^5 to 10^6 bending cycles	Residual stress increased
	(James et al. 2004b)	190 × 150 mm2 butt joints	Al 5083-H321	R=0,0.1, –1, 10^5 to 10^7 bending cycles	Residual stress increased
Numerical	(Dattoma, De Giorgi and Nobile 2004)	220 × 105 mm^2 butt joint	AISI 316	10 Tensile loads (R=0.1) in the longitudinal direction	Residual stress relaxation only in the first cycle
	(Cho and Lee 2016a)	Girth weld	S32750	20 load cycles at R=–1 in the longitudinal direction	Significant relaxation in the first cycle and subsequent cycles.
	(Lee, Chang and Do 2015)	400 × 300 mm^2 butt joint	SM 400	10 load cycles in both transverse and perpendicular to weld at R=0.1	Relaxation
Experimental and Numerical	(Xie et al. 2017)	236 × 40 mm^2 butt joint	316L	50 tensile (R=0.1) load cycles along the weld	Relaxation with most in the first cycle.

Based on the shortcomings above, it is understood that the complex mechanism of welding residual stress relaxation or redistribution under applied loadings are difficult to develop experimentally. FEA analysis can predict the redistribution of residual stresses with reasonable accuracy during mechanical loading(Wang et al. 2017b). However, generalising a particular relaxation behaviour at a range of applied load is not looked at yet. As this study focused on a particular load, formulation of generalised equations was not considered, instead a procedure for analysing the redistribution behaviour based on a shakedown region is presented.

Also, the relaxation models are often too complex because of their attempt to capture residual stress relaxation over a large number of load cycles. However, it is shown that, in previous discussions, a significant amount of residual stress relaxation occurs in the first few load cycles and is hence most significant in structural integrity assessments. To study the residual stress relaxation in welded plates, a novel method is considered to represent both residual stresses and the geometric parameter, which is the shakedown limit in a shakedown regime diagram.

6.10.1Shakedown regime

Based on the numerically obtained shakedown limit and assumed residual stress equivalent to the yield strength of the parent material (DH36), a shakedown regime is defined for each specimen as shown in Figure 6.8. The shakedown region is defined by normalised applied stress and normalised residual stress. The applied stress is normalised by the yield strength of the parent material. A few assumptions are considered in defining the shakedown limits as below:

- The applied load is assumed to be axial to the residual stress direction.
- The applied load, if above the design load of a component, is assumed to occur only for a few hundred cycles.
- A linear boundary is considered in the shakedown regime

If the residual stress after the first few cycles together with the applied load is within the shakedown region, it can be said that the structure will enter a shakedown state. Like the ASME pressure vessel code, where a maximum limit of 2 times yield is specified for a loading corresponding to primary plus secondary loads. Here the shakedown region can be used to check if the residual stresses (secondary stresses) will be inside the shakedown regime or not after a few initial load cycles.

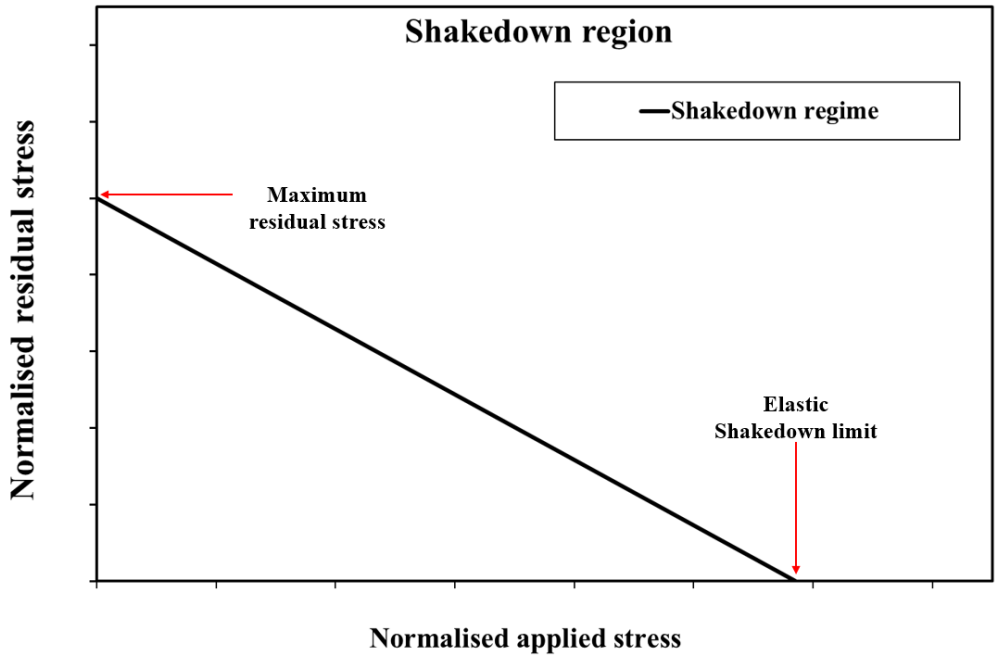

Figure 6.8: Shakedown region defined by normalised applied stress and normalised residual stress.

Prior to the shakedown limit analysis described in this chapter, preliminary 2D FE models were evaluated to estimate an approximate shakedown limit for each specimen. The approximate shakedown limits along with typical load levels experienced in load bearing members in a double bottom configuration of a container ship were considered to choose a cyclic load for the experimental procedures defined in Chapter 3.

6.10.1.1 Redistribution of residual stress in butt-welded plate in shakedown regime

In butt welded plates, critical locations, that is weld centre and weld toe region, are considered for discussion here. The coordinates of the points considered as per Figure 3.17a and 3.17b for the butt welded plate with the short weld and the long weld are as below:

- Weld centre at Y=10.2mm: X=0mm, Y=10.2mm, Z=0mm
- Weld centre at Y=2.5mm: X=0mm, Y=2.5mm, Z=0mm
- Weld toe at Y=10.2mm= X=0mm, Y=10.2mm, Z=6.35mm
- Weld toe at Y=2.5mm= X=0mm, Y=2.5mm, Z=6.35mm

Figure 6.9 and 6.10 shows the redistribution of transverse residual stress in the butt-welded plate with short weld and redistribution of longitudinal residual stress in the butt-welded plate with the long weld respectively, in the above four points under ten load cycles obtained from neutron diffraction. Here the applied load is 0.75 times the yield

strength of the parent material. As explained in Chapter 5 the transverse residual stress in the butt-welded plate with the short weld at Y=10.2mm shows significant relaxation whereas at the weld centre at Y=2.5mm shows an increase in residual stress. On the other hand, the longitudinal residual stress in the butt-welded plate with the long weld shows significant relaxation in the first cycle itself.

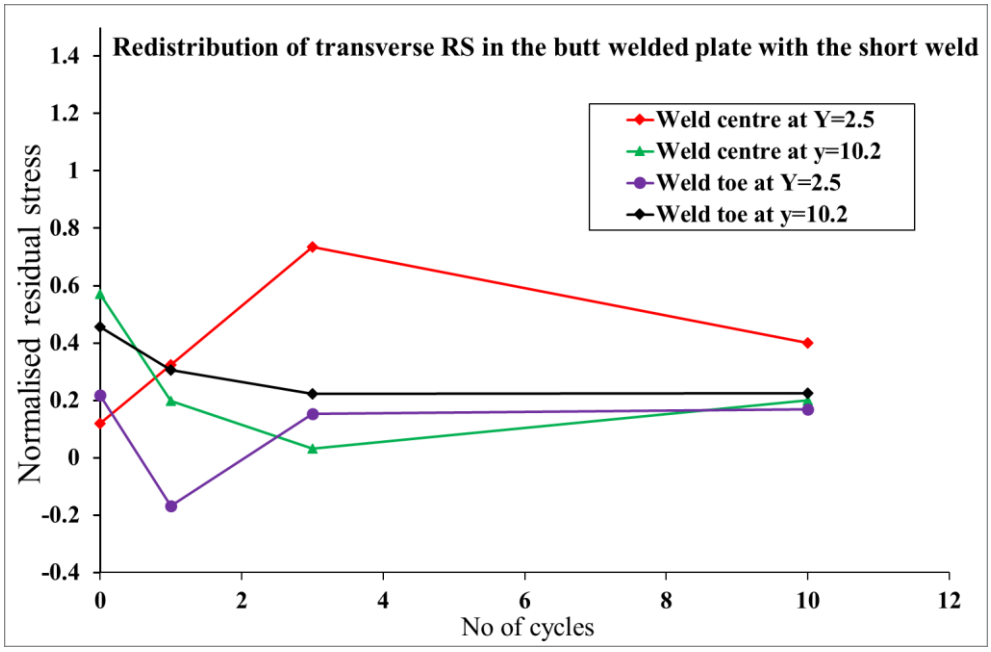

Figure 6.9: Redistribution of transverse residual stresses in butt-welded plates with the short weld in the weld centre and weld toe at Y=2.5mm and 10.2mm.

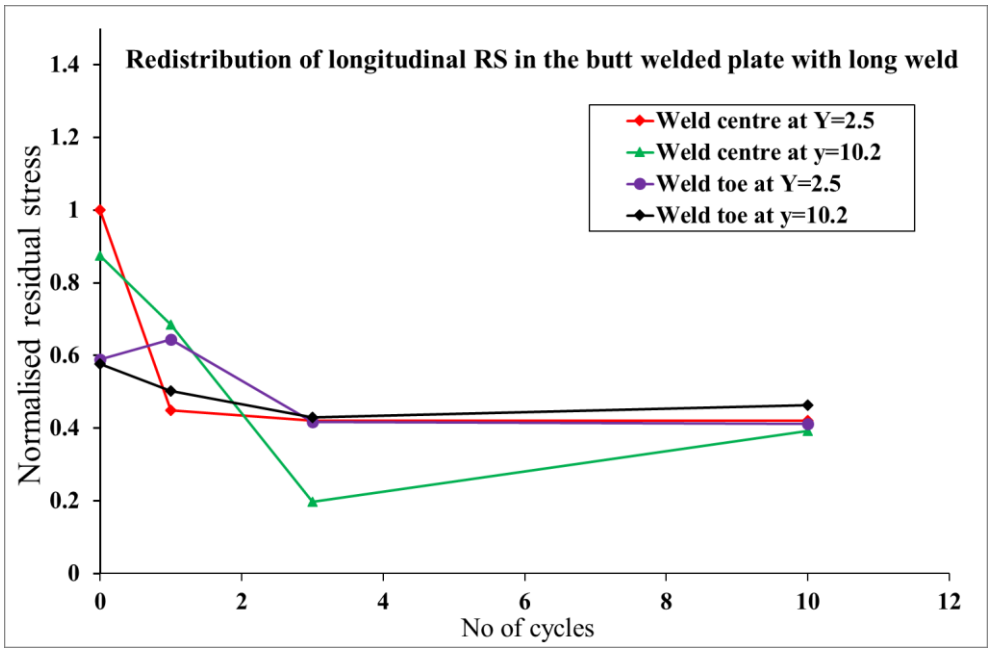

Figure 6.10: Redistribution of longitudinal residual stresses in butt-welded plates with the long weld in the weld centre and weld toe at Y=2.5mm and 10.2mm.

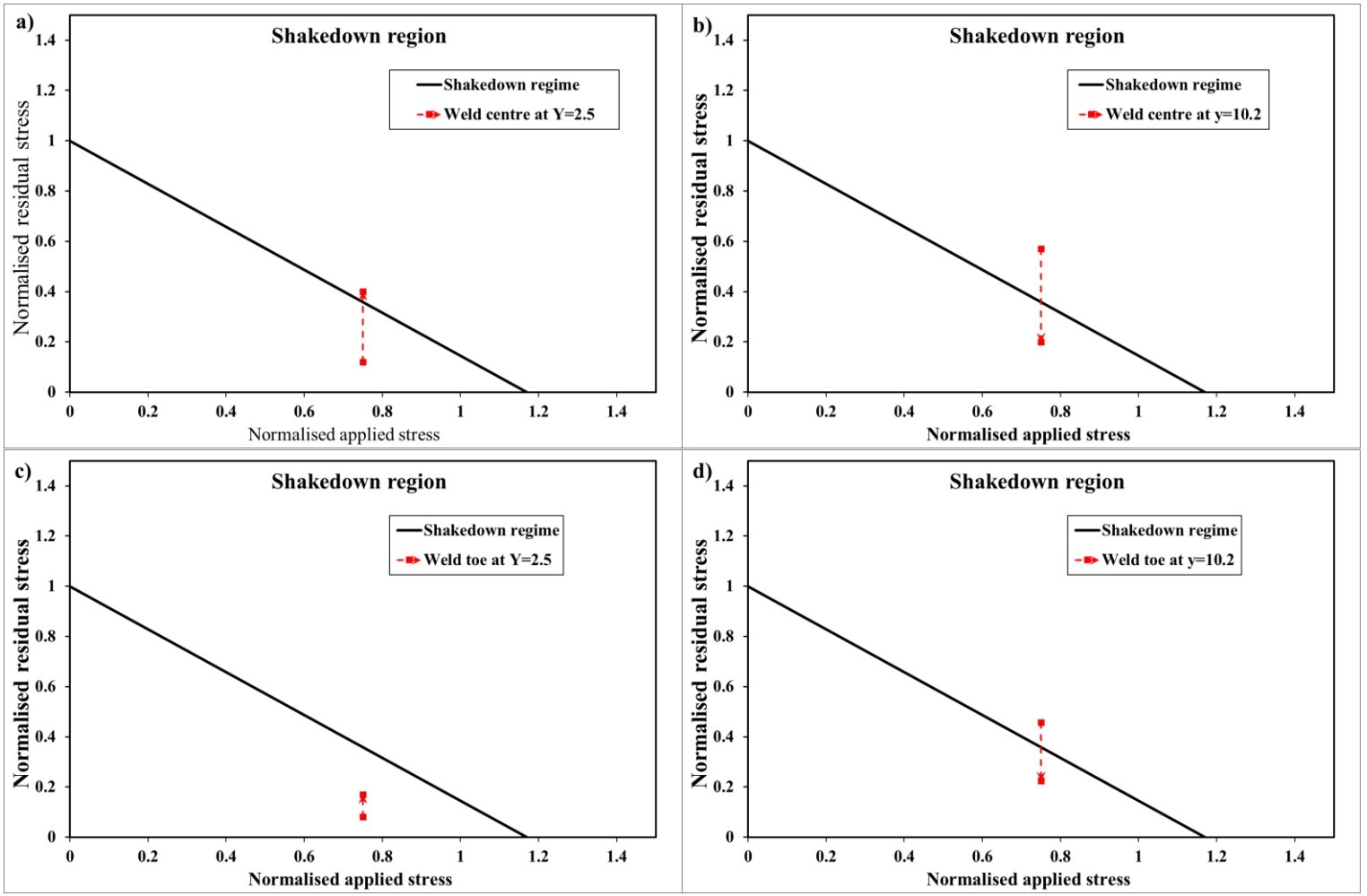

Figure 6.11: Transverse residual stress redistribution after ten load cycles at 0.75 times yields strength of parent material in the butt-welded plate with the short weld represented in the shakedown regime: a)Weld centre at Y=10.2mm, b) weld centre at Y=2.5mm, c) weld toe at Y=2.5mm and, d) weld toe at Y=10.2mm

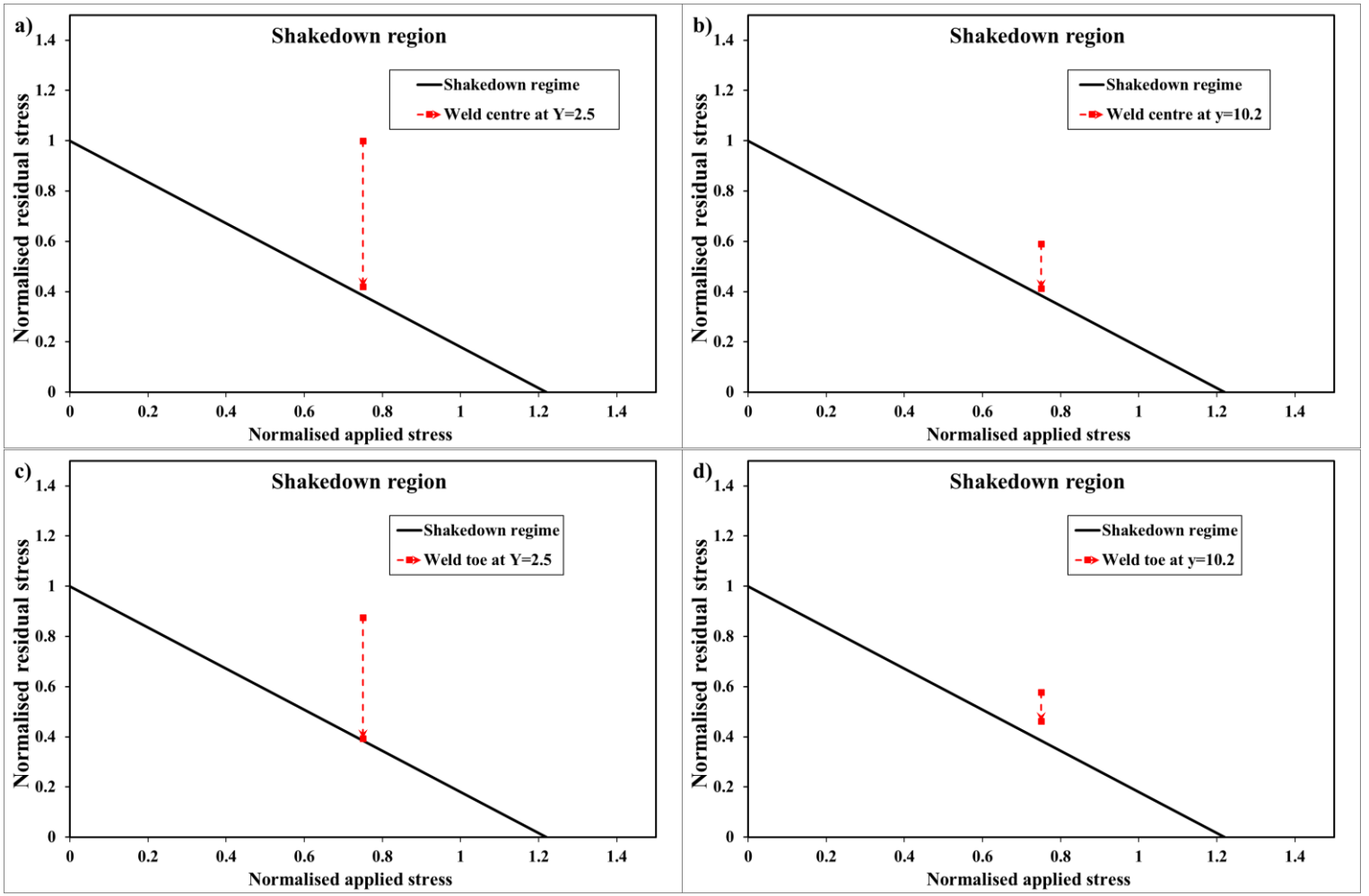

Figure 6.12: Longitudinal residual stress redistribution after ten load cycles at 0.75 times yields strength of parent material in the butt welded plate with the long weld represented in the shakedown regime: a) Weld centre at Y=10.2mm, b) weld centre at Y=2.5mm, c) weld toe at Y=2.5mm and, d) weld toe at Y=10.2mm

Figure 6.11 shows the transverse residual stress redistribution from the as-welded condition to after ten load cycles on four locations stated above in the butt-welded plate with the short weld represented in the shakedown region. Here the residual stresses are normalised by the yield strength of the weld material. It can be noted that except for the values at the weld centre at Y=2.5mm, all other points fall inside the defined shakedown boundary (Figure 6.11a, 6.11b, and 6.11d). In the case of the weld centre at Y=2.5mm (Figure 6.11c), the transverse residual stress after ten load cycles is on the shakedown boundary. Here the increase in transverse residual stress after ten cycles could be due to the internal equilibrium as a result of significant relaxation on the locations above this region. It is noted that preloading weld plates for relieving tensile stresses can be useful on the top surface or weld toe of the plate, but it can also introduce tensile stresses through the thickness.

Figure 6.12 shows the longitudinal residual stress redistribution from the as-welded condition to after ten load cycles on the four locations stated above in the butt-welded plate with the long weld represented in the shakedown region. Here the initial welding residual stresses are relaxed to near the shakedown boundary under ten load cycles. Figure 6.11 indicates the shakedown state after ten cycles as a relatively stable value are measured after three and ten load cycles. Like the butt-welded plate with the short weld, here the plate is expected to reach shakedown state.

6.10.1.2 Redistribution of residual stress in fillet welded plate in shakedown regime

In fillet welded plates, four critical locations, that is two points near the fillet weld toe on each side of the vertical plate, are considered for discussion here. The coordinates of the points considered as per Figure 3.21a and 3.21b for the fillet welded plate with the short weld and the long weld respectively are as below:

- Weld toe side 1 at Y=10.2mm: X=0mm, Y=10.2mm, Z= –9.4mm
- Weld toe side 2 at Y=10.2mm: X=0mm, Y=10.2mm, Z= +9.4mm
- Weld toe side 1 at Y=15.2mm: X=0mm, Y=15.2mm, Z= –9mm
- Weld toe side 2 at Y=15.2mm: X=0mm, Y=15.2mm, Z= +9mm

Figure 6.13 and 6.14 shows the redistribution of transverse and longitudinal residual stresses in the fillet welded plate with the short weld and the long weld respectively, in the above four points under three load cycles obtained from neutron diffraction. Here the applied load is 0.65 times the yield strength of the parent material. As explained in

Chapter 5, unlike the butt welded plates, both the fillet welded plates show significant redistribution to the tensile zone from the as-welded stresses after three load cycles.

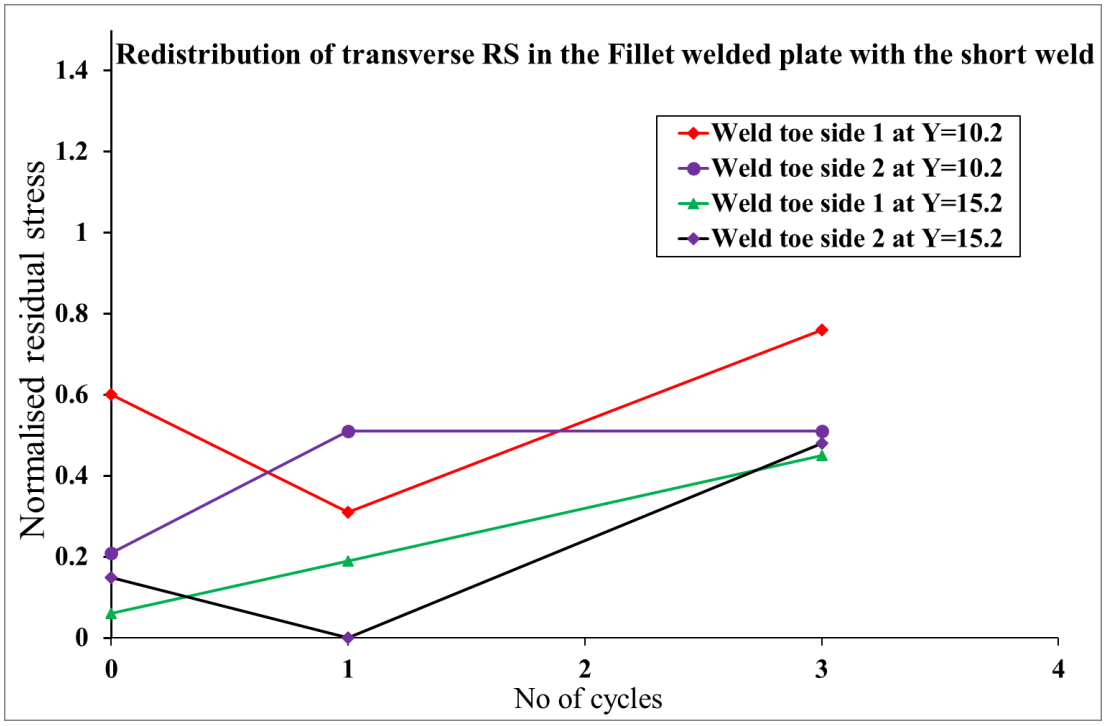

Figure 6.13: Redistribution of transverse residual stresses in fillet welded plates with the short weld in the weld toe region in side 1 and side 2 at Y=10.2mm and 15.2mm.

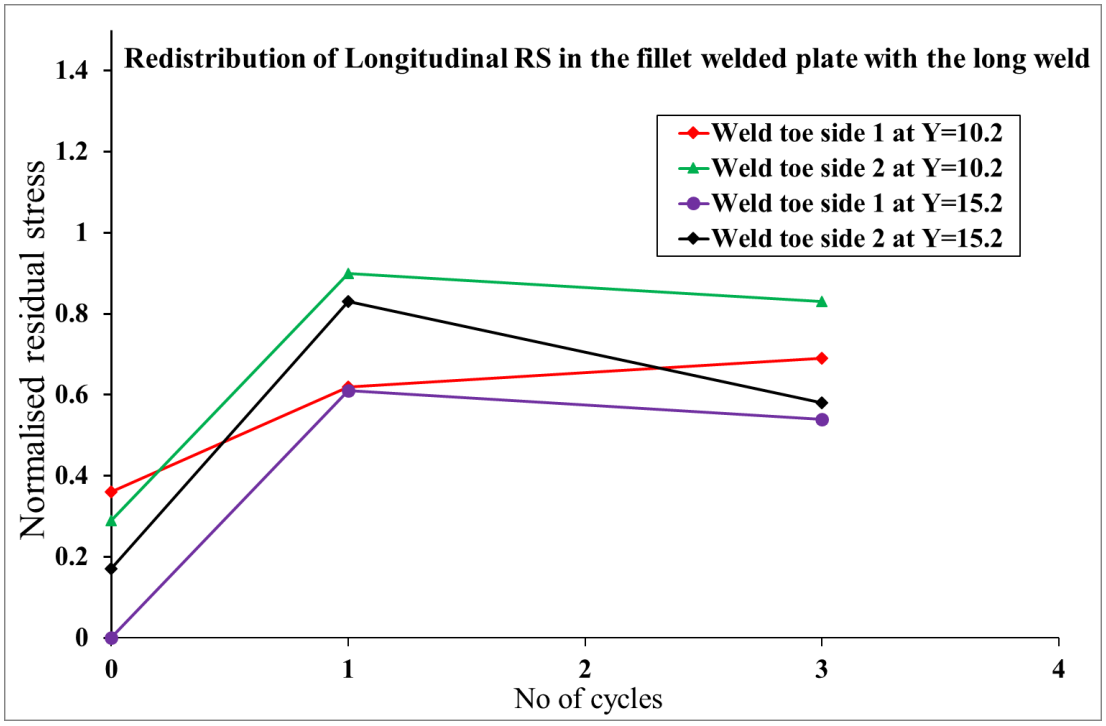

Figure 6.14: Redistribution of longitudinal residual stresses in fillet welded plates with the long weld in the weld toe region in side 1 and side 2 at Y=10.2mm and 15.2mm.

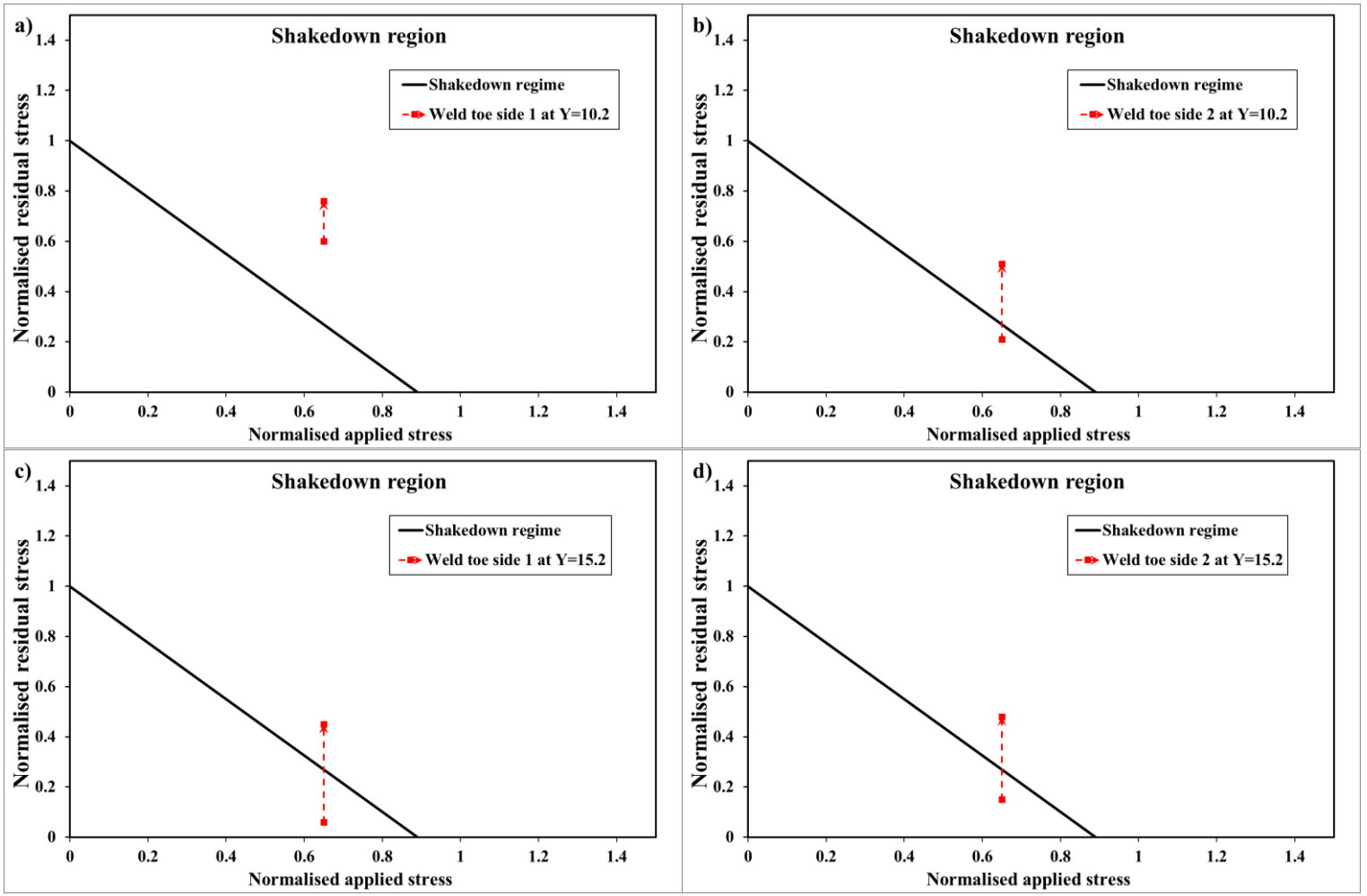

Figure 6.15: Transverse residual stress redistribution after three load cycles at 0.65 times yields strength of parent material in the fillet welded plate with the short weld represented in the shakedown regime: a) Weld toe side 1 at Y=10.2mm, b) weld toe side 2 at Y=10.2mm, c) weld toe side 1 at Y=15.2mm and, d) weld toe side 2 at Y=15.2mm.

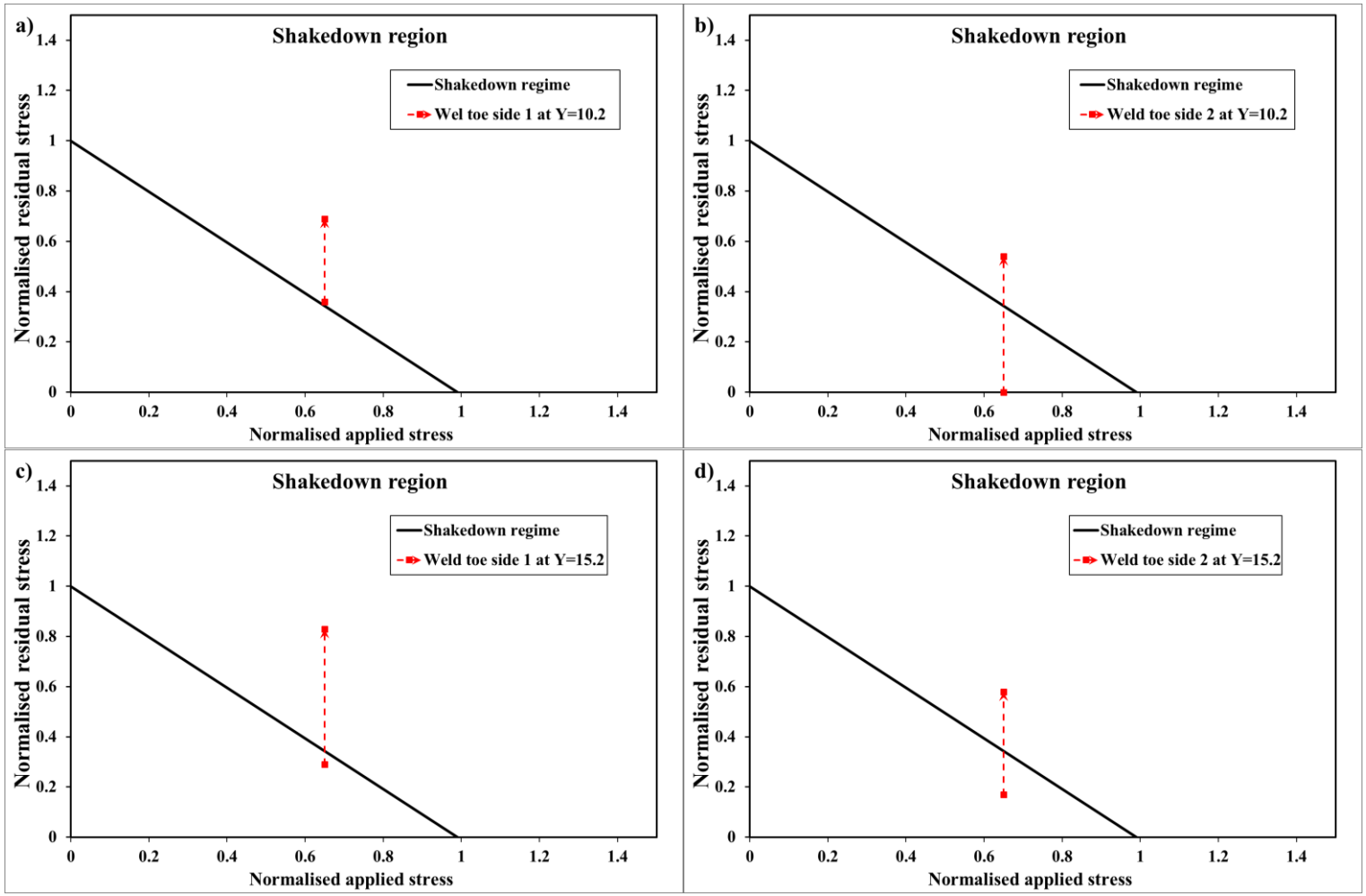

Figure 6.16: Longitudinal residual stress redistribution after three load cycles at 0.65 times yields strength of parent material in the fillet welded plate with the long weld represented in the shakedown regime: a) Weld toe side 1 at Y=10.2mm, b) weld toe side 2 at Y=10.2mm, c) weld toe side 1 at Y=15.2mm and, d) weld toe side 2 at Y=15.2mm

Figure 6.15 shows the transverse residual stress redistribution from the as-welded condition after three load cycles on the selected locations stated above in the fillet-welded plate with the short weld represented in the shakedown region. It can be noted that after the first load cycle, the residual stress values at all stated locations fall outside the defined shakedown boundary. As per the defined shakedown boundary, this indicates that the fillet welded plate cannot achieve shakedown state at this load level.

Figure 6.16 shows the longitudinal residual stress redistribution from the as-welded condition to after three load cycles on the selected locations stated above in the fillet-welded plate with the long weld represented in the shakedown region. Similar to the fillet welded plate with the short weld, all stated locations fall outside the defined shakedown boundary which indicates that the fillet welded plate cannot achieve shakedown state at this load level.

6.11 Summary

In this chapter, a numerical simulation for shakedown limit analysis based on the energy method was implemented for butt and fillet welded plates manufactured using DH36 shipbuilding steel. The conditions of achieving shakedown steady state in a structure defined in R5 was confirmed from the results of the shakedown limit model. The limit analysis is defined for the specific experimental case studied in this work. Further, a shakedown region is defined based on the determined shakedown limits for each weld plates.

The redistribution of residual stresses in the shakedown region was investigated for each specimen at specific points. The residual stress redistribution of butt-welded plates indicated that it could achieve shakedown state whereas the fillet welded plates showed ratcheting behaviour under the applied load condition.

CHAPTER 7.KEY FINDINGS AND LIMITATIONS

7.1 Key findings

In section 1.3 of this thesis, the main research objectives were presented; these are restated below:

- Objective 1: To implement a shakedown limit analysis optimised to the problem in hand to define shakedown limits in the specimens under study.
- Objective 2: To quantify residual stresses in butt and fillet welded plates fabricated using established welding procedures in shipbuilding using both numerical and experimental methods.
- Objective 3: To evaluate the extent of residual stress redistribution under selected cyclic loads representing extreme loads experienced in ship structures and, in the range of the elastic shakedown using experimental techniques.
- Objective 4: To characterise the residual stress state under cyclic load applied and to define an effective FE model to simulate residual stress redistribution.
- Objective 5: To investigate the effects of shakedown limit on the redistribution of residual stresses.

In this Chapter, each of the objectives described above is discussed, and the key findings in pursuit of these objectives are highlighted.

7.1.1 Objective 1

The shakedown limit analysis of 3-dimensional weld plates under uniaxial mechanical loading was implemented using an incremental FEA and energy-based method (Chapter 6). Shakedown limits in butt and fillet welded plates were different from each other primarily due to the geometric features and the direction of the load application. The plastic work done at the end of each load cycle was considered as the shakedown criterion based on the principles of energy method. The limit analysis was simplified to the specific problem in this work using a reduced basis technique to minimise the computation required. It was shown that the plastic work done at the end of each load cycle could be used to determine the shakedown limit.

The butt-welded plate with the short and, the long weld obtained a shakedown limit of $1.17\times\sigma_y$ and $1.22\times\sigma_y$ respectively, where σ_y is the parent material yield strength. Also, the

fillet welded plate with the short and, the long weld obtained a shakedown limit of $0.89\times\sigma_y$ and $0.99\times\sigma_y$. Based on the obtained shakedown limits on the butt and fillet welded plates in this work, the design limits specified in BS 7608 (BS 7608 2014) limits for extreme working conditions ($0.8\times\sigma_y$) are conservative. This could be due to the specific material properties considered in this work. BS 7608 does not provide design curves for different materials, instead provide a general fatigue curve for each weld detail. Earlier studies on the material hardening behaviour and low-cycle fatigue have shown cyclic hardening for yield to tensile strength ratio below 0.7 but cyclic softening for yield to tensile strength ratio above 0.83 on a wide range of metallic materials (Hirschberg, Manson and Smith 1963; Tanaka et al. 1981). Unlike BS 7608, the ASME code (ASME BPVC Section VIII.2 2015) places some limits on the magnitude of primary load (not greater than 1.5×basic code allowable stress) and primary plus secondary load (not greater than 3×basic code allowable stress or 2×yield strength).

It was found that the simulation results greatly depend on the hardening behaviour considered in the material model and accurate representation of plate geometry was also found to be influential in the solution.

7.1.2 Objective 2

As-welded residual stresses in both butt and fillet welded plates were determined using both numerical and experimental techniques. Neutron diffraction was used for experimental measurement. 3D welding process simulation using "chunking method" was used to predict as-welded residual stresses in the specimens. Although assumptions and approximations were introduced in the weld process simulations, the overall trend of stress profiles predicted from the FEA model was in good agreement with the measured results. Additionally, an iterative technique was proposed to map residual stress values based on a self-equilibrating stress profile for a geometry with a large area of incompatibility. The residual stress mapping technique was implemented on the butt-welded plate with the short weld.

Through-the-thickness measurement of different residual stress components in butt and fillet welded plates provided valuable information. Unlike single pass welding, the through-thickness residual stress state in multi-pass welding is complex. Residual stress component in the through thickness (normal) direction of the butt-welded plates was

mostly insignificant in terms of stress magnitude. The residual stress magnitude on the top, middle and bottom region of the butt and fillet welded plates were considerably different particularly at the weld zone. However, in the case of butt-welded plates, moving away from the weld zone, similar residual stress distributions were measured on the top, middle and bottom region of the plates. Transverse residual stress measured in butt-welded plates were much lower than longitudinal residual stresses. The residual stress in the cross-section of the fillet welded shows high tensile longitudinal and traverse residual stress on both sides of the web plate, but compressive or near zero stresses in the middle region. It was found that the transverse and longitudinal residual stress in fillet welded joints had similar magnitudes, unlike butt welded plates. In the case of fillet welded plates, it was necessary to set-up the plates in various positions in order to minimise the beam path so that lattice spacing can be measured as quick as possible with reasonable accuracy. The Scanning Simulation Software SScanSS was very helpful in defining sample positioning for minimal beam path before neutron diffraction experiments (James et al. 2004a; James and Edwards 2007), especially in fillet welded plates.

The residual stress outputs from the mapping technique applied on the butt-welded plate with short weld were compared with those obtained from welding process simulation and with experimental results measured using neutron diffraction. It was found that self-balancing stress equations can play an essential role in supporting residual stress mapping techniques from a limited number of measurement data, where data are typically obtained from a relatively small region of interest only.

7.1.3 Objective 3

Residual stress redistributions were measured using neutron diffraction in all four specimens. Weld plates with the short weld were especially looked for the effects in transverse residual stressed whereas the plates with long weld were especially looked for the effects in longitudinal residual stress under cyclic loading.

In butt welded plates, the residual stresses measurement under ten tensile (R=0) load cycles of magnitude 0.75 times yield strength of the parent material (DH36) showed significant relaxation within the first load cycle. The relaxation was significant in the stress component parallel to the applied load. However, it was found that there was

significant redistribution in the residual stress component, perpendicular to the applied load direction.

In fillet welded plates, the residual stresses measurement under three tensile (R=0) load cycles of magnitude 0.65 times yield strength of the parent material (DH36) showed significant redistribution in all three load cycles. Redistribution was seen in both transverse and longitudinal residual stress when the applied load was parallel and perpendicular to the weld. Interestingly, the residual stress in most of the locations in the mid cross section of the plate showed an increase in residual stress following three load cycles of magnitude 0.65 × yield strength of the parent material. This could be due to three reasons. Firstly, the distortion in the horizontal plate of the fillet weld resulting in bending stresses as a result of axial fatigue load gripping. Secondly, the load applied was only on the horizontal plates causing the constraint effects from the attachment and through the fillet weld to introduce bending stresses. The second reason is evident in the case of residual stress redistribution in both welds. Finally, the stress concentration factor in the case fillet welds is higher than the butt-welded plates due to the weld toe angles.

7.1.4 Objective 4

Residual stress redistribution was numerically simulated using an FE model consisting of the as-welded residual stress results from welding process simulations. In ABAQUS, mesh-to-mesh solution mapping capability was employed to transfer of all variables from the previous analysis to a new analysis. This enabled a comprehensive residual stress profile to be predefined on the FE model before the application of cyclic load. This technique has been used in recent years by several teams is promising in residual stress relaxation or redistribution analysis. (Cho and Lee 2016b; Lee, Chang and Van Do 2015; Wang et al. 2017a; Xie et al. 2017).

The numerical simulations were able to predict the redistribution of residual stress in the butt-welded plate with reasonable accuracy in terms of both magnitude and trend. The simulations were able to capture the trend in the variation of residual stress through the thickness of the plate. On the other hand, the numerical simulations on fillet welded plates were only able to predict the trend in the redistribution of residual stress. The magnitudes seen in the fillet welded plates were often away from the measurement results. In both

butt and fillet welds, the deviation in the residual stress values could be due to the underprediction of as-welded residual stresses.

7.1.5 Objective 5

A method was defined to see how the shakedown limits in each weld plate affected the residual stress redistribution under applied load conditions. Based on the numerically obtained shakedown limit and the residual stress which was assumed to be equal to the yield strength of the parent material (DH36) a shakedown regime is defined for each specimen as shown in Figure 6.12. The shakedown region is defined by normalised applied stress and normalised residual stress. The applied stress is normalised by the yield strength of the parent material. If the residual stress after the first few cycles together with the applied load is within the shakedown region, it can be said that the structure will enter a shakedown state. The shakedown region can be used to check if the residual stresses (secondary stresses) will be inside the shakedown regime or not after a few initial load cycles.

Based on the measurement data, residual stress redistribution in butt-welded plates indicated that the weld plates were achieving shakedown after ten load cycles of magnitude equivalent to 0.75 × yield strength of the parent material. However, the measured residual stress redistribution in fillet welded plates indicated that the weld plates were not achieving shakedown after the first three load cycles of magnitude equivalent to 0.65 × yield strength of the parent material.

7.2 Limitations of the work

7.2.1 On the experimental plan

One of the main limitations presented in the experimental plan is that the measurement of residual stresses was not conducted in-situ, which could have avoided the set-up error while measuring after different number of load cycles. Because this work focused on the redistribution of residual stresses, it was initially planned to use in-situ loading rig at ENGIN-X for the load application. However, the load capacity of the in-situ stress rig at ENGIN-X was not sufficient to introduce the required stress levels in the specimens. As a result, the loading was performed at TWI Ltd. and the plates were transported to ENGIX-X for residual stress measurements.

A load amplifier which works on the principle of a second-class lever was designed for the stress rig at ENGIN-X, which would essentially increase the load capacity by 3 times. However, as the manufacturing of the load amplifier was delayed due to unforeseen issues, this part of the work is not included in this thesis.

7.2.2 Numerical simulation of the welding process

The numerical simulation of residual stress strongly depends on the temperature dependent material property used in the analysis. The temperature-dependent material mechanical properties used in this work had to assume similar properties for both parent and weld material except the yield strength. The actual welding had an overmatching filler material when compared to the parent material. The assumption that the material property of the weld material, when compared to the parent material only differs in the yield strength, is not ideal. This could be one of the reasons for the underprediction of residual stresses on the weld zone.

Moreover, the computation time required for multi-pass 3D plates for 400mm length is very high. It was possible to increase efficiency by reducing the number of weld chunks considered in each weld pass. However, that would reduce the accuracy, and the number chosen in this work is based on achieving a reasonable accuracy. The best option to capture strain hardening accurately is to employ combined/mixed hardening models in the simulations but would require more computational time. Since the FE models in this work were 3D, the hardening behaviour was assumed to be isotropic with stress-strain data defined at different temperatures, which provided reasonable accuracy with efficient computation.

7.2.3 Numerical simulation of residual stress redistribution

The main limitation in residual stress redistribution analysis is that the plates after welding did not consider the distortion in the welded plates. The distortion in the butt-welded plates was very minimal. However, the residuals stress redistribution results from measurement in fillet welded plates show that there was an effect of bending stress and were not able to capture in the numerical simulation.

7.2.4 Shakedown limit

One of the main limitations of incremental FEA method for shakedown limit analysis in welded plates is the notch effects from weld toe affecting the limit determined. Incremental FEA techniques primary depends on the evolution and accumulation of plastic strains and their effect on the mechanical behaviour of the material in the plate. Standards such as IIW (Hobbacher 2009) recommends avoiding the stress values right at the weld toe as they may represent unrealistic values.

The application of shakedown limit analysis presented in this work, if applied in complex loading condition would reduce the computational efficiency. The experimental validation of shakedown limits in the weld plates was not conducted in this work.

The defined shakedown region from the limits obtained was under the assumption that the applied load is axial to the residual stress component under investigation. Also, the boundary considered between the residual stress and applied load is assumed to linear.

CHAPTER 8.RELEVANCE AND FUTURE RECOMMENDATIONS

8.1 Relevance in industry

This PhD research work was funded in part by Lloyd's Register Foundation and was conducted in collaboration with the Asset and Fracture Management (AFM) section at TWI Ltd. The AFM section under Integrity Management Group conducts Engineering Critical Analyses (ECAs) to TWI member companies. These ECAs are often performed based on the procedures detailed in structural integrity standards such as BS 7910, "Guide to methods for assessing the acceptability of flaws in metallic structures" (BS 7910:2013+A1:2015 2013) and require the consideration of residual stress distributions as recommended by the standard. Welding residual stress distributions and magnitudes can be estimated using the polynomial functions that depend on the weld plate geometry and material properties as detailed in assessment procedures such as BS 7910 and R6 (R6 Revision 4 2015). The polynomial functions represent yield level residual stresses on the surface of the plate. Consequently, an accurate consideration of welding residual stress distribution could improve assessments in welded structures (Hadley. I and Pisarski 2013).

R6 recently included guidelines for welding process simulation to consider a comprehensive residual stress distribution which is included in Section III.15. The work presented in this thesis used this technique and was able to obtain reasonable accuracy in the residual stress predictions. Even though the modelling guidelines are simple, the computational requirement for a 3D weld process simulation is still very high. Alternatively, an iterative residual stress mapping technique suitable for butt welded plate is proposed in this work which improves the computational efficiency while keeping the accuracy secure in the region of interest.

BS 7910 assumes some global relief of residual stresses on welded structures when subjected to primary loading. It was found that the stress relaxation after global relief due to the same applied load studied on the FE models (both weld model and the residual stress mapping model) is highly conservative. As mentioned in Chapter 5, when the stress relaxation in the weld toe region only relaxed by ~26% based on BS 7910, the level of relaxation in the weld model and mapped model was ~56% and ~70% respectively.

8.1.1 Relevance to the ship structures

This PhD research work was also conducted in collaboration with Lloyd's Register Marine (LR Marine). As per the recommendations from LR marine, this work was aimed at investigating residual stress redistribution in load bearing members in ship structures. However, due to limitations in the experimental equipment, it was decided to study small scale specimens manufactured according to the welding procedures used in ship structures and similar plate thicknesses. To this reason, GMAW was used as the manufacturing process. Maximum restraints were used while performing welding to represent welding in ship structures which are constrained due to surrounding members. A ship structural steel, DH 36 was used for the work as they are one of the most common steels used for manufacturing plating's and stiffeners.

LR Marine was involved in defining the essential parameters for the research problem such as the specimen dimensions, welding procedures and the load levels. LR Marine in their design calculations for ship structures uses maximum permissible stress of about 75% of yield stress for mild steels. In the case of high strength steels such as DH36, a maximum permissible stress of about 68% of yield stress is considered.

In ship structures, it is unlikely to do any post weld treatments to alleviate the residual stresses. The knowledge of the as-welded residual stress distribution and its redistribution from the as-welded condition is valuable for a number of reasons.

Firstly, knowing the as-welded stresses that are present after fabrication is a valuable input to calculate how the residual stress state changes during subsequent loading. Models can be developed to predict how the material will respond to the combination of residual stresses and extreme loading. The residual stress redistribution as a result of cyclic loading is less severe than welding. Therefore, the simulation of residual stress redistribution presents fewer challenges than the simulation of welding. The residual stress mapping technique presented in section 4.9 will contribute to the development of the numerical simulation of residual stress redistribution. Moreover, the information obtained on the through thickness residual stress profiles in fillet welded plates is also is valuable as there not many literatures available on residual stress distributions in fillet welds.

Secondly, the redistribution of residual stresses, following cyclic loading presents valuable input to structural integrity assessment because the level of residual stress in the crack opening locations can be crucial. The process of residual stress redistribution is identified because of plastic flow in the initial few cycles. However, a structure is considered safe only if the residual stress shakedown is stable in the first few cycles.

The shakedown limit analysis presented in this work can be used to define shakedown limits on a geometry undergoing a cyclic loading. The proposed method can be upscaled to a flat bar stiffener so that permissible stress on the location critical in fatigue crack can be estimated. It can be used for subsequent development of a procedure for allowance of elastic shakedown in design calculations.

8.2 Future work and recommendations

Based on the work presented in this thesis recommendations for future work include the following:

1. A continuation of the application of load cycles on both butt and fillet welded plates are recommended for future work. Any future residual stress redistribution measurement is recommended to be done in-situ as it reduces the time and cost while increasing the accuracy of the measurements.
2. It is suggested that an additional destructive or semi-destructive technique such as contour method or deep hole drilling to be used which can generate through thickness stress profiles or full stress map which could be potentially used to validate the results obtained from a non-destructive technique.
3. Future work on the numerical simulation of residual stress redistribution could be to include welding induced distortions in the FE model to capture the bending stress effects.
4. FEA of welding process could be improved by considering the effect of phase transformation in ferritic DH36 steel and the accurate temperature-dependent material properties (mainly the yield strength and modulus of elasticity), plastic deformation.
5. The fillet welded plates represent the welding parameters, thickness and material sued in flat bar stiffeners. Therefore, the work can be upscaled to be used in the

double bottom configuration of a ship structure by using as-welded residual stress values in this work for the implementation of residual stress redistribution in flat bar stiffeners.

References

Abaqus Manual (2013) Version 6.13-2. Rhode Island, USA: Dassault Systems Simulia Corporation

Abdel-Karim, M. (2005) 'Shakedown of Complex Structures According to various Hardening Rules'. International Journal of Pressure Vessels and Piping 82 (6), 427-458

Abou-Hanna, J. and McGreevy, T. E. (2011) 'A Simplified Ratcheting Limit Method Based on Limit Analysis using Modified Yield Surface'. International Journal of Pressure Vessels and Piping 88 (1), 11-18

Anderson, T. L. (1991) Fracture Mechanics: Fundamentals and Applications. Boca Raton, Fla.: CRC Press

API 579-1 (2016) Fitness-for-Service. 3rd edn: American Petroleum Institute

ASME BPVC Section VIII.2 (2015) Rules for Construction of Pressure Vessels Division 2-Alternative Rules. Two Park Avenue, New York NY 10016-5990: ASME

Bao, R., Zhang, X., and Yahaya, N. A. (2010) 'Evaluating Stress Intensity Factors due to Weld Residual Stresses by the Weight Function and Finite Element Methods'. Engineering Fracture Mechanics 77 (13), 2550-2566

Barsoum, Z. and Barsoum, I. (2009) 'Residual Stress Effects on Fatigue Life of Welded Structures using LEFM'. Engineering Failure Analysis 16 (1), 449-467

Bate, S. and Smith, M. (2016) 'Determination of Residual Stresses in Welded Components by Finite Element Analysis'. Materials Science and Technology 32 (14), 1505-1516

Bertini, L., Fontanari, V., and Straffelini, G. (1998) 'Influence of Post Weld Treatments on the Fatigue Behaviour of Al-Alloy Welded Joints'. International Journal of Fatigue 20 (10), 749-755

Bleich, H. (1932) 'Uber Die Bemessung Statisch Unbestimmter Stahltragwerke Unter Berucksichtigung Des Elastisch-Plastischen Verhaltens Des Baustoffes'. Bauingenieur 19/20, 261 on

Borkowski, A. and Kleiber, M. (1980) 'On a Numerical Approach to Shakedown Analysis of Structures'. Computer Methods in Applied Mechanics and Engineering 22 (1), 101-119

Bragg, W. L. (1929) 'The Diffraction of Short Electromagnetic Waves by a Crystal'. Scientia 23 (45), 153

Bree, J. (1967) 'Elastic-Plastic Behaviour of Thin Tubes Subjected to Internal Pressure and Intermittent High-Heat Fluxes with Application to Fast-Nuclear-Reactor Fuel Elements'. The Journal of Strain Analysis for Engineering Design 2 (3), 226-238

BS 7608 (2014) Guide to Fatigue Design and Assessment of Steel Products. 2nd edn: BSI Standards Limited

BS 7910:2013+A1:2015 (2013) Guide to Methods for Assessing the Acceptability of Flaws in Metallic Structures.: BSI

BSI (2015) '7910: Guide to Methods for Assessing the Acceptability of Flaws in Metallic Structures'. British Standards Institute

Chen, H., Ponter, A. R., and Ainsworth, R. (2006) 'The Linear Matching Method Applied to the High Temperature Life Integrity of Structures. Part 1. Assessments Involving Constant Residual Stress Fields'. International Journal of Pressure Vessels and Piping 83 (2), 123-135

Cho, J. and Lee, C. (2016a) 'FE Analysis of Residual Stress Relaxation in a Girth-Welded Duplex Stainless Steel Pipe Under Cyclic Loading'. International Journal of Fatigue 82, 462-473

Cho, J. and Lee, C. (2016b) 'FE Analysis of Residual Stress Relaxation in a Girth-Welded Duplex Stainless Steel Pipe Under Cyclic Loading'. International Journal of Fatigue 82, 462-473

Connor, L. P. and American, W. S. (1987) Welding Handbook, Vol. 1 : Welding Technology. 8th ed... edn. Miami, Fla.: Miami, Fla. : American Welding Society

Coules, H. E., Smith, D. J., Abburi Venkata, K., and Truman, C. E. (2014) 'A Method for Reconstruction of Residual Stress Fields from Measurements made in an Incompatible Region'. International Journal of Solids and Structures 51 (10), 1980-1990

Dattoma, V., De Giorgi, M., and Nobile, R. (2004) 'Numerical Evaluation of Residual Stress Relaxation by Cyclic Load'. The Journal of Strain Analysis for Engineering Design 39 (6), 663-672

Dawson, R. and Moffat, D. (1980) 'Vibratory Stress Relief: A Fundamental Study of its Effectiveness'. Journal of Engineering Materials and Technology 102 (2), 169-176

Del Puglia, A. and Nerli, G. (1973) Experimental Research on Elasto-Plastic Behaviour and Collapse Load of Statically Indetermined Space Tubular Beams. Berlin, Germany: IASMiRT

Deng, D. and Murakawa, H. (2006) 'Prediction of Welding Residual Stress in Multi-Pass Butt-Welded Modified 9Cr–1Mo Steel Pipe Considering Phase Transformation Effects'. Computational Materials Science 37 (3), 209-219

Deng, D., Liang, W., and Murakawa, H. (2007) 'Determination of Welding Deformation in Fillet-Welded Joint by Means of Numerical Simulation and Comparison with Experimental Measurements'. Journal of Materials Processing Technology 183 (2-3), 219-225

Dieter, G. E. and Bacon, D. J. (1986) Mechanical Metallurgy.: McGraw-hill New York

DNVGL-ST-F101 (2017) Submarine Pipeline Systems. October 2017, amended December 2017 edn: Det Norske Veritas

Do, S., Serasli, K., and Smith, D. (eds.) (2013) ASME 2013 Pressure Vessels and Piping Conference. 'Combined Measurement and Finite Element Analysis to Map Residual Stresses in Welded Components': American Society of Mechanical Engineers

Dong, P. and Hong, J. K. (2002) Recommendations for Determining Residual Stresses in Fitness-for-Service Assessment.: Welding Research Council

Eckerlid, J. and Ulfvarson, A. (1995) 'Redistribution of Initial Residual Stresses in Ship Structural Details and its Effect on Fatigue'. Marine Structures 8 (4), 385-406

Erny, C., Thevenet, D., Cognard, J., and Körner, M. (2012) 'Fatigue Life Prediction of Welded Ship Details'. Marine Structures 25 (1), 13-32

Eyre, D. G. and Galambos, T. (1970) 'Shakedown Tests on Steel Bars and Beams'. Journal of the Structural Division 96, 1287-1304

Eyres, D. J. (2007) '1 - Basic Design of the Ship'. in Ship Construction (Sixth Edition). ed. by Eyres, D. J. Oxford: Butterworth-Heinemann, 3-9

Faghidian, S. A., Goudar, D., Farrahi, G. H., and Smith, D. J. (2012) 'Measurement, Analysis and Reconstruction of Residual Stresses'. The Journal of Strain Analysis For 47 (4), 254-264

Farajian, M., Nitschke-Pagel, T., and Dilger, K. (2010) 'Mechanisms of Residual Stress Relaxation and Redistribution in Welded High-Strength Steel Specimens Under Mechanical Loading'. Welding in the World 54 (11), R366-R374

Farajian-Sohi, M., Nitschke-Pagel, T., and Dilger, K. (2010) 'Residual Stress Relaxation of Quasi-Statically and Cyclically-Loaded Steel Welds'. Welding in the World 54 (1), R49-R60

Farajian-Sohi, M., Nitschke-Pagel, T., and Dilger, K. (2009) 'Residual Stress Relaxation in Welded Joints Under Static and Cyclic Loading'. International Centre for Diffraction Data

Farrahi, G., Faghidian, S., and Smith, D. (2010) 'An Inverse Method for Reconstruction of the Residual Stress Field in Welded Plates'. Journal of Pressure Vessel Technology 132 (6), 061205

Farrahi, G. H., Faghidian, S. A., and Smith, D. J. (2009) 'Reconstruction of Residual Stresses in Autofrettaged Thick-Walled Tubes from Limited Measurements'. International Journal of Pressure Vessels and Piping 86 (11), 777-784

Ficquet, X. (2007) 'Development and Application of the Deep Hole Drilling Method'. Development and Application of the Deep Hole Drilling Method

Fricke, W., von Lilienfeld-Toal, A., and Paetzold, H. (2012) 'Fatigue Strength Investigations of Welded Details of Stiffened Plate Structures in Steel Ships'. International Journal of Fatigue [online] 34 (1), 17-26. available from <http://www.sciencedirect.com/science/article/pii/S0142112311000387>

Fricke, W. and Paetzold, H. (2010) 'Full-Scale Fatigue Tests of Ship Structures to Validate the S–N Approaches for Fatigue Strength Assessment'. Marine Structures [online] 23 (1), 115-130. available from <http://www.sciencedirect.com/science/article/pii/S0951833910000055>

Fricke, W. and Kahl, A. (2005) 'Comparison of Different Structural Stress Approaches for Fatigue Assessment of Welded Ship Structures'. Marine Structures [online] 18 (7), 473-488. available from <http://www.sciencedirect.com/science/article/pii/S0951833906000165>

Fu, G., Lourenco, M. I., Duan, M., and Estefen, S. F. (2014) 'Effect of Boundary Conditions on Residual Stress and Distortion in T-Joint Welds'. Journal of Constructional Steel Research 102, 121-135

Ganguly, S., Edwards, L., and Fitzpatrick, M. E. (2011) 'Problems in using a Comb Sample as a Stress-Free Reference for the Determination of Welding Residual Stress by Diffraction'. Materials Science and Engineering: A [online] 528 (3), 1226-1232. available from <http://www.sciencedirect.com/science/article/pii/S0921509310012049>

Gannon, L., Pegg, N., Smith, M., and Liu, Y. (2013) 'Effect of Residual Stress Shakedown on Stiffened Plate Strength and Behaviour'. Ships and Offshore Structures 8 (6), 638-652

Gao, H., Zhang, Y., Wu, Q., and Song, J. (2017) 'Experimental Investigation on the Fatigue Life of Ti-6Al-4V Treated by Vibratory Stress Relief'. Metals 7 (5), 158

Gokhfeld, D. A. and Charniavsky, O. (1980) Limit Analysis of Structures at Thermal Cycling. Rockville, Maryland - USA: Sijthoff & Noordhoff

Goldak, J., Chakravarti, A., and Bibby, M. (1984) 'A New Finite Element Model for Welding Heat Sources'. Metallurgical and Materials Transactions B 15 (2), 299-305

Gordo, J. (2013) 'Residual Stresses Relaxation of Welded Structures Under Alternate Loading'. Developments in Maritime Transportation and Exploitation of Sea Resources, Taylor & Francis, London, UK, 321-328

Goudar, D., Hossain, S., Truman, C., and Smith, D. (eds.) (2008) ASME 2008 Pressure Vessels and Piping Conference. 'Uncertainty in Residual Stress Measurements': American Society of Mechanical Engineers

Groß-Weege, J. (1997) 'On the Numerical Assessment of the Safety Factor of Elastic-Plastic Structures Under Variable Loading'. International Journal of Mechanical Sciences 39 (4), 417-433

Grüning, M. (1926) Die Tragfähigkeit Statisch Unbestimmter Tragwerke Aus Stahl Bei Beliebig Häufig Wiederholter Belastung. Berlin: J. Springer

Gurney, T. R. (1979) Fatigue of Welded Structures. 2nd edn: Cambridge University Press

Hadley. I and Pisarski, H. (2013) 'Overview of BS 7910:2013'. ESIA12 – Where are we Now?

Haigh, R. D., Hutchings, M. T., James, J. A., Ganguly, S., Fitzpatrick, M. E., Mizuno, R., Ogawa, K., Okido, S., and Paradowska, A. M. (2013) 'Neutron Diffraction Residual Stress Measurements on Girth-Welded 304 Stainless Steel Pipes with Weld Metal Deposited Up to Half and Full Pipe Wall Thickness'. International Journal of Pressure Vessels and Piping 101, 1-11

Hamelin, C. J., Muránsky, O., Smith, M. C., Holden, T. M., Luzin, V., Bendeich, P. J., and Edwards, L. (2014) 'Validation of a Numerical Model used to Predict Phase Distribution and Residual Stress in Ferritic Steel Weldments'. Acta Materialia 75, 1-19

Hao, H., Ye, D., Chen, Y., Feng, M., and Liu, J. (2015a) A Study on the Mean Stress Relaxation Behavior of 2124-T851 Aluminum Alloy during Low-Cycle Fatigue at Different Strain Ratios [online] . available from <http://www.sciencedirect.com/science/article/pii/S026130691400939X>

Hao, H., Ye, D., Chen, Y., Feng, M., and Liu, J. (2015b) 'A Study on the Mean Stress Relaxation Behavior of 2124-T851 Aluminum Alloy during Low-Cycle Fatigue at Different Strain Ratios'. Materials & Design 67, 272-279

Heinze, C., Schwenk, C., and Rethmeier, M. (2012) 'Numerical Calculation of Residual Stress Development of Multi-Pass Gas Metal Arc Welding'. Journal of Constructional Steel Research [online] 72, 12-19. available from <http://www.sciencedirect.com/science/article/pii/S0143974X11002252>

Heiple, C. and Burgardt, P. (1985) 'Effects of SO2 Shielding Gas Additions on GTA Weld Shape'. Welding Journal 64 (6), 159-162

Hirschberg, M., Manson, S., and Smith, R. (1963) Fatigue Behavior of Materials Under Strain Cycling in Low and Intermediate Life Range. national Aeronautics and Space Administration, Washington: NASA Technical Note D-1574

Hobbacher, A. (2009) Recommendations for Fatigue Design of Welded Joints and Components. New York: Springer

Hodapp, D. P., Collette, M. D., and Troesch, A. W. (2015) 'Stochastic Nonlinear Fatigue Crack Growth Predictions for Simple Specimens Subject to Representative Ship Structural Loading Sequences'. International Journal of Fatigue [online] 70, 38-50. available from <http://www.sciencedirect.com/science/article/pii/S0142112314002138>

Holden, T. M., Suzuki, H., Carr, D. G., Ripley, M. I., and Clausen, B. (2006) 'Stress Measurements in Welds: Problem Areas'. Materials Science and Engineering: A [online] 437 (1), 33-37. available from <http://www.sciencedirect.com/science/article/pii/S0921509306004874>

Holzapfel, H., Schulze, V., Vöhringer, O., and Macherauch, E. (1998) 'Residual Stress Relaxation in an AISI 4140 Steel due to Quasistatic and Cyclic Loading at Higher Temperatures'. Materials Science and Engineering: A 248 (1–2), 9-18

Holzapfel, H., Vöhringer, O., and Macherauch, E. (eds.) (1990) . 'Relaxation of Shot Peening Residual Stresses of the Steel 42 CrMo 4 by Tensile Or Compressive Deformation' at Tokyo: International conference of shot peening

Homma, H., Ohkida, S., Matsuda, and Yamamoto, K. (1987) 'Improvement of HAZ Toughness in HSLA Steel by Introducing Titanium Oxide'. Welding Journal 66, 301-s

James, J., Santisteban, J., Edwards, L., and Daymond, M. (2004a) 'A Virtual Laboratory for Neutron and Synchrotron Strain Scanning'. Physica B: Condensed Matter 350 (1-3), E743-E746

James, J. A. and Edwards, L. (2007) 'Application of Robot Kinematics Methods to the Simulation and Control of Neutron Beam Line Positioning Systems'. Nuclear Instruments and Methods in Physics Research Section A: Accelerators, Spectrometers, Detectors and Associated Equipment 571 (3), 709-718

James, M. N., Hughes, D. J., Hattingh, D. G., Mills, G., and Webster, P. J. (2009) Residual Stress and Strain in MIG Butt Welds in 5083-H321 Aluminium: As-Welded and Fatigue Cycled [online] . available from <http://www.sciencedirect.com/science/article/pii/S014211230800114X>

James, M. N., Hughes, D. J., Hattingh, D. G., Bradley, G. R., Mills, G., and Webster, P. J. (2004b) 'Synchrotron Diffraction Measurement of Residual Stresses in Friction Stir Welded 5383-H321 Aluminium Butt Joints and their Modification by Fatigue Cycling'. Fatigue & Fracture of Engineering Materials & Structures 27 (3), 187-202

Jhansale, H. and Topper, T. (1973) 'Engineering Analysis of the Inelastic Stress Response of a Structural Metal Under Variable Cyclic Strains'. Astm Stp 519, 246-270

Jun, T. and Korsunsky, A. M. (2010) 'Evaluation of Residual Stresses and Strains using the Eigenstrain Reconstruction Method'. International Journal of Solids and Structures 47 (13), 1678-1686

Justin Mach, Casey Gales, Jun-Sang Park, John Okasinski, Christopher Budrow, Armand Beaudoin, Kenneth Swartz, Matthew Miller, and Thomas Gnaupel-Herold (2019) 'FD&E Total Life T-Sample Residual Stress Analytical Predictions and Measured Results'. SAE Technical Paper 2019-01-0528

Kandil, F. A., Lord, J. D., Fry, A. T., and Grant, P. V. (2001) A Review of Residual Stress Measurement Methods - A Guide to Technical Selection.: National Physical Laboratory

Kartal, M. E., Liljedahl, C. D. M., Gungor, S., Edwards, L., and Fitzpatrick, M. E. (2008) 'Determination of the Profile of the Complete Residual Stress Tensor in a VPPA Weld using the Multi-Axial Contour Method'. Acta Materialia [online] 56 (16), 4417-4428. available from <http://www.sciencedirect.com/science/article/pii/S135964540800356X>

Kim, M. H., Kang, S. W., Kim, J. H., Kim, K. S., Kang, J. K., and Heo, J. H. (2010) 'An Experimental Study on the Fatigue Strength Assessment of Longi-Web Connections in Ship Structures using Structural Stress'. International Journal of Fatigue [online] 32 (2), 318-329. available from <http://www.sciencedirect.com/science/article/pii/S0142112309002023>

Kirk, M. T. and Dodds Jr, R. H. (1991) The Effect of Weld Metal Strength Mismatch on the Deformation and Fracture Behavior of Steel Butt Weldments: University of Illinois Engineering Experiment Station. College of Engineering. University of Illinois at Urbana-Champaign.

Kodama S (1972) 'The Behavior of Residual Stress during Fatigue Stress Cycles'. Proceedings of the International Conference on Mechanical Behavior of Metals II. Kyoto: Society of Material Science 2, 111–118

Koiter, W. T. (1956) 'A New General Theorem on Shakedown of Elastic-Plastic Structures'. Proc. Koninkl. Ned. Akad. Wetenschap B59, 24-34

Koiter, W. T. (1964) 'General Theorems for Elastic Plastic Solids'. Progress of Solid Mechanics, Ed. by Hill, R. and Sneddon, I., 2nd Edition, North Holland Publishing Company, Amsterdam 2, 167-219

Konig, J. and Kleiber, M. (1978) 'On a New Method of Shakedown Analysis'. Bull. Acad. Polon. Sci.-Ser. Sci. Techn. 26 (4), 165

König, J. A. (2012) Shakedown of Elastic-Plastic Structures.: Elsevier

Korsunsky, A. M. (2009) 'Eigenstrain Analysis of Residual Strains and Stresses'. The Journal of Strain Analysis For 44 (1), 29-43

Kou, S. (2002) Welding Metallurgy. Second edn. Hoboken, New Jersey.: John Wiley & Sons, Inc

Kou, S. (2003) Welding Metallurgy. Second edn. Hoboken, New Jersey: John Wiley & Sons, Inc

Krawitz, A. D. and Winholtz, R. A. (1994) 'Use of Position-Dependent Stress-Free Standards for Diffraction Stress Measurements'. Materials Science and Engineering: A [online] 185 (1), 123-130. available from <http://www.sciencedirect.com/science/article/pii/0921509394909350>

L. Wei and M. Gallegillo (2012) 'Methods for Measurement and Prediction of Residual Stresses in Pipe Girth Welds in Clad Pipes'. TWI Core Research Project Report

Lee, C., Chang, K., and Van Do, V. N. (2015) 'Finite Element Modeling of Residual Stress Relaxation in Steel Butt Welds Under Cyclic Loading'. Engineering Structures 103, 63-71

Lee, S., Coratella, S., Brügger, A., Clausen, B., Brown, D., Langer, K., Fitzpatrick, M., and Noyan, I. (2018) 'Boundary Effects in the Eigenstrain Method'. Experimental Mechanics 58, 799-814

Lee, C., Chang, K., and Do, V. N. V. (2015) 'Finite Element Modeling of Residual Stress Relaxation in Steel Butt Welds Under Cyclic Loading'. Engineering Structures 103, 63-71

Leggatt, R. (1986) 'Residual Stress and Distortion in Multipass Butt Welded Joints in Type 316 Stainless Steel'. Residual Stresses in Science and Technology. 2, 997-1004

Leggatt, R. H. (2008) 'Residual Stresses in Welded Structures'. International Journal of Pressure Vessels and Piping 85 (3), 144-151

Lei, Y., O'dowd, N., and Webster, G. (2000) 'Fracture Mechanics Analysis of a Crack in a Residual Stress Field'. International Journal of Fracture 106 (3), 195-216

Lemaitre, J. and Chaboche, J. (1994) Mechanics of Solid Materials.: Cambridge University Press

Li, T., Chen, H., Chen, W., and Ure, J. (2011) 'On the Shakedown Analysis of Welded Pipes'. International Journal of Pressure Vessels and Piping 88 (8-9), 301-310

Liljedahl, C., Zanellato, O., Fitzpatrick, M., Lin, J., and Edwards, L. (2010) 'The Effect of Weld Residual Stresses and their Re-Distribution with Crack Growth during Fatigue Under Constant Amplitude Loading'. International Journal of Fatigue 32 (4), 735-743

Liu, Y. H., Carvelli, V., and Maier, G. (1997) 'Integrity Assessment of Defective Pressurized Pipelines by Direct Simplified Methods'. International Journal of Pressure Vessels and Piping [online] 74 (1), 49-57. available from <http://www.sciencedirect.com/science/article/pii/S0308016197000847>

Lodini, A. (2003) 'Calculation of Residual Stress from Measured Strain'. in Analysis of Residual Stress by Diffraction using Neutron and Synchrotron Radiation. ed. by Fitzpatrick, M. E. and Lodini, A. : Taylor and Francis, 47-59

Lotsberg, I. and Landet, E. (2005) 'Fatigue Capacity of Side Longitudinals in Floating Structures'. Marine Structures 18 (1), 25-42

M. Farajian and T. Nitschke-Pagel (2012) 'Relaxation of Welding Residual Stresses-Part I Under Quasi Static Loading'. International Journal of Microstructure and Materials Properties 7 (1), 3-15

Mackenzie, D., Boyle, J., Hamilton, R., and Shi, J. (1996) 'The Elastic Compensation Method in Shell-Based Design by Analysis'. Proceedings of the 1996 ASME Pressure Vessels and Pinpping Conference 338, 203

Mackenzie, D., Boyle, J. T., and Hamilton, R. (2000) 'The Elastic Compensation Method for Limit and Shakedown Analysis: A Review'. The Journal of Strain Analysis for Engineering Design 35 (3), 171-188

Maddox, S. J. (1991) Fatigue Strength of Welded Structures.: Woodhead Publishing

Mahapatra, M. M., Datta, G. L., and Pradhan, B. (2006) 'Three-Dimensional Finite Element Analysis to Predict the Effects of Shielded Metal Arc Welding Process Parameters on Temperature Distributions and Weldment Zones in Butt and One-Sided Fillet Welds'. Proceedings of the Institution of Mechanical Engineers, Part B: Journal of Engineering Manufacture 220 (6), 837-845

Martin, J. B. (1975) Plasticity: Fundamentals and General Results.: MIT press

Masubuchi, K. and Martin, D. C. (1966) Investigation of Residual Stresses in Steel Weldments

Mattson, R. and Coleman, W. (1954) 'Effect of Shot-Peening Variables and Residual Stresses on the Fatigue Life of Leaf-Spring Specimens'. SAE Technical Paper 540262

McDill, J., Runnemalm, K., and Oddy, A. (2001) 'An 8-to 16-Node Solid Graded Shell Element for Far-Field Applications in Thermal-Mechanical FEA'. J Math Model Sci Comput 13, 177-192

Melan, E. (1938a) 'Zur Plastizität Des Räumlichen Kontinuums'. Archive of Applied Mechanics 9 (2), 116-126

Melan, E. (1938b) 'Zur Plastizität Des Räumlichen Kontinuums'. Ingenieur-Archiv 9 (2), 116-126

Morrow J, S. G. (1958) 'Cycle-Dependent Stress Relaxation'. Symposium on Basic Mechanisms of Fatigue, ASTM STP 237. American Society for Testing and Materials

Mura, T. (1987) Micromechanics of Defects in Solids. 2nd edn: Martinus Nijhoff Publishers, Dordrecht

Nur Syahroni (2012) '3D Finite Element Simulation of T-Joint Fillet Weld: Effect of various Welding Sequences on the Residual Stresses and Distortions'. Numerical Simulation - from Theory to Industry 10, 583-606

O'Meara, N., Smith, S. D., and Francis, J. A. (eds.) (2015) ASME 2015 Pressure Vessels and Piping Conference. 'Calibrating Phase Transformation and Grain Growth Models and Measuring Phase Dependent Material Properties for use in Fe Simulations of Welds': American Society of Mechanical Engineers

O'Meara, N., Smith, S. D., and Francis, J. A. (2015) 'Calibrating Phase Transformation and Grain Growth Models and Measuring Phase Dependent Material Properties for use in FE Simulations of Welds'. Pressure Vessels and Piping Conference (56987), V005T09A016

Paradowska, A. M., Price, J. W. H., Ibrahim, R., and Finlayson, T. R. (2006) 'The effect of Heat Input on Residual Stress Distribution of Steel Welds Measured By neutron Diffraction'. Journal of Achievements in Materials and Manufacturing Engineering 17 (1-2), 385-388

Pavelic, V. (1969) 'Experimental and Computed Temperature Histories in Gas Tungsten Arc Welding of Thin Plates'. Welding Journal Research Supplement 48, 296-305

PD 5500:2018 (ed.) (2018) Specification for Unfired Fusion Welded Pressure Vessels. 7th edn. : BSI Standards Limited

Phạm, P. T. and Staat, M. (2014) 'FEM-Based Shakedown Analysis of Hardening Structures'. Asia Pacific Journal on Computational Engineering 1 (1), 1-13

Polezhayeva, H., Kang, J., Lee, J., Yang, Y., and Kudryavtsev, Y. (eds.) (2010) The Twentieth International Offshore and Polar Engineering Conference. 'A Study on Residual Stress Distribution and Relaxation in Welded Components'. held 20-25 June at Beijing, China: International Society of Offshore and Polar Engineers

Prager, W. (1956) 'A New Method of Analyzing Stresses and Strains in Work-Hardening Plastic Solids'

Prevey, P.,S. (1996) 'Current Applications of X-Ray Diffraction Residual Stress Measurement'. Dev. Mater. Charact. Technol. Symp. Held Dur. 28th Annu. Tech. Meet. Int. Metallogr. Soc. 513, 103-110

Qian, Z., Chumbley, S., Karakulak, T., and Johnson, E. (2013) 'The Residual Stress Relaxation Behavior of Weldments during Cyclic Loading'. Metallurgical and Materials Transactions A 44 (7), 3147-3156

R5 (ed.) (2014) Assessment Procedure for the High Temperature Response of Structures. 3rd edn. : EDF Energy Nuclear Generation Ltd

R6 Revision 4 (2015) Assessment of the Integrity of Structures Containing Defects. United Kingdom: EDF Energy Nuclear Generation Ltd

Rahman Chukkan, J., Vasudevan, M., Muthukumaran, S., Ravi Kumar, R., and Chandrasekhar, N. (2015) 'Simulation of Laser Butt Welding of AISI 316L Stainless Steel Sheet using various Heat Sources and Experimental Validation'. Journal of Materials Processing Technology 219 (0), 48-59

Reimers, W., Broda, M., Brusch, G., Dantz, D., Liss, K. -., Pyzalla, A., Schmackers, T., and Tschentscher, T. (1998) 'Evaluation of Residual Stresses in the Bulk of Materials by High Energy Synchrotron Diffraction'. Journal of Nondestructive Evaluation 17 (3), 129-140

Reißner, H. (1931) 'Eigenspannungen Und Eigenspannungsquellen'. ZAMM - Journal of Applied Mathematics and Mechanics / Zeitschrift Für Angewandte Mathematik Und Mechanik 11 (1), 1-8

Rosenthal, D. (1946) 'The Theory of Moving Sources of Heat and its Applications to Metal Treatments' 68, 849-866

Rossini, N. S., Dassisti, M., Benyounis, K. Y., and Olabi, A. G. (2012) 'Methods of Measuring Residual Stresses in Components'. Materials & Design [online] 35, 572-588. available from <http://www.sciencedirect.com/science/article/pii/S0261306911005887>

Santisteban, J., Daymond, M., James, J., and Edwards, L. (2006) 'ENGIN-X: A Third-Generation Neutron Strain Scanner'. Journal of Applied Crystallography 39 (6), 812-825

Schajer, G. S. (2010) 'Advances in Hole-Drilling Residual Stress Measurements'. Experimental Mechanics 50 (2), 159-168

Seshadri, R. (1995) 'Inelastic Evaluation of Mechanical and Structural Components using the Generalized Local Stress Strain Method of Analysis'. Nuclear Engineering and Design [online] 153 (2), 287-303. available from <http://www.sciencedirect.com/science/article/pii/0029549395900209>

Smith, D., Farrahi, G., Zhu, W., and McMahon, C. (2001) 'Experimental Measurement and Finite Element Simulation of the Interaction between Residual Stresses and Mechanical Loading'. International Journal of Fatigue 23 (4), 293-302

Smith, M., Bouchard, P., Turski, M., Edwards, L., and Dennis, R. (2012) 'Accurate Prediction of Residual Stress in Stainless Steel Welds'. Computational Materials Science 54, 312-328

Staat, M. and Heitzer, M. (2001) 'LISA — a European Project for FEM-Based Limit and Shakedown Analysis'. Nuclear Engineering and Design [online] 206 (2), 151-166. available from <http://www.sciencedirect.com/science/article/pii/S0029549300004155>

Stacey, A., MacGillivary, H., Webster, G., Webster, P., and Ziebeck, K. (1985) 'Measurement of Residual Stresses by Neutron Diffraction'. The Journal of Strain Analysis for Engineering Design 20 (2), 93-100

Stein, E., Zhang, G., and Mahnken, R. (1993) 'Shake-Down Analysis for Perfectly Plastic and Kinematic Hardening Materials'. in Progress in Computational Analysis of Inelastic Structures. ed. by Anon: Springer, 175-244

Stokoe (1996) Reed's Ship Construction for Marine Students.: Thomas Reed Publications

Sun, Y., Shen, S., Xia, X., and Xu, Z. (2013) 'A Numerical Approach for Predicting Shakedown Limit in Ratcheting Behavior of Materials'. Materials & Design 47, 106-114

Taleb, L. (2013) 'About the Cyclic Accumulation of the Inelastic Strain Observed in Metals Subjected to Cyclic Stress Control'. International Journal of Plasticity 43, 1-19

Tanaka, K., Nishijima, S., Matsuoka, S., and Kouzu, F. (1981) 'Low-and High-cycle Fatigue Properties of various Steels Specified in JIS for Machine Structural Use'. Fatigue & Fracture of Engineering Materials & Structures 4 (1), 97-108

Taran, Y. V., Balagurov, A. M., Schreiber, J., and Stuhr, U. (2008) 'Residual Stresses in a Shape Welded Steel Tube by Neutron Diffraction'. Journal of Physics: Condensed Matter 20 (10), 1-4

Tekriwal, P. and Mazumder, J. (1991) 'Transient and Residual Thermal Strain-Stress Analysis of GMAW'. Journal of Engineering Materials and Technology 113 (3), 336-343

Trufyakov, V. I. (1958) 'Welded Joints and Residual Stresses'. Avt.Sv.no.5, 1956, and Br.Weld.J. 5 (11), 491-498

Trufyakov, V. I. (1956) 'The Role of Residual Stresses in Reducing the Endurance of Welded Joints'. Automatecheskaya Svarka 5, 90-103

Walker, C. (2011) 'A Theoretical Review of the Operation of Vibratory Stress Relief with Particular Reference to the Stabilization of Large-Scale Fabrications'. Proceedings of the Institution of Mechanical Engineers, Part L: Journal of Materials: Design and Applications 225 (3), 195-204

Wang, Q. and Liu, X. (2017) 'Non-Saturated Cyclic Softening and Uniaxial Ratcheting of a High-Strength Steel: Experiments and Viscoplastic Constitutive Modeling'. Mechanics of Materials 113, 112-125

Wang, Q., Liu, X., Yan, Z., Dong, Z., and Yan, D. (2017a) 'On the Mechanism of Residual Stresses Relaxation in Welded Joints Under Cyclic Loading'. International Journal of Fatigue 105, 43-59

Wang, Q., Liu, X., Yan, Z., Dong, Z., and Yan, D. (2017b) 'On the Mechanism of Residual Stresses Relaxation in Welded Joints Under Cyclic Loading'. International Journal of Fatigue 105, 43-59

Williams, J., Dyson, I., and Kapoor, A. (1999) 'Repeated Loading, Residual Stresses, Shakedown, and Tribology'. Journal of Materials Research 14 (04), 1548-1559

Withers, P. J., Turski, M., Edwards, L., Bouchard, P. J., and Buttle, D. J. (2008) 'Recent Advances in Residual Stress Measurement'. International Journal of Pressure Vessels and Piping 85 (3), 118-127

Withers, P. J. and Webster, P. J. (2001) 'Neutron and Synchrotron X-Ray Strain Scanning'. Strain 37 (1), 19-33

Withers, P. J. (2007) 'Mapping Residual and Internal Stress in Materials by Neutron Diffraction'. Comptes Rendus Physique 8 (7–8), 806-820

Xie, X., Jiang, W., Luo, Y., Xu, S., Gong, J., and Tu, S. (2017) 'A Model to Predict the Relaxation of Weld Residual Stress by Cyclic Load: Experimental and Finite Element Modeling'. International Journal of Fatigue 95, 293-301

Yaghi, A. H., Hyde, T. H., Becker, A. A., Sun, W., Hilson, G., Simandjuntak, S., Flewitt, P. E. J., Pavier, M. J., and Smith, D. J. (2010) 'A Comparison between Measured and Modeled Residual Stresses in a Circumferentially Butt-Welded P91 Steel Pipe'. Journal of Pressure Vessel Technology 132 (1), 011206-011206-10

Young, B. W. (1981) Energy Methods of Structural Analysis: Theory, Worked Examples and Problems.: Macmillan

Yuan, K. and Sumi, Y. (2013) 'Welding Residual Stress and its Effect on Fatigue Crack Propagation After Overloading'. Analysis and Design of Marine Structures (CRC Press)

Zerbst, U., Ainsworth, R., Beier, H. T., Pisarski, H., Zhang, Z., Nikbin, K., Nitschke-Pagel, T., Münstermann, S., Kucharczyk, P., and Klingbeil, D. (2014) 'Review on Fracture and Crack Propagation in Weldments–a Fracture Mechanics Perspective'. Engineering Fracture Mechanics 132, 200-276

Zhuang, W. Z. and Halford, G. R. (2001) 'Investigation of Residual Stress Relaxation Under Cyclic Load'. International Journal of Fatigue 23, Supplement 1, 31-37

Zouain, N., Herskovits, J., Borges, L. A., and Feijóo, R. A. (1993) 'An Iterative Algorithm for Limit Analysis with Nonlinear Yield Functions'. International Journal of Solids and Structures 30 (10), 1397-1417

Appendix A: Welding process details

Welding Procedure Specification – 001/AME

WPQR-001P_AME

Created and approved by TWI Test house Date: 11th January 2017

Photographs of completed weld – Radiographic identity C2451

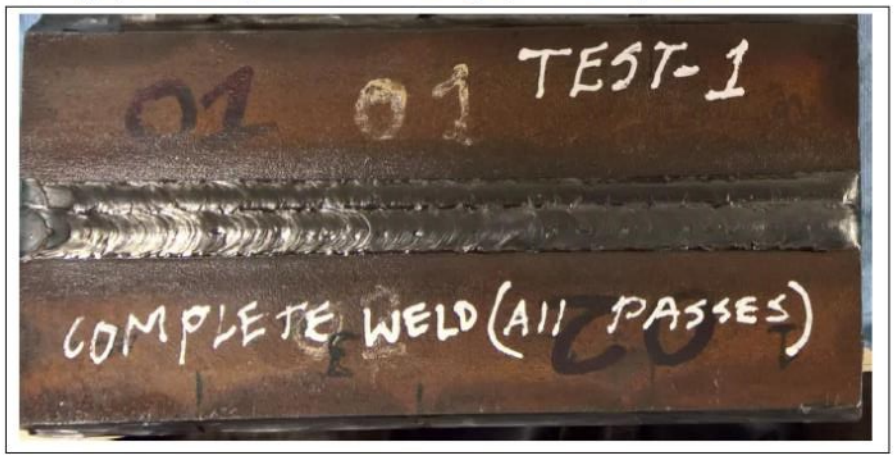

Photographs of completed weld – Radiographic identity C2453

Photographs provided by Jazeel Chukkan

Date: 11th January 2017

Appendix B: Residual strains determined from neutron diffraction